# Damage to Masonry Houses due to a Riverine Dyke Breach

*A hydraulic and structural approach*

Max Teeuwen
4021770
13 February 2019

Photo on front cover:
Ouderkerk aan den IJssel, February 1st, 1953 North Sea Flood, izi.travel

**Graduate**
Beekstraat 19
5931 ER, Tegelen
Mobile: 06-47335762
Email: M.F.M.Teeuwen@student.tudelft.nl
Email: maxteeuwen@hotmail.com

**Master track**
Hydraulic Engineering & Structural Engineering

**Committee Members**

| | | |
|---|---|---|
| Prof. dr. ir. S.N. Jonkman | (Hydraulic Engineering) | Chairman |
| Ir. W.F. Molenaar | (Hydraulic Engineering) | Supervisor |
| Dr. ir. P.C.J. Hoogenboom | (Structural Engineering) | Supervisor |

# *Abstract*

The Netherlands has always been in close proximity to water, whether its rivers or the sea. This proximity to water and the need for land to settle and farm, led to vast amounts of land reclamation by constructing dykes along the water features to prevent flooding of the new earned land. This newly reclaimed land started to subside over the years, increasing the difference between the high water in the rivers and the low-lying land even more. With an expanding population, rising water levels and increasingly severe storms, the consequences of a future flood due to a riverine dyke breach are ever rising.

The Dutch protect their land using dykes. These dykes are constructed along nearly every water feature, rivers, lakes and the sea. As the water rises to the top of the dyke, failure might occur. The most dangerous failure mechanisms are shearing and sliding of the inner slope, since these can cause rapid failure of a dyke causing flood waves. Even though normal sand dykes follow several generic stages and will not fail suddenly as a whole, peat dykes and other flood defences might fail suddenly and catastrophically.

The aim of this thesis followed from the increasing consequences, the way the Dutch protect their land using dykes and from the traditional Dutch house being constructed using masonry. This led to the aim to determine the potential structural damage to a masonry house due to a dyke breach leading to a riverine flood.

This sudden failure in turn releases a flood wave. To determine the flow velocity and inundation depth of this wave, several approximations have been used. Individually, these proved to be unable to properly determine the flow velocity and inundation depth, which led to an estimate of the flow velocity and inundation depth rather than an exact determination.

Behind the dykes in the Netherlands there are often masonry house, as masonry is the building material most commonly used. When the flood wave reaches the masonry house several loads will be imposed by the water on the house. The most important loads for this thesis are the hydrostatic water pressure and the hydrodynamic bore impact. Where the hydrostatic water pressure speaks for itself, the hydrodynamic bore impact requires some additional information. When this bore impacts the house, a so-called ‘church roof’ pressure distribution follows, a high peak followed by a quasi-static part.

These hydraulic loads are used to determine the structural response of a masonry house. Since, as stated above, it is the most commonly used material for the construction of houses in the Netherlands. Especially in the early 1900 most of the houses were built using masonry. First the construction consisted of mainly single solid walls, later on followed by cavity walls for better isolation. These masonry houses generally had wooden door and window frames as well as wooden floors.

Besides these major building components, there are also components which are smaller either in size or in relevance. Doors, for example, are found in most outer walls and are generally a weak point, failing well before the walls do. Cavity walls also have wall ties, these connect the outer façade with the inner, load bearing, wall. However, this connection might not be so strong as to be able to structurally connect to inner and outer walls. Cavity walls therefore can be significantly weaker than their single solid wall counterpart.

To get a first approximation of the water-masonry interaction, several preliminary calculations have been done. Starting with a simple analytical approach, just a beam connected at the top

and bottom with hinges, and ending with a plastic hinge model which assumed a rigid connection at the top and bottom with plastic deformation for moment redistribution. These first approximation provided inundation depth for the first cracks and failure of a single solid wall which where around 3.0 m and 3.35 m respectively.

Since a masonry house is too complex to calculate by hand, a finite element program, DIANA, has been used to perform these calculations. In order to compare the many different possible scenarios, several cases have been formulated for a cavity and a single solid wall masonry house. Starting with a house without any inner walls, doors and windows, after which these features were added one by one. Of course, the results of these calculations needed to be interpreted. Therefore, a failure criterion based on the displacement characteristics of the masonry was formulated to objectively compare the different cases.

The calculations showed the importance of the inner walls on the structural strength of the houses, increasing the failure load of the dynamic load for the cavity walls up to 40% and even up to 100% for the single solid walls. The static calculations proved to be much more rigid with only small increases or decreases between the different cases. Between the cavity wall and single solid wall there were large differences, where an inundation depth of around 2.5 m led to failure for the cavity wall, an inundation depth of 4-5 m was required for similar damage in the case of the single solid wall. The dynamic load also showed this same tendency, an increase for the failure load from about 2-2.5%, of the dynamic load, for the cavity wall to 6-10%, of the dynamic load, for the single solid wall. The percentages follow from the loading scheme in DIANA, the load is increased step by step until failure occurs.

As is evident from the low percentages for failure due to the dynamic load, there is something unusual going on. This can already greatly be explained by the use of a wrong inundation depth and flow velocity. After correcting these, the force due to the dynamic load reduces to approximately 25% of the dynamic load used in the DIANA calculations. Furthermore the dynamic load was schematised as a static load in the model, which does not fully take into account the short duration of the pressure peak on which the dynamic load is based. This leads to the conclusion that even though those percentages are low, for some cases, it might very well be possible that the masonry house is able to withstand the dynamic bore impact. Although, it is unlikely that no structural damage will occur for any of the cases.

# *Acknowledgements*

This thesis concludes the double track Master of Science programme ‘Hydraulic Engineering’ and ‘Structural Engineering’ at Delft University of Technology.

I would like to thank my professor, S.N. Jonkman as well as my supervisors, W.F. Molenaar and P.C.J. Hoogenboom for their patience, support and feedback. Meetings providing new ideas and insights have helped me along a great deal.

Furthermore I would like to thank my friends and family for their unwavering confidence and never-ending support during this process.

Max Teeuwen, Tegelen February 13th, 2019

# Table of Contents

# 1 Introduction

## 1.1 Background

The Netherlands is a small, low-lying country at the North Sea with lots of rivers, streams and other water related features. Due to the proximity to all this water, land to live and farm upon has always been scarce. Land reclamation in previous centuries has led to new fertile farming areas. This was done through the construction of dykes along the rivers, and other water features, and then pumping the water out. However, the soil in a lot of these reclaimed areas consists of a substantial amount of peat. This peat slowly shrinks when it dries, causing enormous subsiding of these reclaimed areas over the past centuries. Normally the rivers would alter their course to form a new equilibrium. However, the Dutch protected their hard-earned land by improving the dykes along the rivers. This has led to many of these reclaimed areas of land next to rivers to lie several metres below the riverbed. In order to settle on these new low lying areas, the Dutch constructed many permanent masonry houses. How these masonry houses will respond in the case of a dyke failure is however mostly unknown and consequences are still evaluated in hindsight to predict the consequences of future floods.

There are two types of floods, coastal and riverine. Coastal floods are usually caused by a storm surge or tsunami. There are, of course, factors such as the tide which can increase the water level even further. The most well-known Dutch example of a coastal flood is the North Sea Flood of 1953, which flooded 2.000 $km^2$, killing 1836 people and leaving about 100.000 homeless[1]. A more recent coastal flood is the tsunami induced flood caused by a seaquake in Japan, killing more than 25.000 people and causing the meltdown of several nuclear reactors in Fukushima.[2] This meltdown was so severe that on the INES scale it was placed in scale 7. For reference, there has been only one other scale 7 event, the Chernobyl disaster.[3]

Riverine floods are generally preceded by intense rain or melting of snow in the catchment area of the river. This water will then make its way downstream and due to the effect called hysteresis, see also 4.4, it will lump together, thus enhancing the flood wave. Well-known Dutch riverine floods are the floods of 1993 and 1995. The 1993 flood of the river Meuse caused a record discharge of 3120 $m^3/s$ and a record water level of 45.90 m +NAP at Borgharen and flooded large parts of the Dutch province Limburg, causing damage for approximately 115 million euros. In 1995 again, high water levels were recorded. Not only in the river Meuse but also the Rhine and Waal. Parts of Limburg were flooded and the unprotected villages of Itteren and Borgharen were severely hit. More than 250.000 people were evacuated but no more protected areas were flooded. Even though a dyke near the village of Ochten started to slide; hundreds of soldiers and tonnes of sand bags prevented its collapse.[4]

In response to the floods in the Netherlands, the Dutch created the Delta Commission. The first was installed in 1953 following the flood of that year and the second in 2007. The first commission

[1] Omroep Zeeland [52]
[2] NEMO Kennislink [53]
[3] IAEA [54]
[4] NOS [55]

consisted mostly of civil engineers and its main task was to determine measures to prevent a next flood. Amongst other things, this led to the construction of the storm surge barrier and a dam to close the Eastern Scheldt.[5] The 2007 commission had a larger mix of disciplines, apart from civil engineers there were ecologists, economists and specialists with regard to spatial planning. Its goal was to advise on matters such as the rising seawater, the increasing discharges of the Dutch rivers, (drinking) water management as well as possible strategies for sustainable development of the Dutch coast. This led to 12 recommendations for the short- and middle-long-term. Both delta commissions have led to the current protection norms in the Netherlands.[6]

## 1.2 Knowledge Gaps

Even though these newer norms are used, there are still knowledge gaps in both the hydraulic and structural sections.

After the breaching of the dyke or flood defence, a flood wave will follow, especially is this breaching is sudden. The hydraulic loads following from this flood wave are still partially unknown and subject of research. The main hydraulic load which is not yet fully known is the first impact of the flood wave against a structure. Although research shows the familiar church roof pressure distribution[7][8], the pressure peak seemed to be dependent on the time scale of the measurements. The shorter the time scale, the higher the peak.

The structural damage can always be assessed after a flood event has occurred. Using predictions or measurements of the inundation depth and flow velocity, a certain the structural damage could be attributed to a certain combination of the inundation depth and flow velocity. However, what actually happens with the structure, in this thesis the focus will be on a masonry house, is not yet determined.

With the changes in climate, water levels rising and increasing severity of storms and floods, there is an increasing chance of a flood occurring which could lead to dyke failure. A good example is hurricane Katrina, which ravaged parts of North America in 2005 or the high water events in Germany in 2013 leading to the evacuation of several cities close to the Elbe.

All the more reason to bridge these knowledge gaps to improve safety estimations and mitigate consequences as much as possible.

## 1.3 Research Questions

The following main research question has been formulated:

“What is the potential structural damage to masonry houses in the Netherlands due to a dyke breach leading to a riverine flood?”

The objective of this thesis is to identify and quantify the hydraulic loads on masonry houses due to a riverine flood following from a dyke breach in the Dutch River Lek. As well as to accurately determine the structural properties and the damage to a masonry house due to a riverine flood in the Netherlands.

---

[5] Deltacommissie [47]
[6] Steenepoorte [56]
[7] Peregrine [29]
[8] Ramachandran et al. [32]

### 1.3.1 Sub-questions

In order to answer the research question, several sub-questions are formulated. These sub-questions are associated with the structural properties of a masonry house in the Netherlands as well as the identification and quantification of the riverine flood loads for the case study.

These sub-questions are:

- What is the worst possible dyke breach?
- What are the flow velocity and inundation depth due to this dyke breach?
- What are the loads due to the flow velocity and inundation depth and what are their quantities?
- What are the structural weak points of a masonry house?
- What is the interaction between the different structural components of the masonry house?
- How does a masonry house at a certain distance from the breach react to flood loads?
- What would be necessary for this house to survive this flood event?

## 1.4 Approach

In order to answer the main research question and the sub-questions, several steps have to be taken. These steps are:

- Literature study
- Preliminary calculation
- Case Study

The first step is conducting a literature study. This provided the background information regarding riverine floods and the accompanying loads. Furthermore, it provided the necessary information regarding the composition of masonry houses and possible failure mechanisms of these houses. Doing this lead to the identifying of the knowledge gaps.

The second step is preliminary calculations. These are with regard to the inundation depth and flow velocity following a dyke breach as well as to the interaction between the water and the masonry house as a consequence of that dyke breach.

Finally, a model of the masonry house will be tested with the determined hydraulic loads to determine the structural response of the masonry house. From this the failure mechanisms and loads can be determined.

## 1.5 Case

Besides the hydraulic aspects during floods, there are more aspects which play a role in the effect of a flooding on its surroundings. The first is the characteristics of the flood defence at the specific location and second, the objects behind that flood defence. As mentioned in the Introduction there are many low-lying areas in the Netherlands with high dykes and masonry houses for the people to live in. As mentioned in 1.2, the hydraulic loads that occur shortly after the breach are not all known, the structural response of a masonry house to those loads is also unknown. In order to determine the specific masonry housing type, flood defence characteristics and subsequent flood loads for a case study, first a location needs to be selected based on a high potential difference between the ground level and the water level, in other words a high inundation depth. This high potential inundation depth will also lead to significant flow velocities when the dyke breaches, both are required in order to obtain structural damage. This led to a stretch of dyke next to the river Lek in dyke ring 16 near the village of Streefkerk in the Province of South Holland. This stretch of dyke has

the following characteristics; the dyke width, 45m, crest level, 5.8m and hinterland level -1.0m and therefore the maximum inundation depth is 6.8m. This is however an academic maximum, the factual maximum follows from the hydraulic boundary conditions and is approximately 3.5m, see also Appendix C. The calculations in this report are based on the, worst case, academic maximum.

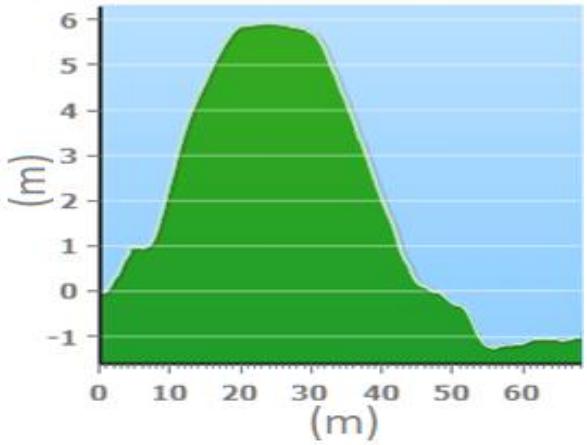


Figure 1 - Cross-section of the dyke (distorted scale)[9]

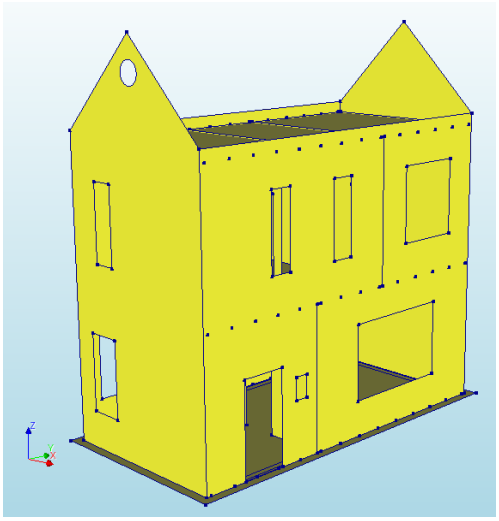

Figure 2 - Overview of the model of the masonry house

In the Netherlands a large part of the (older) houses are built using masonry, if a dyke were to break this housing type is expected to be the one most affected. With regard to the chosen dyke section, this is especially true since almost all buildings are built using masonry, with the majority being from pre-1930. The masonry wall can be a cavity wall which means it consists of an inside load bearing wall and an outside façade connected to each other using wall ties or a single wall without cavity. The floors will be constructed using wooden beams and planks. See Figure 2 for a first impression of the model used in the case study.

## 1.6 Report Structure

For an overview of the structure of this report, see Figure 3. First is the investigation of the composition of dykes in general and the possible dyke failure mechanisms in chapter 2. After the initial breach, the propagation of the damage as well as the water is determined in chapter 3. From this the potential flood loads follow which are discussed in chapter 4 which concludes the hydraulic part.

In chapter 5, the damage propagation in the polder after the dyke breach is discussed. Next in chapter 6, the different properties of masonry are discussed as well as the properties of the other building materials used in the construction of a masonry house. Following this in chapter 7, is the strength of minor building components of the masonry house. This includes several calculations regarding these components.

To get an idea of the interaction between the flood wave and the masonry house, discussed in chapters 4 and 6 respectively, preliminary calculations to the masonry-water interaction are done in chapter 8. Following this, the DIANA model properties of a masonry house, which is discussed in chapter 9. This is followed by chapter 10 and 11 which contain the results of the DIANA calculations. Everything is concluded with chapter 12 which contains the conclusions and recommendations.

[9] AHN [43]

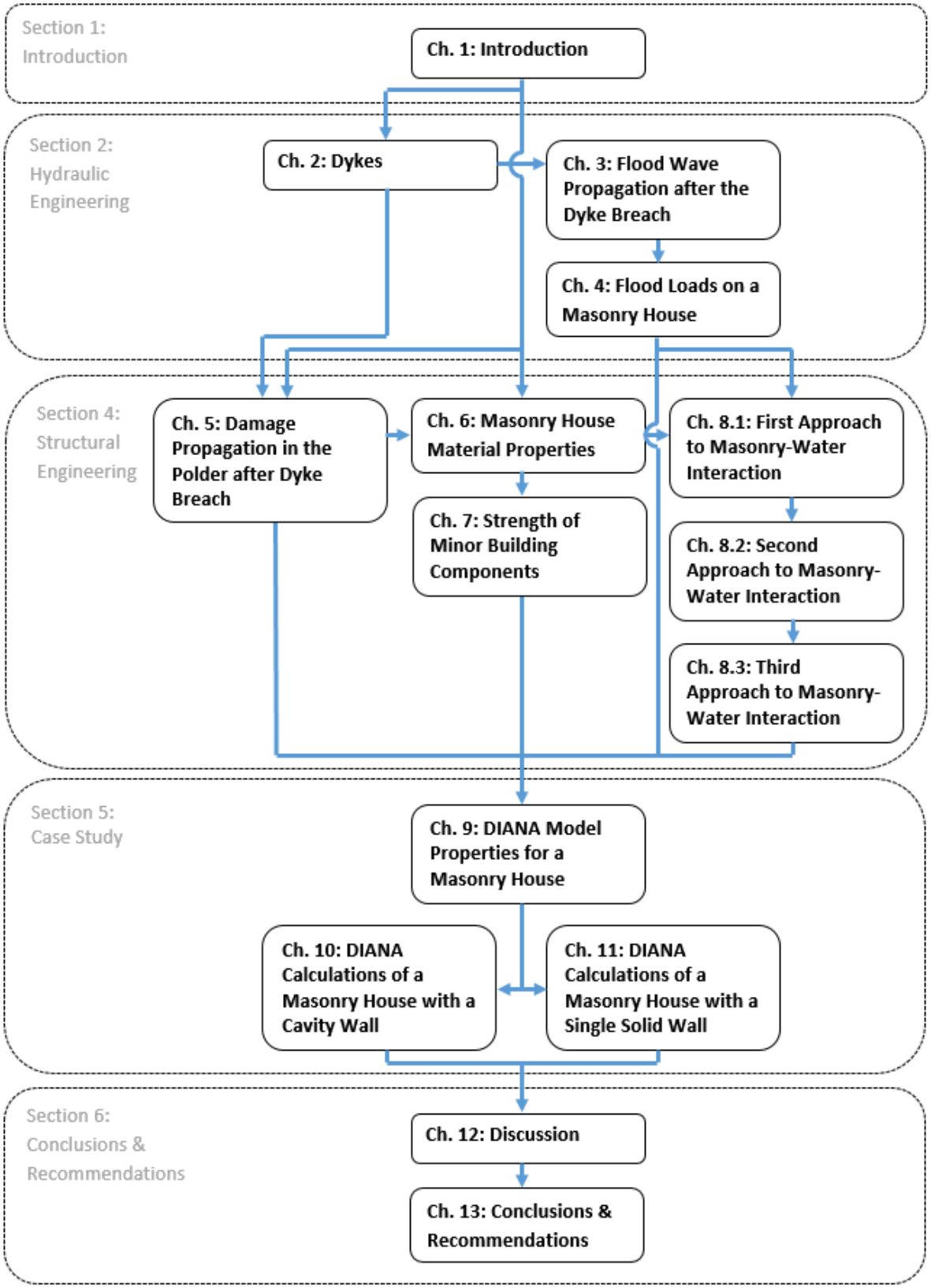


Figure 3 - Structure of the Report

# 2 Dykes[10]

In the Netherlands, an encircled area of land, such as a polder, is protected by a so-called dyke-ring. This dyke-ring is a flood defence which can consist of several types of structures. The four main types are dunes, soils structures (which includes dykes), water retaining structures (cofferdam, retaining wall, sheet piling, etc.) and water retaining hydraulic structures (locks, sluices, tidal flood barriers etc.). This dyke ring is the primary flood defence and, in the Netherlands, usually these consists mostly of dykes. Besides the primary flood defence, the area is also subdivided into smaller sections using secondary defences. Therefore, if a part of the primary flood defence fails, only a small section of the entire dyke-ring will flood, thus containing the damage. These secondary flood defences are often roads built on a smaller dyke.

The focus of this chapter will be on the primary river dyke. In order to give a proper estimation of the flood parameters, failure of this dyke needs to be examined. This is done by first examining the structural design of Dutch river dykes, followed by the failure mechanisms of those dykes.

## 2.1 Structural Design

The structural design follows from the requirements such as the water-retaining height, allowed overtopping and stability of the slopes as well as the local conditions such as the presence of historical dykes and a foreland. Any longitudinal variations or connections to other structures are assumed not to be of significant influence. The focus will therefore be on the composition of the cross-section.

### 2.1.1 Cross-section of the Dyke

The cross-section of a dyke consists of an area of influence which should be considered on both the inner and outer sides of the dyke. The boundaries of this influence area mostly depend on the type of dyke. They should be chosen in such a way that direct danger of failure or collapse of (part of) the dyke will not occur due to changes in external conditions, for example the construction of houses behind the dyke, see Figure 4.

[10] Weijers et al. [25]

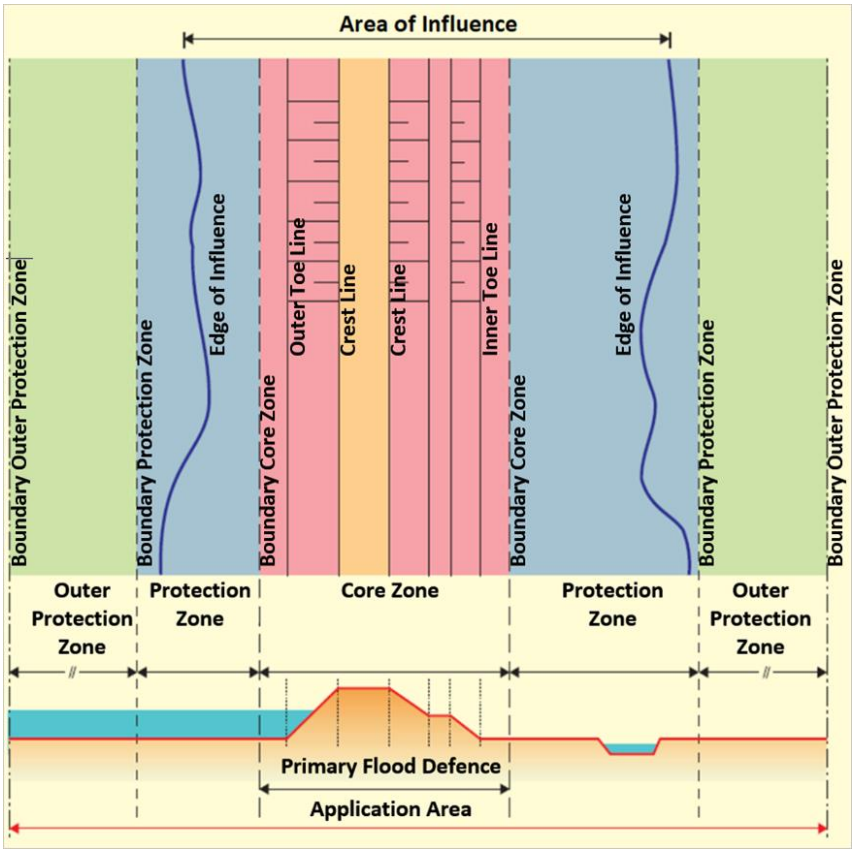


Figure 4 – Area of Influence of a dyke[11]

As can be seen in Figure 5, a dyke consists of many elements within the previously mentioned influence area. The function and presence of the elements depends on the type of dyke. Every dyke however has a base, core, inner and outer slope. It is not uncommon for a riverine flood wave to last a week. This means that a river dyke has to deal with a long period of high water. Therefore, the design focus is mainly on the inner side to protect against piping and improve the inward macro and micro stability.

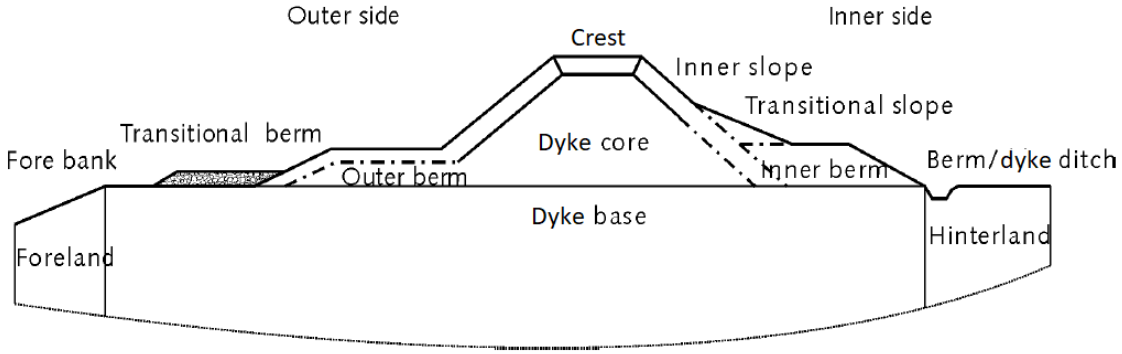


Figure 5 - Transverse profile of a dyke without special elements[12]

[11] Weijers et al. [25]
[12] Weijers et al. [25]

### 2.1.2 Dyke Crest

The dyke crest is essentially the highest part of the dyke and its level is determined by the required water-retaining height. This includes local increases of the water level and wave overtopping. The dyke crest level also depends on the soil properties as well as the geometry of the slopes. Furthermore, soil settlements of the dyke are taken into account. Dykes therefore often, if not always, have a building height higher than the design height.

Besides the settlement of the dyke itself, the soil on which the dyke is built, the subsoil, will most likely also subside due to the extra weight of the dyke. Some other reasons for a reduction in the soil level can be extraction of gas or oil and oxidation of organic components, for example in peat. Also, (ground)water extraction, to adapt to a certain polder level, can cause settlements of the soil. These are also taken into account in the building height of the dyke as much as possible.

To ensures that the final dyke crest is equal to the design height, settlements are calculated and monitored during the dyke's construction. For the designed lifetime of 50 years in the Netherlands, these settlement predictions are updated every five years on the basis of measurements. If necessary, the settlements will be countered by an extra increase of the crest height. These settlements are, of course, also dependent on the secondary function of the dyke crest. Some dykes are grazed by sheep and other animals, some support roads or have trees and other plants growing on them.

### 2.1.3 Dyke Core

The core of the dyke is the load bearing element on which various other elements are placed. The first requirement is for it to be stable under both external loading and the other dyke elements. Again, the soil properties are used to calculate the dimensions. The sensitivity to settling flow needs to be taken into account when determining the construction method as well as the soil types.

To protect against lateral displacements, the shear strength with the substratum due to the weight of the dyke core needs to be sufficiently high.

### 2.1.4 Inner Slopes, Outer Slopes and Berms

Slopes and berms are of great influence on the stability of a dyke. Overall the gentler the slope and/or the wider the berm, the greater the stability.

Normally the outer slope's design is mostly related to wave loading and overtopping. For river dykes however, waves are not as significant as for coastal dykes although wave overtopping can still initiate damage. The main design points remaining for river dykes are the angle of the slope and the berm width. During construction there might be temporary increases in water pressure, a wider berm then gives more stability than a gentler slope. The outer berm also improves the macro stability of the outer slope as well as the resistance against piping by increasing the length of the seepage line.

The design of the inner slope is related to overtopping water, which can lead to micro and macro instabilities. This can be mitigated by decreasing the permeability of the outer layer, for example by adding a clay layer, and increasing the permeability of the core. Furthermore, during very high water levels, lateral stability can become a problem. To prevent this a transitional slope can be used, see Figure 5. The stability of the inner slope can be increased using an inner berm. This berm, just like the outer berm helps the increase resistance against piping.

### 2.1.5 Subsoil

With the construction of a dyke on the subsoil, this subsoil becomes (a part of) the foundation of the dyke. This means that the subsoil must not only support the weight of the dyke, but also its position and stability when retaining water. To get an accurate view of the subsoil, the various layers should be investigated to assess their characteristics.

The first consideration regarding the substratum is soil settlements due to the weight of the dyke on top. This is governed by the weak Holocene covering layers. Second is the macro stability of the core, slopes and berms which is mainly influenced by the properties of the weak subsoil layers. These weak layers usually do increase in strength when loaded from above, however this takes time. In the meantime, the load is carried by the pore water which is a major concern for stability, especially during construction. Vertical drainage can be used to increase this stability as well as reduce residual settling. Third, since the substratum is part of the structure it means that with high water levels there is a hydraulic gradient over the dyke base. If there is a sand aquifer in the subsoil, the ground water flow can cause erosion, piping and heave of a covering layer in the hinterland. Finally, failure mechanisms as a result of variations in the substratum can greatly threaten the water retaining capabilities of a dyke.

## 2.2 Dyke Failure Mechanisms

The way a dyke fails determines what kind of flood wave will occur in the land behind the dyke. Therefore, it is important to determine what failure mechanism occurs when and what kind of flood wave they will cause. In Figure 6 an overview of the most prominent failure mechanisms for dykes are given.

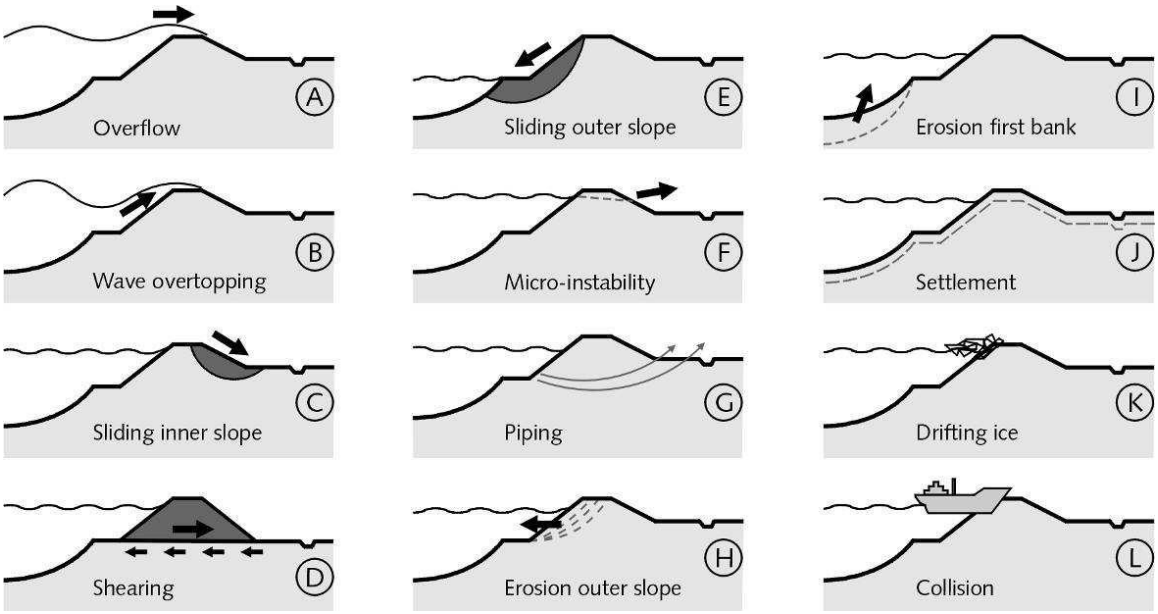


**Figure 6 - Failure mechanisms of a dyke[13]**

A. The most obvious failure is overflowing of the dyke when it is simply not high enough. However, this does not necessarily need to be catastrophic, depending on the amount of

[13] Weijers et al. [25]

overflowing water, the capacity of the hinterland to store water and the resistance of the inner slope to erosion.

B. Related to normal overflow is wave overtopping. Due to the small wave height in rivers the significance is limited since the overflow amount is also limited, however wave overtopping can still initiate damage.
C. Sliding of the inner slope however can be a more dangerous failure mechanism for river dykes due to the saturation of the dyke under a high water wave of multiple days or even weeks. Although it is possible for this mechanism to occur while the dyke still remains capable of retaining the water.
D. Shearing or horizontal sliding of the dyke body is potentially the most dangerous failure mechanism since it will create an immediate gap equal to the retaining height of the dyke.
E. This failure mechanism is more likely to occur after a high water wave which saturated a dyke body. The rapid decrease of the water level cannot be followed by the water inside the dyke, causing the dyke to slide towards to water. Although this can cause severe damage to a dyke it will only cause major problems if a second high water wave will follow shortly after.
F. Micro instability is when seepage water reaches the inner slope of a dyke and causes smaller particles, hence the name ‘micro’ to erode due to the water pressure from inside. Often the damage is minor, however if the build-up pressure is high enough it threatens the integrity of the entire structure.
G. Similar to micro instability is piping, but now the erosion happens underneath a cohesive layer of the subsoil. With a sufficient gradient, soil particles will erode and a ‘pipe’ will be formed underneath the dyke. The gradient is dependent on the type of subsoil.
H. Outer slope erosion can be the start of the failure of a dyke. To prevent this usually some kind of protective top layer is placed depending on the load. Since the load is rather low for river dykes, this cover is usually just grass.
I. Erosion of the first bank can occur if there is a steep underwater slope. If the saturated soil for some reason is moving into a denser state, the water pressure in the soil can rise quickly. If this pressure is not relieved within time the soil will change into a so-called settlement flow, a thick sandy subsoil fluid in this case. Although erosion of the first bank itself will not lead to failure of the dyke it can kick-start the instability of the outer slope of the dyke.
J. Settlement of the dyke is mostly a long-term phenomenon, the fast-acting settlements will be dealt with during the design phase. These long-term settlements, for example creep, can be monitored with maintenance programs and will therefore usually not lead to any problems for river dykes in the Netherlands.
K. Although drifting ice was a major problem historically seen, it has not caused a problem for the Dutch river dykes for over 100 years. Although this does not give any guarantees, ice is not seen as a major problem anymore.
L. Vessel collision is potentially a very big problem. However, shipping is prohibited on Dutch rivers when the highest water levels of a flood wave occur. A collision is therefore very unlikely.

## 2.3 Breach Propagation

Breach propagation follows several generic stages from stable, no breach initiation, to breach formation[14].

- Stage 1:
  The dyke is stable, no breach initiation yet.
- Stage 2:
  Start of the breach initiation in the form of seepage through or over the dyke.
- Stage 3:
  Progression of the breach initiation through the ongoing removal of soil and/or increased loading. The flow is usually still small with a very slow rate of change.
- Stage 4:
  Transition of breach formation, a critical stage where the upstream face of the dyke is reached starting rapid and often irreversible breach growth.
- Stage 5:
  Breach formation, ongoing erosion of the dyke in vertical and lateral direction with the vertical erosion being rapid. Rapid increase in discharge due to the lowering of the controlling crest level of the dyke.
- Stage 6:
  Breach expansion, the widening and deepening of the breach as a result of the increased discharge. Eventually the breach become somewhat stable after the water levels on both sides are about equal stopping discharge through the breach.

Whether or not these stages occur during the failure of a certain dyke depends on the loading conditions and the type of dyke. A properly designed dyke with a sand core and clay top will follow these stages, a peat dyke however might fail suddenly under shear. An example of such a sudden failure is the breach at Wilnis in 2003.

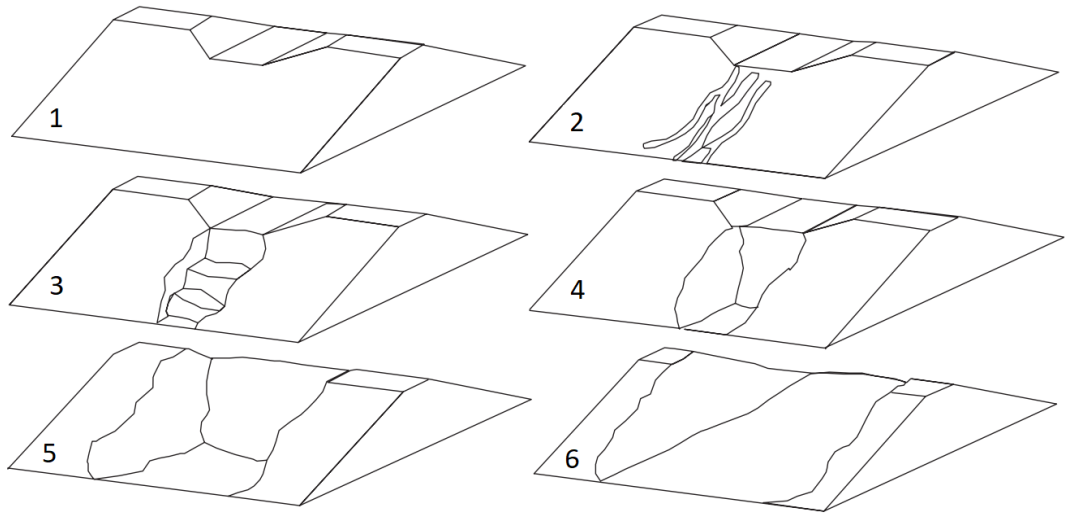


Figure 7 - Breaching stages[15]

[14] Morris [24]
[15] Zhu [26]

## 2.4 Conclusions

- For river dykes there are several important failure mechanisms. These are overflow, sliding of the inner slope, shearing, micro instability and piping. Especially shearing and sliding of the inner slope can cause rapid breaches and large flood waves.
- Breaches usually follow several generic stages, these can however vary depending on the failure type of the dyke. This is influenced by the composition of the dyke itself. A peat dyke, for example, will fail differently than a properly designed sand dyke.
- The highest hydraulic load possible for a river dyke follows from a sudden and entire collapse of that dyke, creating a gap (almost) equal to the height of the dyke. Although this is very unlikely for a normal sand dyke, which compose all major dykes in the Netherlands, it could occur for a peat dyke or other types of flood defences. An example of a peat dyke failing suddenly, is the breach at Wilnis in 2003 and an example of a flood defence failing suddenly is the breach at the Lower Ninth Ward in New Orleans. Since this will provide the highest loading, the assumption is made that this sudden failure of the dyke happens and creates a breach with a width of 30 m with the bottom of the breach at 1.00 NAP.

# 3 Flood Wave Propagation after the Dyke Breach

In this chapter the propagation of the flood water will be determined. The assumption of the previous chapter regarding the sudden collapse of the dyke and the location data mentioned in the introduction is used to make this determination. In Figure 8 an overview is provided of the flood wave during and after the dyke breach, with the last image being the completely flooded polder. The first schematisation is based on the 'long crested weir equations', the second approximation is done using the method of characteristics and a third approximations is based on a numerical model. Keep in mind that the determinations in this chapter are to determine the first wave of water, not the somewhat stable situation that occurs after a while.

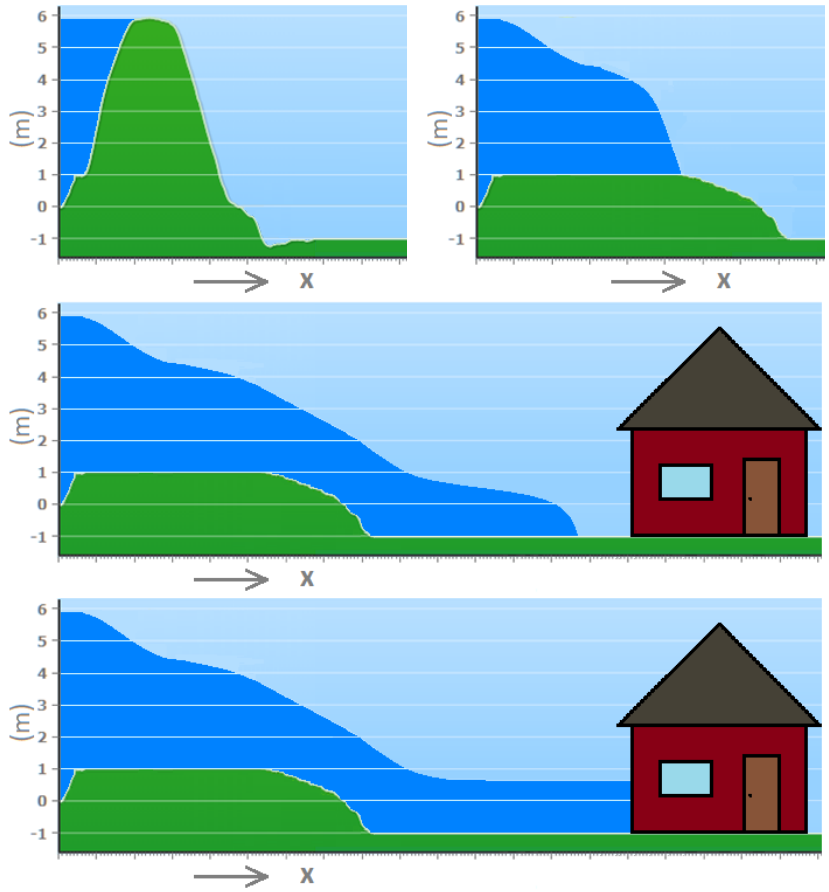


Figure 8 - Overview of the flood wave during and after breaching

## 3.1 Schematisation of the Breach

In order to determine the velocity and water level shortly after the breach, relations between the velocity and water level before and at the breach are required. To define these, the assumed dimensions of the breach are also required. The breach is therefore schematized as a rectangle with an area equal to the cross-sectional area of the breach, Figure 9. The width of the breach, $B_2$, takes into account the streamlines and represents the actual flow width. In Figure 11 and Figure 13 the locations are provided with a number, (1) before the breach, (2) at the breach and (4) 50 m after the breach. The breach is at the centre of the dyke. Furthermore, two assumptions are made. The first being that the water level, $d_1$, will reach until the dyke crest. The second assumption is that the sill height, a, see Figure 13, is equal to the remaining height of the unprotected outer toe of the dyke. This is at 1.00 NAP, see Figure 10. Usually the height of a, is determined by the toe of the dyke, since the outer protection has not (yet) been removed by the flood water and acts as the edge of the long crested weir. At the chosen location such a protection is not present.

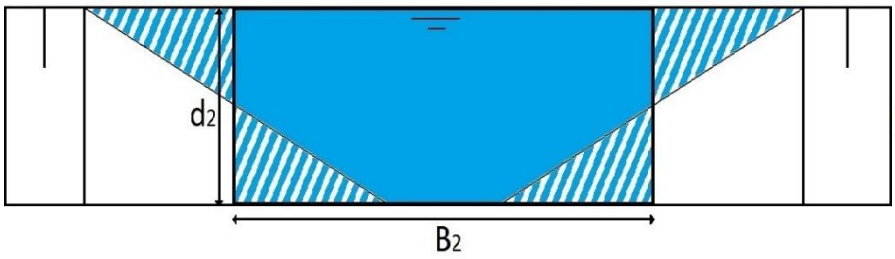


Figure 9 - Approximation of an actual breach schematized as a rectangle

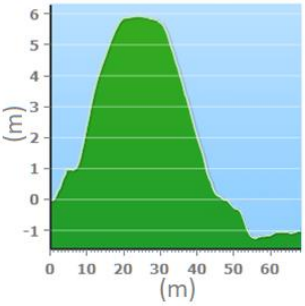


Figure 10 - Cross-section dyke[16] (distorted scale)

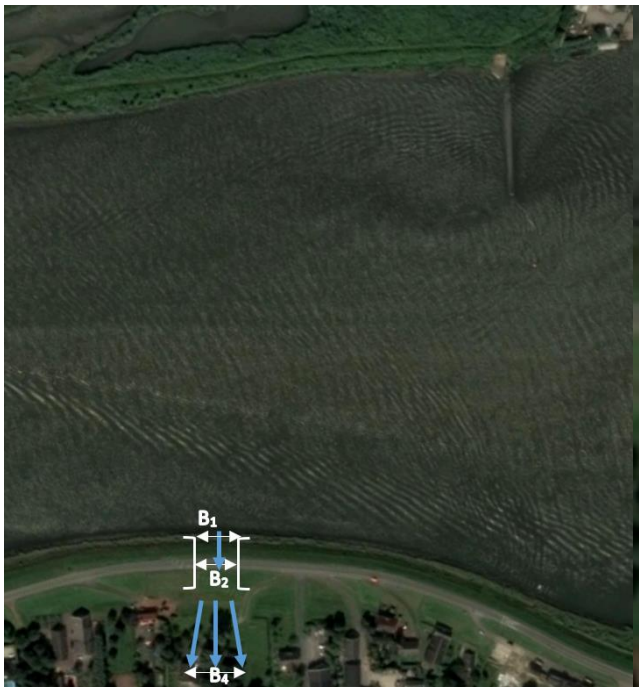


Figure 11 - Top view river and dyke including the breach location

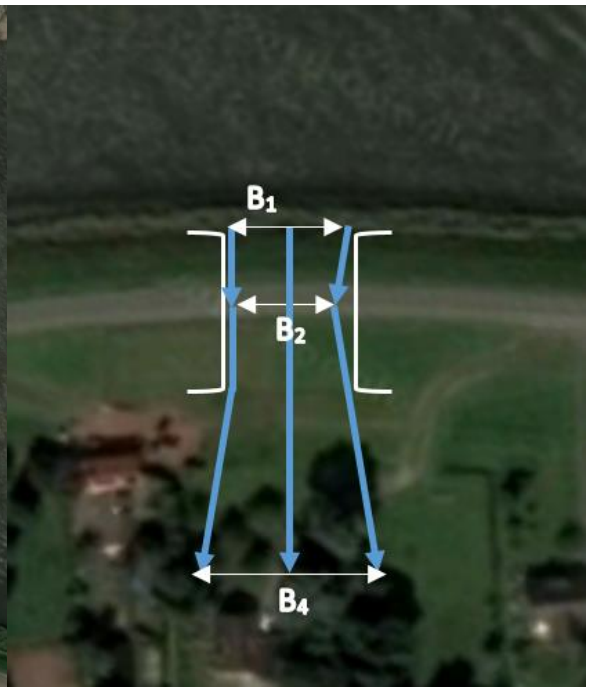


Figure 12 - Top view of the breach, enlarged

## 3.2 Long Crested Weir Approximation

With the information from the previous paragraph it is now possible to calculate the 3D situation using the so-called '2D long crested weir equations'. The make it possible to calculate the velocity and water level at and after the breach.

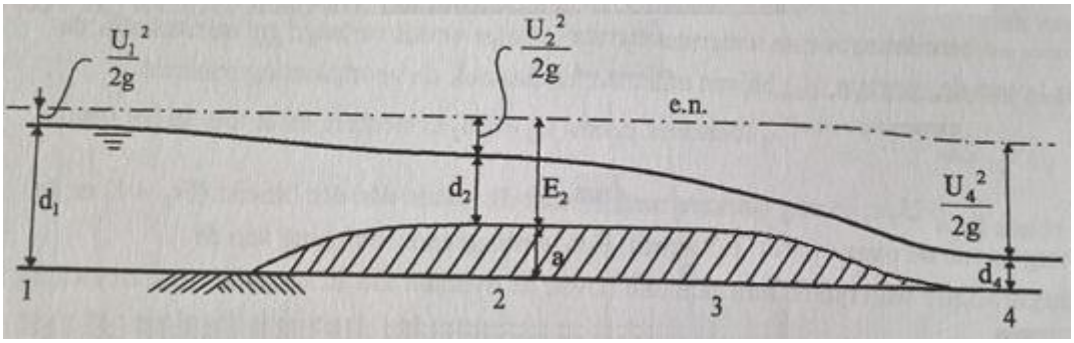


Figure 13 – Long crested weir (Based on[17])

As noted before several relations are required to determine all the variables needed. These are, for all locations, the preservation of volume:

$$Q_1 = Q_2 = Q_4 \rightarrow U_1 d_1 B_1 = U_2 d_2 B_2 = U_4 d_4 B_4$$

From location one to location two, the preservation of energy:

$$H_1 = H_2 = \left(\frac{1}{2}\frac{{U_1}^2}{g} + h_1\right) * B_1 = \left(\frac{1}{2}\frac{{U_2}^2}{g} + h_2\right) * B_2$$

With $h_2 = a + d_2$.

And from location 2 to location 4, the preservation of impulse:

$$I_2 = I_4 = \left(\frac{1}{2}\rho g(a + d_2)^2 + \rho {U_2}^2 d_2\right) * B_2 = \left(\frac{1}{2}\rho g {d_4}^2 + \rho {U_4}^2 d_4\right) * B_4$$

In which:

| | | |
|---|---|---|
| $Q_i$ | is the discharge at location i | ($m^3$) |
| $U_i$ | is the flow velocity at location i | (m/s) |
| $d_i$ | is the water depth at location i | (m) |
| $B_i$ | is the flow width at location i | (m) |
| $H_i$ | is the energy at location i | (m) |
| g | is the gravitational constant | ($m/s^2$) |
| $h_i$ | is the water level with respect to the reference plane | (m) |
| a | is the height of the crest | (m) |
| $I_i$ | is the impulse at location i | (N) |
| ρ | is the density of the water | ($kg/m^3$) |

For an elaborate derivation of these three relations, extended calculations and explanations, see Appendix A.

### 3.2.1 Baseline Weir

The widths are kept at a uniform length to obtain a baseline result, afterwards the actual width could be used to calculate the actual situation.

#### *3.2.1.1 Input*

There is a total of 12 variables, of which $\rho, g, a, d_1, B_1, B_2 \; and \; B_4$ are known. Assuming a critical flow over the weir[18], $d_2 = 2 * \frac{1}{2}\frac{{U_2}^2}{g} = \frac{{U_2}^2}{g}$, the last required variable is obtained to determine the four remaining variables, $u_1$, $u_2$, $u_4$ and $d_4$.

#### *3.2.1.2 Results*

The results for the 1 meter wide baseline weir are:

**Table 1 - Flow velocities and depth for the baseline weir**

| | | |
|---|---|---|
| $U_1$ | 3.032 | (m/s) |
| $U_2$ | 5.870 | (m/s) |
| $U_4$ | 3.196 | (m/s) |
| $d_4$ | 6.452 | (m) |

[16] AHN [43]
[17] Battjes [27]
[18] Paul Visser

From the values of $d_4$ and $U_4$ it follows that a hydraulic jump has occurred. This is not the situation that is sought after for shortly after the breach, but the situation that occurs after the polder has almost completely flooded. The calculation using the actual widths is left aside since the above calculation did not provide a viable answer. Introducing the actual widths would not change that.

### 3.2.2 Submerged Baseline Weir

The above result is actually for a situation where there should not be critical flow at location two. Therefore a recalculation is done with a submerged weir setting to determine the water depth at location two. To do so, the flow is assumed to be half of the previous setting since the height difference has mostly disappeared, see Figure 14, therefore $U_1 = 1.5\ m/s$.

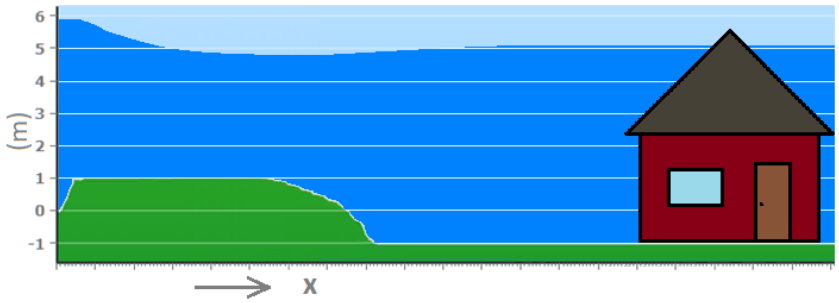


Figure 14 - Submerged Weir situation when the polder is almost fully flooded

#### *3.2.2.1 Results*

The results for this 1 meter wide submerged baseline weir are:

Table 2 - Flow velocities and depth for the submerged baseline weir

| | | |
|---|---|---|
| $U_2$ | 2.183 | (m/s) |
| $U_4$ | 1.505 | (m/s) |
| $d_2$ | 4.672 | (m) |
| $d_4$ | 6.777 | (m) |

## 3.3 Area Filling Approximation

Due to the unfortunate situation of the lack of a result from the weir equations that fits with the super critical flow situation that occurs immediately after the breach, the flow velocity and depth need to be determined in a different manner. To determine the flow velocity a method of filling an area is used. Simply said, an area behind the dyke is filled with the flood water until a certain height. Dividing the horizontally travelled distance with the time required to do this, provides the flow velocity. After determining the flow, only an approximation of the water depth is needed to determine the flow velocity.

### 3.3.1 Input

To determine the flow, the 'long crested weir' equations are used. Based on the assumption that there should be critical flow[19], we know that $d_2 = \frac{2}{3} * H_2 = \frac{2}{3} * H_1$. The initial velocity at location one at the moment of breaching, $U_1$ is set to 0, the water is still stationary. This means that $d_2 = \frac{2}{3} * 4.8 = 3.2\ m$ and $U_2 = \sqrt{d_2 * g} = 5.6\ m/s$ and $q = 17.93\ m^3/s$.

[19] Paul Visser

Next, an approximation of the width at location 2 and location 4, $B_2$ and $B_4$ respectively, is required. To determine this, the breach width of 30 meters is used, see paragraph 2.4. Using streamlines to reduce the width of the breach, $B_2$ is determined to be equal to $30 - 1 * \frac{45}{2} * \frac{1}{6} = 30 - 3.75 = 26.25$ m. The streamlines are only taken into account on one side due to the direction of the incoming flow. The flow, Q, is thus $17.93 * 26.25 = 470.7\ m^3/s$.

$B_4$ is rewritten as the breach width + x/3. This is based on the assumption that the width at location four will be equal to the width of the breach plus streamlines. These streamlines will have a ratio of 1:6, meaning for every 6 metres travelled from the breach the width on both sides will increase with 1 m. Therefore, with a distance of x metres behind the foot of the dyke this width increases by x/3.

### 3.3.2 Results

Considering that in actuality the water depth will have decreased after the flood wave enters the polder, a lower limit for the velocity follows from assuming that the water depth remains the same, 3.2 m. This provides the minimum flow velocities as in Table 3. For the location of the house, at a distance of 27.5 meters behind the dyke, this minimum flow velocity is 3.75 m/s.

**Table 3 - Flow velocity for a water depth of 3.2 m**

| Distance, x (m) | Minimum Flow Velocity (m/s) |
|---|---|
| 10 | 4.41 |
| 20 | 4.01 |
| 30 | 3.68 |
| 40 | 3.39 |
| 50 | 3.15 |

The numeric approximation in paragraph 3.5 provides a water depth of approximately 1.5 m at the location of the masonry house. When changing the water depth in the method used above to the numeric result of 1.5 m, the results of Table 4 are obtained. For the location of the house the flow velocity would then now be 8.01 m/s.

**Table 4 - Flow velocity for a water depth of 1.5 m**

| Distance, x (m) | Minimum Flow Velocity (m/s) |
|---|---|
| 10 | 9.41 |
| 20 | 8.56 |
| 30 | 7.84 |
| 40 | 7.24 |
| 50 | 6.72 |

## 3.4 Method of Characteristics Approximation[20]

The 'long crested weir' approximation did not provide the results as expected and the area filling approximation is a rough approximation, heavily based on the assumed water depth of the wave front. Therefore another approximation is used, the method of characteristics.

[20] Chanson [61]

The method of characteristics is used to solve systems of differential equations. This mathematical technique can be used on the Saint-Venant equations to determine the wave characteristics of a dyke breach wave. Expressed in terms of the water depth d, the continuity equation is:

$$\frac{\partial d}{\partial t}+\frac{A}{B}\frac{\partial u}{\partial x}+u\frac{\partial d}{\partial x}+\frac{u}{B}\left(\frac{\partial A}{\partial x}\right)_{d=constant}=0$$

In which:

| | | |
|---|---|---|
| d | is the water depth | (m) |
| t | is the time | (s) |
| A | is the flow area, B*d | ($m^2$) |
| B | is the flow width | (m) |
| u | is the flow velocity | (m/s) |
| x | is the distance in the flow direction | (m) |

The dynamic equation is:

$$\frac{\partial u}{\partial t}+u\frac{\partial u}{\partial x}+g\frac{\partial d}{\partial x}+g\left(S_f-S_0\right)=0$$

In which:

| | | |
|---|---|---|
| g | is the gravitational constant | ($m/s^2$) |
| $S_f$ | is the friction slope | (-) |
| $S_0$ | is the bed slope | (-) |

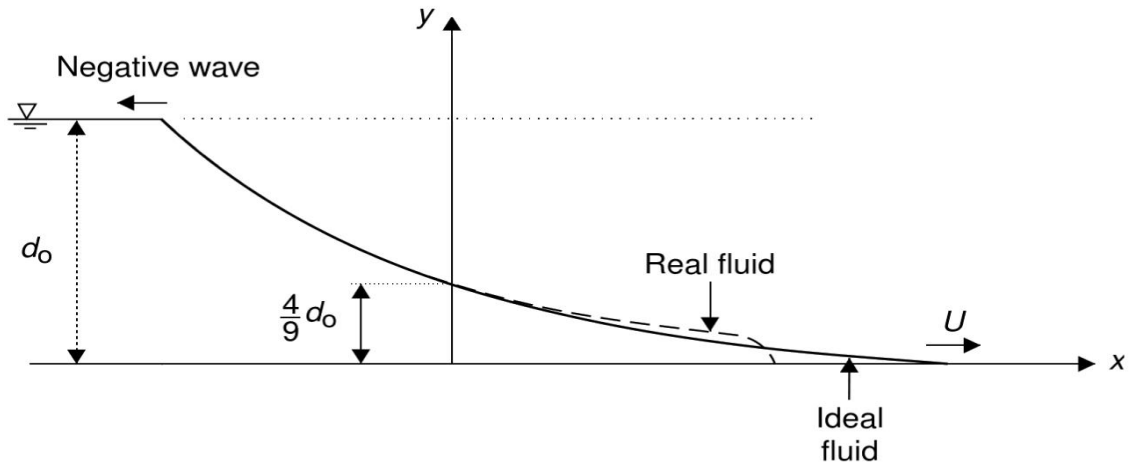


Figure 15 - Dyke Breach Wave on a dry horizontal bed (Based on [21])

The immediate dyke breach causes a negative wave to propagate upstream and a positive wave to propagate downstream, see Figure 15. The celerity of this wave is for an irregular channel equal to $c=\sqrt{g(\frac{A}{B})}$ in which A is the cross-section of the flow and B is the width of the free surface. For a dyke breach wave over a dry horizontal bed the positive wave travels with a speed of $u+2c$ and the negative wave travels with a speed of $u-2c$. In this u is the flow velocity.

The velocity of the wave front, v, of this dyke breach wave equals:

[21] Chanson [61]

$$v = 2c_0 = 2\sqrt{gd_0}$$

In which $c_0$ is the initial negative wave celerity and $d_0$ is the initial water depth.

Based on the parameters from 3.1 this would provide a velocity of:

$$v = 2\sqrt{9.81 * 4.8} = 13.7\ m/s$$

With the velocity of the wave front determined, the actual height of the wave needs to be determined as well. This can be done using the inverse slope of a backward characteristic of the wave front. Since the initial backward characteristic is a straight line, the inverse slope is a constant:

$$\frac{dx}{dt} = u - c = 2c_0 - 3c$$

Integration gives the profile of the water surface for a certain time, thus t is constant. This provides the free surface profile between the negative wave front and the wave front:

$$\frac{x}{t} = 2\sqrt{gd_0} - 3\sqrt{gd} \qquad \text{for } -\sqrt{gd_0} \leq \frac{x}{t} \leq 2\sqrt{gd_0}$$

However, this cannot be used to accurately determine the depth of the wave front, since it is implicitly assumed to be 0, see Figure 15.

## 3.5 Numerical Approximation

Although the method of characteristics was able to provide an approximation of the velocity of the wave front, it did not succeed in providing a depth of said wave front. Therefore a third, numerical, approximation is used. This numeric approximation is a courtesy of Svašek Hydraulics and calculated using Finel2D. This provided the following results:

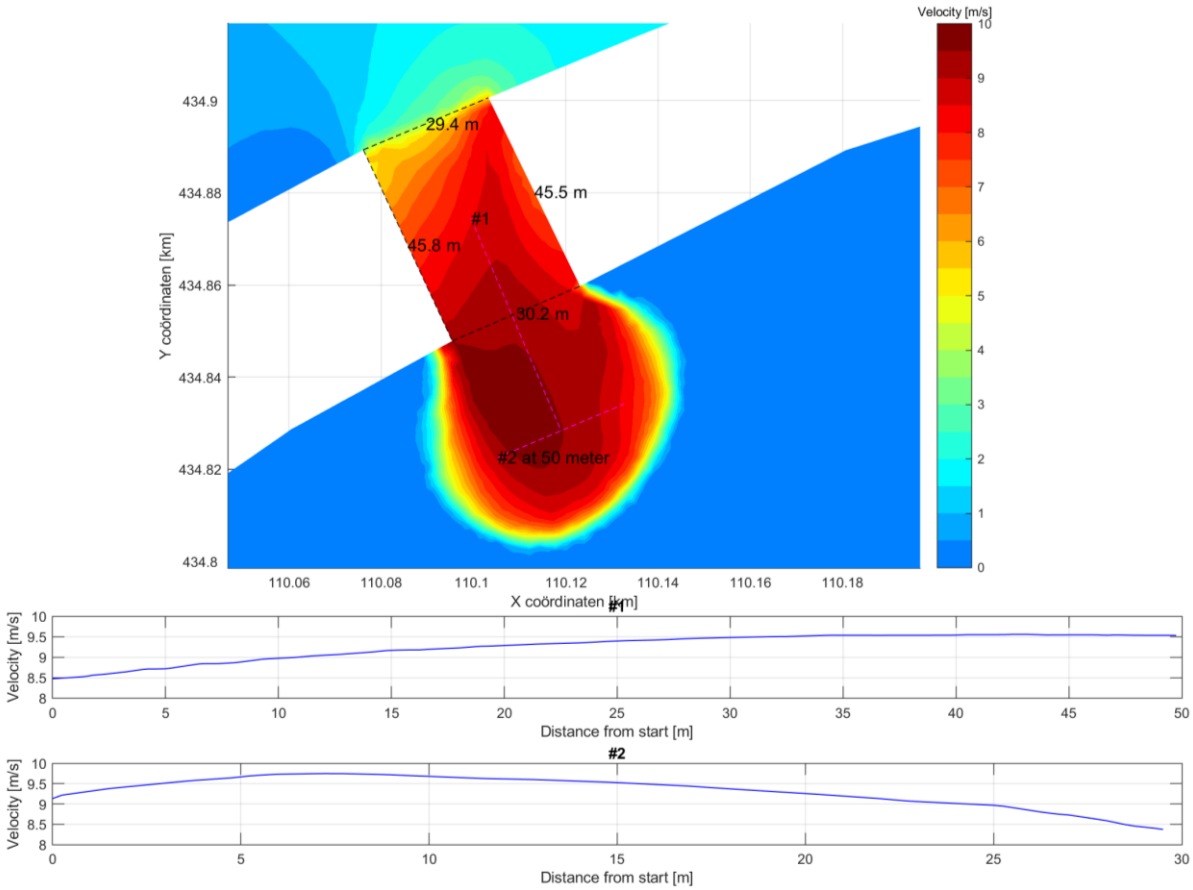


Figure 16 - Numerical approximation of the flow velocity near the breach[22]

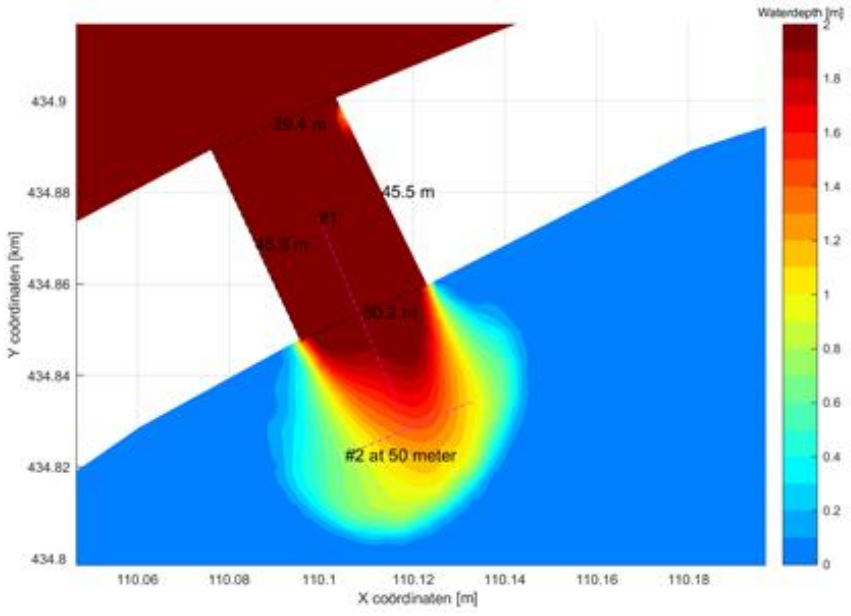


[22] Finel2D provided by Svašek Hydraulics

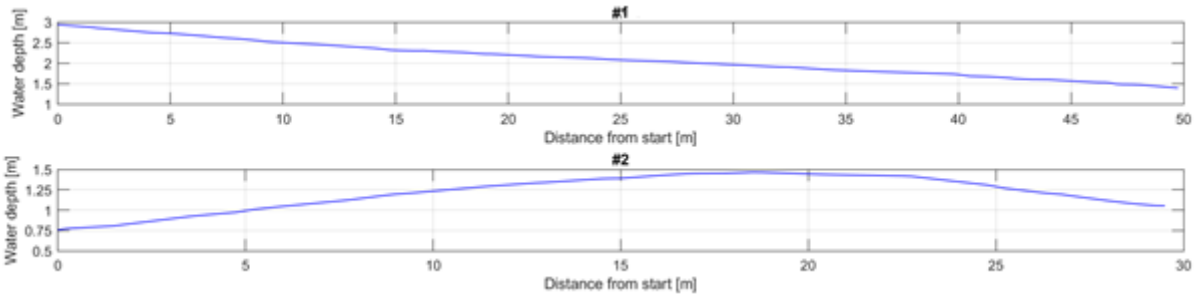


Figure 17 - Numerical approximation of the water depth near the breach, part 2[23]

The numerical approximation predicts a flow velocity of about 9.5 m/s and a water depth of approximately 1.5 m at the location of the house, 50 meter behind the centre of the breach. Since this model has not been fully calibrated for the situation used in this thesis, this is a rough first approximation.

## 3.6 Conclusions

The result from the baseline weir do not match the expectations for the situation shortly after the breach. The result that did follow belonged to the situation in which the polder has almost been fully flooded. Since the assumption of critical flow at location two used to obtain this result is not valid in the new situation, a recalculation is done using a submerged weir and a decreased flow due to the decreased height difference.

Neither of those provided a somewhat accurate approximation of the water depth and flow velocity shortly after the breach. Therefore another approximation was done to obtain a minimum flow velocity combined with a maximum water depth of 3.2 meters. At the location of the masonry house, 27.5 meters behind the dyke, the minimum flow velocity would then be 3.75 m/s. When the water depth is changed to 1.5 m, similar to the result from the numeric approximation, the flow velocity at the masonry house is 8.01 m/s.

This results is, however, heavily based on the assumed water depth of the wave front. Therefore another approximation is done using the method of characteristics. Although unable to provide an accurate water depth of the wave front, an approximation of the velocity of the wave front can be obtained. This approximation is:

$$v = 2c_0 = 2\sqrt{gd_0} = 2\sqrt{9.81 * 4.8} = 13.7\ m/s$$

Finally also the results of a numeric approximation show a water depth of about 1.5 m at the location of the breach combined with a flow velocity of around 9.5 m/s.

Due to the differences in the results further research is necessary. Based on all these results, a water depth of 1.5 m and a flow velocity of 10 m/s is used to calculate the dynamic load in 9.2.2.

[23] Finel2D provided by Svašek Hydraulics

# 4 Flood Loads on a Masonry House

In order to determine the extent of the damage to a masonry house it is necessary to know the loads on this house. Since a riverine flood is chosen, only riverine flood loads are taken into account. Accordingly several loads are deemed not relevant, most importantly wave and wind, see Figure 18. The forces following from these loads are explained in more detail in the following sub-sections and shown in Figure 19, except the flow force.

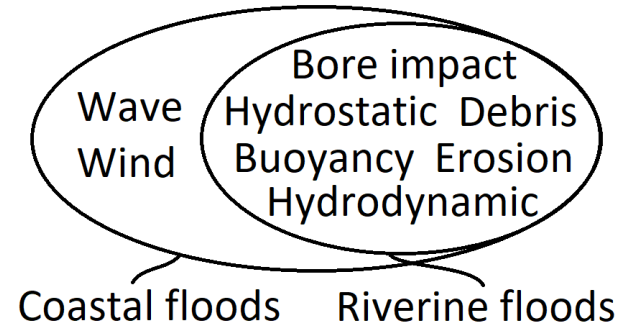


Figure 18 - Load types for coastal and riverine floods

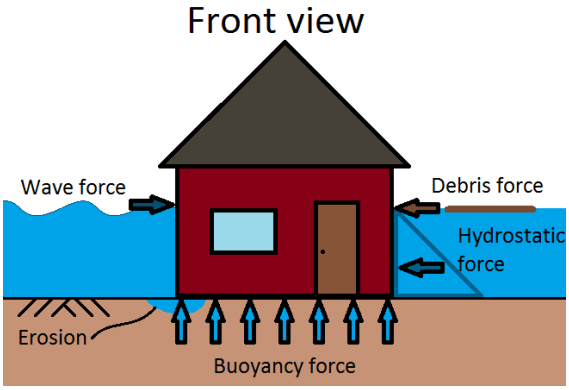


Figure 19 - Overview of the forces due to the flood water

There are also other factors which can cause damage, either directly or indirectly. Examples of these are the season in which the flood takes place, the duration of the flood and the flood type. With respect to direct structural damage their influence is however usually limited and they are therefore left outside the scope of this thesis with the exception of the flood type. Because the flood type is related to the timescale of the flood wave it is of major importance when schematising the flood wave as static, quasi-static or dynamic. This in turn also influences the flood loads. In the case of a dynamic schematisation the Eigen period of the masonry house also becomes a factor to take into account. In Figure 20 is an overview of different types of waves and their frequencies and periods.

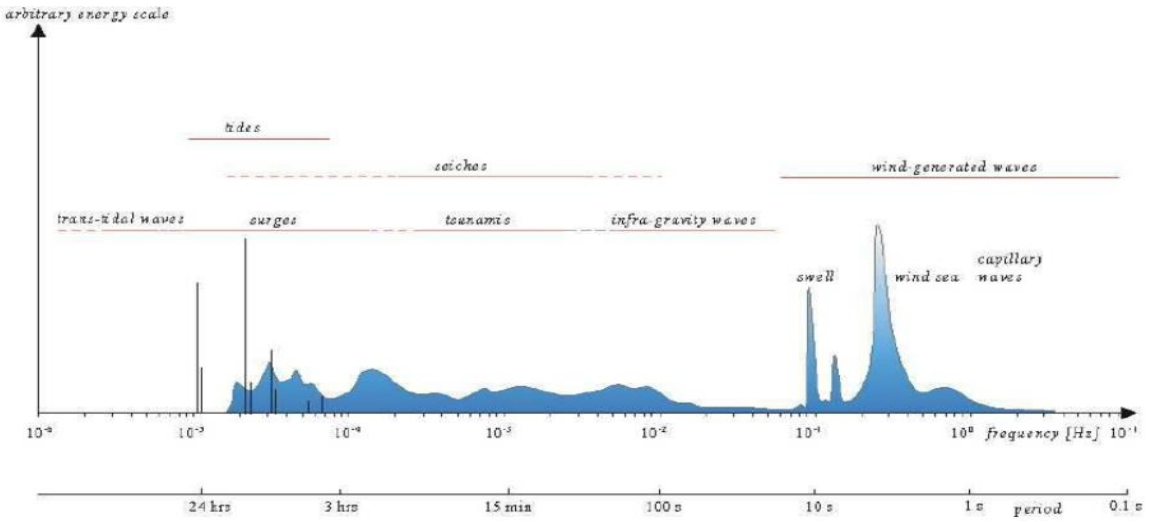


Figure 20 - Frequencies and periods of the vertical motions of the ocean surface[24]

[24] Holthuijsen [37]

## 4.1 Hydrostatic

The hydrostatic force, $F_{HS}$, is the static water pressure exerted against the house. Its main parameter is the inundation depth since the pressure is proportional to this depth. It is also related to the density of the water and the width of the house. Since it is a very well-known force, no derivation is provided. The formula for the hydrostatic force is:

$$F_{HS} = \frac{1}{2} * \rho * g * b * h^2$$

In which:

| | | |
|---|---|---|
| ρ | is the density of the water | (kg/m$^3$) |
| g | is the gravitational constant | (m/s$^2$) |
| b | is the width of the house | (m) |
| h | is the actual height of the water against the house | (m) |

## 4.2 Buoyancy

The buoyancy force, $F_B$, is the force exerted against the bottom surface of the house and it is closely related to the hydrostatic force. The buoyancy force is equal to the weight of the water displaced by the house. Again, this is a very well-known force and no derivation is provided. The formula for the buoyancy force is:

$$F_B = V * \rho * g$$

In which:

| | | |
|---|---|---|
| ρ | is the density of the water | (kg/m$^3$) |
| g | is the gravitational constant | (m/s$^2$) |
| V | is the volume of the submerged section of the house | (m$^3$) |

If there are no changes in the cross-section of the submerged area, the buoyancy formula can be simplified to:

$$F_B = A * \rho * g * h$$

Where A is the surface area of the submerged cross-section in m$^2$ and h is the actual height of the water against the house.

## 4.3 Flow Forces

The total flow force actually consists of three separate forces. Firstly the front force, which is the force of the water pushing against the front of the house. Secondly the friction or drag force, which is the force caused by the friction between the water flowing past the sides of the house and the house itself. And thirdly the suction force, which is the force of the water 'pulling' at the back of the house. This combined flow force occurs after the tip of the flood wave has passed the house and a more or less stable flow around the house has been established. The formula for the combination of these three forces, the flow force, $F_{Flow}$, is[25,26]:

$$F_{Flow} = \frac{1}{2} * C_D * \rho * b * h * u^2$$

[25] Nistor et al. [5]
[26] ASCE [8]

In which:

| | | |
|---|---|---|
| $C_D$ | is the drag coefficient (see Table 5) | - |
| ρ | is the density of the water | (kg/m$^3$) |
| b | is the width of the house | (m) |
| h | is the actual height of the water against the house | (m) |
| u | is the flow velocity | (m/s) |

Table 5 - Drag coefficient, $C_D$[27]

| Width-to-depth ratio (b/h) | Drag coefficient ($C_d$) |
|---|---|
| **1-12** | 1.25 |
| **13-20** | 1.3 |
| **21-32** | 1.4 |
| **33-40** | 1.5 |
| **41-80** | 1.75 |
| **81-120** | 1.8 |
| **>120** | 2.0 |

## 4.4 Long Waves and Translation Waves

### 4.4.1 Riverine Flood Waves and Coastal Tidal Waves

A riverine flood wave is caused by either rain or melting water and characterized by a relatively slow rise and fall of the water level over several days, for example with 0.5 m a day, see Figure 21. This makes them fairly predictable. Due to the variations in the water depth the front of the wave will move slightly slower than the back causing the front to become steeper compared to the back. The increased gradient causes a larger discharge during the rising period compared to the falling period. This effect is called hysteresis and is the reason why local measurements of the water depth not necessarily translate to reliable estimations of the discharge.

The increased gradient causes the flow velocity to also increase during the rising period, with several dm/s in a day. The magnitude of this increase is however very low, and almost solely due to the gradient. Inertia is therefore neglected and gravity is almost in balance with the friction terms[28].

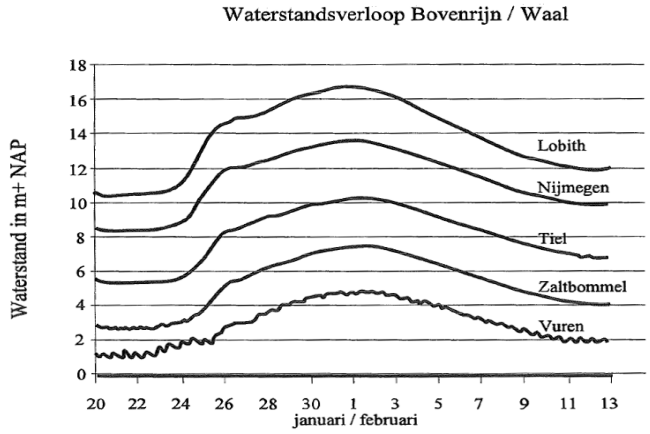


Figure 21 - Riverine flood wave, Netherlands spring 1995[29]

[27] FEMA P-55 [13]
[28] Battjes [38]
[29] Battjes [38]

A coastal tidal wave is, as the name suggests, based on the tide. The tide therefore determines the period which can be semi-diurnal, mixed or diurnal with respect to the moon-day cycle of 24 hours and 50 minutes. Most places on earth have a semi-diurnal tide. For a tidal wave at the ocean friction plays no role due to the large depths, however in coastal areas the friction and inertia are both of equal importance and therefore need to be taken into account. However, the pressure distributions remains approximately hydrostatic.

The depth of a river compared to a coastal area is relatively small. Furthermore the period of a riverine flood wave is usually significantly longer than a coastal tidal wave, both however have a long period for waves. For a coastal tidal wave a hydrostatic approximation is already valid, for a riverine flood a hydrostatic approximation is unquestionably an accurate approximation.

### 4.4.2 Long Wave and Translation Wave Theory[30]

Long wave theory, also known as the De Saint-Venant equations, is a set of equations to determine two unknowns, the water depth and the discharge, for waves which have a much larger wave length than the water depth. Depending on the situation certain parts of these equation might be neglected.

$$B\frac{\partial d}{\partial t}+\frac{\partial Q}{\partial x}=0$$
$$\frac{\partial Q}{\partial t}+\frac{\partial}{\partial x}\left(\frac{Q^2}{A_s}\right)+gA_s\frac{\partial d}{\partial x}+c_f\frac{|Q|Q}{A_sR}=0$$

In which:

| | | |
|---|---|---|
| B | is the flow width | (m) |
| d | is the inundation depth | (m) |
| t | is the time | (s) |
| Q | is the discharge | ($m^3/s$) |
| x | is the distance in the flow direction | (m) |
| $A_s$ | is the flow area | ($m^2$) |
| g | is the gravitational constant | ($m/s^2$) |
| $c_f$ | is the coefficient of friction | (-) |
| R | is the hydraulic diameter | (m) |

Since both tidal and riverine waves have a wave length which is much greater than the water depth long wave theory is applicable. This was already clear due to the approximately hydrostatic pressure distribution for both waves which is a prerequisite for the long wave theory. An easy way to estimate if a wave fits with the long wave theory is to check the following:

$$\frac{\omega^2 d}{g}\ll 1$$

In which $\omega$ is the wave period, d the water depth and g the gravitational constant.

For riverine flood waves, the inertia term can be neglected as stated before. For coastal waves, however, inertia and friction have an approximately equal importance depending on the exact coastal situation.

[30] Battjes [38]

Translation wave theory refers to more or less pulse-shaped waves instead of oscillating waves. In principle, translation waves have a wave speed sufficiently high such that no effects of local friction may be assumed. If the height of the translation wave can be neglected the advective term can be neglected as well.

A principle related to high translation waves is that the deeper part of the wave moves faster than the shallower part since the wave celerity is dependent on the water depth. This means for a translation wave that moves faster than the flow velocity, the front of the wave becomes ever steeper. This is seen in both riverine flood waves as well as in coastal tidal waves. If the front gets steep enough the wave can turn into a bore. This happens in certain rivers as well as during dyke breaches, see 4.6.

## 4.5 Short Waves

The opposite of the long wave is the short wave. The difference between the two is in the wavelength and period. Where a long wave has a period of several minutes up to several hours, the short wave has a period which remains in the seconds. Furthermore the wavelength follows the same pattern, relatively long for long waves and short for short waves, see also Figure 20.

Another distinct difference is the generation of the waves, short waves are generally caused by wind. This means that the magnitude of the short wave is dependent on the wind characteristics. These are the wind direction, wind speed, fetch length and duration. In the situation of a dyke breach short waves can occur after the water level stabilizes. Fetch lengths will however mostly be very small. Therefore, only relatively small short waves are expected to occur.

Short waves can be described by summing a large number of independent harmonic waves. These harmonic waves can be understood through linear (Airy) wave theory which describes these waves thoroughly. The main requirement for this theory is that the amplitude of the wave is small relative to the wave length and water depth. The theory uses two equations, the continuity equation derived from the mass balance equation and the momentum balance equation. To solve these equations the velocity potential equation is used which provides all the kinematic aspects without considering any dynamic aspects. The consequence of this is that both free and forced (wind) waves can be described with this theory[31]. See Figure 22 for a summary of the results of the linear (Airy) wave theory in shallow, transitional and deep water.

[31] Holthuijsen [37]

| Relative depth Characteristics | Shallow Water $\frac{h}{L}<\frac{1}{20}$ | Transitional water depth $\frac{1}{20}<\frac{h}{L}<\frac{1}{2}$ |
|---|---|---|
| Wave Celerity | $c=\frac{L}{T}=\sqrt{g\,h}$ | $c=\frac{L}{T}=\frac{gT}{2\pi}\tanh kh$ |
| Wave Length | $L=T\sqrt{g\,h}$ | $L=\frac{gT^2}{2\pi}\tanh kh$ |
| Group Velocity | $c_g=c=\sqrt{g\,h}$ | $c_g=nc=\frac{1}{2}\left[1+\frac{2kh}{\sinh 2kh}\right]\cdot c$ |
| Energy Flux (per m width) | $F=Ec_g=\frac{1}{2}\rho g a^2\sqrt{g\,h}$ | $F=Ec_g=\frac{1}{2}\rho g a^2 nc$ |
| Particle velocity | | |
| Horizontal | $u=a\sqrt{\frac{g}{h}}\sin\theta$ | $u=\omega a\frac{\cosh k(h+z)}{\sinh kh}\sin\theta$ |
| Vertical | $w=\omega a\left(1+\frac{z}{h}\right)\cos\theta$ | $w=\omega a\frac{\sinh k(h+z)}{\sinh kh}\cos\theta$ |
| Particle displacement | | |
| Horizontal | $\xi=-\frac{a}{\omega}\sqrt{\frac{g}{h}}\cos\theta$ | $\xi=-a\frac{\cosh k(h+z)}{\sinh kh}\cos\theta$ |
| Vertical | | $\zeta=a\frac{\sinh k(h+z)}{\sinh kh}\sin\theta$ |
| Subsurface pressure | $p=-\rho g z+\rho g a\sin\theta$ | $p=-\rho g z+\rho g a\frac{\cosh k(h+z)}{\cosh kh}\sin\theta$ |
| $a=\frac{H}{2}$ $\omega=\frac{2\pi}{T}$ $k=\frac{2\pi}{L}$ $\theta=\omega t-kx$ | | |

Figure 22 - Summary of linear (Airy) wave theory[32]

### 4.5.1 Breaking Wave

A wave where the front becomes too steep will break. This will mostly happen to short waves as they tend to have higher gradients. The force and pressure distribution of the breaking wave differs in both time and space and can therefore be split into two parts, the distribution in time and the distribution in space. Both are discussed as pressure distributions which can be integrated to obtain the force distributions. The breaking wave is also very closely related to the Bore Impact discussed in 4.6.

#### *4.5.1.1 Breaking Wave Pressure Distribution in Time*

A wave impacting a vertical wall has a very distinct pressure distribution, the shape resembles a church roof, see Figure 24. At the moment of first impact there is a very high peak due to the hydrodynamic properties of the wave. This is followed by a longer lasting lower part, which is governed by gravity and is quasi-hydrostatic. The pressure peak from this pressure distribution is the starting point for the rest of this section.

[32] Molenaar et al. [42]

The pressure peak originates from when the front part of the advancing wave already reaches the wall, causing a rapid ascent of the water level at the wall. The ascent is so quick that the wave height reduces rapidly and the free surface moves as if going to a single point in 2D or a line when in 3D. At some moment during this process the water at the wall accelerates so fast that a vertical jet occurs. This quick acceleration requires large pressure gradients which explains the pressure peak. The smaller the area into which the water converges, the narrower and more violent the pressure peak will be. The surface roughness of the obstacle and wave are however factors which prevent the conversion into a small area. A completely smooth obstacle and wave would therefore theoretically give the highest peak pressure. Anything which increases the surface roughness causes a decrease of the pressure peak. Trapped air due to a wave breaking earlier also decreases the pressure peak since the air works somewhat like an airbag smearing out the force over a larger area.[34]

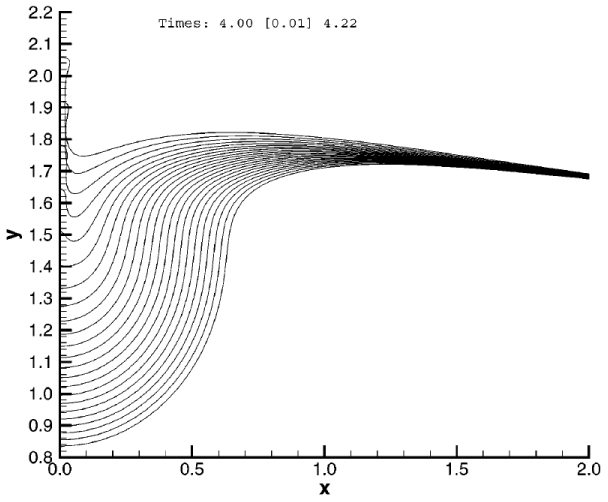


Figure 23 - Detail of wave profiles close to an obstacle. Successive profiles "focus" toward the point where a jet forms (space units are in terms of the initial depth at the wall)[33]

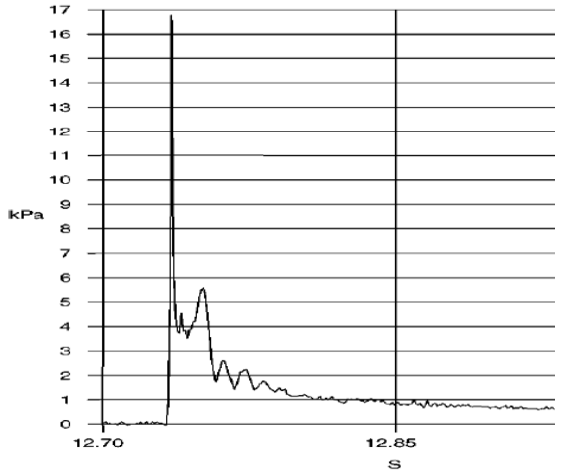


Figure 24 - Time history of the impact pressure of a single wave in a laboratory flume[35]

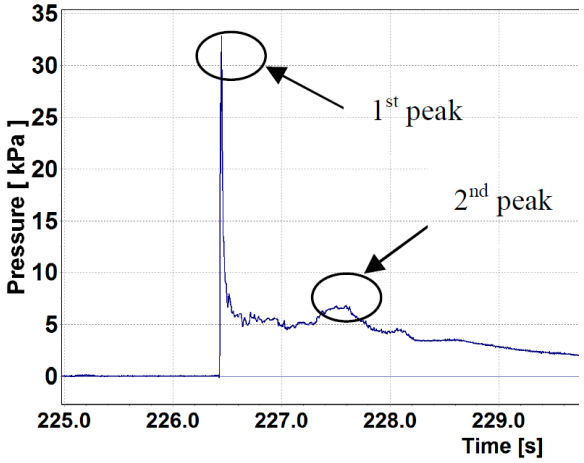


Figure 25 - Time history of the impact pressure of an overtopping bore[36]

### 4.5.1.2 *Breaking Wave Pressure Distribution in Space*

Besides the overall pressure distribution in time, the pressure also differs in space. Simply said, the pressure is not equally distributed over the height of the obstacle, see Figure 26. This can be of importance since knowing which parts receive the largest pressures also tells you which parts might

[33] Peregrine [29]
[34] Peregrine [29]
[35] Peregrine [29]
[36] Ramachandran et al. [32]

need extra attention. The extra attention can be, for example, in the form of protection, mitigation or strengthening of the obstacle.

As one might expect, this distribution in space is also influenced by certain factors. The main factor being the depth of the incoming water, the wave height and the wavelength.

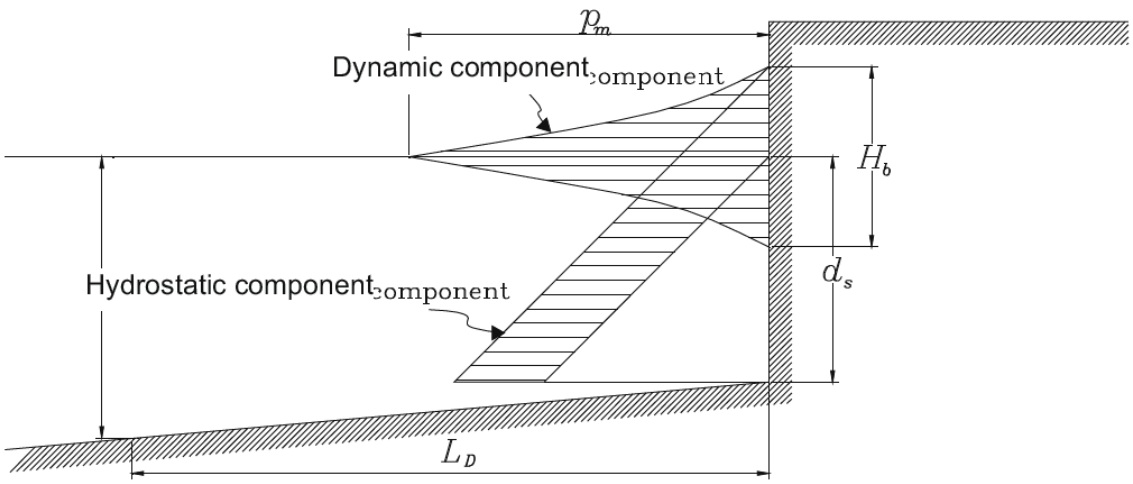


Figure 26 - Minikin: broken wave pressure distribution[37]

The maximum pressure, $P_{max}$, and resulting force, F, following this assumed distribution are as follows:[38]

$$P_{max} = \frac{1}{2} C_{mk} \pi \rho g \frac{H_b}{L_{H_L}} \frac{h}{H_L} (H_L + h)$$

$$F = \frac{P_{max} H_b}{3} + \frac{\rho g H_b}{2} \left( \frac{H_b}{4} + h \right)$$

In which:

| | | |
|---|---|---|
| $C_{mk}$ | is the coefficient of impact (≈2) | (-) |
| ρ | is the density of the water | (kg/m³) |
| g | is the gravitational constant | (m/s²) |
| $H_b$ | is the wave height | (m) |
| $L_{HL}$ | is the wavelength at depth $H_L$ | (m) |
| h | is the actual height of the water against the structure | (m) |
| $H_L$ | is the depth at one wavelength in front of the wall | (m) |

### 4.5.2 Standing Wave Force with Complete Reflection

Instead of breaking waves, standing waves could also collide with the house. After the area around the house is inundated the occurrence of these waves could lead to extra loads on the house. These will be the highest when there is complete reflection at the wall of the house and this wall is located at an antinode.

The force can then be calculated using linear theory for non-breaking waves:

$$F = 2\rho g a \left( \frac{e^{kd} - e^{-kd}}{2k \cosh(kd)} + a \right)$$

[37] Molenaar et al. [42]
[38] Molenaar et al. [42]

Assuming a wave with the following properties:

| | | | |
|---|---|---|---|
| ρ | is the density of the water | 1000 | (kg/m$^3$) |
| g | is the gravitational constant | 9.81 | (m/s$^2$) |
| a | is the wave amplitude (H/2) | 0.25 | (m) |
| k | is the wave number of the incoming wave | $\frac{2\pi}{L}$ | (1/m) |
| L | is the wavelength | 7.5 | (m) |
| d | is the inundation depth | 2 | (m) |

The resulting force will then be 4.9 kN/m.

### 4.5.3 Slenderness of the House

A structure can be seen as slender in relation to a wave when its width is much smaller than the inundation depth. The result will be that the sides of the structure will influence the pressure distribution of the front face of that structure. If this is not the case, i.e. the pressure distribution of the front of the structure is seemingly uniform, then the structure is not slender.

Since the width of the house is at its smallest 4.0 m [39] whilst the inundation depth cannot be more than 6.8 m[40] this means that the ratio is at its slenderest 4/6.8≈0.6. If we take a look at more realistic values then the inundation depth will be more around 3-4 m which would give a slenderness ratio of about 1. This means that the house will be in between both extremes, there will be some influence of the sides of the house on the overall pressure distribution and the walls cannot be schematized as infinitely long.

## 4.6 Bore Impact

The bore impact force is the force following from a bore impacting against a house. At first this seems like an odd phenomenon in regards to a riverine flood. However, the water wave appearing from the dyke breach can be compared to a bore at the location of the masonry house since water depth and velocity will be approximately constant in time for a certain location, see Figure 27. The water depth and velocity of this bore is of course different, but still approximately constant in time, for each location shortly after the dyke breach.

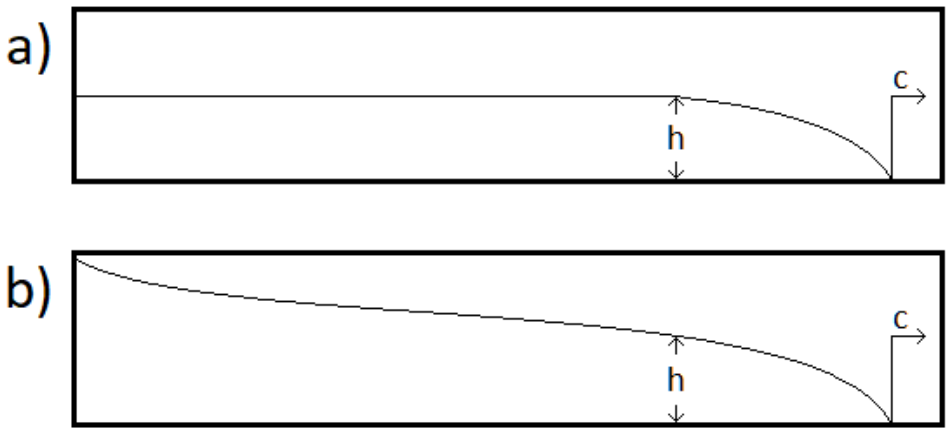


Figure 27 - Wave shape of a bore (a) and a dam break wave (b) with water depth h and celerity c

[39] See chapter 6 Masonry House Material Properties or chapter 9 DIANA Model Properties for a Masonry House

[40] See chapter 1 Introduction

A bore in its place is very similar to a wave breaking on a dyke crest, from now on referred to as an overtopping bore, as well as tsunami waves on land. All of these are, at least for a certain time, a water mass with approximately constant depth and speed. Furthermore, the water mass, more than one wave height away from the wall at the moment of first impact, has little effect on the total impulse on the wall during first impact.[41] This suggests that the wave can be divided into 2 parts, the part during first impact and the stream of water that immediately follows, improving the comparison between bore and overtopping bore. This first part is where 4.6 will focus on, building on the theory from 0,
Breaking Wave. Since the research done in the fields of tsunamis and breaking waves is much more extensive than the research done to dyke breach waves, it will lead to better estimations for the dyke breach itself. The second part can be related to the flow force discussed in 4.3.

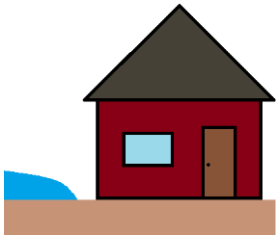

Figure 28 - Bore just before it reaches the house

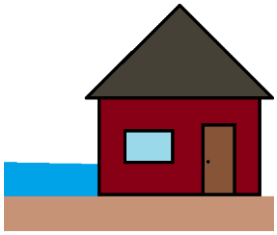

Figure 29 – Bore at the moment of first impact

Figure 30 – Bore at the moment when the rest of the wave reaches the house

Figure 31 - Bore just after the impact and just before the 'normal' flow situation

### 4.6.1 Bore Pressure Distribution in Time

The "church roof" pressure distribution is applicable to bores, tsunamis and overtopping bores too, see Figure 30. The main difference is in the height of the pressure peak, several circumstances can decrease this peak height. One of the main circumstances is the presence of a residual water layer as it can cause the peak to decrease or even disappear. The water layer redirects the first impact to a higher location on the obstacle and disperses it onto a larger area. It therefore seems to hinder the single point convergence which causes the pressure peak. Another circumstance as mentioned earlier, is the amount of entrained air in the approaching water mass. While water itself is very difficult to compress, air is very compressible. This means that entrained air will act as damper, a higher amount of entrained air will thus decrease the height of the peak.

For a wave breaking on a dyke crest there is usually a significant water layer already present due to the amount of incoming waves. This is however not the case for most tsunamis or bores caused by a dyke breach. Since there is thus no redirecting of the first impact, on average, a higher pressure peak is expected for these events compared to the overtopping bore. The results from the wave breaking, the overtopping bore, can therefore be seen as a lower limit for the bores pressure peak.

### 4.6.2 Bore Pressure Distribution in Space

As one might expect this bore pressure distribution in space is also influenced by certain factors. The main factor being the water depth of the incoming bore. The depth is however assumed to be constant. Other factors that can influence the pressure distribution are the bottom roughness and more importantly the presence of a water layer. A high bottom roughness, for example due to small objects before the actual obstacle is reached, will slow down the lower part of the incoming water. The presence of a water layer however, practically acts like a continuous string of small objects. This

[41] Cooker and Peregrine [28]

will cause the water to impact higher up on the wall and over a larger area, see Figure 32 and Figure 33. As can be seen Figure 32 belongs to a force distribution, however as stated above the principal still holds for the pressures.

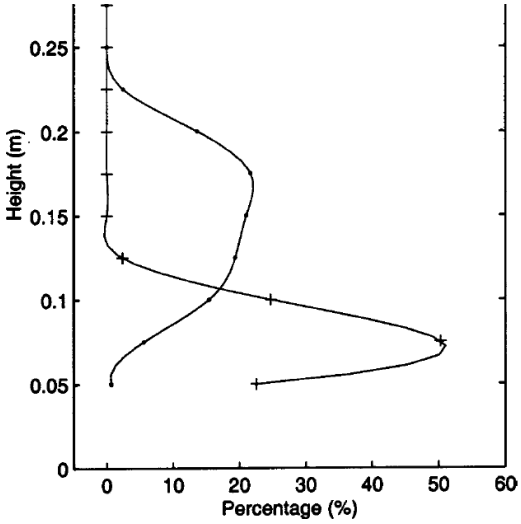


Figure 32 - Vertical distribution of the force during impact, with and without an already present water layer[42]

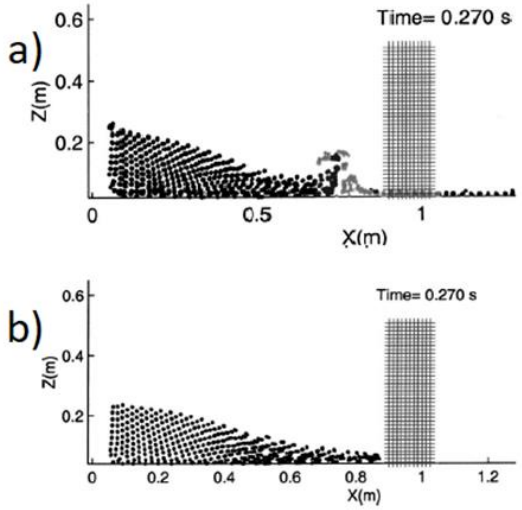


Figure 33 - Water propagation with (a) and without (b) an initial water layer present[43]

Another factor of course is time. Depending on time, the pressure distribution in space also changes. At first the high pressure peak will occur, which will act on the obstacle below the initial water depth of the incoming wave. This resembles the dynamic pressure peak from 4.5.1.2. Next the quasi-hydrostatic peak will occur, acting on a larger area of the obstacle. Both of these situations can be seen in Figure 34. In between the pressure changes of course which means that these two situations do not necessarily capture the highest pressure at each location.

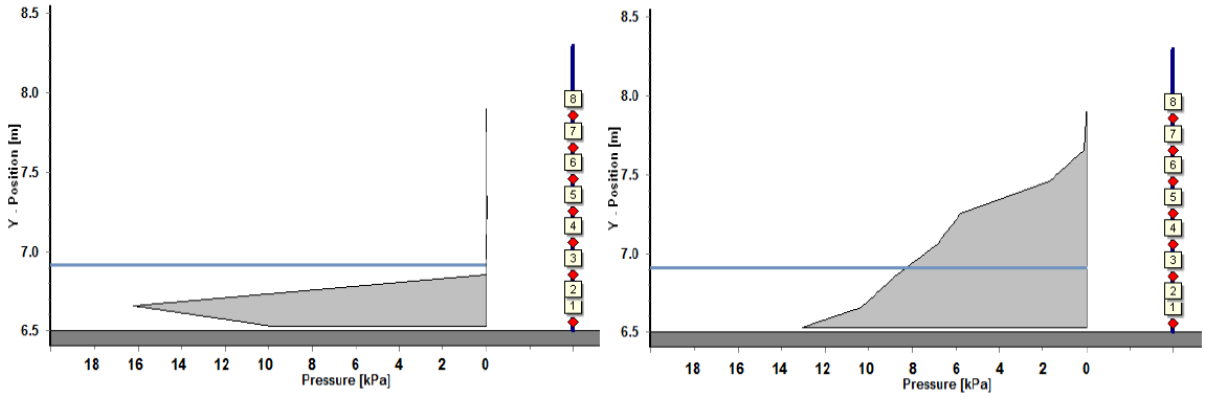


Figure 34 - Vertical pressure distribution of the hydrodynamic peak (left) and the quasi-hydrostatic peak (right),[44] the blue line indicates the water depth of the incoming water, 42cm.

### 4.6.3 Force Distributions

There are two ways of determining the force distribution, either via direct measurements of the force or through the integration of the pressure distribution. This means that again a difference in

[42] Gomez-Gesteira et al. [31]
[43] Gomez-Gesteira et al. [31]
[44] De Rouck et al. [33]

time and in space can be observed. Furthermore, the factors which influence the pressures will therefore also influence the forces. For those factors and circumstances see 0, 4.6.1 and 4.6.2. In Figure 35 a time history of both force distribution methods can be seen.

As can be seen these match rather well, especially after the second peak. This is due to the fact the distribution is quasi-hydrostatic from that moment onwards. Therefore less local peaks occur and the integration matches the force measurements better. During the first part however this is not a given. Due to the short duration of the first pressure peak, a local pressure difference might occur. If this is on a pressure sensor it will give a different result compared to the direct force measurement. Most of the differences between both methods can be decreased with a more accurate method to measure both forces and pressures. By increasing the numbers of locations were pressures are measured, the integration area of each pressure sensor will decrease. This will decrease the influence of local pressure differences and will increase the overlap between both measurement methods.

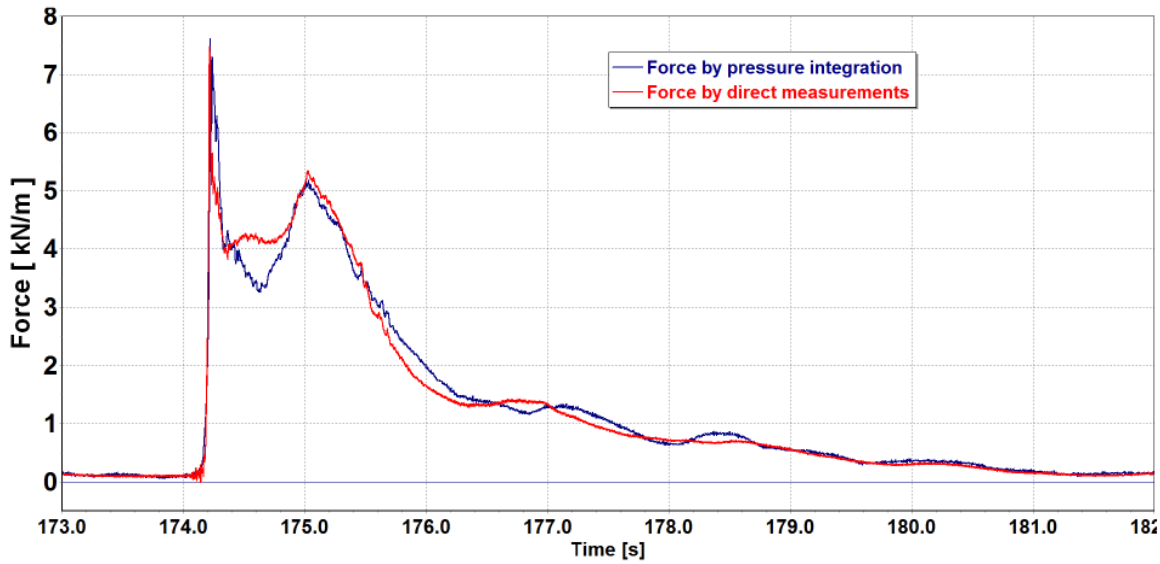


Figure 35 - Time history of a force distribution by pressure integration and by direct measurements[45]

### 4.6.4 Quantification

A theoretical formula is used in order to give an estimation of the quantities related to the pressures and forces. These are only related to the pressure peak, not to the quasi-hydrostatic part of the distributions. Furthermore diffusing circumstances, such as an initial water layer, are not present.

[45] Ramachandran et al. [32]

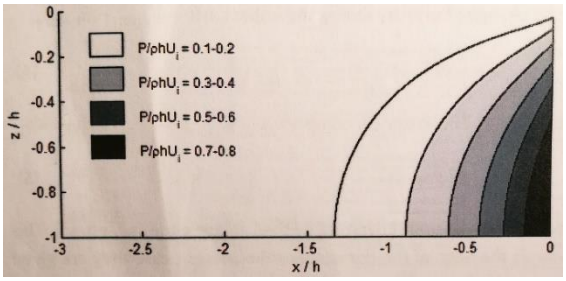


Figure 36 - Theoretical pressure impulse field of a steep bore impact[46]

#### 4.6.4.1 Maximum Pressure

The maximum theoretical pressure impulse, P, follows from a series of mathematical derivations.[47]

This P is at the bottom of the structure approximately equal to:

$$P = 0.742 * \rho * h_b * u_n \left(\frac{N}{s * m^2}\right)$$

In which:

| | | |
|---|---|---|
| ρ | is the density of the water | (kg/m$^3$) |
| $h_b$ | is the water depth of the bore | (m) |
| $u_n$ | is the normal component of the velocity | (m/s) |

Assuming the pressure peak has an isosceles triangular shape, the maximum pressure, $p_{max}$, would then be:

$$p_{max} = \frac{1.484 * \rho * h_b * u_n}{\Delta t} \left(\frac{N}{m^2}\right)$$

In which Δt is the duration of the pressure peak, which is usually in the order of 0.1 seconds.

#### 4.6.4.2 Maximum Force

The total force during this pressure peak follows from the same series of mathematical derivations.[48] This total force, $F_{tot}$, is approximately equal to:

$$F_{tot} = \frac{0.543 * \rho * b * h^2 * u_n}{\Delta t} \ (N)$$

In which b stands for the width of the obstacle.

## 4.7 Debris

Debris is a collection of different objects and solids in the flood that can have an impact on a house. Its importance is greatly related to the availability and type of debris. Furthermore it depends on the inundation depth which causes debris to float and the flow velocity which is the main variable in determining the impact force of the debris. Examples of debris are floating vehicles but also pieces from collapsed buildings, floating furniture or even sediment in the flow.

Debris loads can be divided into two main types, static and dynamic. Static forces are for example due to sediment accumulation against the side of the house and dynamic forces are related to the impact of the debris on the house. The static debris loads are presumed to be negligible compared

[46] Hofland [36]
[47] Cooker and Peregrine [28]
[48] Hofland [36]

to the other static loads, this is augmented by the fact that it takes quite some time for these static debris loads to develop. The dynamic force can be subdivided into concentrated (impact) and distributed forces. Concentrated forces are forces on a small surface area such as a log colliding with a wall. Distributed forces are caused by, for example, sediment entrained in the flow flowing around a structure[49]. For this report two types of impact debris are taken into account, cars and branches or other log-like debris.

### 4.7.1 Impact Debris

Depending on the type of debris, its impact on the house will differ. Therefore more than one debris impact force formula is used. $F_{D,\,gen}$, is for general debris impact forces which is defined by the mass of the debris and the rate of deceleration. $F_{D,\,log}$, on the other hand, takes beside the mass and impact velocity also the stiffness of the debris and house into account. This formula is designed for impacting logs and poles and will therefore be used for the impacting branches and other log-like debris. These formulas are defined as:[50,51]

$$F_{D,gen} = m_D * \frac{u_D}{\Delta t}$$
$$F_{D,log} = u_D * \sqrt{k * m_D}$$

In which:

| | | |
|---|---|---|
| $m_D$ | is the mass of the debris impacting the house | (kg) |
| $u_D$ | is the velocity of the debris | (m/s) |
| $\Delta t$ | is the impact duration | (s) |
| k | is the constant effective stiffness between the debris and the house | (N/m) |

A representative value for k, for the upper envelope of the collected data, is found to be $2.4*10^6$ N/m.

### 4.7.2 Distributed Debris

The formula for the distributed debris force, $F_{D,\,distri}$, is presumed to be similar to the flow force:

$$F_{D,distri} = \frac{1}{2} * C_D * \rho_f * A * u^2$$

However ρ is now $\rho_f$ which is not the density of the water, but the density of the fluid including the suspended solids. All the other variables are the same.

## 4.8 Erosion

Erosion is the removal of soil or rock at a certain location. There are two principal phenomena which make erosion possible, the entrainment of sediment and the horizontal movement of this entrained sediment.

Erosion can have a large impact on a house, since erosion can cause the foundation of that house to fail and therefore lead to its (partial) collapse. Erosion takes place mainly on locations with increased turbulence, since this increased turbulence is capable of causing sediment entrainment. This

[49] Kelman et al. [4]
[50] Nistor et al. [5]
[51] ASCE [8]

entrained sediment will then be transported away from this location which leads to erosion at that location. Examples of this are the flow of water around buildings or around bridge pillars.

The formula for the estimation of time-dependent local scour or erosion next to a house, z(t), is adapted from an estimation of the maximum scour depth by introducing a time-scale, $K_t$ and a land-cover correction factor $K_n$[52]:

$$z(t) = 1.4 * b^{0.65} * Fr^{0.43} * d^{0.35} * K_a * K_t * K_n$$

$$K_a = \sin(\theta)$$

$$K_t = e^{-0.145 * \left|\frac{u_c}{u} * \ln(\frac{t}{t_u})\right|^{1.36}}$$

$$K_n = \frac{0.138}{{n_c}^{0.43}}$$

In which:

| | | |
|---|---|---|
| b | is the width of the house | (m) |
| Fr | is the Froude number | (-) |
| d | is the inundation depth | (m) |
| $K_a$ | is the approach angle correction factor | (-) |
| θ | is the angle of approach in degrees | (°) |
| $u_c$ | is the critical velocity for sediment entrainment | (m/s) |
| t | is the time during which u occurs | (s) |
| $t_u$ | is the time needed to reach the ultimate scour depth | (s) |
| $n_c$ | is the Manning's coefficient for actual field conditions | (-) |

Another formula for local scour around vertical wall or enclosures, z, is estimated by[53]:

$$z = 0.15 * L$$

Where L is the horizontal length along the side of the house and z is limited to 10ft, roughly 3m.

## 4.9 Conclusions

There are six different loads discussed in this chapter, hydrostatic, buoyancy, flow forces, bore impact, debris and erosion. Long and short wave are not loads of themselves, short waves provide the introduction for the breaking wave and thus the bore impact assessment. Not all of these six loads can be taken into account when answering the main research question. Loads with regard to overall stability, such as buoyancy and more or less also erosion are not taken into account. The focus will be on more direct loads. From the remaining four, the flow forces are similar to the bore impact. The bore impact, however, is larger in magnitude and therefore leading. Hydrostatic is the other load chosen, debris is a very broad subject and is therefore something for further investigation.

Therefore, to answer the main research question, two distinct and different loads will be used to calculate the structural response. These are the hydrostatic water pressure, 4.1, and the hydrodynamic bore impact, 4.6.

To provide an idea of the magnitude of the loads, the total force for a bore impact is calculated using the flood parameters from chapter 3, a flow velocity of 10 m/s and an inundation depth of 1.50 m

[52] Caraballo et al. [7]
[53] FEMA P-55 [13]

and a $\Delta t$ of 0.1 seconds. Entering these parameters into the maximum force formula from paragraph 4.6.4.2 provides the following result:

$$F_{tot} = \frac{0.543 * \rho * h^2 * u_n}{\Delta t} = \frac{0.543 * 1000 * 1.50^2 * 10}{0.1} = 122175\ (N/m) = 122.2\ (\mathrm{kN/m})$$

This is the total force exerted by the bore and needs a distribution over the height to be used in calculations, this distribution is shown in Figure 37. The total area of the distribution corresponds to the maximum force.

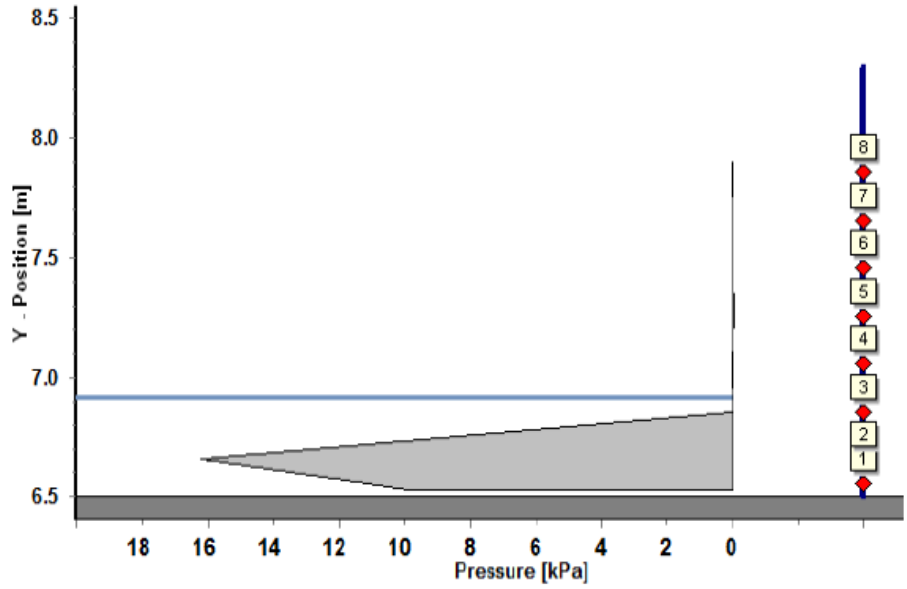


**Figure 37 - Vertical pressure distribution of the hydrodynamic peak[54], the blue line indicates the water depth of the incoming water, 42cm.**

[54] De Rouck et al. [33]

# 5 Damage Propagation in the Polder after the Dyke Breach

After the dyke has been breached and the hinterland is being flooded, damage will also start to occur. There are two related types of damage, structural damage can occur due to the direct impacts of the flood on the building. Economic damage can occur due to structural damage, but also due to damage to the contents of the buildings and repair costs. A simple way to estimate damage is to use so-called damage curves. Furthermore, some possible failure mechanisms of the masonry house will be discussed.

## 5.1 Damage Curves[55]

A damage curve relates the load at a certain location to the damage. These loads are almost always the inundation depth, often also the duration and sometimes the flow velocity. Others are used but more scarcely. A damage curve is based on either data from previous floods and/or case study data from models.

Using standardised types for the categories one can determine the damage of an entire area, by selecting the standardised type most closely to the actual type. This can for example be a type of crop but also a type of road or building. With this, it is then possible to determine the total damage of an area and doing so for all categories, thus for the entire flooded area.

However, this is not a very precise method for determining the damage to a single specific building, road etc. The reason this method is still fairly accurate is because it works with averages. Therefore, if you have a large enough flooding and thus a large amount of these specific buildings, roads etc., the results will still be quite accurate.

Even though it is possible to also consider indirect flood damage and more categories than damage to masonry houses, those fall outside the scope of this thesis.

Some examples of damage curves are shown in Figure 38.

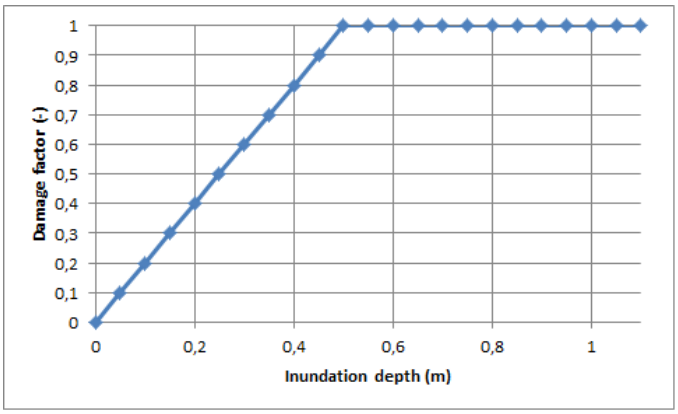


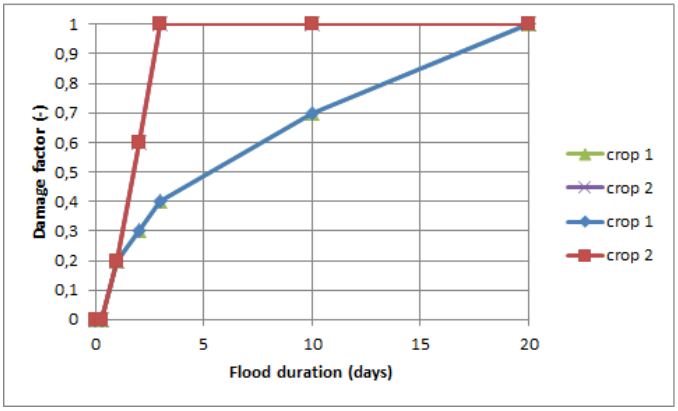


[55] Hoes et al. [2]

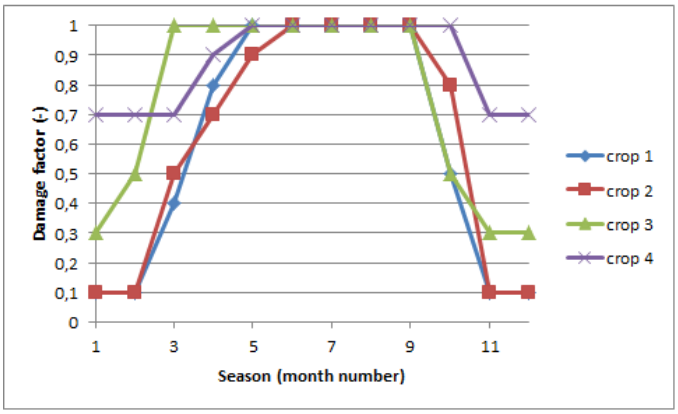


Figure 38 - Examples of damage curves

## 5.2 Failure Mechanisms of the House

When the water and other possible objects reach the house they will have some effect. In the worst case this will lead to structural failure of the house. There are several groups of failure mechanisms which can lead to partial or complete structural failure, these are shown in Figure 39.

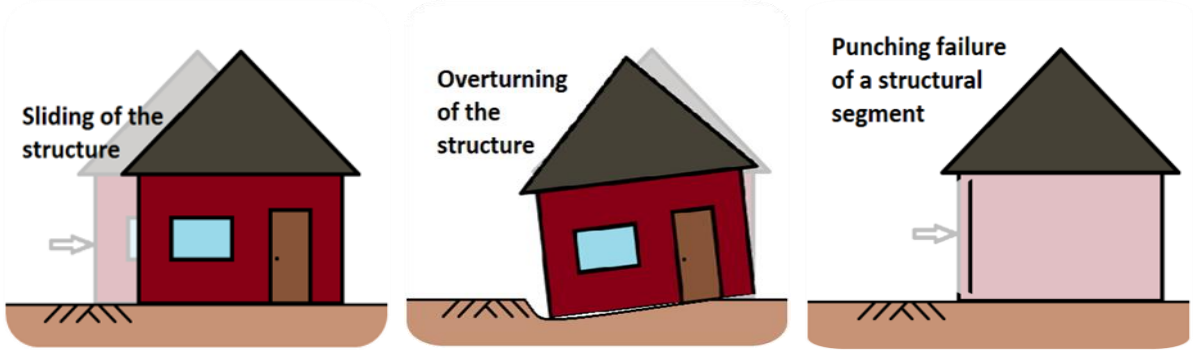


Figure 39 - Failure mechanisms of a house

The first failure mechanism is sliding of the entire house. With a sufficiently deep foundation this is very unlikely to happen. Not only would the structure with the foundation need to slide, the surrounding soil as well. The second mechanism is overturning, which means that part of the foundation has subsided causing the house on top to overturn. This might occur with shallow foundation and locations close to the breach were the flow velocities are high, causing large scour holes. For foundations on poles, this should not pose a very large threat. The third and most dangerous failure mechanism is punching failure of a specific segment especially when it is a load bearing segment. Failure of such a segment will cause partial or entire collapse of the house and requires less specific circumstances than the first and second failure mechanism.

## 5.3 Conclusions

- The current practice of using damage curves can provide accurate results for larger sample sizes and it is used in this way to estimate economic damage.
- For single buildings or small areas a structural damage curve would lack accuracy since it does not take the actual loads and resistances into account. Therefore a, structural, model is needed to accurately determine the damage.

# 6 Masonry House Material Properties

After determining the loads in chapter 4 it is now time to take a look at the structural side of this thesis. Since damage curves only work after the occurrence of a flood in order to predict the damage for future floods, this realisation made it clear that it would be beneficial to take an extensive look at what actually happens with a house during a flood. If it is possible to predict structural damage based on the expected flood parameters, mitigation measures can be taken to prevent the worst outcomes, loss of life and structural damage.

Therefore, in the second part of this thesis the structural side is investigated. First the material properties of the house are determined, here in chapter 6. As was mentioned in chapter 1, the houses in question are constructed using masonry. Since masonry and other construction materials varied immensely over the years, a specific time period helps to narrow down these material properties. This time period has been based on the houses at the chosen location for the case study. These houses are from pre-1930 and the quality and composition of the different building materials is thus based on this time period.

The masonry houses consist of three main material groups, masonry, wood and concrete. Since it is a masonry house, the presence of masonry speaks for itself. Wood was used to construct not only the doors and window frames, as is still often done today, but also to construct the floors. Concrete and masonry were used to construct foundations. Concrete was also sometimes used to construct the ground floor, especially when there was a basement underneath. In this thesis, the walls are constructed using masonry, the floors using wood and the foundation using concrete.

Next, in chapter 7, the strength of minor building components is calculated and checked to determine whether or not local failure might occur. This can have both positive and negative consequences on the overall damage. With regard to structural damage, small local failure might actually prevent larger structural damage. For example, failure of a door could lead to flooding of the house. This, however, prevents a large pressure differential between the inside and outside of the house and therefore decreases structural damage.

A preliminary approach to the masonry-water interaction is performed in chapter 8. Starting with a simple approach using hinged connections, the complexity and realism are then increased step by step ending with a plastic hinge model.

This is followed by the DIANA model properties in chapter 9. Here all the required properties to perform the DIANA calculations are determined. These properties are then used to perform the DIANA calculations in chapter 10 and 11.

Figure 40 and Figure 41 give an impression of the masonry house used to determine the model for the case study. The house itself as well as the model for the case study are discussed in more detail in chapter 9.

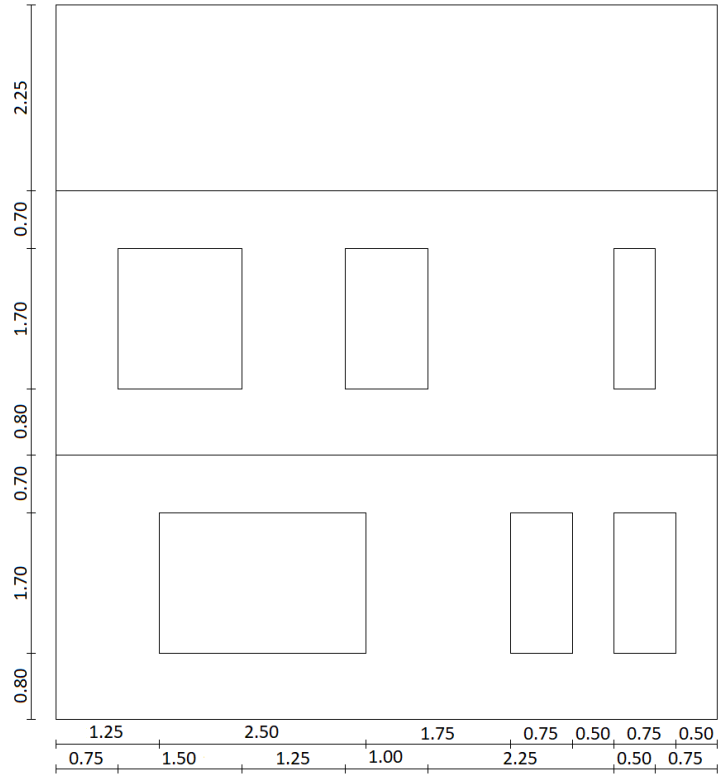


Figure 40 - Front view of the masonry house, measurements in metres

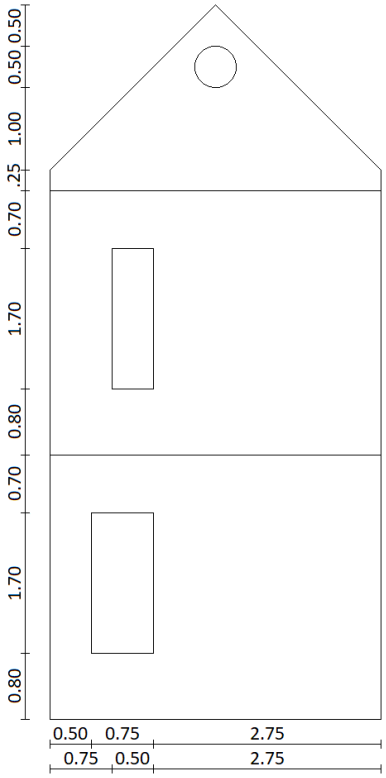


Figure 41 - Side view of the masonry house, measurements in metres

## 6.1 Masonry Properties[56]

As is well known masonry consists of interlaid bricks, held together with mortar. This can be either in a cavity wall or in a solid brick wall. Currently only the cavity wall is used with an increasingly large cavity used for isolation, see Figure 42 and Figure 43. The properties of masonry depend therefore on several parameters, most importantly the bricks themselves, the mortar, the brick-mortar interface and the applied masonry bond, the pattern in which the bricks are laid. The influence of these parameters varies, the strength properties mostly depend on the weakest link, which is usually the mortar or brick-mortar interface. The influence of the masonry bond and the bricks is just minor. Furthermore the properties of the individual components vary with their specific composition which has changed over time. In Figure 44 an overview of the different parameters of a masonry wall is provided.

Although there are a lot of different brick sizes and possible joint thicknesses, the Dutch standard 'Waalformaat 50mm' has been used with a slight alteration. Due to a mistake in the Preliminary Calculations in Chapter 8 instead of a length of 210 mm, a length of 220 mm was used. In order to keep all calculations based on the same principles, this mistake has been carried on into the DIANA calculations. The effect of this on the masonry properties and on the results of the calculations is limited. The main difference is the increase of the single wall thickness from 210 mm to 220 mm.

[56] For more background information see Van Noort [15]

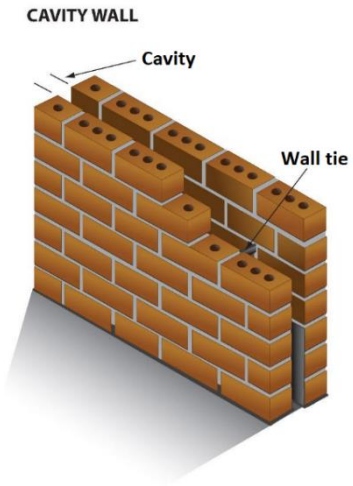


Figure 42 - A masonry cavity wall[57]

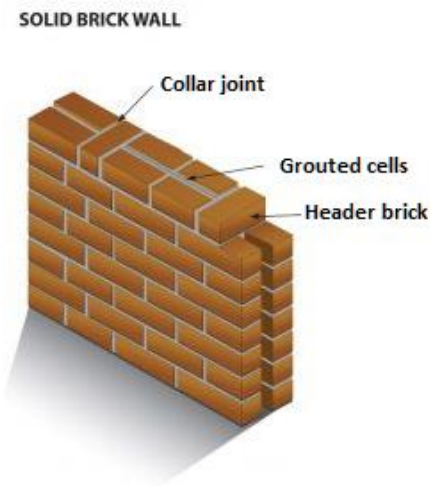


Figure 43 - A masonry solid wall[58]

Depending on the load direction there are several ways masonry can fail, through:

- cracks in the bed joint
- cracks in both bed and head joint
- cracks through both bricks and mortar

The bed joint is always part of the cracking pattern in masonry. The cracks in both the bed and head joint are the so called diagonal staircase cracks. These can often be observed when an earthquake shook the masonry houses, for example in Groningen. The cracks through both bricks and mortar only occur when the bricks are weaker or close to the strength of the mortar. In that case the cracks will not pass around the bricks but go straight through them.

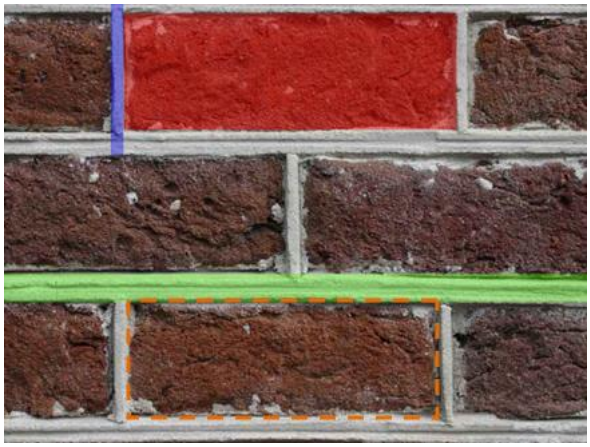

Figure 44 – Masonry wall, bricks (red), bed joint (green), heat joint (blue) and the brick-mortar interface (orange)[59]

The finite element program used for the case study, DIANA, requires several properties as input. These properties are as described above of the bricks, mortar, a combination of both or of the brick/mortar interface.

- Young's moduli (both)
- Shear modulus (both)
- Mass density (both)
- Compressive strength (brick)
- Factor to strain at compressive strength (brick)
- Fracture energy in compression (mortar)
- Unloading factor (-)

[57] Abbot [59]
[58] Abbot [59]
[59] Van Noort [15]

- Friction angle (interface)
- Cohesion (interface)
- Fracture energy in shear (interface)
- Crack bandwidth specification (-)
- Head-joint failure type (some require additional properties):
    - 1) Head-joint failure not considered.
    - 2) Direct input head-joint tensile strength:
        - Head-joint tensile strength.
    - 3) Diagonal stair-case cracks:
        - Angle between stepped diagonal crack and bed-joint.
    - 4) Tensile strength head-joint defined by friction.
        - Minimum tensile strength head-joint (optional)
        - Angle between stepped diagonal crack and bed-joint.
- Bed-joint tensile strength (interface)
- Residual tensile strength (interface)
- Fracture energy in tension (interface)

A few of these properties might be unknown and are therefore clarified a bit. Factor to strain at compressive strength, $= \frac{E*\varepsilon_{peak}}{f_c}$. The unloading factor relates to unloading of the masonry, which is only of importance for cyclic loading. Cohesion, after cracks have occurred there is still some cohesion between brick and mortar due to the roughness of both surfaces. Crack bandwidth specification, the specific method to determine the crack bandwidth, either Rots' element method, Govindjee's projection method or direct input. Head-joint failure type, the way the head-joint fail or not, the chosen type should be based on the expected way of failure. See Table 6 for an overview of the values used for the masonry properties required for DIANA.

**Table 6 - Masonry Properties Outside Walls for DIANA[60][61]**

| | | |
|---|---|---|
| Young's modulus ($E_x$) | 6024 | ($N/mm^2$) |
| Young's modulus ($E_y$) | 6092 | ($N/mm^2$) |
| Shear modulus | 2423 | ($N/mm^2$) |
| Mass density | 1800 | ($N/mm^3$) |
| Compressive strength | 14.2 | ($N/mm^2$) |
| Factor to strain at compressive strength | 4 | - |
| Fracture energy in compression | 20.7 | (N/mm) |
| Unloading factor, 1=secant, 0=linear | 1 | - |
| Friction angle | 36.87 | (°) |
| Cohesion | 0.85 | ($N/mm^2$) |
| Fracture energy in shear | 0.11 | (N/mm) |
| Crack bandwidth specification | Rots | - |
| Head joint failure type | diagonal | - |
| Angle between stepped diagonal crack and bed-joint | 27.55 | (°) |
| Bed-joint tensile strength | 0.71 | ($N/mm^2$) |
| Residual tensile strength | 0 | ($N/mm^2$) |
| Fracture energy in tension | 0.022 | (N/mm) |

[60] Van Noort [15]
[61] Van der Pluijm [50]

### 6.1.1 Inner Wall Masonry Properties

Besides the masonry for the outside walls, the inner walls will also have been constructed using masonry or something of the sort, albeit with lesser materials. The properties have therefore been altered to match these lesser materials and thus provide an accurate strength. Where the higher strength mortar was partially stronger than the bricks, for the lower strength mortar and brick, the mortar is the lesser one for all the properties used. Table 7 provides an overview of the properties for these inner walls.

**Table 7 - Masonry Properties Inner Walls for DIANA[62][63]**

| | | |
|---|---|---|
| Young's modulus ($E_x$) | 1989 | ($N/mm^2$) |
| Young's modulus ($E_y$) | 1960 | ($N/mm^2$) |
| Shear modulus | 790 | ($N/mm^2$) |
| Mass density | 1800 | ($N/mm^3$) |
| Compressive strength | 6.2 | ($N/mm^2$) |
| Factor to strain at compressive strength | 4 | - |
| Fracture energy in compression | 9.9 | (N/mm) |
| Unloading factor, 1=secant, 0=linear | 1 | - |
| Friction angle | 36.87 | (°) |
| Cohesion | 0.65 | ($N/mm^2$) |
| Fracture energy in shear | 0.085 | (N/mm) |
| Crack bandwidth specification | Rots | - |
| Head joint failure type | diagonal | - |
| Angle between stepped diagonal crack and bed-joint | 27.55 | (°) |
| Bed-joint tensile strength | 0.56 | ($N/mm^2$) |
| Residual tensile strength | 0 | ($N/mm^2$) |
| Fracture energy in tension | 0.017 | (N/mm) |

## 6.2 Wood Properties

For the construction of the window frames, doors, floor beams and planks wood was used. The main type used in the Netherlands for this pre-1930 was spruce. Since wood is anisotropic the properties will be different in all directions. See Table 8 for an overview of the properties used in this report. Since there are different types of spruce, their values have been averaged to get the best estimate. The Young's moduli are increased by 10% to remove the effect of shear deflection. This is possible since shear deflection is expected to only be of minor influence. Since the shear moduli are expressed as a percentage of the Young's moduli, they also increase with 10%.

**Table 8 - Wood Properties (averaged over the spruce types) [64]**

| | | |
|---|---|---|
| Young's modulus (longitudinal) | $1.10*10^{10}$ | $N/m^2$ |
| Young's modulus (radial) | $1.13*10^{9}$ | $N/m^2$ |
| Young's modulus (tangential) | $5.61*10^{8}$ | $N/m^2$ |
| Poisson ratio (LR) | 0.397 | - |
| Poisson ratio (LT) | 0.465 | - |
| Poisson ratio (RT) | 0.483 | - |
| Shear modulus (LR) | $1.03*10^{9}$ | $N/m^2$ |
| Shear modulus (LT) | $9.96*10^{8}$ | $N/m^2$ |

[62] Van Noort [15]
[63] Van der Pluijm [50]
[64] Green et al. [49]

| | | |
|---|---|---|
| Shear modulus (RT) | $7.15*10^7$ | $N/m^2$ |
| Mass density | 400 | $kg/m^3$ |
| Maximum shear strength | $8.00*10^6$ | $N/m^2$ |
| Rolling shear strength | $2.00*10^6$ | $N/m^2$ |
| Tension perpendicular to the grain | $2.50*10^6$ | $N/m^2$ |

## 6.3 Concrete Properties

The foundation of the house is constructed using concrete, in order to model this concrete three properties are required, the mass of the concrete, the modulus of elasticity and the Poisson ratio.

The mass of concrete[65] is approximately 2400 $kg/m^3$ and the Poisson ratio[66] is about 0.20. In order to determine the modulus of elasticity the compressive strength is needed. Over the years the concrete used in constructing buildings has changed. In Table 9 there is an overview of the compressive strength at the time and the compressive strength normalised to 2003. These values are based on an expert's opinion[67].

**Table 9 - Concrete material properties over the years**

| | Before 1905 | 1905-1944 | 1945-1974 | 1975-1994 | 1995-2002 |
|---|---|---|---|---|---|
| $f_{cc}$ | 18 | 20.5 | 23 | 28 | 33 |
| **Upgrade factor** | 2.5 | 2.5 | 2 | 1.7 | 1.4 |
| $f_{cc,\ upgr}$ | 45 | 51.3 | 46 | 47.6 | 46.2 |

Since the house is from pre-1930 the $f_{cc}$ of 51.3 $N/mm^2$ is used to determine the modulus of elasticity using the following formula[68]:

$$E_c = \frac{1}{24.4} * {m_c}^{1.5} * \sqrt{f_{cc}} = \frac{1}{24.4} * 2400^{1.5} * \sqrt{51.3} = 34513.24\ N/mm^2$$

In which:

| | | |
|---|---|---|
| $E_c$ | is the modulus of elasticity (Young's modulus) | $N/mm^2$ |
| $m_c$ | is the mass of the concrete | $kg/m^3$ |
| $f_{cc}$ | is the compressive strength of the concrete after 28 days | $N/mm^2$ |

**Table 10 - Concrete Properties**

| | | |
|---|---|---|
| Young's modulus | $3.45*10^4$ | $(N/mm^2)$ |
| Mass | $2.40*10^3$ | $(kg/m^3)$ |
| Poisson ratio | 0.20 | (-) |

[65] Roos, W. [1]
[66] Engineering ToolBox [51]
[67] Roos, W. [1]
[68] Wikipedia [12]

# 7 Strength of Minor Building Components

The resistance of a building not only consists of the resistance of its major building component, there are also other minor building components, such as doors, windows, wall ties and frames. Usually these minor components will have completely different resistances than the major building components. Several important minor building components are discussed in this chapter. Although frames can be important in supporting (failing) major building components due to their toughness, they have been left outside the scope of this thesis.

## 7.1 Doors

Doors are essentially plates, however they are hinged on one side, have one or more rigid point connections on the opposing side and are not connected on the top and bottom. A door can swing two ways, towards the inside and towards the outside. This has a large effect on their resistance against a water load, a door that opens against the load has the benefit that the door is supported around the edges by the frame, making failure less likely. Outside doors are therefore presumed to swing towards the inside and only have one point connection at the height of the handle, the latch bolt. If the door is locked there are 2 or more point connections, this will also increase the resistance, especially if they are divided over the height of the door. Divided point connections also mitigate the lever effect of the door somewhat. Since the top of the door will in reality function as the rotation point of a lever with the resistance of the point connections and the force of the water acting on that lever. If the resulting force of the water acts below the point connections, this will have a negative effect on the resistance and if it acts above, there will be a positive effect.

Since the presumed door is now hinged on one side and connected with a single point on the other side, whether or not the door will be able to resist the load comes down to whether or not the point connection is able to cope with the load. This load is transferred through the door to the latch bolt and onward to the door frame. For a pre-1930 Dutch masonry house the material used to construct the door frame is assumed to be wood, spruce to be more precise. In order to transfer the load from the latch bolt to the frame a steel plate is placed on top of the wooden frame. See Figure 45 for a top view of a door and its components.

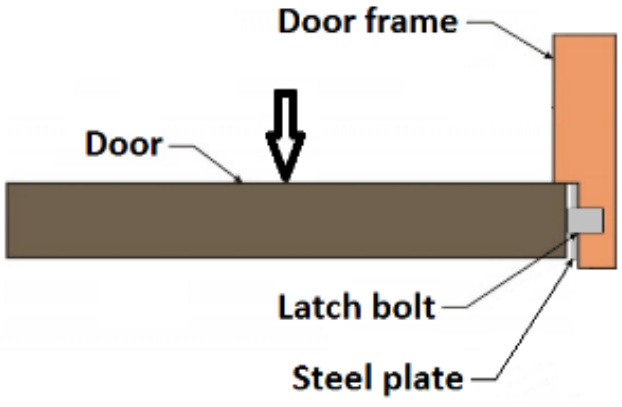


Figure 45 - Top view of a door

### 7.1.1 Failure mechanisms

To calculate the minimum force required for the failure of the connection, several failure mechanisms have been determined. Depending on the specific dimensions of the lock, see Figure 47, the governing mechanism can be determined.

- The first failure mechanism is the tensile failure of the steel plate next to the latch (and dead) bolt. No possible shear failure of the wood is included as to get a bottom approximation.
- The second failure mechanism is a kind of punching failure. The wood next to the screws is pushed out by the screws causing the entire steel plate to disconnect and thus failure of the connection.
- The third failure mechanism is linked to the second. However now not the wood next to the screws is pushed out, but the entire section between the top and bottom screw is pushed out as a whole.
- The fourth and final failure mechanism is failure of the screws connecting the steel plate to the frame.

Figure 46 - Steel plate on the wooden door frame

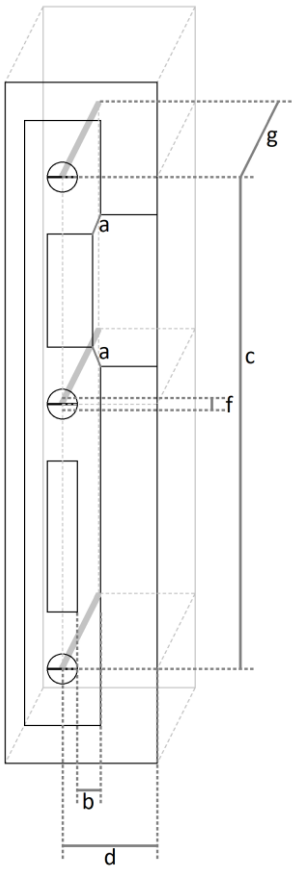


Figure 47 - Lock schematisation

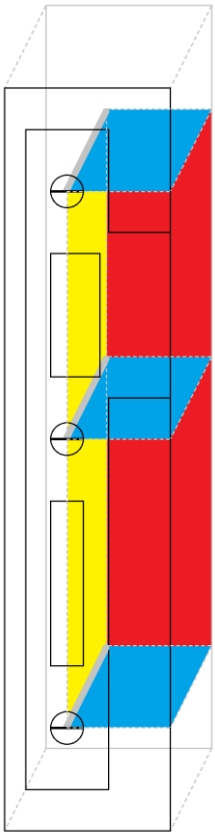

Figure 48 - Failure areas of the wooden door frame

Figure 47 shows the different dimensions of the lock and its related parts. Figure 48 shows the different areas of failure for the wooden frame, the blue areas are active in maximum shear, the red areas are active in rolling shear and the yellow areas are active in tension perpendicular to the grain.

Based on the four failure mechanisms and the dimensions from Figure 47 and Figure 48, resistance formulas can be made. For example calculations see Appendix D.

- For the steel plate to fail the strike plate near the latch bolt has to fail. This consists of two parts with equal length, a. The cross-section depends on the thickness of the steel plate which is assumed to be 'e'. The resistance of this mechanism is then:

$$F_{fail,latch} = A_{s,t} * f_{t,steel} = 2 * a * e * f_{t,steel}$$

If the door is locked another component needs to be added which is the part of the steel that fails due to the dead bolt:

$$F_{fail,dead} = A_{s,t} * f_{t,steel} = 2 * b * e * f_{t,steel}$$

The total for the first failure mechanism then is:

$$F_{fail1} = F_{fail,latch} + F_{fail,dead} = 2 * (a + b) * e * f_{t,steel}$$

| | | |
|---|---|---|
| $F_{fail,latch}$ | is the force required for tensile failure of the steel plate next to the latch bolt | (N) |
| $F_{fail,dead}$ | is the force required for tensile failure of the steel plate next to the dead bolt | (N) |
| $F_{fail1}$ | is the force required for failure mechanism 1 of the door | (N) |
| $A_{S,t}$ | is the area of the steel active in tension | ($mm^2$) |
| $f_{t,\ steel}$ | is the ultimate tensile strength of the steel | ($N/mm^2$) |
| A | is the length of the steel plate next to the latch bolt | (mm) |
| e | is the thickness of the steel plate | (mm) |
| b | Is the length of the steel plate next to the dead bolt | (mm) |

- The area that is pushed out by the screws depends on the width, f, and length, g, of the screws, assuming that the screws push over their entire length against the wood. Furthermore the kind of failure within the wood and its direction also influence the resistance. The resistance of the second mechanism is:

$$F_{fail2} = 3 * \left(A_{w,s} * f_{s,wood} + A_{w,srol} * f_{srol,wood}\right)$$
$$= 3 * \left(2 * d * g * f_{s,wood} + d * f * \frac{1}{4} * f_{s,wood}\right)$$
$$= \frac{3}{4} * d * f_{s,wood} * (8 * g + f)$$

| | | |
|---|---|---|
| $F_{fail2}$ | is the force required for failure mechanism 2 of the door | (N) |
| $A_{w,s}$ | is the area of the wood active in shear | ($mm^2$) |
| $f_{s,wood}$ | is the maximum shear strength of the wood | ($N/mm^2$) |
| $A_{w,srol}$ | is the area of the wood active in rolling shear | ($mm^2$) |
| $f_{srol,wood}$ | is the rolling shear strength of the wood (≈¼$f_{s,wood}$) | ($N/mm^2$) |
| d | is the distance between the screw and the side of the frame | (mm) |
| g | is the length of the screw | (mm) |
| f | Is the width of the screw | (mm) |

- Similar to the previous mechanism this resistance also depends on the length of the screws, g, as well as the kind of failure and direction within the wood. The rolling shear strength is approximately ¼ of the maximum shear strength. For the third mechanism the resistance is:

$$F_{fail3} = A_{w,s} * f_{s,wood} + A_{w,srol} * f_{srol,wood} + A_{w,t} * f_{t,wood}$$
$$= 2 * d * g * f_{s,wood} + d * c * \frac{1}{4} * f_{s,wood} + g * c * f_{t,wood}$$
$$= \frac{1}{4} * d * f_{s,wood} * (8 * g + c) + g * c * f_{t,wood}$$

| | | |
|---|---|---|
| $F_{fail3}$ | is the force required for failure mechanism 3 of the door | (N) |
| $A_{w,t}$ | is the area of the wood active in tension | ($mm^2$) |
| $f_{t,wood}$ | is the tensile strength of the wood perpendicular to the grain | ($N/mm^2$) |
| c | Is the distance between the bottom and top screw | (mm) |

- The final and fourth mechanism depends solely on the width of the screws. Again extra resistance will likely be provided by the wood, but none is taken into account to get a bottom approximation. This leads to the following resistance:

$$F_{fail4} = 3 * (A_{s,s} * f_{s,steel})$$
$$= 3 * \left(\frac{1}{4} * \pi * f^2 * f_{s,steel}\right)$$

| | | |
|---|---|---|
| $F_{fail4}$ | is the force required for failure mechanism 4 of the door | (N) |
| $A_{s,s}$ | is the area of the steel active in shear | ($mm^2$) |
| $f_{s,steel}$ | is the shear strength of the steel | ($N/mm^2$) |

## 7.2 Wall Ties

The inner and outer part of the walls will be connected in the case of a cavity wall. This connection is achieved using wall ties. Wall ties are small metal strips are rods which are placed during construction between the inner and outer wall. They will therefore transfer loads on from the outer wall to the inner wall. It is assumed that when the load increases beyond the capacity of the wall ties, it will start to deform with the outer wall until the outer wall is against the inner wall. kni

There are many different types of wall ties, mostly circular or rectangular. For simplicity a single type of wall tie is chosen, a rectangular steel wall tie, see Figure 49q with the dimension 200x22x1mm. The holes however decrease the minimal cross-section to approximately 17x1mm.

Figure 49 - Wall tie

For Streefkerk, a house below 11 m in height and a cavity of less than 150 mm, an equivalent of 2.8 wall ties per $m^2$ are required.[69] In order to bend a single wall tie, the entire cross-section will be plastic. Assuming a steel grade of S235 leads to a strength of 4kN per wall tie or 11.2 $kN/m^2$.

This strength is rather high, it is more likely that the wall tie will buckle. The buckling load, $F_B$, for a wall tie is:

$$F_B = \frac{\pi^2 * E * I}{l^2}$$

In which:

| | | |
|---|---|---|
| E | is the young's modulus | ($N/mm^2$) |
| I | is the area moment of inertia | ($mm^4$) |
| l | is the length of the cavity | mm |

With a young's modulus of $2.0*10^5$ $N/mm^2$, an I of $\frac{17*1^3}{12} = 1.42$ $mm^4$ and a cavity length for a pre-1930 house of 50 mm, the buckling load is at most 1.12 kN per wall tie.
Therefore the maximum load that the wall ties can transfer is no more than 3.132 $kN/m^2$.

[69] Wienerberger [48]

# 8 Preliminary Calculations to Masonry-Water Interaction

## 8.1 General Information for the preliminary calculations

To get an idea of how the masonry house responds to the loads, a single wall of the house is loaded and evaluated with some hand calculations. Only a small section of the wall, 0.4 m wide, see Figure 50, is used and undergoing a hydrostatic load and the self-weight of the house. To ease the calculations, the wall has been simplified into 2 large bricks connected with 1 layer of mortar at the breaking point. This breaking point has been assumed to be at the same location as the point of maximum bending.

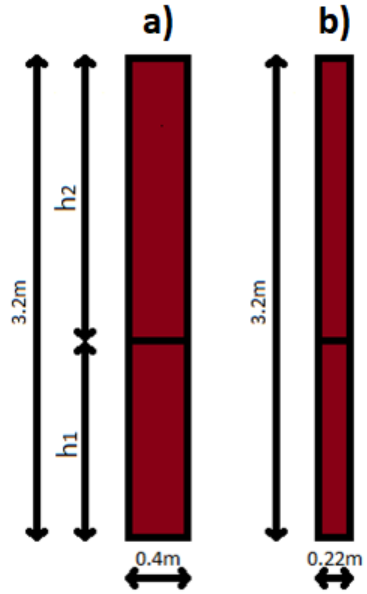


Figure 50 - Front view (a) and side view (a) of the small wall section

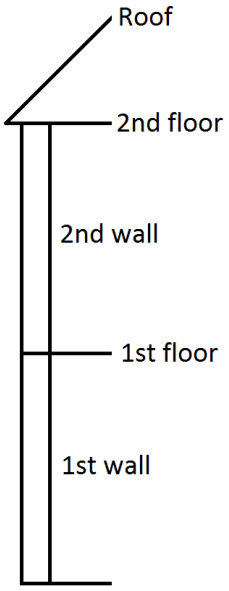


Figure 51 - Overview of the house

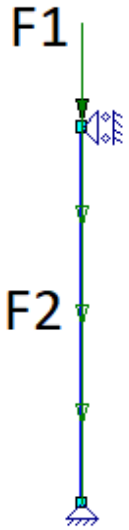


Figure 52 - Self-weight loads of the wall section

Since not all assumed dimensions are clear from Figure 50 and Figure 51, some additional information is required. The effective length for the floors working on the wall section is assumed to be 4 m. Since the roof is under a 45° angle, the effective length of the roof assumed to work on this section of wall is then 4*√2 m. Using the properties from chapter 6 the force corresponding to the self-weight of the 1st wall, $F_2$, can be determined. The self-weight corresponding to the rest of the house, $F_1$, can be determined after assumptions regarding the roof weight are made. The woodwork supporting the roof is assumed to be equal to the weight of a normal wooden floor and the weight of the ceramic roofing tiles is assumed to be 500 N/m².[70]

$$
\begin{aligned}
F_1 &= 1st\ floor + 2nd\ wall\ + 2nd\ floor\ + roof \\
&= (0.65\ kN/m^2 + 0.5\ kN/m^2) * 0.4m * 4m \\
&+ 3.96\ kN/m^2 * 0.4m * 3.2m \\
&+ (0.65\ kN/m^2 + 0.5\ kN/m^2) * 0.4m * 4m \\
&+ (0.65\ kN/m^2 + 0.5\ kN/m^2) * 0.4m * 4m + 4m * \sqrt{2} * 0.4m * 0.5\frac{kN}{m^2} \\
&= 1.84\ kN + 5.0688\ kN + 1.84\ kN + 2.97\ kN = 11.72\ kN
\end{aligned}
$$

$$
F_2 = 3.96\ kN/m^2 * 0.4m = 1.584\ kN/m
$$

[70] Monier B.V. [21]

### 8.1.1 Moment capacity calculation

For the first and second approach, the moment capacity is derived from the maximum moment and the load on top of the wall using a linear elastic stress distribution. In order to determine the moment capacity more exactly for the third approach, a stress distribution for concrete under tension has been examined[71]. Since concrete and bricks have a similar brittle way of failing, the concrete stress distribution represents the brick stress distribution quite accurately when scaling with the maximum stress of both materials. Using the trendline plotted through that stress distribution, a linear approximation for the elastic part, the non-elastic part as well as for the non-elastic (partially) cracked part was determined, see Figure 53.

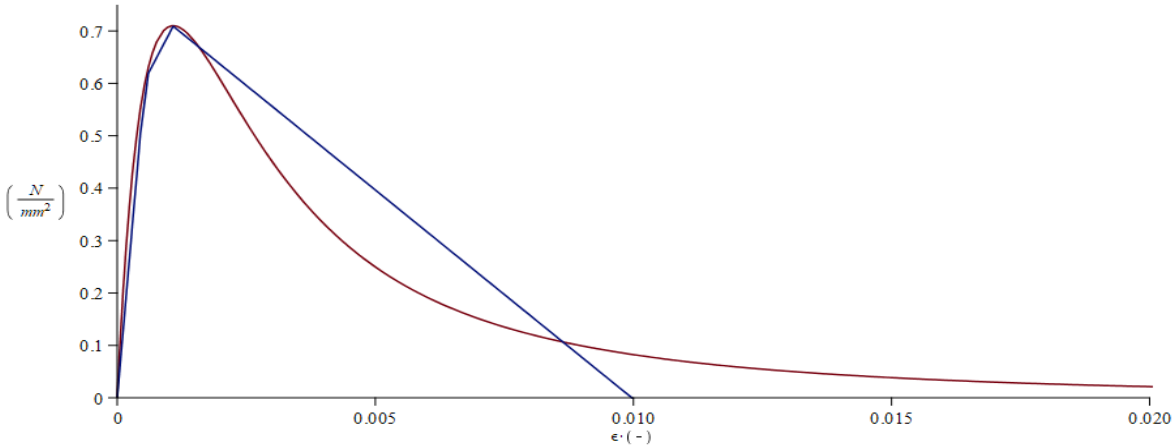


Figure 53 - Stress distribution for tension from the trendline as well as the linear approximations

Using these three linearized parts of the stress distribution it is possible to determine the stress distribution for all different crack lengths, assuming the compression part is always in the linear elastic stage. Crack length has been determined as the length after reaching the maximum tensile strength of the mortar. See Figure 54 and Figure 55 for examples of stress distributions for different crack lengths.

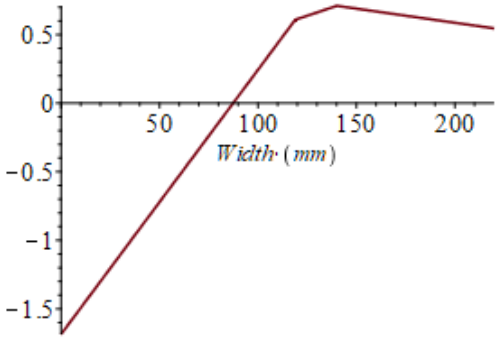


Figure 54 - Stress distribution (N/mm²) for a crack length of 80 mm

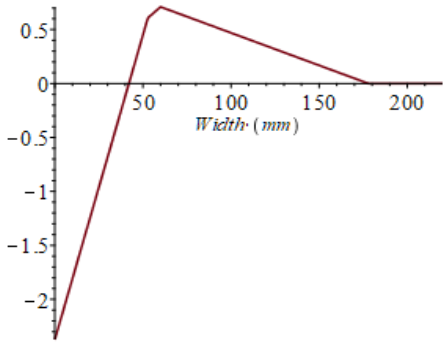


Figure 55 - Stress distribution (N/mm²) for a crack length of 160 mm

From these stress distributions the moment capacity of the cross-section has been determined by multiplying the areas under the distribution with the width of the wall and the distance to the point where compression changes to tension. This leads to a moment capacity distribution dependent on the crack length, see Figure 56.

[71] 2TM7 Lecture notes, figuur 5 and figuur 6 [22]

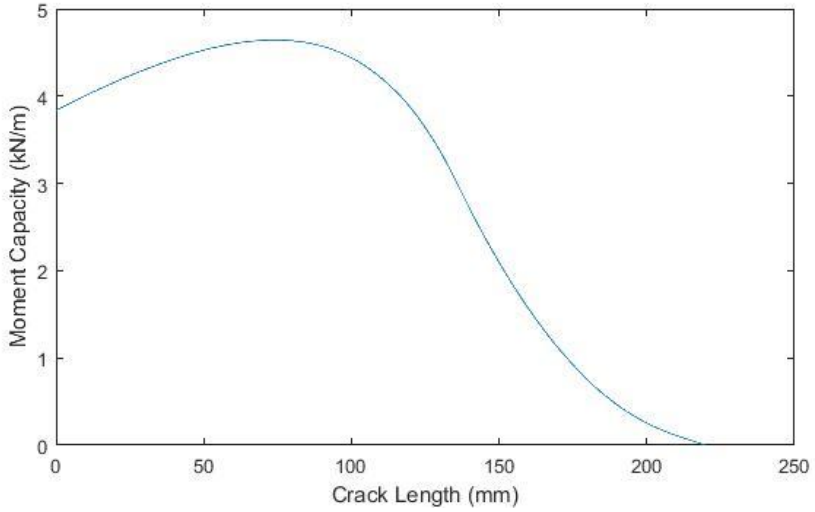


Figure 56 - Moment capacity distribution at the bottom of the wall

A remark has to be made regarding Figure 56 and the maximum compressive stress. When the crack length reaches 214 mm, the maximum compressive stress reaches 15 N/mm$^2$, any results after that are therefore not accurate anymore. In reality when this point is reached not only the tension part but also the compression part of the cross-section will start to fail.

The maximum moment capacity in this cross-section is 4.64 kN/m, while the moment capacity when the maximum tensile strength is reached is 3.84 kN/m and the moment capacity at the end of the elastic stage is at most 3.30 kN/m. The maximum moment capacity at the bottom of the wall increases with respectively 20.8% and 40.6%.

Table 11 - Moment capacities under different circumstances at the bottom, field and top location

| | Bottom (kN/m) | Field (at a height of 1.4 m) (kN/m) | Top (kN/m) |
|---|---|---|---|
| $M_{max}$ | 4.6430 | 4.5210 | 4.3724 |
| $M_{ftmax}$ | 3.8374 | 3.6849 | 3.5008 |
| $M_{el}$ | 3.2978 | 3.1284 | 2.9244 |

## 8.2 First Approach to Masonry-Water Interaction

The first approach assumes no resistance at the top and bottom of the 1st wall, i.e. a hinged connection and only one load type, a hydrostatic load, $F_3$, Figure 57 shows these features.

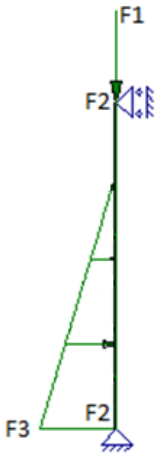


Figure 57 - Side view of the model including the hydrostatic load

### 8.2.1 Hydrostatic load

The hydrostatic load, $F_3$, was determined using a hydrostatic distribution. This gives the following forces:

$$F_3 = 0.5 * \rho * g * b * h^2$$
$$= 0.5 * 1.000 * 9.81 * 0.4 * h^2$$
$$= 1.962 * h^2\ kN$$

At the breaking point, the stresses can be determined which can then be compared to the material properties to determine whether or not failure occurred. In order to swiftly run several inundation depths, different values of h, a simple elastic 1D MatrixFrame model is used, see Figure 57. Since MatrixFrame does not have the material properties for masonry, concrete with a tensile strength closest to masonry is used, C12/15. This gives the following results for the hydrostatic load:

**Table 12 - Mmax and Sigmatmax due to the hydrostatic load**

| h (m) | Mmax (kNm) | sigmatmax (N/mm²) |
|---|---|---|
| 0.5 | 0.07 | -0.162 |
| 1.0 | 0.49 | -0.027 |
| 1.5 | 1.45 | 0.275 |
| 1.97 | 2.85 | 0.712 |
| 2.0 | 2.96 | 0.746 |
| 2.5 | 4.95 | 1.365 |
| 3.0 | 7.27 | 2.086 |
| 3.2 | 8.25 | 2.390 |

$Sigma_{tmax}$ is negative for h<1 m since there is no tensile stress in the cross-section yet. The maximum tensile force of the mortar is 0.71 N/mm², so for h>1.97 m cracking occurs. Since the material is brittle and the supports are hinged it seems logical to assume that once a tensile crack occurs, this will lead to failure. Since the area transferring the tensile load will decrease and thus the stress on the remaining part will increase. For this to be true an entirely linear stress distribution is required. However a higher load is transferable, due to the change in the stress distribution. This has been calculated in 8.1.1.

## 8.3 Second Approach to Masonry-Water Interaction

The assumptions made considering a hinged connection at the top and bottom of the wall were not realistic, at the bottom the wall is connected to the foundation and at the top to a floor and a roof or another wall in this case. This means the connections are more rigid than assumed in section 8.2. Therefore a second estimation has been made assuming a rigid connection at the top and bottom, see Figure 58, using the same load as in 8.2.1 the following results were obtained, see Table 13.

In Figure 60 the moment distribution at h=2.5 m can be seen. This clearly shows that the maximum moment is at the left (bottom) connection, this is therefore the dominant location and value.

Table 13 - Mmax and sigmatmax due to the hydrostatic load

| h (m) | Mmax (kNm) | sigmatmax (N/mm²) |
|---|---|---|
| 0.5 | 0.07 | -0.17 |
| 1.0 | 0.47 | -0.05 |
| 1.5 | 1.32 | 0.22 |
| 1.97 | 2.49 | 0.58 |
| 2.0 | 2.58 | 0.61 |
| 2.12 | 2.92 | 0.71 |
| 2.5 | 4.11 | 1.08 |
| 3.0 | 5.76 | 1.59 |

Figure 58 - Second model, rigid at the top and bottom

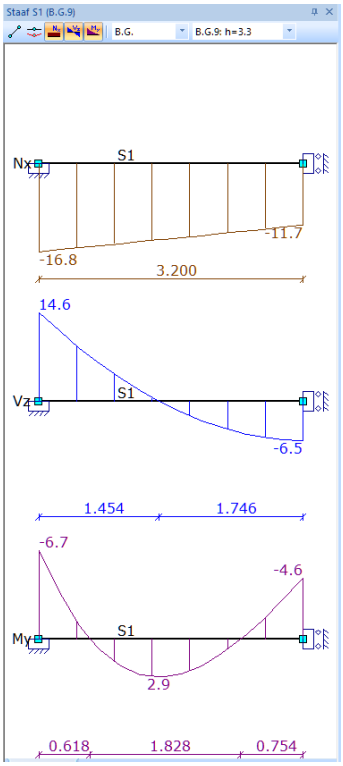


Figure 59 - Force distribution due to the hydrostatic load with an inundation depth of h=3.3 m

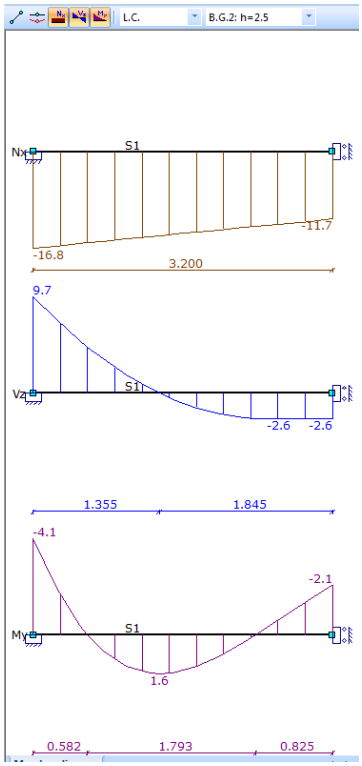


Figure 60 - Force distribution due to the hydrostatic load with an inundation depth of h=2.5 m

As can be seen from Table 13, the maximum inundation depth that can be withstood increased slightly with the assumption of rigid connections at the top and bottom. The location of the maximum moment also moves to the bottom of the wall. Although the moment distribution changed significantly in value, it did not in shape, the differences between hinged and rigid are small based on their impact on when first crack occurs.

For the hinged connection equilibrium is no longer possible after the moment capacity of the cross-section has been reached which therefore determines the failure load. The rigid connection will be able to withstand at least that load and fail at or before the moment capacity is reached at all three locations, field, top and bottom. This moment capacity appeared to be about 2.9 kNm, see Table 12

and Table 13 and was reached at the third, field, location at h=3.3 m, see Figure 59. The accompanying moment at the top and bottom however grossly exceed the moment capacity, making this an unrealistic upper value for the failure load.

## 8.4 Third Approach to Masonry-Water Interaction

### 8.4.1 Plastic hinge model calculation

The scenarios used in the first and second approach are not completely realistic, thus a more realistic situation will be discussed in this section assuming three plastic hinges. The first two hinges are located at the bottom and top of the wall, the third plastic hinge is assumed to be at the location of the maximum field moment.

The same MatrixFrame model as in section 8.3 has been used, however now when the moment capacity, $M_{max}$, of the cross-section is reached, a plastic hinge will appear. This will allow for a redistribution of the forces.

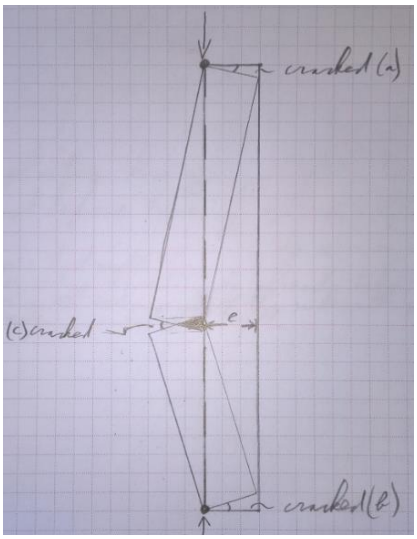


**Figure 61 - More realistic situation with three plastic hinges**

#### *8.4.1.1 Plastic model calculations*

To determine in what order and when these hinges will appear several steps were taken. First the actual moment capacity of the cross-sections was determined, starting at $M_{el}$ after which some plastic deformation occurs and $M_{ftmax}$ is reached. Second the load was increased in order to find the location of the first hinge. After finding the first hinge the load was increased to find the second hinge whilst lowering the resistance of the first hinge in order to prevent the moment at that location from being greater than $M_{ftmax}$. When hinge two was found the same procedure was followed as before to find the third hinge, only now both existing hinges were prevented from being greater than $M_{ftmax}$. The load at which hinge three appears is when deflections start to increase and the extra moment capacity will be utilised. After the maximum moment capacities, $M_{max}$, are reached equilibrium is no longer possible and failure will occur.

Using the new moment capacities, the following distributions for the hydrostatic load have been obtained, see Figure 62. First without any plastic hinges, then with plastic hinges at the bottom, next with plastic hinges at the top and bottom and finally with plastic hinges at the top, field and bottom.

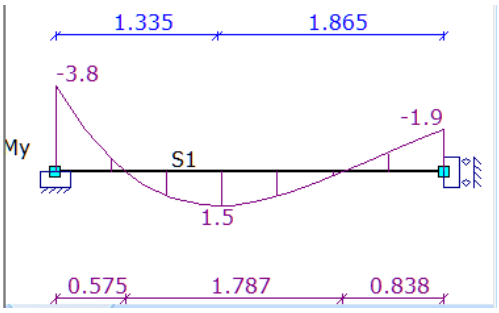


a) No plastic hinges

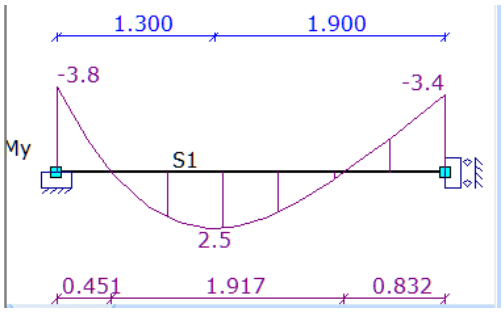


b) Plastic hinge at the bottom

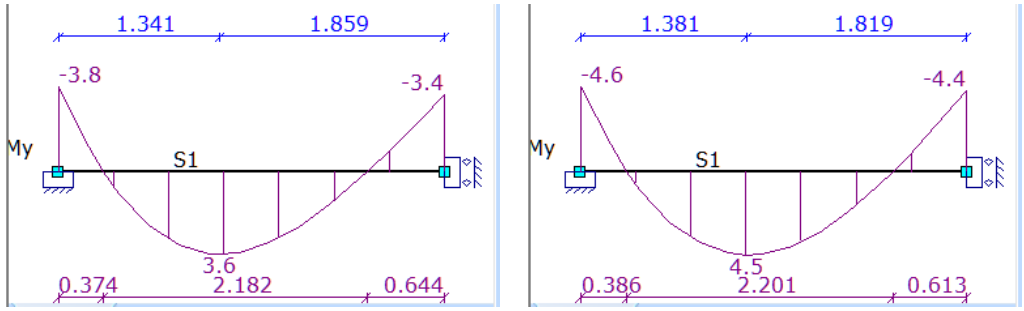


c) Plastic hinges at the top and bottom

d) Plastic hinges at the top, field and bottom

Figure 62 - Moment distribution when the first, second and third plastic hinge occur and when failure occurs

The first plastic hinge appears at h = 2.4 m, the second at h = 2.75 m and the third at h = 3.0 m, then the load can increase untill h = 3.35 m before failure occurs. Compared to the previous paragraphs the load increases due to the increased moment capacity. The load at which failure occurs also increases slightly, due to the higher maximum moment capacity. Previously this was reached at or before h = 3.3 m and with the higher maximum moment capacity this value is increased to an inundation depth of 3.35 m.

### 8.4.2 Plastic hinge hand calculation

Instead of using a computer program it is also possible to do the plastic hinge calculation by hand. Using the sign conventions as seen in Figure 63 and Figure 64 the following equations can be derived:

$$h = 3.2\ m = h_1 + h_2$$

$$\delta\theta_1 = \frac{h_2}{h_1} * \delta\theta_2 \ \rightarrow\ \delta\theta_2 = \frac{h_1}{h_2} * \delta\theta_1$$

$$\delta A = 0 = -Mp_1 * \delta\theta_1 - Mp_2 * \delta\theta_1 - Mp_2 * \delta\theta_2 - Mp_3 * \delta\theta_2 + F_1 * \delta\theta_2 * \left(\frac{1}{3} * (h_1 - h_3) + h_2\right) + F_2 * \delta\theta_1 * \frac{1}{3} * h_1 + F_3 * \delta\theta_1 * \frac{1}{2} * h_1$$

$$\rightarrow 0 = -Mp_1 * \delta\theta_1 - Mp_2 * \left(\delta\theta_1 - \frac{h_1}{h_2} * \delta\theta_1\right) - Mp_3 * \frac{h_1}{h_2} * \delta\theta_1 + F_1 * \frac{h_1}{h_2} * \delta\theta_1 * \left(\frac{1}{3} * (h_1 - h_3) + h_2\right) + F_2 * \delta\theta_1 * \frac{1}{3} * h_1 + F_3 * \delta\theta_1 * \frac{1}{2} * h_1$$

$$\rightarrow 0 = \delta\theta_1 * \left(-Mp_1 - Mp_2 * \left(1 + \frac{h_1}{h_2}\right) - Mp_3 * \frac{h_1}{h_2} + F_1 * \frac{h_1}{h_2} * \left(\frac{1}{3} * (h_1 - h_3) + h_2\right) + F_2 * \frac{1}{3} * h_1 + F_3 * \frac{1}{2} * h_1\right)$$

$$\rightarrow Mp_1 + Mp_2 * \left(1 + \frac{h_1}{h_2}\right) + Mp_3 * \frac{h_1}{h_2} = F_1 * \frac{h_1}{h_2} * \left(\frac{1}{3} * (h_1 - h_3) + h_2\right) + F_2 * \frac{1}{3} * h_1 + F_3 * \frac{1}{2} * h_1$$

$$F = \frac{1}{2} * \rho * g * b * h^2, with\ \rho = 1000 \frac{kg}{m^3}, g = 9.81 \frac{m}{s^2}, and\ b = 0.4\ m$$

$$\rightarrow F = 1.962 * h^2$$

$$F_1 = 1.962 * (h_3 - h_1)^2$$

$$F_2 = 1.962 * {h_1}^2$$

$$F_3 = 3.924 * h_1 * (h_3 - h_1)$$

$$\rightarrow Mp_1 + Mp_2 * \left(1 + \frac{h_1}{h_2}\right) + Mp_3 * \frac{h_1}{h_2}$$

$$= 1.962 * \left((h_3 - h_1)^2 * \frac{h_1}{h_2} * \left(\frac{1}{3} * (h_1 - h_3) + h_2\right) + \frac{1}{3} * {h_1}^3 + {h_1}^2 * (h_3 - h_1)\right)$$

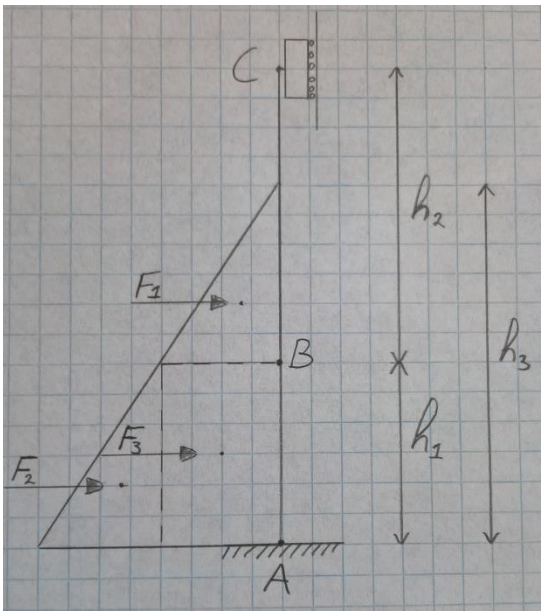


Figure 63 - Sign convention plastic hinge hand calculation

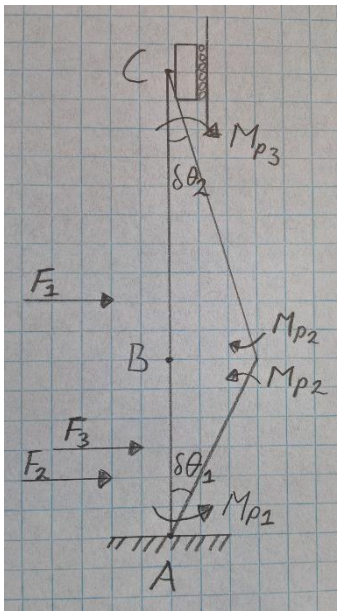


Figure 64 - Sign convention plastic hinge hand calculation

From the unknowns left in the final equation, $Mp_1$, $Mp_2$ and $Mp_3$ can be determined using the moment capacity relation obtained in 8.1.1. The only thing needed to be able to solve this equation is a relation between $h_3$ and one of the other h. Assuming point B is at the location of the maximum field moment it is possible to calculate $h_1$ for the inundation depth, $h_3$, using the MatrixFrame model from the previous paragraphs. After plotting these values in a graph a trendline can be drawn through these value to provide the relation needed, see Figure 65. This relation will however only be valid for $0<h_3<4.5$ m.

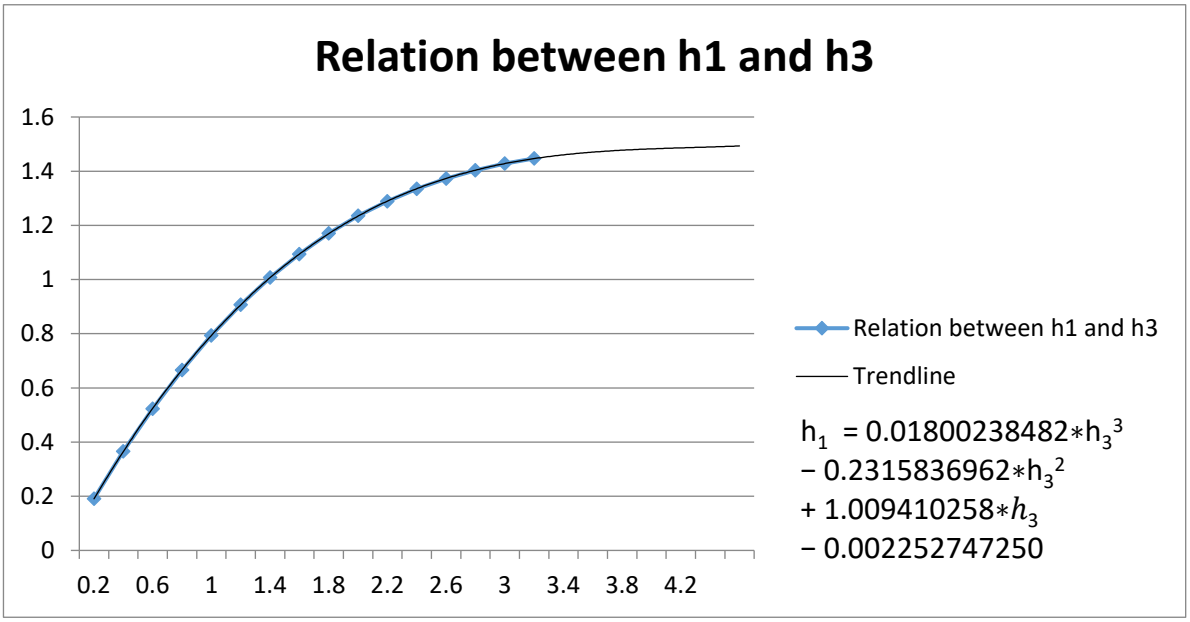


Figure 65 - Relation between $h_1$ and $h_3$

Since the remaining formula is rather unpleasant to work out by hand, Maple is used to solve the equation.

This gives the following result after narrowing down with restrictions regarding h and $h_1$:

$h_1 = 1.4612$ m $h_2 = 1.7388$ m $h_3 = 3.3658$ m

Rerunning the calculation again with the moment capacity before any major deformations take place, $M_{ftmax}$, where $Mp_1 = 3.8374$ kNm, $Mp_2 = 3.6849$ kNm, $Mp_3 = 3.5008$ kNm, gives the following results after applying the same restrictions as before:

$h_1 = 1.4308$ m $h_2 = 1.7692$ m $h_3 = 3.0276$ m

## 8.5 Conclusions

When comparing the first model calculations with the later plastic calculations there are some relatively big differences, see Table 14. With increased realism of the approaches so do the maximum inundation depth increase too. These difference and increases can be largely contributed to the difference in the stress distributions and model schematisations. Since the first and second approach lack a certain degree of realism, the focus will be on the results of the third approach, both computer and hand calculations.

**Table 14 - Overview of h and Mmax for first crack and failure**

| | | h (m) | Mmax (kNm) |
|---|---|---|---|
| First approach | First crack | 1.97 | 2.9 |
| | Failure | 2.43 | 4.5 |
| Second approach | First crack | 2.12 | 2.9 |
| | Failure | 2.65 | 4.6 |
| Third approach (model) | First crack | 3.00 | 3.8 |
| | Failure | 3.35 | 4.6 |
| Third approach (hand) | First crack | 3.03 | 3.8 |
| | Failure | 3.37 | 4.6 |

In order to properly compare both plastic hinge calculations they were done for $M_{max}$ and $M_{ftmax}$. The results are almost the same, for $M_{ftmax}$, $h_3 = 3.35$ m compared to $h_3 = 3.37$ m. And for $M_{max}$, $h_3 = 3.0$ m while the hand calculation gives $h_3 = 3.03$ m. The difference can be explained by the lack of accuracy in the model calculation, $h_3$ is accurate within about 0.05m, while the hand calculation gives a result with an accuracy of several decimals. Besides that the changing circumstances between the model and hand calculation cause small differences such as the relation between $h_1$ and $h_3$ which changes due to the deformations of the cross-sections. And lastly the use of C12/15 as a representative for the properties of masonry. Since both different methods independently give similar results, the results can be taken as fairly accurate.

From this it follows that from the moment the first crack appears the next cracks follow rather quickly but quite some margin is left before the failure load is reached. This means that although failure will be quick and sudden, there is a distinct warning period, which unfortunately will not be visible to the naked eye since the cracks are too small.

# 9 DIANA Model Properties for a Masonry House

The anisotropic behaviour of the construction materials for a masonry house combined with the complexity of the structure itself make it very difficult, if not impossible, to calculate the response of the house to a (complex) load by hand. To be able to do so, a finite element approach provides a solution. For this thesis the finite element program used is DIANA. In order to do the finite element calculations with DIANA, a model needs to be constructed with specific properties. To provide some oversight, the properties which are used for each model are all discussed here. These properties are the model dimensions, load cases, engineering masonry model, element data, elements and tyings. Furthermore the error of the model and the failure criterion used will be explained.

## 9.1 Model Dimensions

The masonry house is modelled in several ways, as a cavity wall and as a single solid wall, with and without windows and door, with and without an inside wall. These options are chosen since most of the house built pre-1930 did not have a cavity wall. However the two walls of the cavity wall will not act as one, since the loads are much higher than the force that the wall ties are able to transfer. A cavity wall of 100 mm thickness will thus be significantly weaker than a single wall of 220 mm thickness.

As stated before the floors planks and beams are constructed out of wood, the wooden floor planks are 21 mm thick and the wooden beams are rectangular with 200mm*50mm. The floor planks are modelled as a sheet and placed at the centre of the beams as to prevent a collaboration between the floor sheet and the beams. This collaboration is not possible since the floor planks are only loosely connected to one another.

In Figure 66, Figure 67, Figure 68 and Figure 69 an overview is provided of the dimensions of the masonry house[72]. These dimensions will be used to perform all analyses and calculations. The ground floor consists of a living room, kitchen and toilet. Furthermore it contains the stairs towards the first floor, with underneath those stairs the fuse box. The first floor consists of a bathroom, two bedrooms, two built-in closets and the stairs towards the attic. This is however too much detail to model, therefore only the outside windows and door are modelled. Of the inside walls only the walls which are between the front and the back of the house are modelled. See the yellow lines in Figure 66 and Figure 67. The inner walls have the same thickness as the cavity walls, 100 mm and this thickness is used in all models with inner walls.

[72] Roos, W. [1]

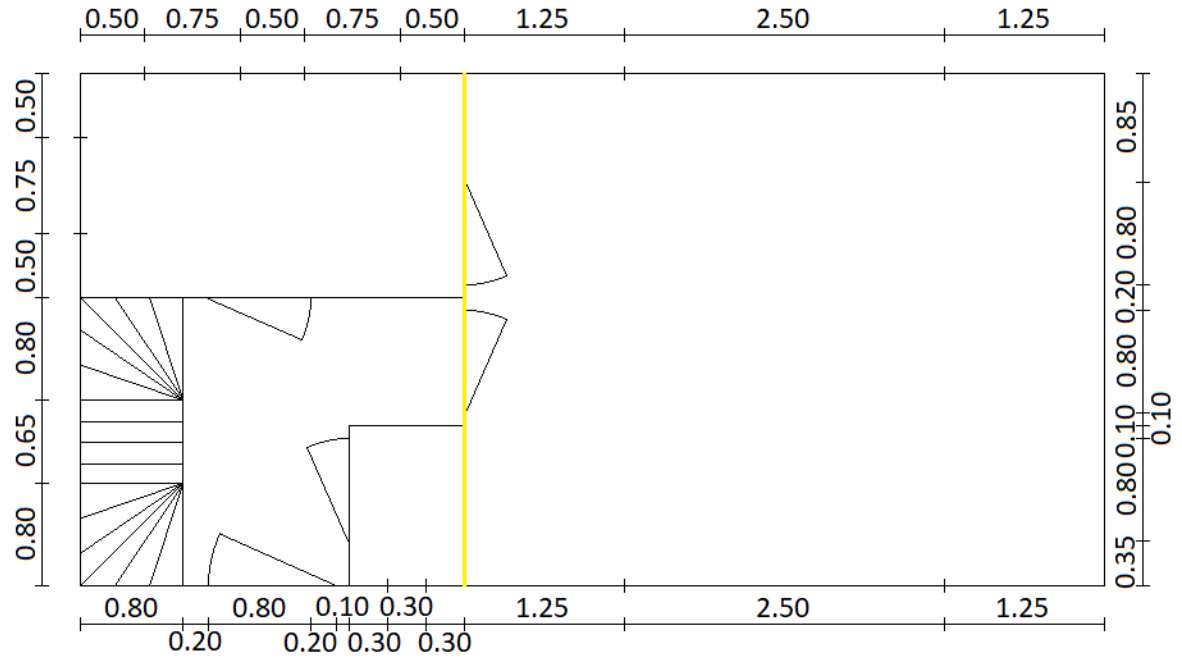


Figure 66 - Ground floor of the masonry house, measurements in metres

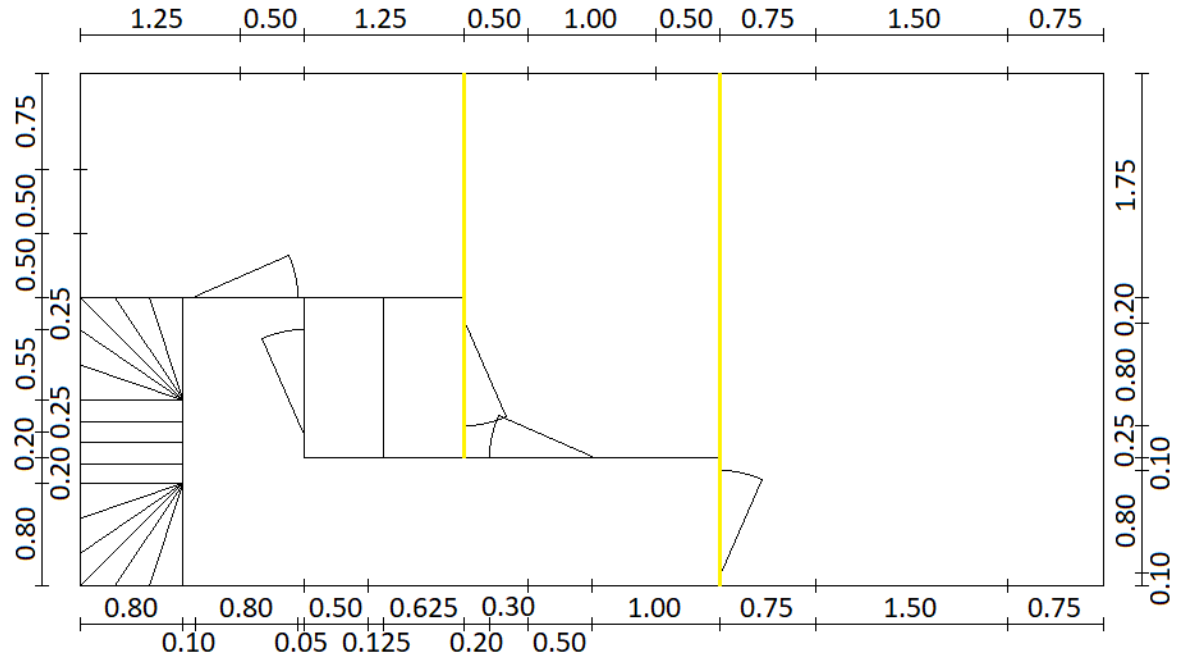


Figure 67 - First floor of the masonry house, measurements in metres

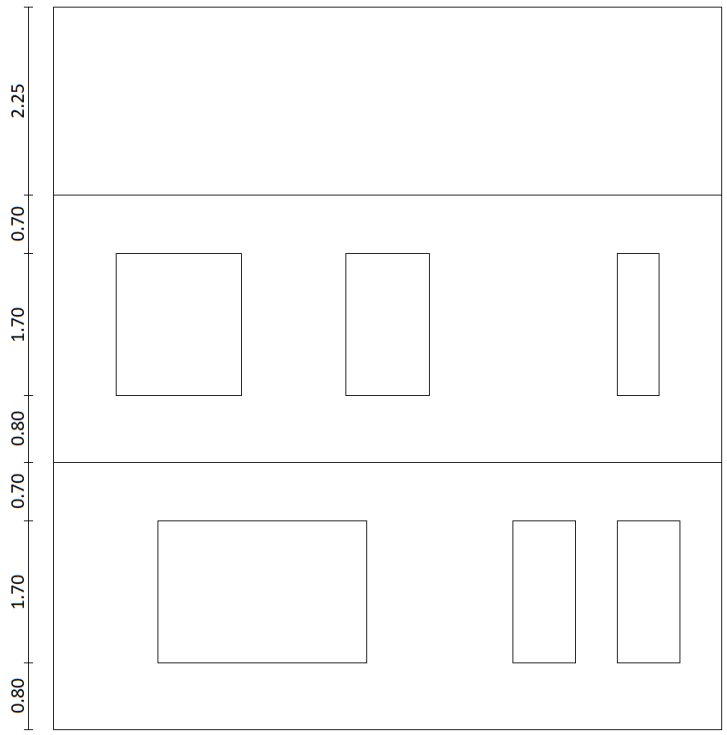


Figure 68 - Front view of the masonry house, measurements in metres

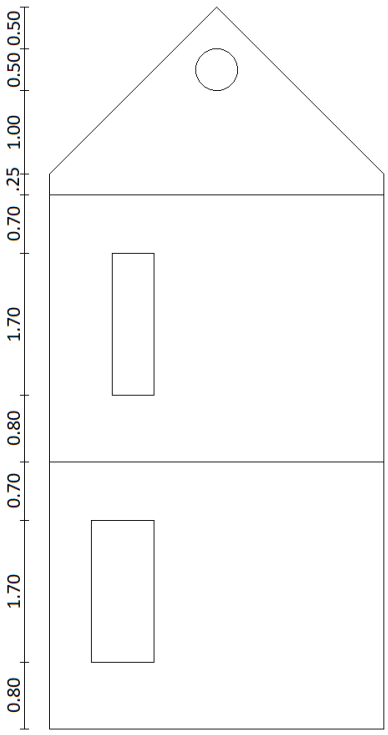


Figure 69 - Side view of the masonry house, measurements in metres

## 9.2 Load Cases

There are two distinct load cases, the hydrostatic pressure after the inundation of the flood area and the bore impact. The dynamic calculations in chapters 10 and 11 are however based on a different distribution, see Appendix K, which has been outdated in the meantime. Redoing all dynamic DIANA calculations would be too time-consuming, unfortunately.

### 9.2.1 Static

For the hydrostatic load case the models will be loaded with increasing inundation depths until, in the end, failure occurs. The hydrostatic and the bore impact pressure distributions are shown in Figure 70.

### 9.2.2 Dynamic

The load for the dynamic bore impact follows from the calculations in chapter 3 and is based on a water level of 1.50 m and a velocity of 10 m/s. To determine the force due to the bore impact the total force formula from 4.6.4.2 is used without inputting the width and with a $\Delta t$ of 0.1 seconds:

$$F_{tot} = \frac{0.543 * \rho * h^2 * u_n}{\Delta t} = \frac{0.543 * 1000 * 1.50^2 * 10}{0.1} = 122175\ (N/m) = 122.2\ (\mathrm{kN/m})$$

The pressure distributions for the bore impact peak over the entire wave height is then scaled using Figure 34. The hydrostatic and the bore impact pressure distributions are shown in Figure 70.

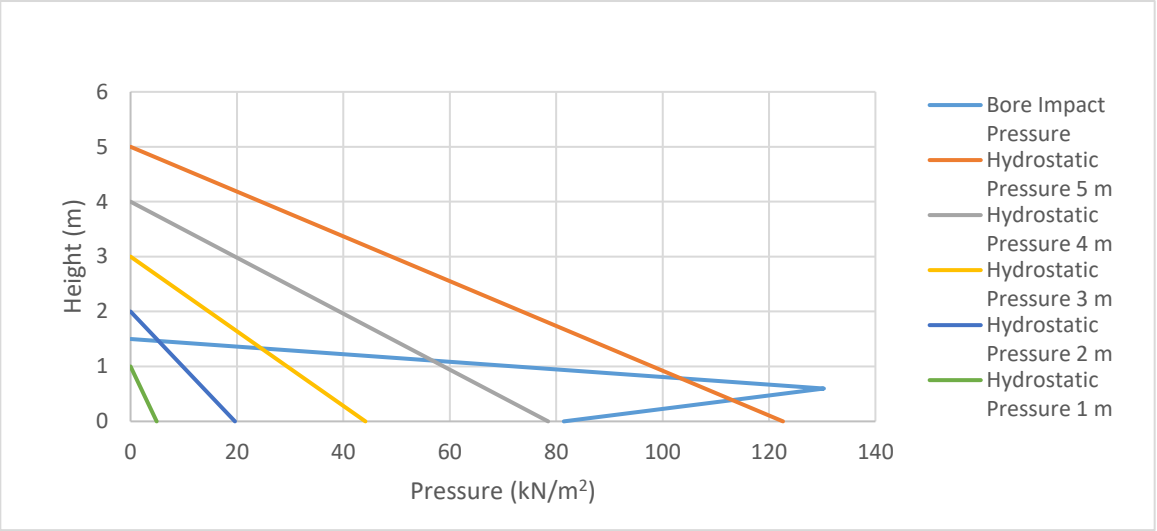


Figure 70 - Modelled Pressure Distribution Bore Impact and Hydrostatic Pressures

Figure 71 and Figure 72 show how these load case will look like in DIANA.

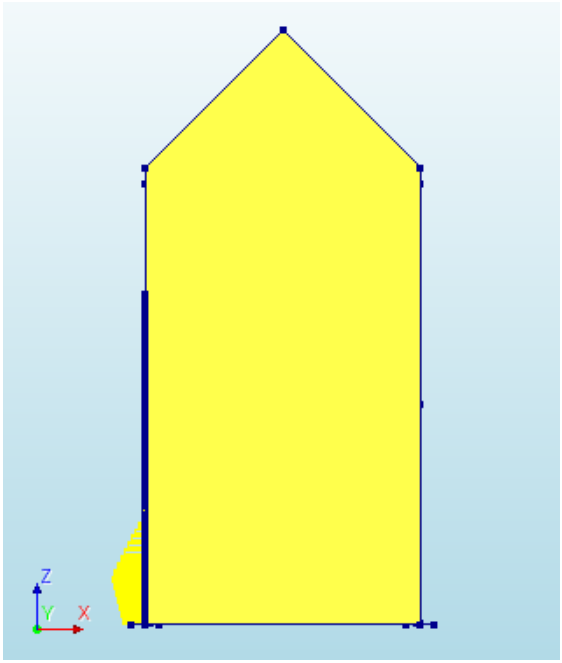

Figure 71 - Bore Impact pressure distribution in DIANA

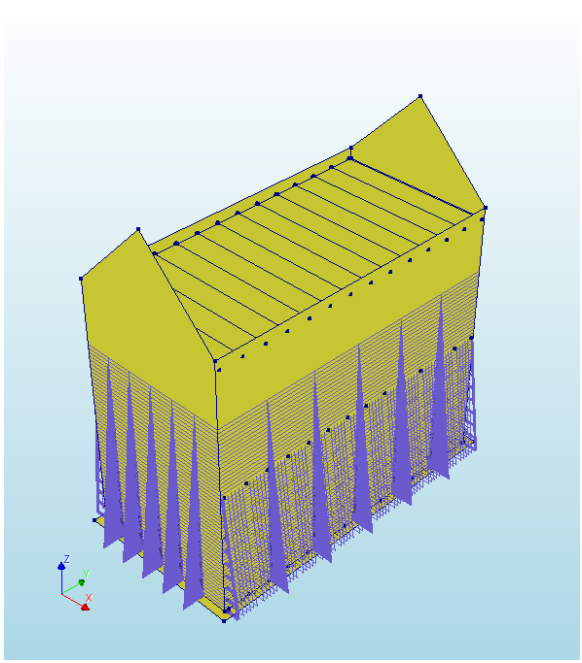

Figure 72 - Hydrostatic pressure distributions in DIANA

## 9.3 Engineering Masonry Model

The Total Strain Crack model in DIANA is used for the failure simulations of brittle materials such as masonry. However, it has two shortcomings, it was derived for isotropic materials, which masonry definitely is not and it underestimates the energy dissipation under cyclic loading. Therefore the Engineering Masonry Model was developed.

The Engineering Masonry Model is a smeared failure model which can be used with either membrane or curved shell elements. The EMM is a continuum model based on total strain. It covers tensile, shear and compressive failure, can crack in the bed-joint and head-joint direction as well as two, user predefined, stair-case cracks. Furthermore it can be orthotropic by using different properties for the two directions.

The model is based on lab tests, defines four potential cracks on each iteration point and uses the active crack procedure. This means it check whether the diagonal cracks are active and if not it

assumes no coupling between the stiffness of the normal components in x- and y-direction and that of the in-plane shear component. Essentially, it assumes a Poisson's ratio of zero.[73]

## 9.4 Elements

Four elements are used, one to model the beams, one for the walls, one for the floors and one for the foundation.

The beams are modelled using class-III 3D beam elements. In contrast to the class-I and class-II beam elements, the class-III beam elements do take shear deformation into account. Furthermore the rotations and displacements of the beam axis normal are independent and interpolated from the nodal rotations and displacements. Although class-II beam elements might suffice as well, class-III beam elements do not require much more computing time and are therefore the better choice.

The walls are modelled using regular curved shells. As mentioned in 9.3, the engineering masonry model has either plane stress or curved shell elements. Plane stress elements are not able to have any loading perpendicular to the element, since for the plane stress elements the stress in this direction has to be zero. The regular curved shell elements however do not have this limitation. Since all the loading is perpendicular to the elements, the regular curved shell elements are used.

The floors are also modelled using regular curved shells. The floor consists of many interconnected planks which essentially form a thin shell. These floor planks are however not connected to each other in a stiff manner and are often connected to the beams with just one or two nails per beam. They will therefore not form a T-beam structure with the beams. To prevent this from happening, the floors are modelled at the same height as the beams, without offset.

The foundation is again modelled using regular curved shells. Although thicker than the floors, the foundation is in essence also a shell, possibly with loading in all directions, therefore the regular curved shell elements are used.

## 9.5 Element Data

In order to accurately perform the non-linear analysis more than the standard 3 layers are required in the thickness direction of the wall. This can be achieved with the THINTE option, thickness integration points. This number of integration points has been set to 7 to be able to accurately perform the required non-linear analysis. An analysis has been performed to determine and confirm that 7 integration points will suffice, see Appendix H.

## 9.6 Tyings

In reality the floor beams are placed on top of the walls. Although they are connected to the walls, this connection is approximately fully hinged, especially in the up/down direction of the beam. In order to make sure that the connection between the beams and the walls is hinged, they are connected using tyings. A tying connects a master point to a slave point, the slave point receives its translations and rotations directly from the master point. By only connecting the translations, the rotations are kept free and thus the connection is hinged. To prevent model instabilities the beams have to be supported for the rotations in the two none hinged directions, this is done by adding a support to all beams for those rotations.

[73] Rots et al. [57]

## 9.7 Error

The error mentioned to indicate the trustworthiness of the results, is the relative displacement variation, of course, smaller is better.

$$Displacement\ norm\ ratio = \frac{\sqrt{\delta u_i^T * \delta u_i}}{\sqrt{\Delta u_0^T * \Delta u_0}}$$

In which $u_0$ is the displacement of the first prediction and $u_i$ is the displacement of the $i^{th}$ iteration. If it is not specifically specified, this displacement norm is evaluated for each element. The result displayed by DIANA is the average of the elements evaluated. It is therefore possible that local failure is missed if there is a large number of elements performing well within the norm. Local failure could also skew the results, if the opposite is true, a relatively small amount of elements and a large deviation in the elements of the local failure.[74]

## 9.8 Failure Criterion

In order to determine when structural damage occurs, most importantly when failure occurs, a failure criterion is needed. This criterion is needed in order to interpret the results from the DIANA calculations. The simplest criterion would be displacement based, i.e. failure occurs when a certain displacement is reached. However, masonry is brittle and therefore failure might occur at different displacement magnitudes. What does fit with a brittle material is a rapid increase in displacement when nearing or at failure. Therefore, the point where the displacements start to increase rapidly, is chosen as the failure point. Of course, rapid is a relative term and some interpretation is still required. To aid in the determination of this failure point, it helps to remember that when a brittle material starts to fail, the load hardly increases if not decreases. Thus, the rapid increase of the displacement can be coupled with a flattening of the load vs displacement curves.

Keep in mind that the accuracy of the calculations themselves or lack thereof, might make it difficult to determine an exact failure point or load.

## 9.9 Eigen Frequencies

The loads all have a frequency, an overview of all the wave frequencies was given in Figure 20 (chapter 4). However not only the loads but the house also has an Eigen frequency. If there is a repeating load and both frequencies are very near each other, resonance will occur amplifying the effect of the load. Therefore, the Eigen frequencies of the house have been determined using the DIANA model. These frequencies do vary somewhat between the different cases and walls. However, the biggest difference is between the single solid and cavity wall in general. Overall, they are between about 10 and 20 Hz, where around 20 Hz is only for the side walls and around 10 Hz for the front and back walls as well as part of the side walls.

Besides the difference in frequency also the part of the walls engaged in a certain frequency varies. The cavity walls do not necessarily engage the entire wall, the single solid walls do engage the entire walls due to the increased stiffness of the walls themselves.

An overview of the main patterns and frequencies is given in Figure 73, Figure 74, Figure 75 and Figure 76.

[74] DIANA Manual [60]

As is clear from Figure 20 there are normally speaking no waves with a load near 10-20 Hz. The impulse peak from the bore impact does have a time factor of about 10 Hz, however that is only the impact peak and the actual time of that peak is debatable. Depending on the accuracy of the measurements and the load itself, it can be anywhere between approximately 2-1000 Hz. Since this peak loads the house only once, resonance is not expected to be of any concern. Although resonance is not expected to be of any concern it is advised to determine a dynamic amplification factor to scale the load, if need be. For this thesis however, this is not taken into account.

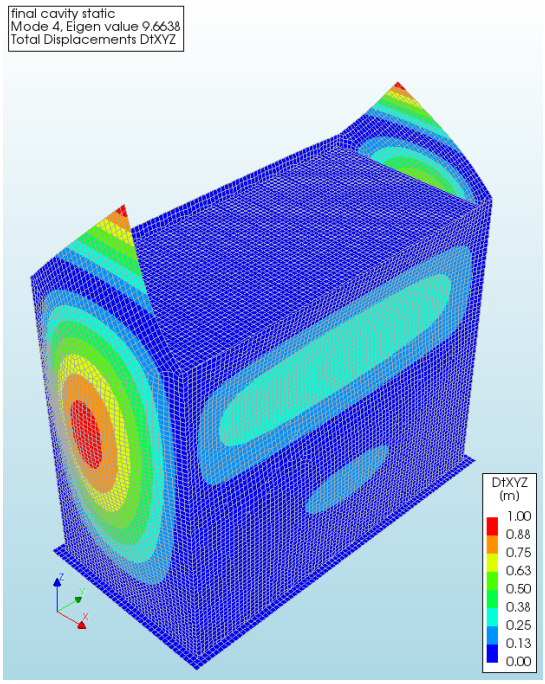


Figure 73 - Eigen frequency for the side walls of the Cavity Wall Masonry House

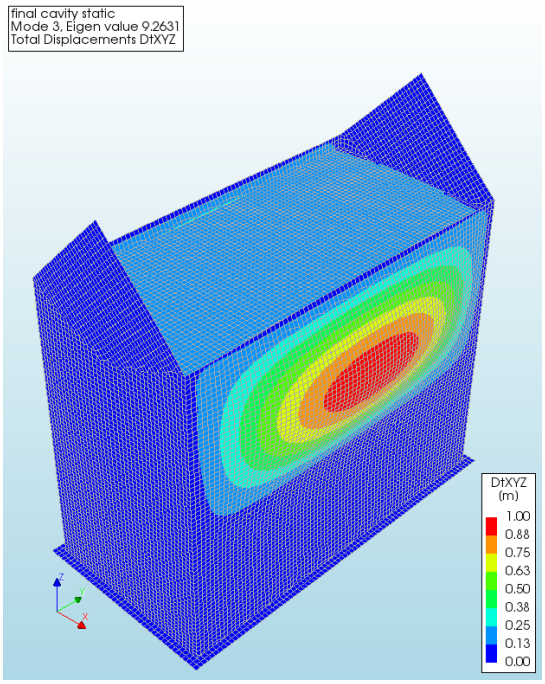


Figure 74 - Eigen frequency for the front and back walls of the Cavity Wall Masonry House

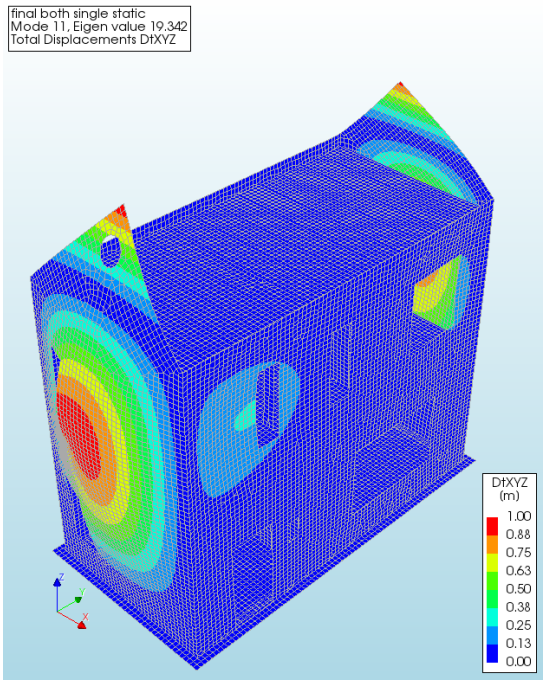


Figure 75 - Eigen frequency for the side walls of the Single Wall Masonry House with Door, Windows and Inner Walls

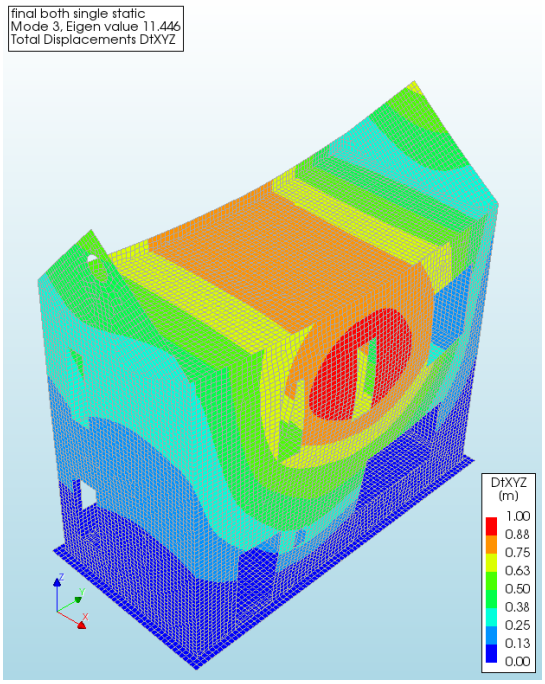


Figure 76 - Eigen frequency for the front and back walls of the Single Wall Masonry House with Door, Windows and Inner Walls

# 10 Diana Calculations of a Masonry House with a Cavity Wall

The DIANA calculations have been split into 2 main groups. The first group is the calculations regarding a masonry house with a cavity wall, those are treated in this chapter. The second group regards the calculations of a masonry house with a single wall, treated in chapter 11.

Next the calculation will increase in detail, first only the foundation, outer walls and floors are modelled. One by one, extra details will be added, door and windows, inner walls and a combination of both.

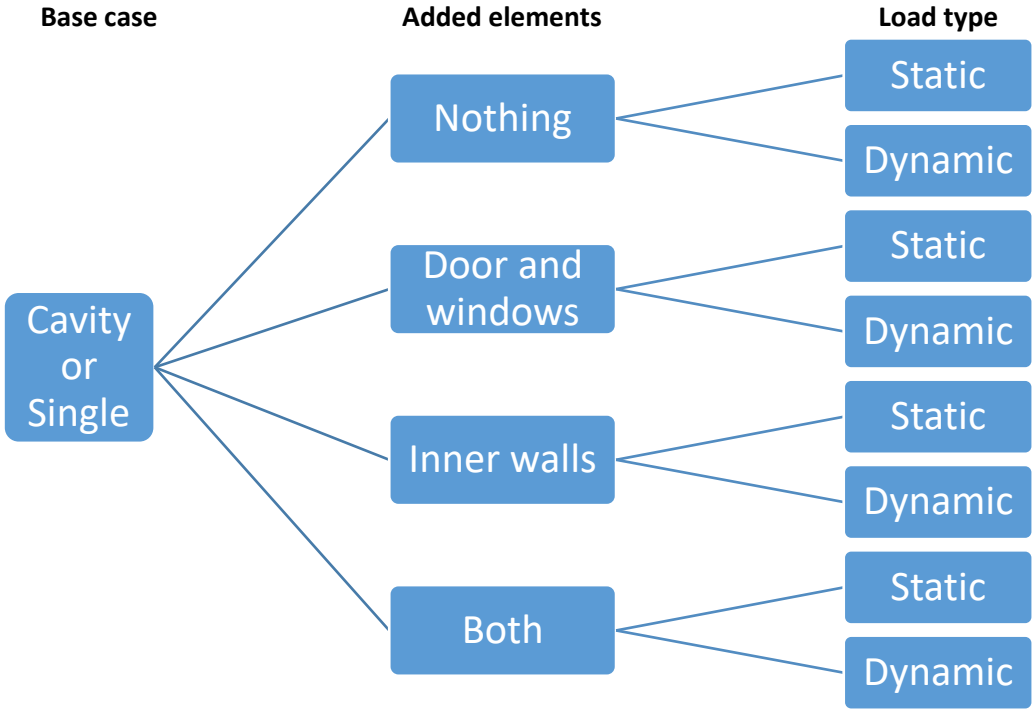


Figure 77 - Overview of the different cases

Only one wall is displayed in the figures to keep the results as clear and readable as possible. If not stated otherwise the displacement at a certain point is the maximum displacement of that wall. A description and image of the displacements and crack widths, is given for the first case to give an idea of the occurring patterns. For an (elaborate) description of the displacements and crack width and their patterns for each case, see Appendix I.

## 10.1 Masonry House

The simplest model, the masonry house with a cavity wall.

### 10.1.1 Static

The cavity wall house has been loaded with a rising water level until it failed. The first cracks started at an inundation depth of approximately 1.0 m. This corresponds with the second-last green dot in Figure 78. The load then still increases and failure occurs between approximately 2.0 and 2.5 m. The maximum displacement of the walls at the three points are respectively 0.65 mm, 3.0 mm and 11.2 mm. Even though those last results are reasonably inaccurate, since convergence did not occur and the error was 0.547, they are used to show the patterns that do occur. The errors due to convergence not being met, will be discussed at each point.

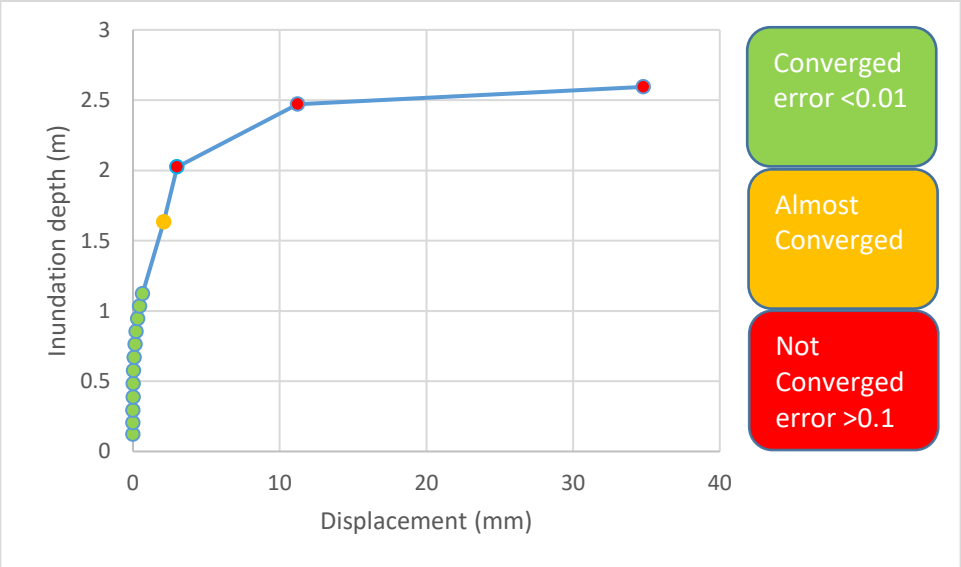


Figure 78 - Inundation depth vs Displacement of the Cavity Wall Masonry House due to the static load

Figure 79 and Figure 80 show the displacements of the house. As is especially visible in Figure 80 there is a sharp bend in the displacements, the locations of the cracks.

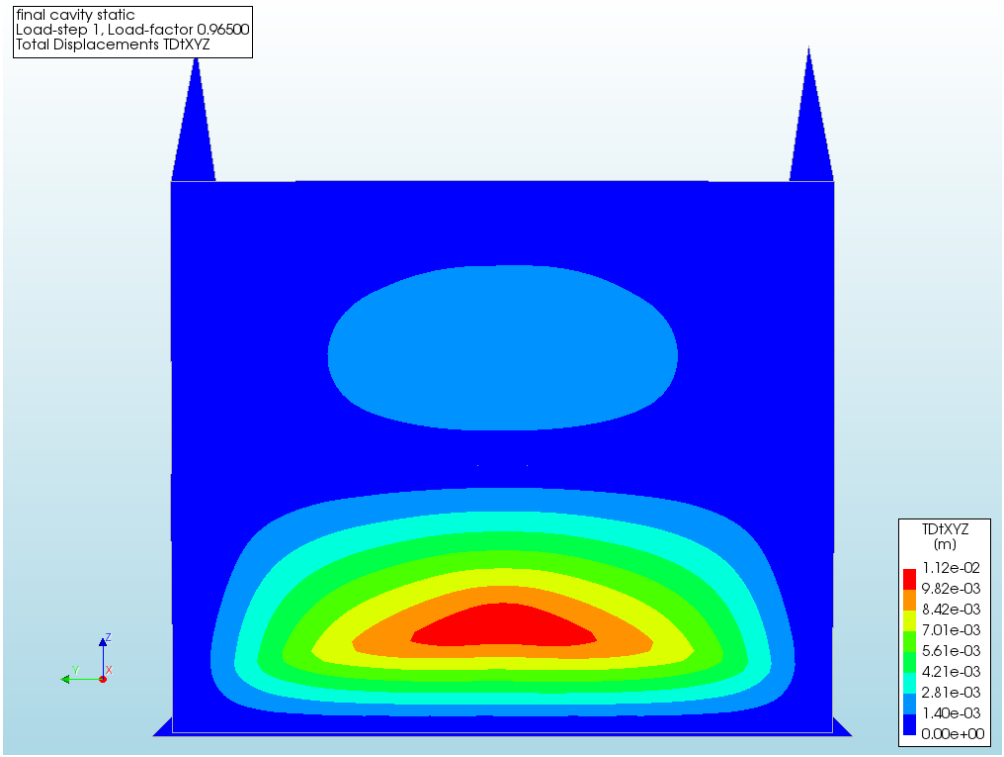


Figure 79 - Displacement of the Cavity Wall Masonry House due to the static load, 2.5 m, front view

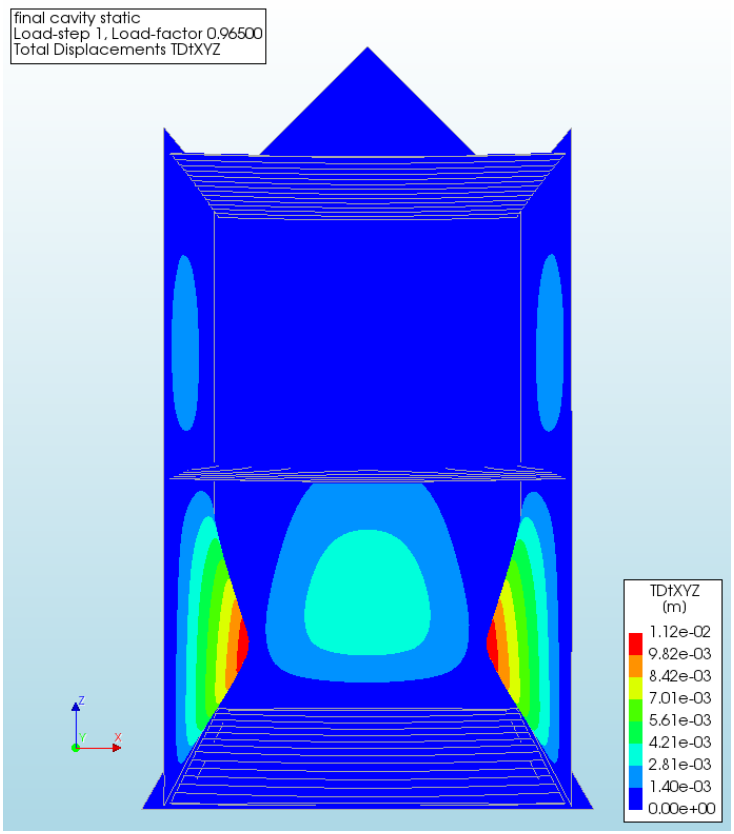


Figure 80 - Displacement of the Cavity Wall Masonry House due to the static load, 2.5 m, side view

Figure 81 shows the crack widths at the inside of the wall, here there are cracks at the middle of the wall, up to several millimetre. Figure 82 shows the crack widths at the outside of the wall, the cracks here are located at the bottom and are also up to several millimetre. Notice that the upper part of the wall has also started to crack. This fits with the deflections seen in Figure 79 and Figure 80.

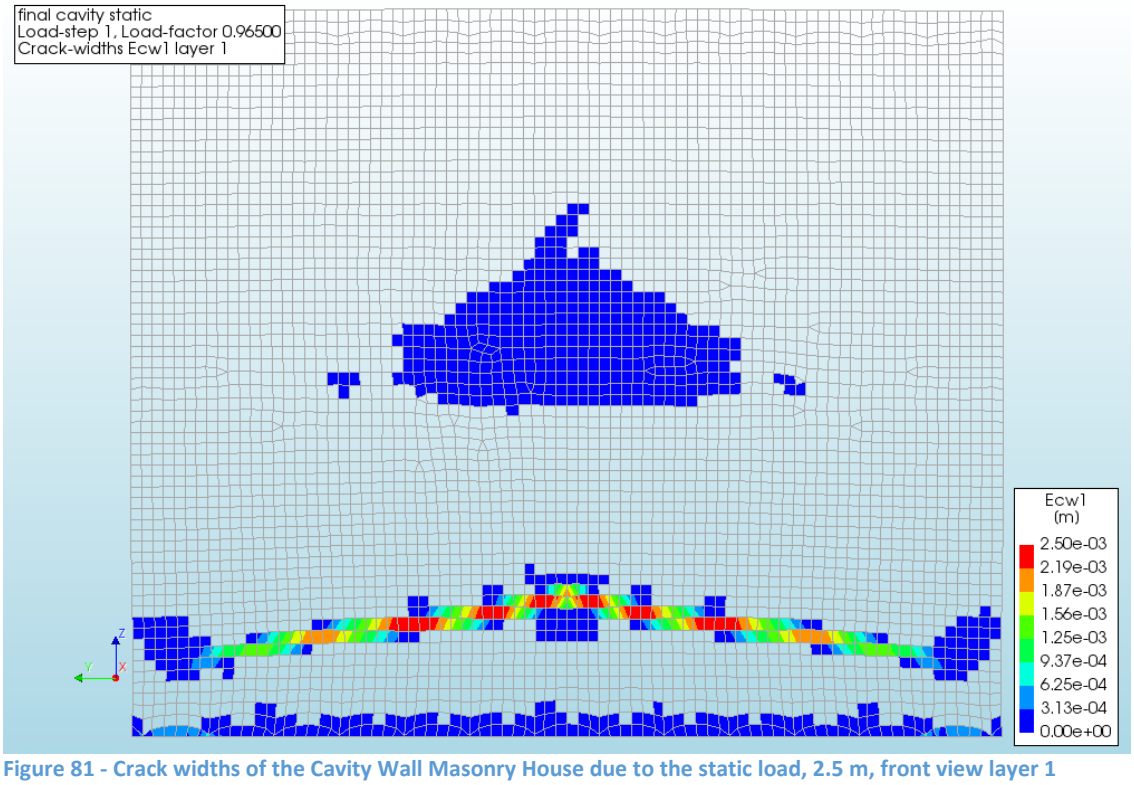


Figure 81 - Crack widths of the Cavity Wall Masonry House due to the static load, 2.5 m, front view layer 1

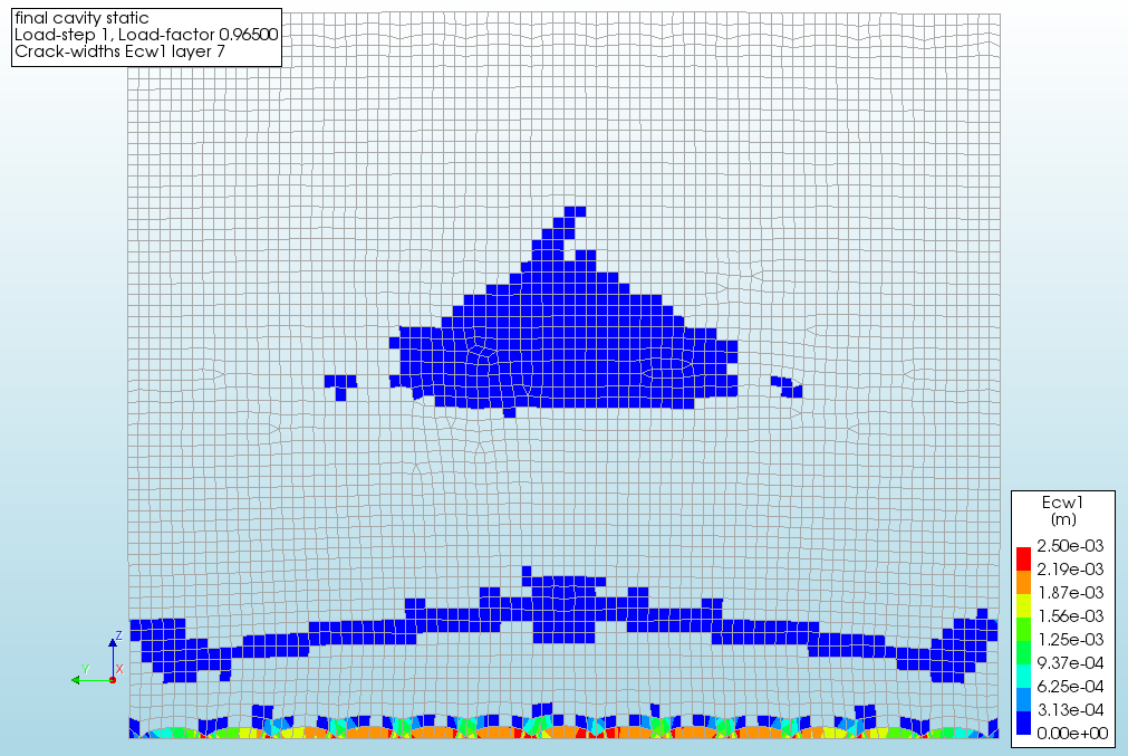


Figure 82 - Crack widths of the Cavity Wall Masonry House due to the static load, 2.5 m, front view layer 7

The cracking locations and relative sizes fit well with the expected results from the preliminary calculations from chapter 8. The largest moments where at the bottom, causing the first and largest cracks to be situated there. Next follows the middle of the wall, since in the calculations performed here, the wall is not restricted by the first floor. It is thus able to rotate, decreasing the stresses, strains and thus crack widths at that location.

### 10.1.2 Dynamic

The masonry house has been loaded with the dynamic load case as defined in 9.2. Convergence only occurred until 0.7% of the actual load, the maximum deflection at that point was 1.0 mm see Figure 83. No convergence is reached for the next steps up to the final 'Almost Converged' step at 1.8% of the load. The error, however, of this final 'Almost Converged' step is 0.021. The results are, therefore, still fairly accurate. Failure seems to occur between this 1.8% and 2.0% of the total load.

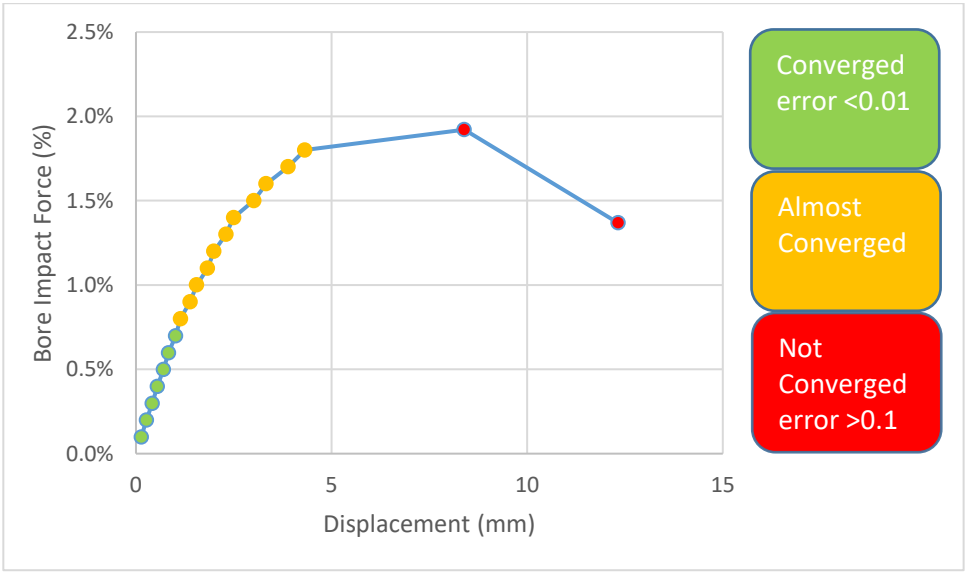


Figure 83 - Bore Impact Force vs Displacement of the Cavity Wall Masonry House due to the dynamic load

Figure 83 and Figure 84 show the displacement of the house at 1.8% of the dynamic load. As can be seen the entire ground floor wall is deformed and via the first floor causes the second wall to deform as well. The second wall provides some additional strength to the first wall in this way.

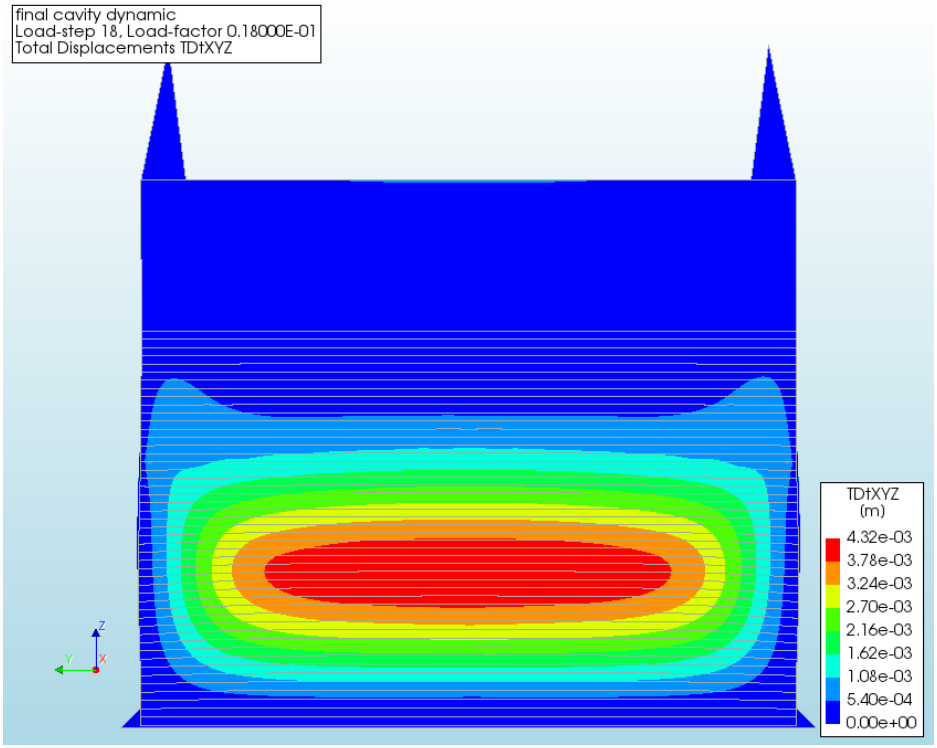


Figure 84 - Displacement of the Cavity Wall Masonry due to the dynamic load at 1.8%, front view

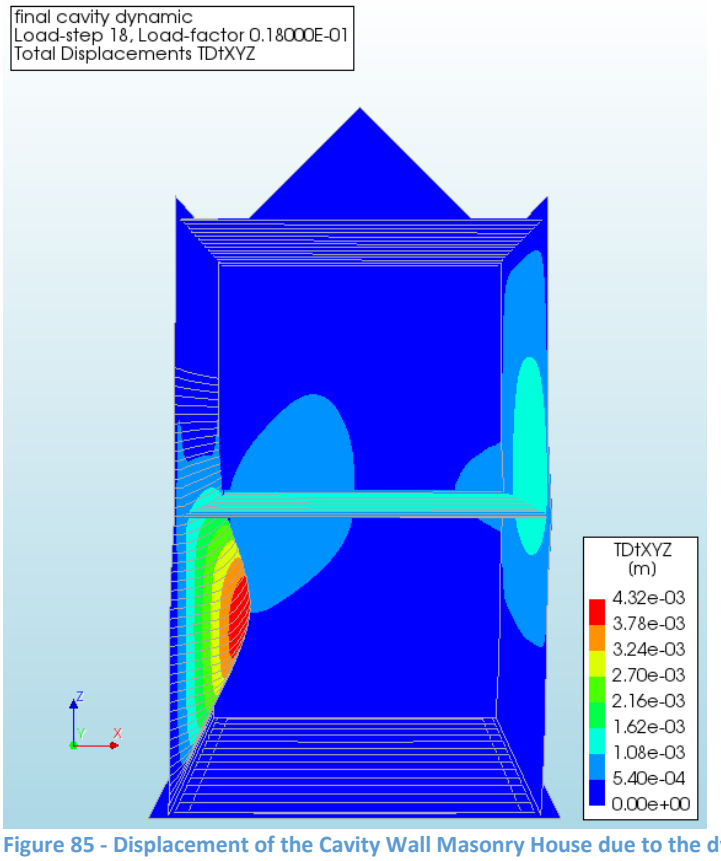


Figure 85 - Displacement of the Cavity Wall Masonry House due to the dynamic load at 1.8%, side view

Although the magnitude of the displacements is not yet very large, only 4-5mm, significant cracks have already formed. Figure 86 and Figure 87 show the crack widths which already reach beyond 1 millimetre. As expected, the largest cracks are located at the bottom, followed by the middle and the top of the ground floor.

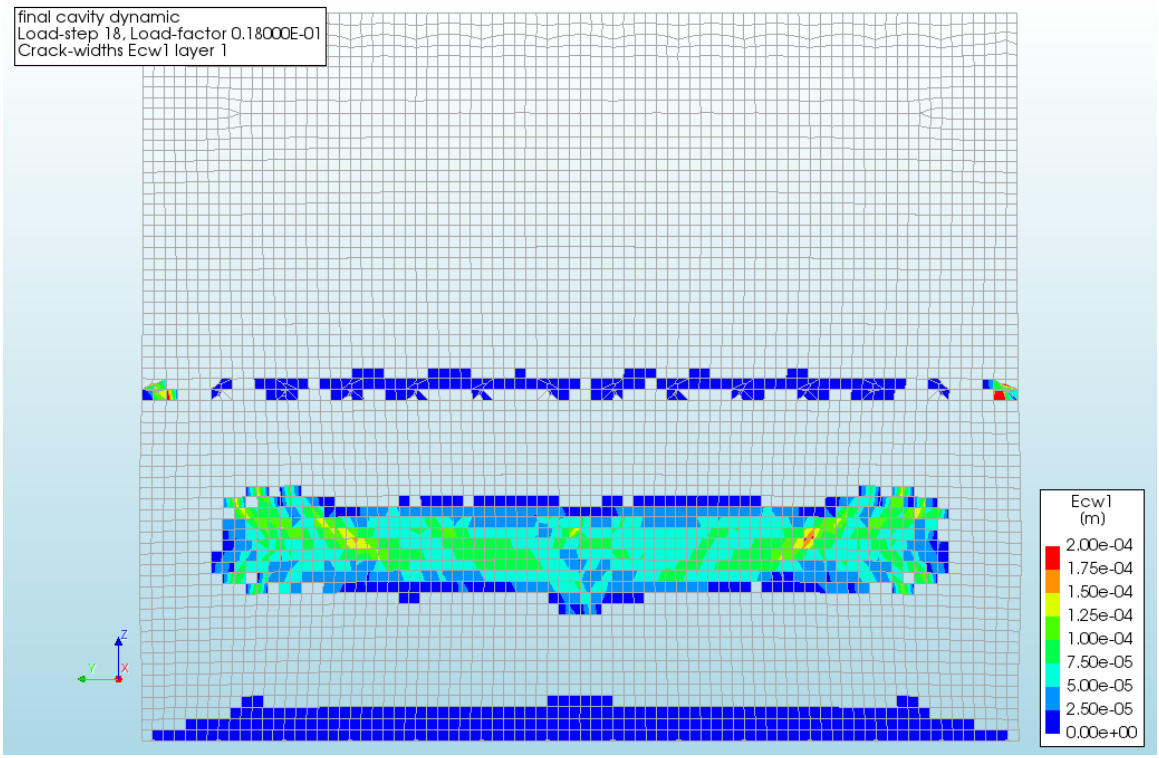


Figure 86 - Crack widths of the Cavity Wall Masonry House due to the dynamic load at 1.8%, front view layer 1

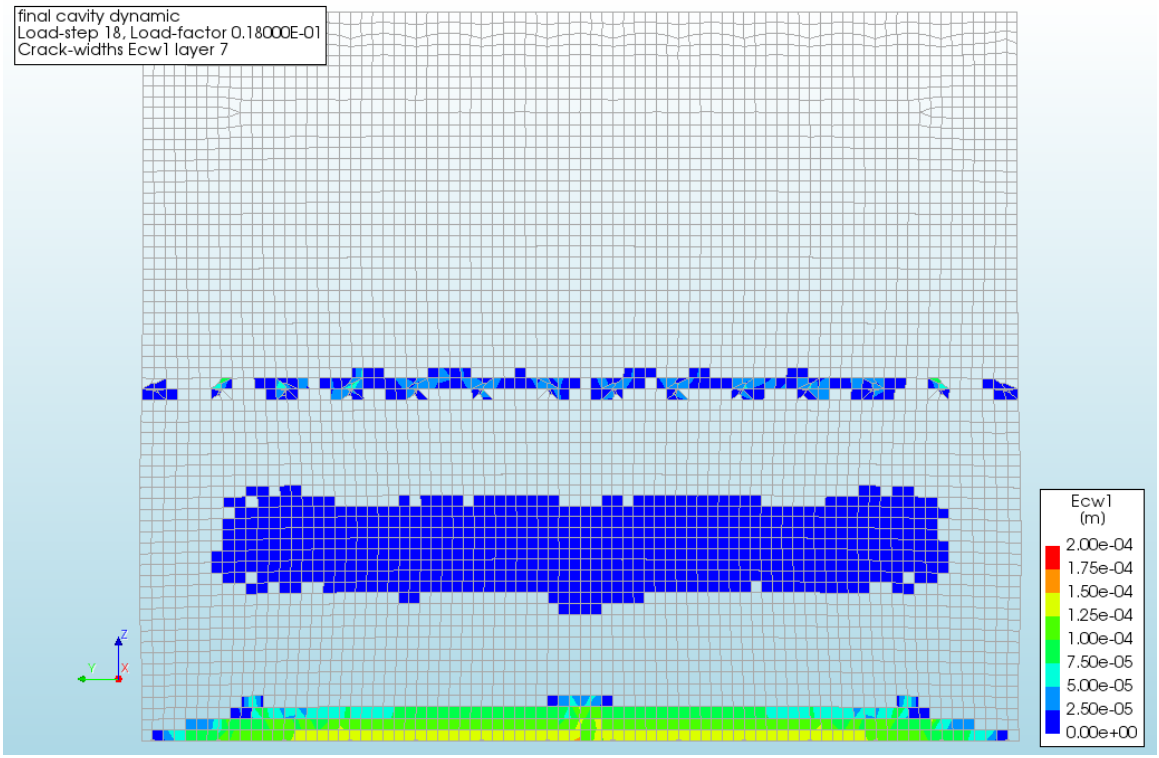


Figure 87 - Crack widths of the Cavity Wall Masonry House due to the dynamic load at 1.8%, front view layer 7

## 10.2 Masonry House with Door and Windows

Increasing the complexity and realism of the model a little, door and windows are added as holes in the walls. The removal of these section from the walls is expected to cause a decrease in the resistance, since smaller sections of the wall will have to carry the same load.

### 10.2.1 Static

Loaded with a rising water level, see Figure 88, first damage occurred at an inundation depth of approximately 1.75 m. The load then increases until collapse, which occurs between an inundation depth of 2.35-2.85 m. This corresponds with the second and third 'Not Converged' steps in Figure 88. However, since the desired cracking and deformation patterns already occur at the first 'Not Converged' step, this first step, with an error of 0.155, is used. Although there is a lack of accuracy, the cracking and deformation patterns overall are fairly accurate. These patterns are not yet visible in the last 'Converged' step. Due to the lack of accuracy it is not possible to determine whether or not a decrease has taken place in the resistance compared to 10.1.1.

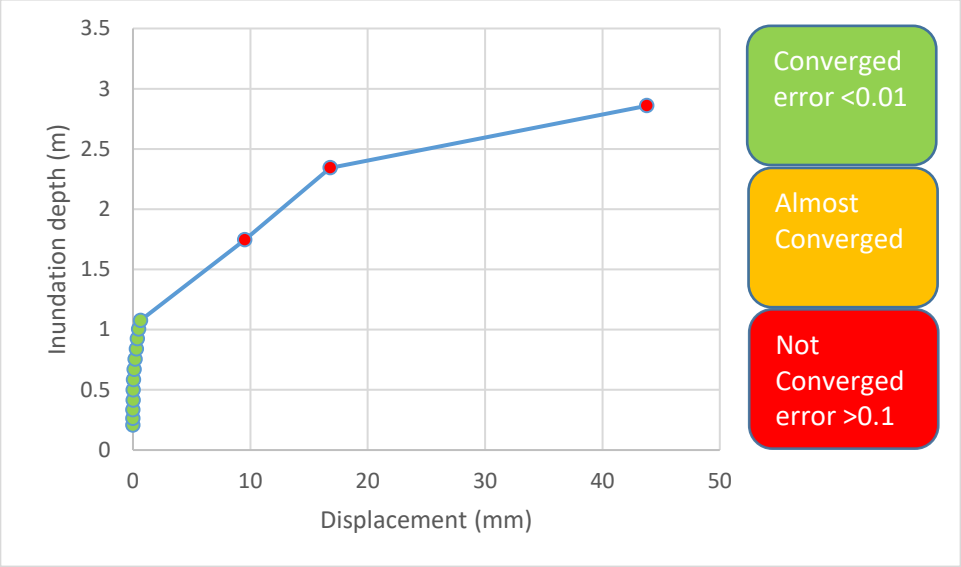


**Figure 88 - Inundation depth vs Displacement of the Cavity Wall Masonry House with Door and Windows due to the static load**

### 10.2.2 Dynamic

Loaded with the dynamic load, the displacement increased until collapse at about 1.6% of the total dynamic load, see Figure 89. The displacement and cracking patterns are already visible at the last 'Almost Converged' step. The error of this last 'Almost Converged' step is 0.029, which makes those results still fairly accurate. As expected the total load slightly decreased compared to 10.1.2.

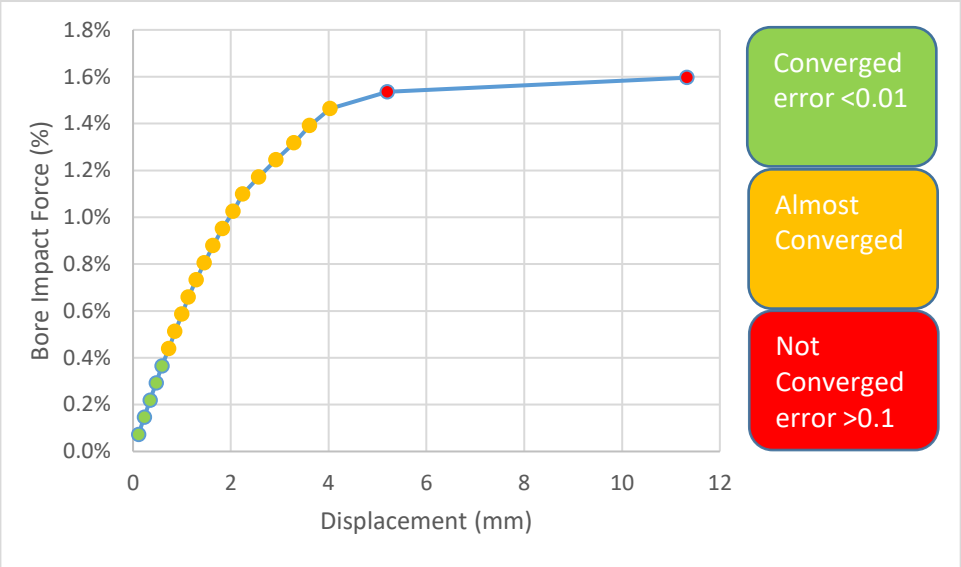


Figure 89 - Bore Impact Force vs Displacement of the Cavity Wall Masonry House with Door and Windows due to the dynamic load

## 10.3 Masonry House with Inner Walls

Again, the complexity is increased, compared to the first, simple model, inner walls have been added. These should provide some out of plane support to the front walls and thus increase their resistance.

### 10.3.1 Static

Again, the model has been loaded with a rising water level. The final 'Almost Converged' step, see Figure 90, already clearly shows the locations of the displacements and cracks. The error of the final 'Almost Converged' step is 0.089, which makes those results still reasonably accurate, especially regarding the patterns. When comparing Figure 90 to Figure 78, there is hardly an increase in the maximum inundation depth. Although the inner wall does provide out of plane support, the remaining width of the wall is still sufficient to cause similar results. Since this remaining width is still larger than the width of the side walls, the front wall is still leading.

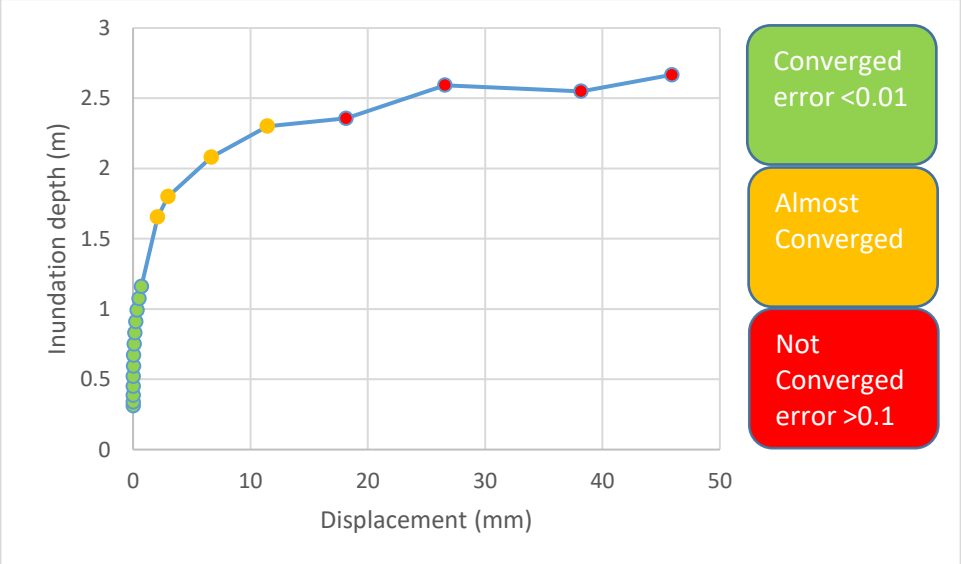


Figure 90 - Inundation depth vs Displacement of the Cavity Wall Masonry House with Inner Walls due to the static load

### 10.3.2 Dynamic

The model is now loaded with the dynamic load until failure. Compared to 10.1.2, a small increase in resistance is expected due to the inner walls. The last 'Almost Converged' step already matches this expectation, see Figure 91 and Figure 83. The house then proceeds to fail, but due to the inaccuracy of the results, the exact load could not be determined. The error of the final 'Almost Converged' step is 0.035, which makes those results still fairly accurate. The error of the following two steps, however, are 0.568 and 0.159 respectively. The expected failure load is expected to be between 2.25-2.75% of the total dynamic load.

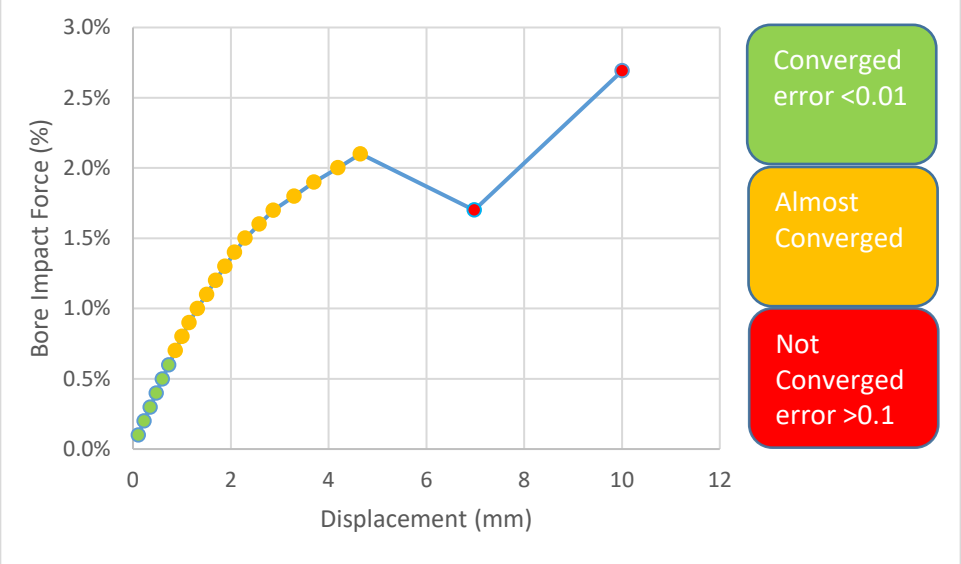


**Figure 91 - Bore Impact Force vs Displacement of the Cavity Wall Masonry House with Inner Walls due to the dynamic load**

## 10.4 Masonry House with Door, Windows and Inner Walls

The final model combines both the door and windows as well as the inner walls. Whether or not this will cause an increase or decrease in the resistance compared to 10.1 is difficult to determine beforehand. One measure seems to increase the resistance, while the other decreases the resistance.

### 10.4.1 Static

Here there are two situations to be shown, the point where first damage occurs and the point where structural collapse occurs.

For first damage the last 'Almost Converged' step from Figure 92 is used. The error of the final 'Almost Converged' step is 0.086, which makes those results still reasonably accurate.

For the point where structural collapse occurs, the last 'Not Converged' step of Figure 93 is used. The error of this 'Not Converged' step is 0.638, which makes those results not very accurate at all. However, the inaccuracy mainly seems to follow for a significant part from the large deflections at the large living room window and the side wall, see Figure 215 in Appendix I. This side wall experiences at this point a load due to an inundation depth of approximately 6.3 m compared to the 3.4 for the front wall.

The side wall fails at an earlier load step but at a higher load, ~4-5 m, between the first and second 'Not Converged' step in Figure 94. These have an error of 0.185 and 0.312 respectively, which is not very accurate. The results are, however, significantly higher than those for the front wall, thus the front wall is leading.

With regard to 10.1.1, damage near the large window seems to occur at the same time. Collapse however seems to increase from about 2.5 m to 3.4 m.

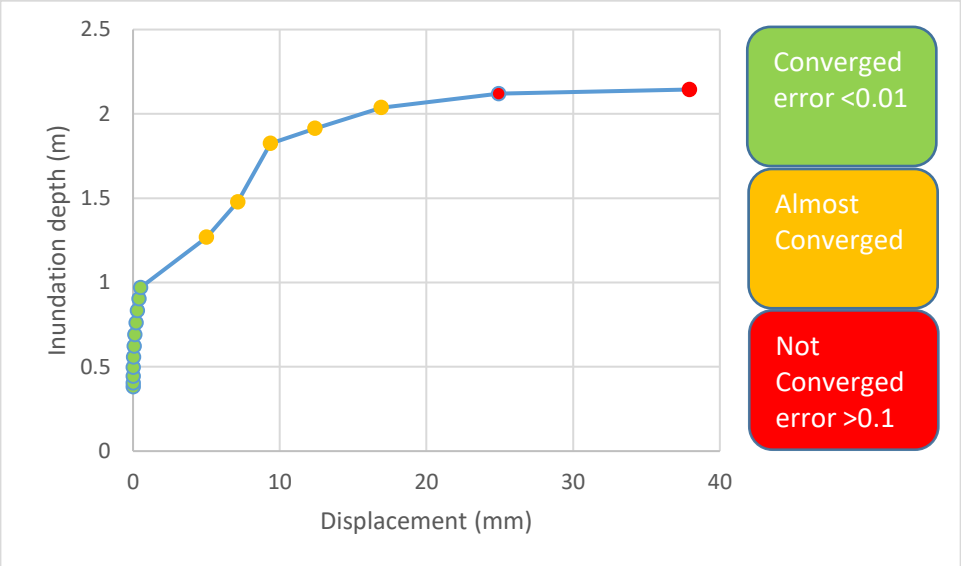


Figure 92 - Inundation depth vs Displacement of the Cavity Wall Masonry House with Door, Windows and Inner Walls due to the static load, entire wall

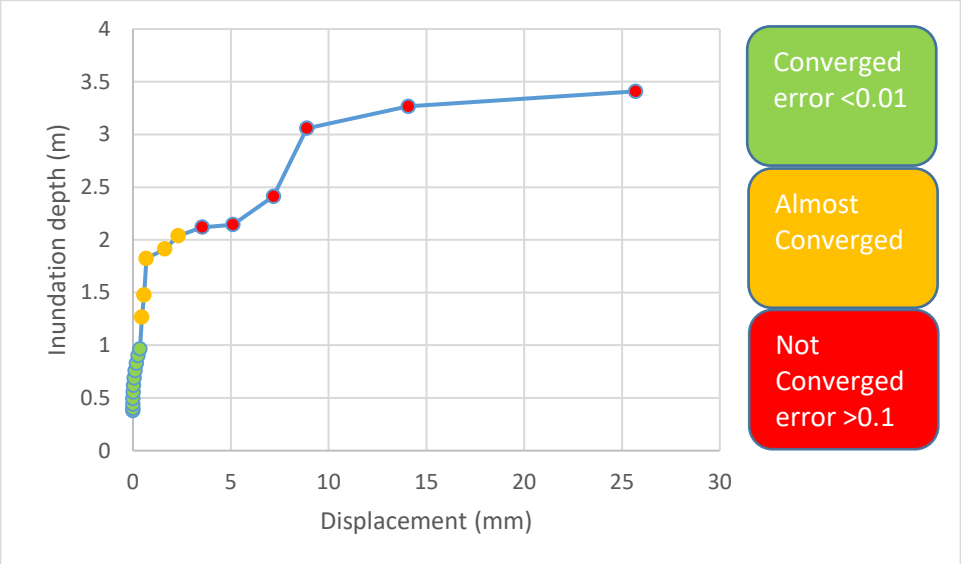


Figure 93 - Inundation depth vs Displacement of the Cavity Wall Masonry House with Door, Windows and Inner Walls due to the static load, section of the wall

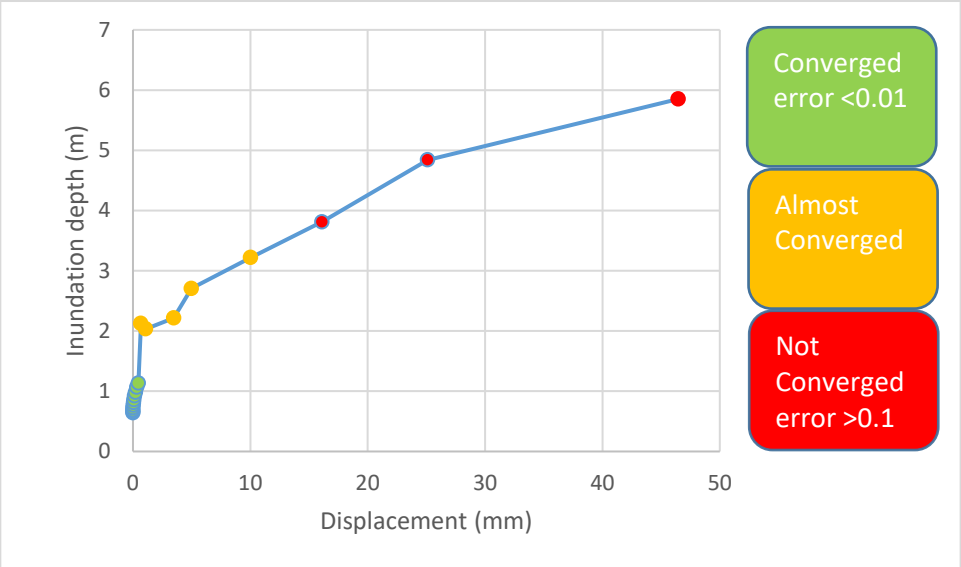


Figure 94 - Inundation depth vs Displacement of the Cavity Wall Masonry House with Door, Windows and Inner Walls due to the static load, side wall

### 10.4.2 Dynamic

Again, the model is loaded with the dynamic load until failure. The error of the final 'Almost Converged' step is 0.034, which makes those results still fairly accurate. The next step has an error of 0.238, which makes it much less trustworthy. The actual maximum load is therefore somewhat difficult to determine, it is expected to be between 2.0-2.5% of the total dynamic load. This makes it weaker than the case with just the inner walls, but stronger than both the other cases.

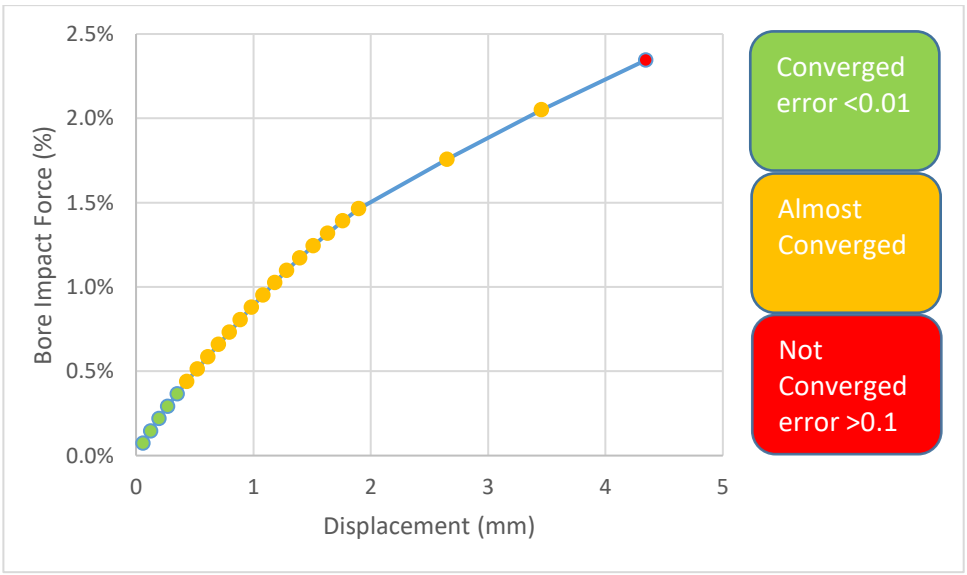


Figure 95 - Bore Impact Force vs Displacement of the Cavity Wall Masonry House with Door, Windows and Inner Walls due to the dynamic load

## 10.5 Conclusions

Four different cases have been investigated for the dynamic and static load. Each case added some complexity and realism to the original model, windows, door and inner walls. These changes also caused differences in the results.

Table 15 - Summary of the estimated failure loads of the Cavity Wall Masonry House

| | Failure load static (m) | Failure load dynamic (%) |
|---|---|---|
| **Original** | 2.0-2.5 | 1.8-2.0 |
| **Door and Windows** | 2.35-2.85 | 1.5-1.6 |
| **Inner Walls** | 2.4-2.6 | 2.25-2.75 |
| **Door, Windows and Inner Walls** | 3.2-3.6 | 2.0-2.5 |

Table 15 shows for the static load that each extra element raises the failure load, increases the accuracy or does both. Especially the combination of door, windows and inner walls increases the failure load tremendously.

For the dynamic load this is not the case, the introduction of door and windows causes a decrease of the failure load. The inner walls do cause a significant increase of the failure load but decrease the accuracy. Combining both, an increase of the failure load compared to the original case is observed at the cost of accuracy.

These results seem partially contradictory, an increase in one case is coupled with a decrease in another and vice versa. Where the door and windows caused a decrease in the maximum load for the dynamic load, there was an increase for the static load. The inner walls caused an increase in the maximum load for both loads. However, for the static load, the increase is only marginal, whereas for the dynamic load the increase is 20-40%. The combined case, door, windows and inner walls caused an increase with regard to the starting case, no door, windows and inner walls, for both loads. For the dynamic load however, there was a decrease with regard to just the inner walls.

The most logical conclusion for these phenomena, is the height at which the loads act on the house. The door and especially the windows are located at the same height as the maximum dynamic load. The maximum static load however is at the bottom of the wall, and therefore is less affected by these door and windows. The inner walls have a larger effect on the dynamic load for the same reason.

# 11 Diana Calculations of a Masonry House with a Single Solid Wall

As mentioned in chapter 10, the DIANA calculations have been split into 2 main groups. The first group is the calculations regarding a masonry house with a cavity wall, those are treated in chapter 10. The second group regards the calculations of a masonry house with a single wall, treated in this chapter.

Next the calculation will increase in detail, first only the foundation, outer walls and floors are modelled. One by one, extra details will be added, door and windows, inner walls and a combination of both, see Figure 77 in chapter 10 for an overview of all the cases.

Only one wall is displayed in the figures to keep the results as clear and readable as possible. If not stated otherwise the displacement at a certain point is the maximum displacement of that wall. A description and image of the displacements and crack widths is given for the first case to give an idea of the occurring patterns. For an (elaborate) description of the displacements and crack width and their patterns for each case, see Appendix J.

## 11.1 Masonry House

A variation on the simplest model, the masonry house with a single wall.

### 11.1.1 Static

The single solid wall house has been loaded with a rising water level until it failed. The first cracks started at an inundation depth of approximately 2.0 m. This corresponds with the last green dot before the first orange dot in Figure 96. The last point of convergence is at an inundation depth of about 3.2 m. The load then still increases until approximately 3.6 m, where the convergence criteria is almost met, the error is 0.061. The wall is definitely cracked at this stage and therefore this point is used for the figures in this paragraph. The maximum deflection of the wall at 2.0 m, 3.2 m and 3.6 m inundation depth are respectively 0.65 mm, 1.78 mm and 4.69 mm. Failure of the wall is most likely to occur between an inundation depth of 4-5 m.

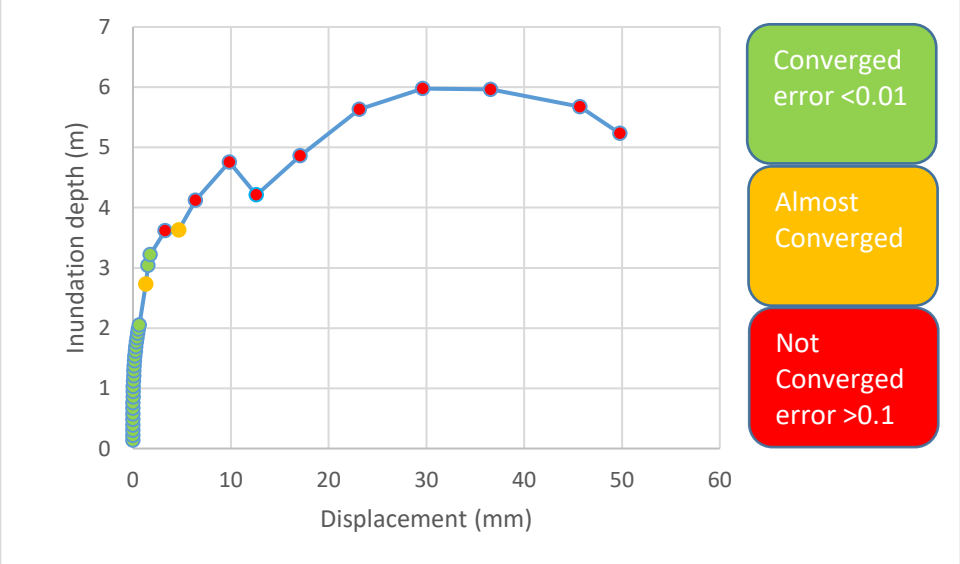


Figure 96 – Inundation depth vs Displacement of the Single Wall Masonry House due to the static load

Figure 97 and Figure 98 show the displacements of the house for all parts. The deflection of the floors is still high compared to the deflection of the walls, which is due to their self-weight and the relatively small deflection overall. Pattern wise they are nearly identical to Figure 79 and Figure 80.

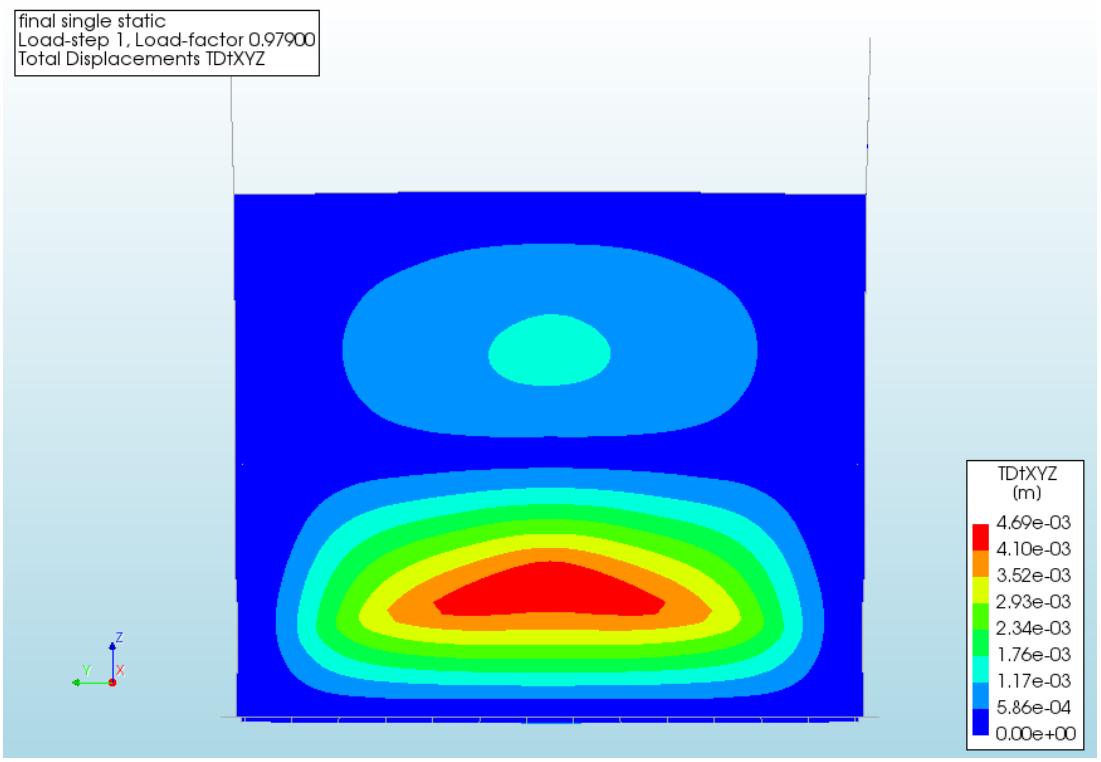


Figure 97 - Displacement of the Single Wall Masonry House due to the static load, 3.6 m, front view

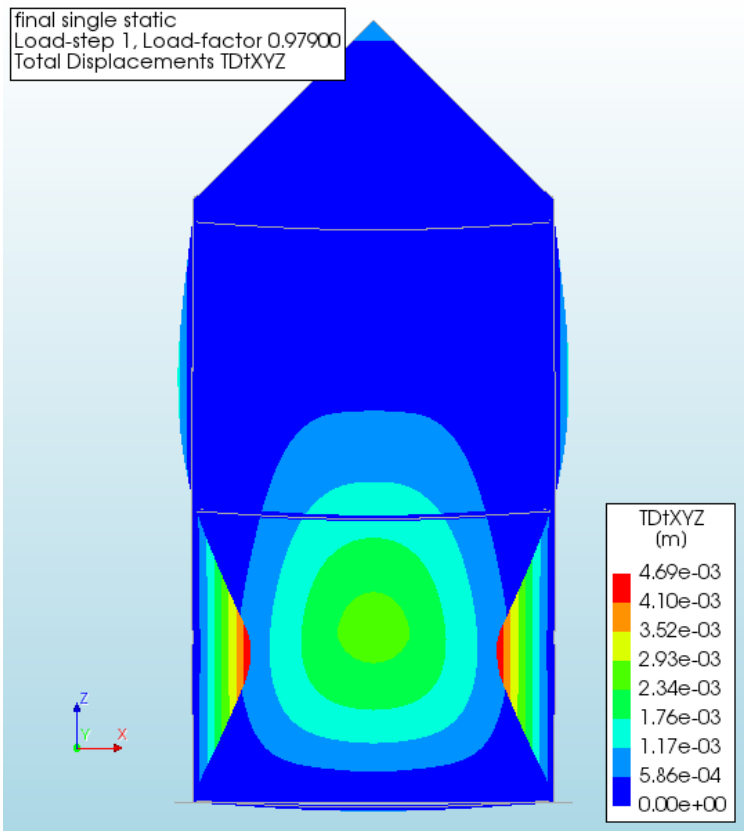


Figure 98 - Displacement of the Single Wall Masonry House due to the static load, 3.6 m, side view

Figure 99 shows the crack widths at the inside of the wall, here there are cracks at the middle of the wall which are up to several millimetre. Figure 100 shows the crack widths at the outside of the wall, the cracks here are located at the bottom and are also up to several millimetre. Notice that the upper

part of the wall has also started to crack. This fits with the deflections seen in Figure 97 and Figure 98. These patterns are as expected and are nearly identical to Figure 81 and Figure 82.

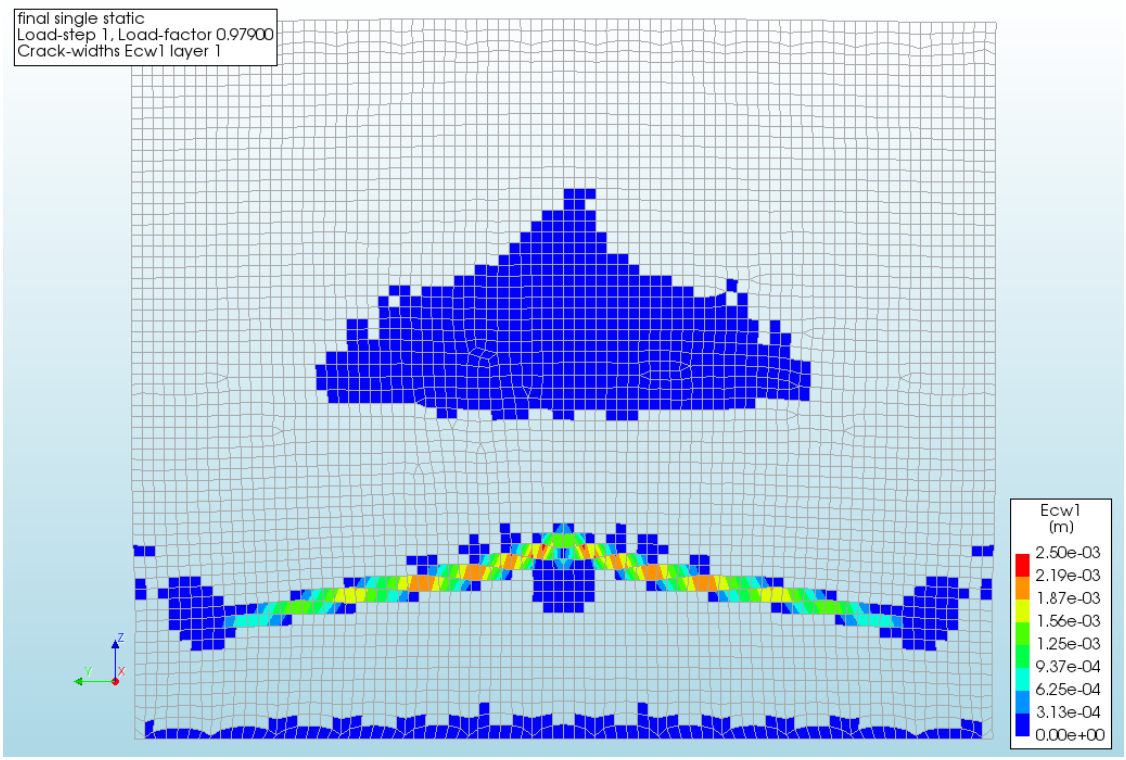


Figure 99 - Crack widths of the Single Wall Masonry House due to the static load, 3.6 m, front view layer 1

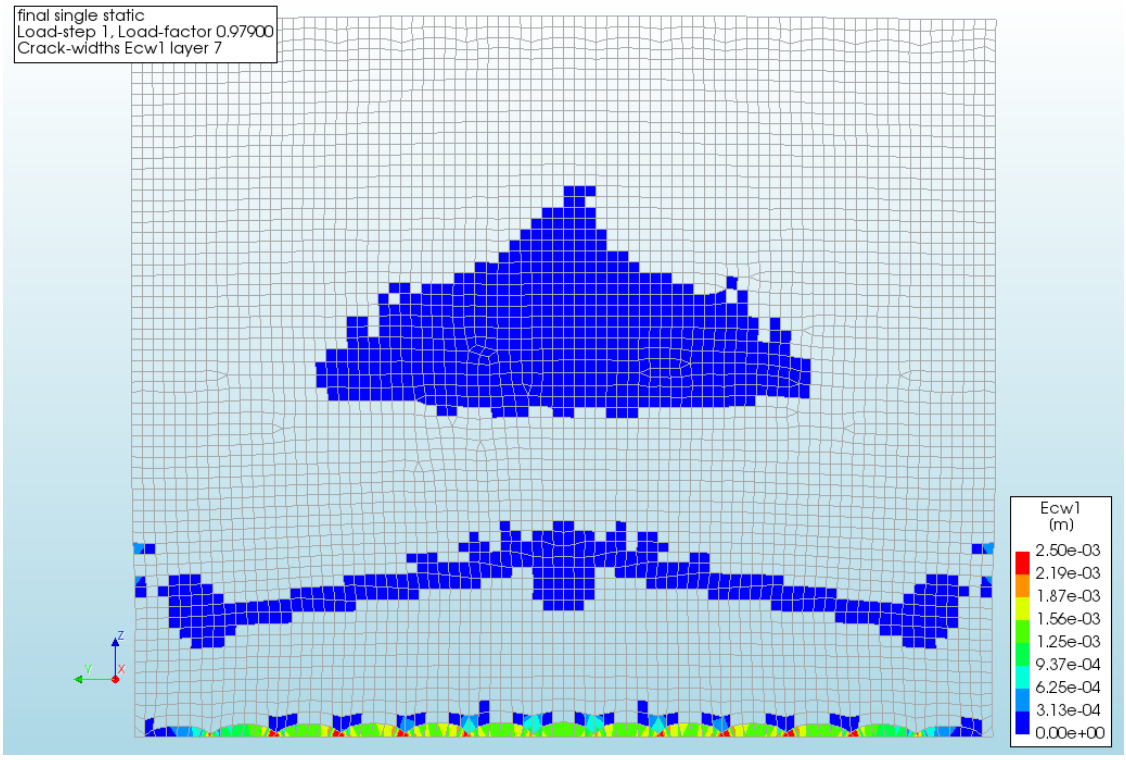


Figure 100 - Crack widths of the Single Wall Masonry House due to the static load, 3.6 m, front view layer 7

The cracking locations and relative sizes fit well with the expected results from the preliminary calculations from chapter 8. The largest moments where at the bottom, causing the first and largest cracks to be situated there. Next follows the middle of the wall since in the calculations performed

here, the wall is not restricted by the first floor and is thus able to rotate decreasing the stresses, strains and thus crack widths at that location.

### 11.1.2 Dynamic

The single wall masonry house has been loaded with the dynamic load case. As was the case in 10.1.2, convergence only occurred for a small part of the steps. Most of the following steps however were very close to the convergence criterion. The first 'Not Converged' step indicates the point where the first major cracks appear, at the bottom of the wall. The load then increases until not only the bottom of the ground floor wall crack, but also the middle and top. This happens at the second 'Not Converged' step, with an error of 0.102. Although the error is significant, the previous steps do support its credibility and displacement and cracking patterns are somewhat better visible in this step than in previous steps. Collapse has not yet occurred at this point, but is expected to have occurred at approximately 5.5-6% of the total dynamic load. Although this cannot be said certainly due to the increased model inaccuracies.

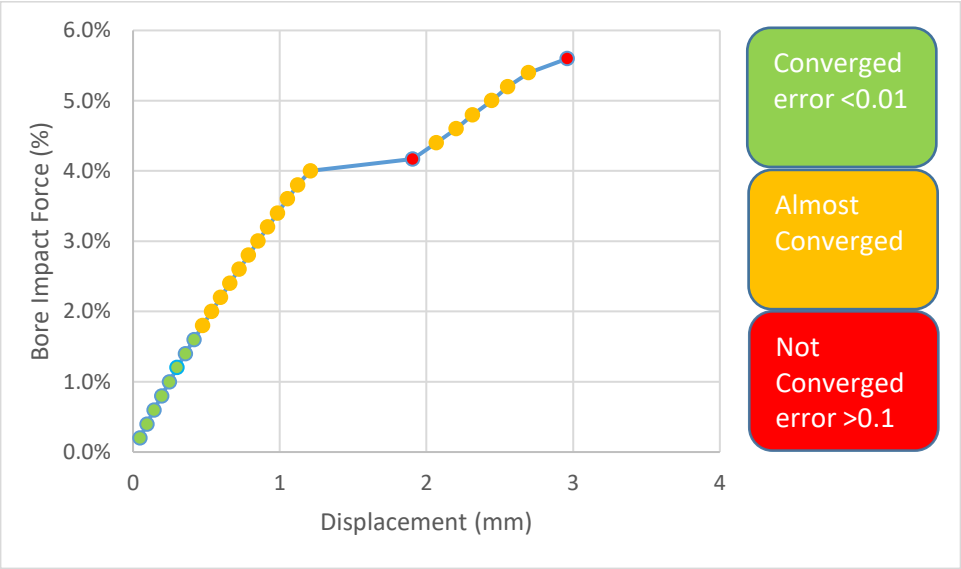


Figure 101 - Bore Impact Force vs Displacement of the Single Wall Masonry House due to the dynamic load

Figure 102 and Figure 103 show the displacement of the single wall masonry house at 5.6% of the dynamic load. These show still a large degree of cooperation between the front and back wall. With increased loading, patterns more like Figure 84 and Figure 85 are expected, where the front ground floor wall experiences the main displacements.

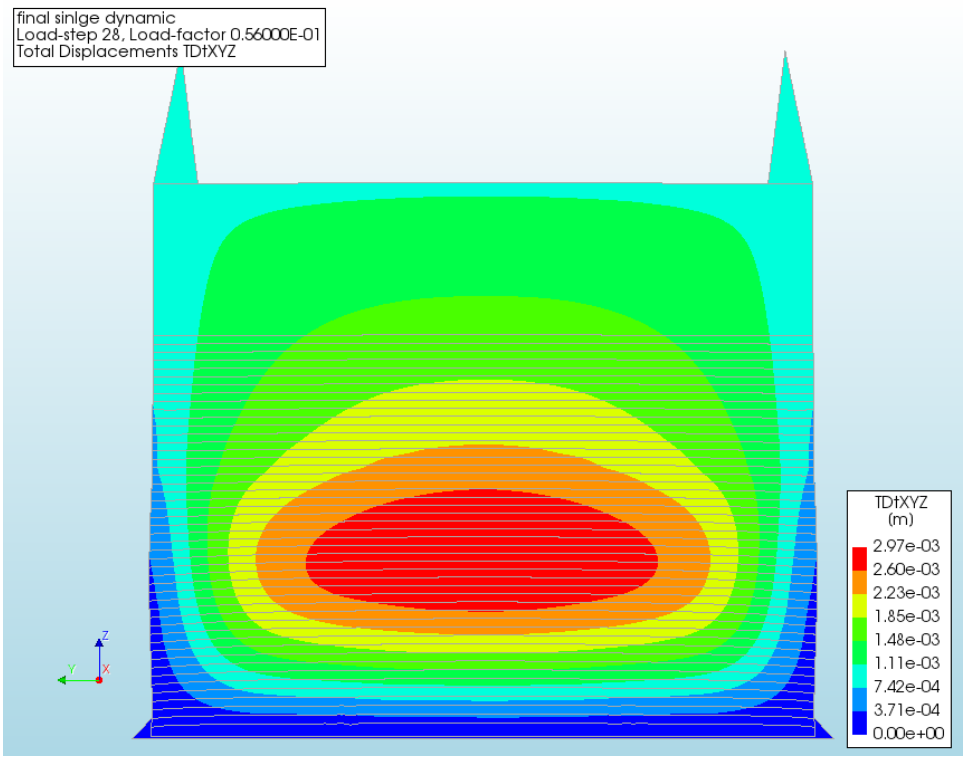


Figure 102 - Displacement of the Cavity Wall Masonry due to the dynamic load at 5.6%, front view

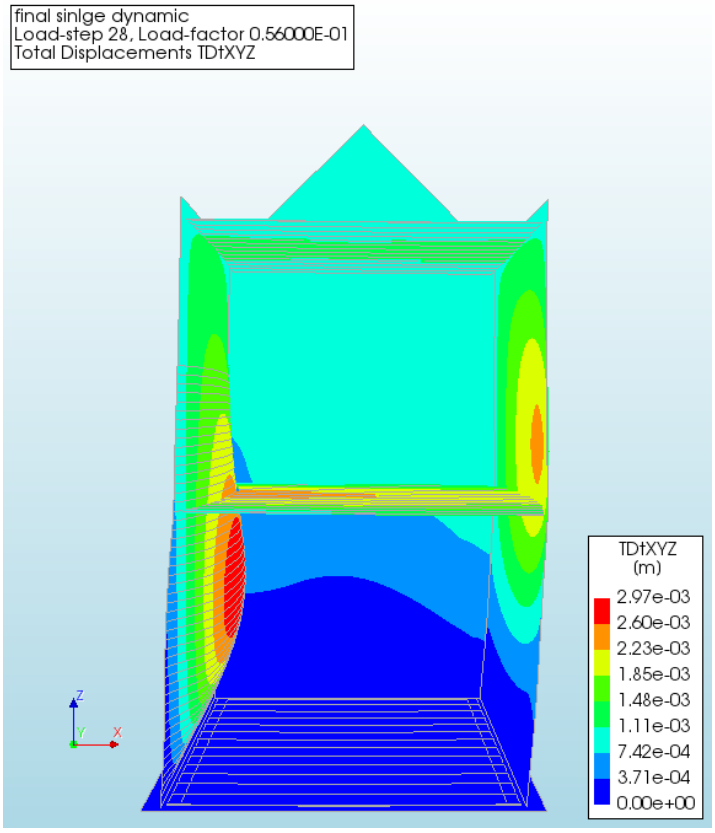


Figure 103 - Displacement of the Cavity Wall Masonry due to the dynamic load at 5.6%, side view

The patterns of the crack widths in Figure 104 and Figure 105 follow the expectations. However, there is still a distinct difference in the size of the crack widths. This fits with the wall not yet having completely cracked, the cracks at the bottom are still far larger than the crack at the middle of the ground floor wall. Cracks at the top of the ground floor wall are not yet present.

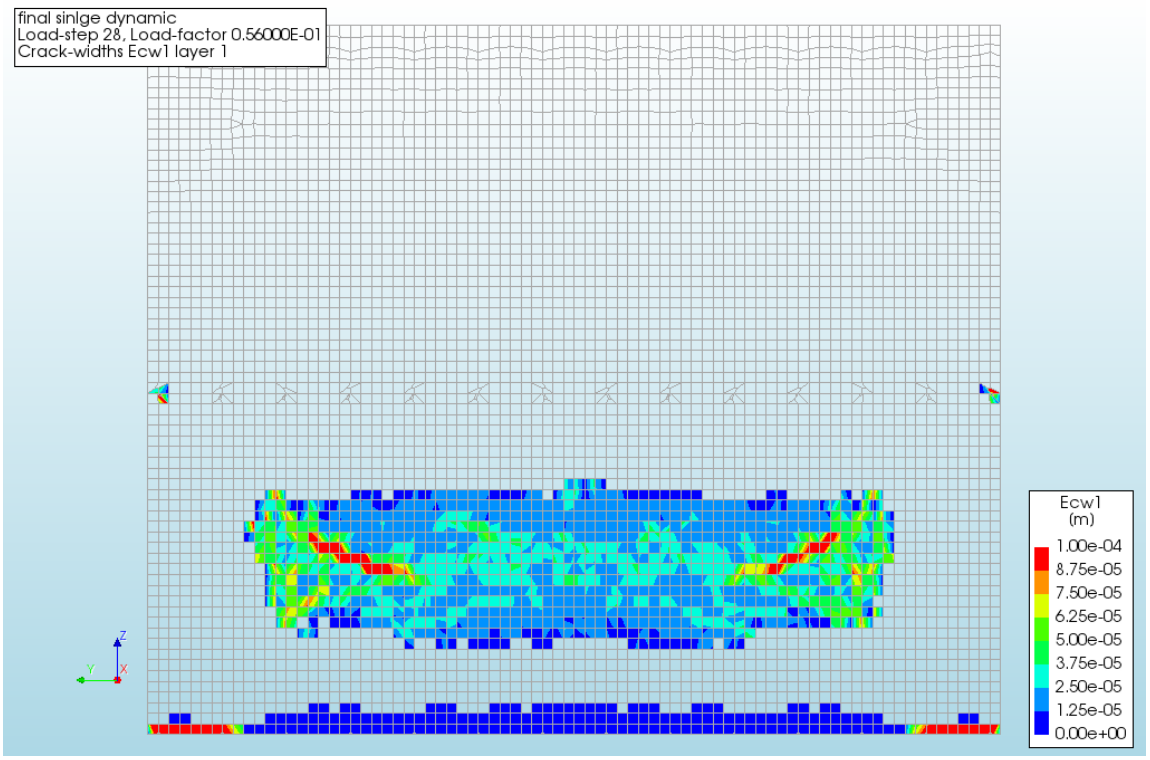


Figure 104 - Crack widths of the Cavity Wall Masonry due to the dynamic load at 5.6%, front view layer 1

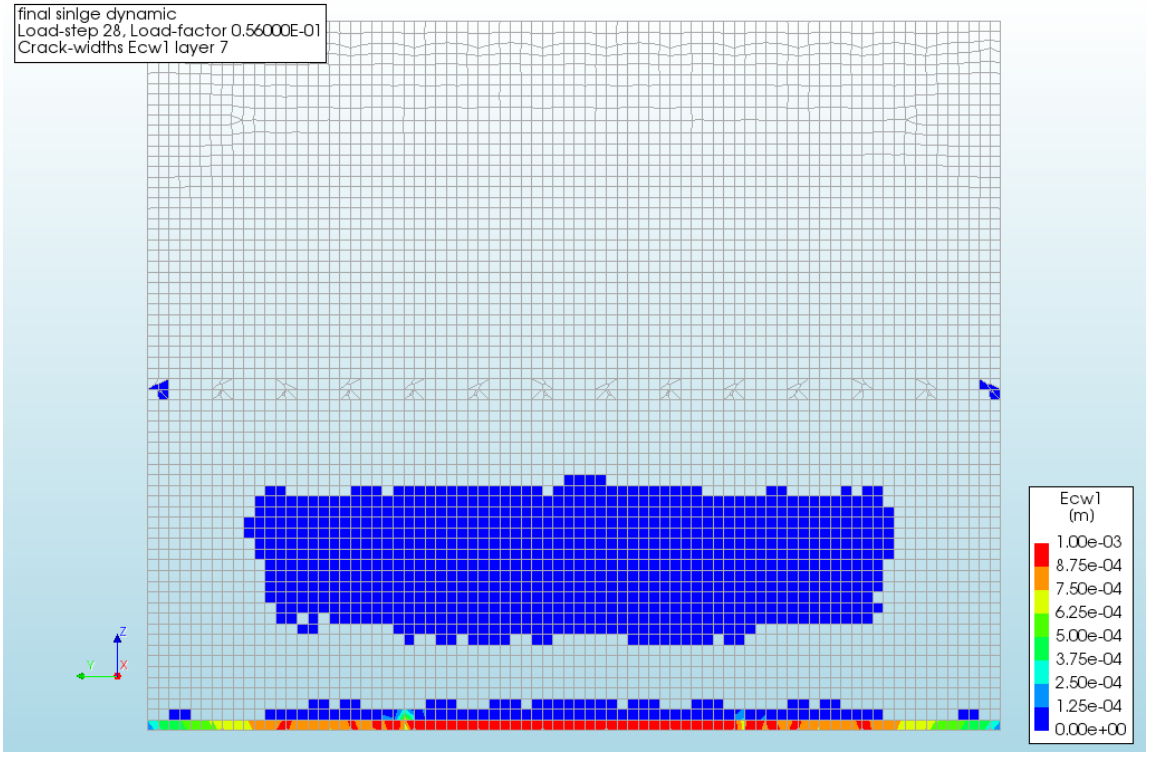


Figure 105 - Crack widths of the Cavity Wall Masonry due to the dynamic load at 5.6%, front view layer 7

## 11.2 Masonry House with Door and Windows

Increasing the complexity and realism of the model a little, door and windows are added as holes in the walls. The removal of these section from the walls is expected to cause a decrease in the resistance, since smaller sections of the wall will have to carry the same load.

### 11.2.1 Static

Loaded with a rising water level, see Figure 106, the single wall masonry house experiences the first damage at an inundation depth of approximately 2.5 m. The load then increases until collapse, which occurs between an inundation depth of 3.75-4.6 m. This large margin follows from the lack of accuracy in the results at those points. For the displacement and cracking patterns, the first point in this margin, the first 'Not Converged' step is used. This step has an error of 0.162, which makes it still somewhat accurate.

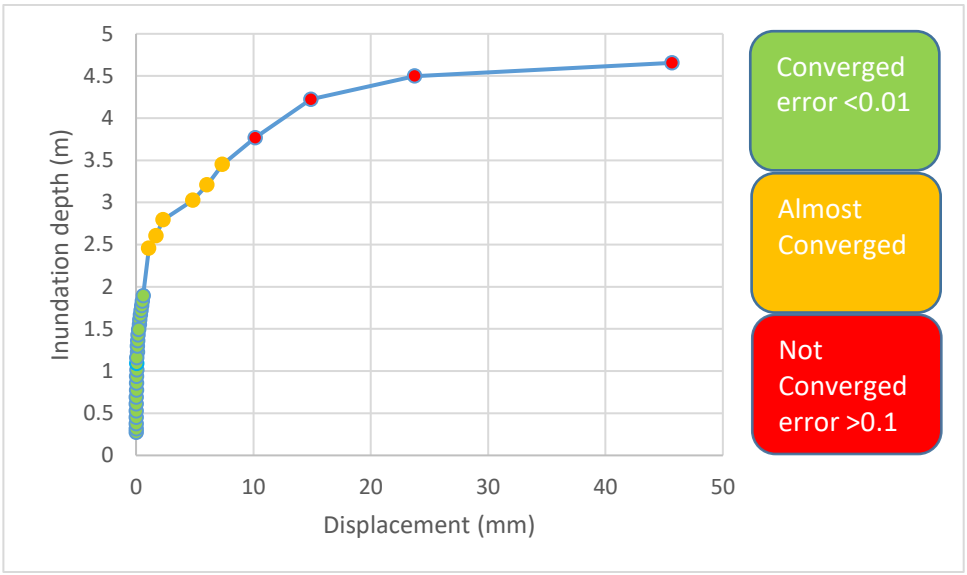


Figure 106 - Inundation depth vs Displacement of the Single Wall Masonry House with Door and Windows due to the static load

### 11.2.2 Dynamic

Loaded with the dynamic load, the displacement increased until failure occurred. The exact point of failure is difficult to determine as the last 'Almost Converged' step still has not fully cracked at any location. The cracking patterns and overall displacement pattern are already visible at this step, which has an error of 0.048. This makes these results still fairly accurate. With increased cracking the failure load will most likely be around 5.5-6%.

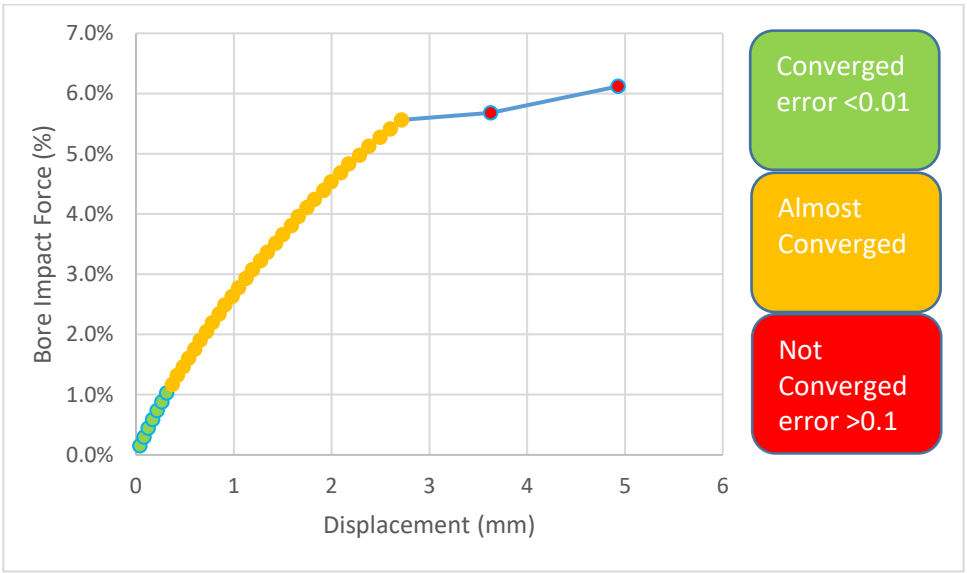


Figure 107 - Bore Impact Force vs Displacement of the Single Wall Masonry House with Door and Windows due to the dynamic load

## 11.3 Masonry House with Inner Walls

Again, the complexity is increased, compared to the first, simple model, inner walls have been added. These should provide some out of plane support to the front walls and thus increase their resistance.

### 11.3.1 Static

Being loaded with the rising water level, the first crack formed at an inundation depth of around 2.5 m. This fits with the transition from 'Converged' steps to 'Almost Converged' steps in Figure 108. The load then keeps increasing and water displacement and cracks start to occur. This starts at an inundation depth of approximately 3.85 m, which corresponds to the second 'Not Converged' step. This step has an error of 0.106, which makes it still somewhat trustworthy. This is partially confirmed by the rest of the load steps, although they are all 'Not Converged' they show a similar pattern. The failure load of this model is therefore estimated to be between an inundation depth of 4-5 m.

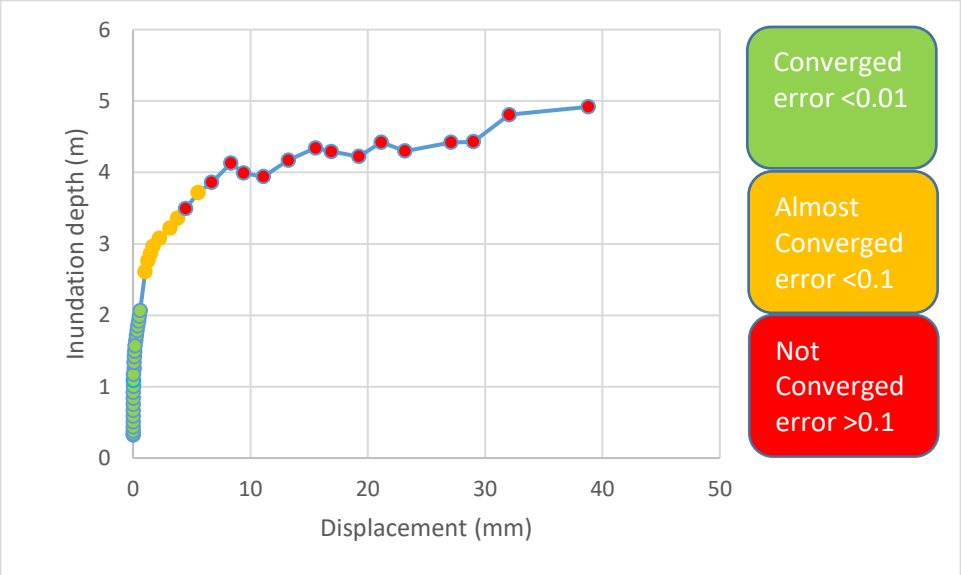


Figure 108 - Inundation depth vs Displacement of the Single Wall Masonry House with Inner Walls due to the static load

### 11.3.2 Dynamic

The model is loaded with an increasing amount of the dynamic load until failure. With respect to 11.1.2 an increase in the maximum load is expected due to the presence of the inner walls. This is confirmed by Figure 109, the maximum load here is expected to be between approximately 9-11% of the total dynamic load. For the displacement and cracking patterns, the last 'Almost Converged' step is used. This step has an error of 0.035, which makes those results still fairly accurate.

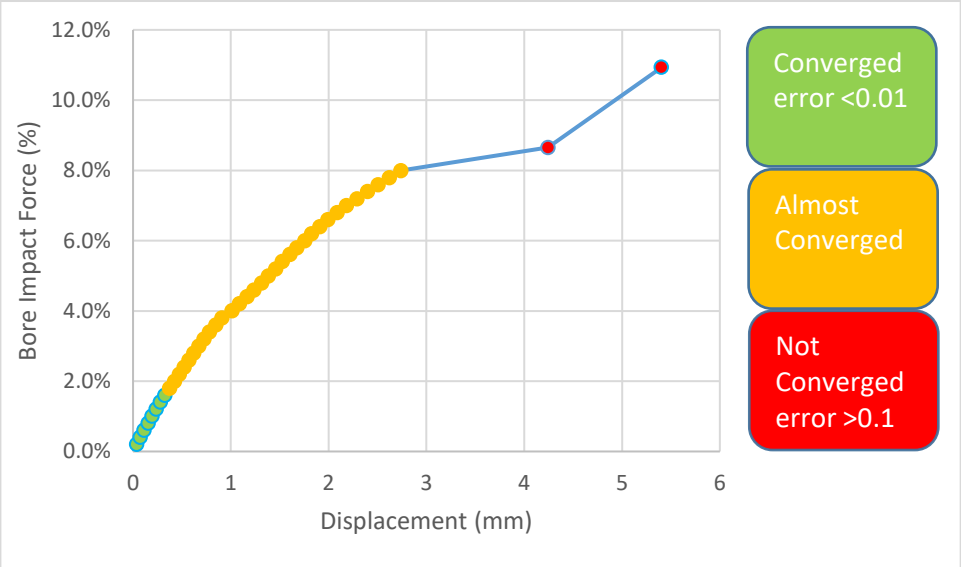


Figure 109 - Bore Impact Force vs Displacement of the Single Wall Masonry House with Inner Walls due to the dynamic load

## 11.4 Masonry House with Door, Windows and Inner Walls

The final model combines both the door and windows as well as the inner walls. Whether or not this will cause an increase or decrease in the resistance compared to 11.1 is difficult to determine. One measure seems to increase the resistance, while the other decreases the resistance.

### 11.4.1 Static

In contrast to 10.4.1, now the section beneath the large window will not fail very early. However, whether or not the side wall will fail before the front wall, still needs to be checked. From Figure 110 and Figure 111 it follows that the side wall is not leading, the front wall is leading. The inundation depth causing failure therefore seems to be between 4-5 m. The front wall starts to show the typical failure behaviour at an inundation depth of approximately 4.0 m, which corresponds to the second 'Not Converged' step of Figure 110. This step is used for the displacement and cracking patterns.

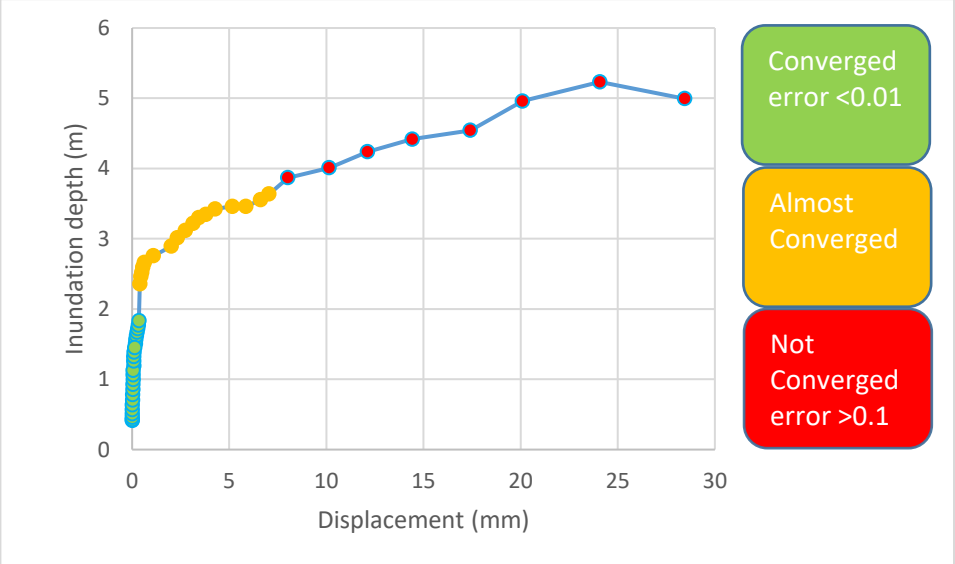


Figure 110 - Inundation depth vs Displacement of the Single Wall Masonry House with Door, Windows and Inner Walls due to the static load, front wall

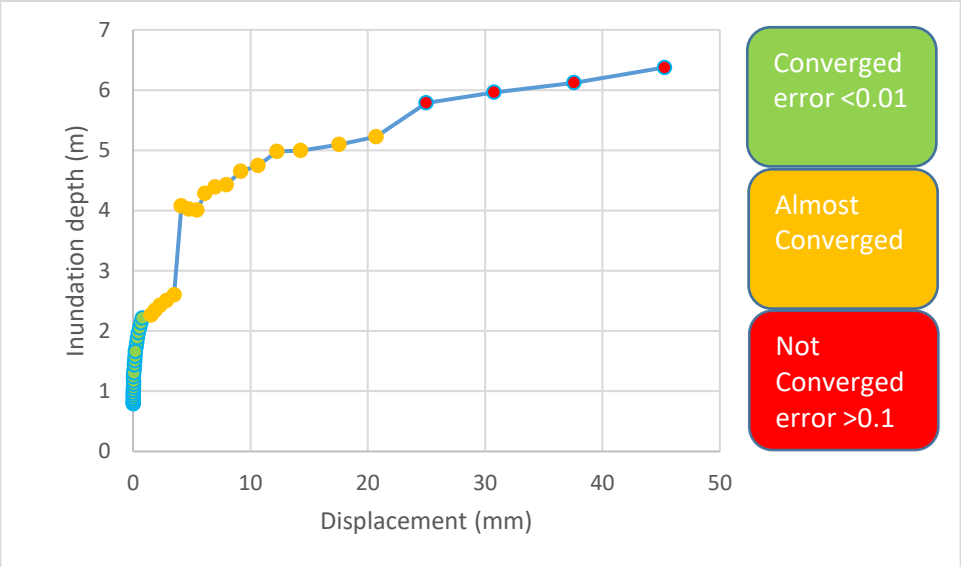


Figure 111 - Inundation depth vs Displacement of the Single Wall Masonry House with Door, Windows and Inner Walls due to the static load, side wall

### 11.4.2 Dynamic

Also, the last model is loaded with the dynamic load until failure. The cracking and displacement patterns for the last steps were all very similar. Therefore, the step with the lowest error is chosen to show these patterns. This is the last step of the 'Almost Converged' steps in Figure 112 and has an error of 0.063. This is still quite accurate, especially for determining the overall patterns. The failure load seems to be between approximately 7-10% of the total dynamic load.

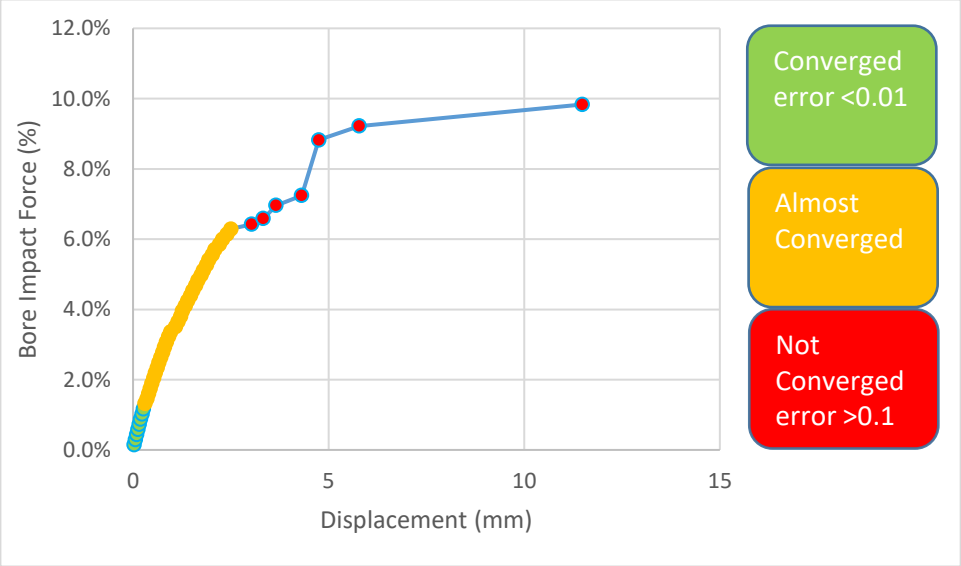


Figure 112 - Bore Impact Force vs Displacement of the Single Wall Masonry House with Door, Windows and Inner Walls due to the dynamic load

## 11.5 Conclusions

Four different cases have been investigated for the dynamic and static load. Again, each case added some complexity and realism to the original model, windows, door and inner walls. These changes also caused differences in the results.

Table 16 - Summary of the estimated failure loads of the Cavity Wall Masonry House

| | Failure load static (m) | Failure load dynamic (%) |
|---|---|---|
| **Original** | 4-5 | 5.5-6 |
| **Door and Windows** | 3.75-4.6 | 5.5-6 |
| **Inner Walls** | 4-5 | 9-11 |
| **Door, Windows and Inner Walls** | 4-5 | 7-10 |

As can be seen for the static load each extra element has little influence on the failure load. Only the door and windows show a small decrease of the failure load.

For the dynamic load this is not the case, the introduction of door and windows causes no decrease of the failure load. The inner walls do cause a significant increase of the failure load but decrease the accuracy. Combining both, an increase of the failure load compared to the original case is observed at the cost of accuracy.

The results seem somewhat contradictory. Where there is hardly any influence in the case of the static load, only a small decline for the door and windows case, there are, major differences for the dynamic load. Especially the influence of the inner walls is clearly visible, increasing the maximum load with about 30-100%. Still, it is difficult to make any hard statements regarding these results since none of the steps near failure loads was very accurate. The results therefore have to be somewhat interpreted and estimated.

The most logical conclusion for these phenomena, is the height at which the loads act on the house. The dynamic load has its maximum at around 2.0 m. This is roughly where the inner wall of the ground floor directly connects the front and back wall, transferring part of this load to this back wall. Since the maximum of the static load is at the bottom of the wall, this transfer is much less present.

# 12 Discussion

Not every result in this thesis proved to be useful or correct, some calculations provided unexpected results and others wrong results. The two main discussion parts are the flow velocity and inundation depth for the bore impact, discussed in 12.1 and the results of the dynamic bore impact calculations in DIANA, discussed in 12.2.

## 12.1 Flood Wave Propagation after the Dyke Breach

As already stated in the conclusions of chapter 3, the results of the weir equations do not match the expectations. The results obtained fit with a more stable situation which could occur later on, after the polder has been flooded.

Although the area filling approximation seemed to provide viable results, it is heavily influenced by the assumed water depth after the breach. This water depth should therefore be determined and checked as accurately as possible.

The method of characteristics had the major flaw that it does not predict the water depth of the wave front accurately, a value of zero is assumed implicitly. It is therefore impossible to determine the dynamic pressure peak with this method.

Finally the results of the rough numeric approximation do seem to validate the magnitude of the flow velocity and water depth. Especially a flow velocity of 10 m/s seems rather large, however this is the extreme just after the dyke has breached and will decay with distance and time.

## 12.2 Dynamic Diana Results

The results of the dynamic calculations in DIANA in chapters 10 and 11 provide very small failure percentages, i.e. a very small percentage of the dynamic load already causes failure. Even though it was expected that the house might not survive the dynamic load, failure this early was unexpected. The main reason for this is the dynamic load used in the calculations. The new load, based on an inundation depth of 1.50 m and a flow velocity of 10 m/s leads to a force of 122.2 kN/m. Pressure-wise, this corresponds to a still water inundation depth of about 3.7 m. Whereas the load used for the calculations was based on an inundation depth of 4.76 m and a flow velocity of 2.92 m/s, which led to a force of 490.9 kN/m. This is over four times larger than the new dynamic force and would correspond to a still water inundation depth of 5.85 m.

Furthermore the load was applied as a static pressure, whereas the load is actually dynamic. The method used does not fully take into account the short duration, 0.1 seconds, and the magnitude of the pressure peak. This affects the results in two ways, the peak force is at least twice as high as the following quasi-static part, which explains part of the difference. Furthermore a dynamic load might load and unload the house before the entire house is able to respond to this dynamic load. Simply said, the inertia of the house will have prevented a quick response to the load and thus failure might not occur.

Taking all these influences into account it is actually very likely that the house is able to withstand the dynamic load. The percentages themselves therefore need not be taken too seriously, the relative results however still stand, both between the static and dynamic calculations and between the dynamic calculations themselves. Note, the actual dynamic load will have a different pressure distribution on the house than the load used in the DIANA model calculations.

# 13 Conclusions and Recommendations

This chapter discusses the conclusions and recommendation of this thesis. First the conclusions in 13.1, followed by the recommendations in 13.2.

## 13.1 Conclusions

The conclusions are separated into three groups, conclusions for the cavity wall masonry house and conclusions for the single wall masonry house and conclusions regarding the research questions.

### 13.1.1 Cavity Wall Masonry House

- A still water difference of at least 2 metres is needed for significant structural damage, below 1.5 metres no structural damage seems to occur at all. The actual failure of the house is not expected until an inundation depth of approximately 2.5 m.
- The bore impact seems to cause large structural damage, failure occurs at as low as 1.6% of the total load and might go up to 3.0%. That this would be the case is mostly confirmed by the fact that following the initial impact of the bore, is a quasi-static part. This quasi-static part is estimated to be up to twice the inundation depth of the original bore. Seen the still water results, the bore may not have a depth higher than 1-1.5 metres. There is therefore a small possibility for a house under these specific circumstances to survive this impact.
- The model in DIANA was increased in realism in several steps, adding gaps where normally windows and doors would reside as well as adding inner walls. Overall, the addition of the windows caused no major changes, a small increase in one situation and a small decrease in another. The inner walls caused only small increases in the maximum possible load, mainly they provided more accuracy in the model results. An odd result is, when combining the door and windows with the inner walls, there was a large increase in the maximum inundation depth up to 3.2-3.6 metres. A possible reason might be, that by adding the door and windows, the load acting on those areas was removed as well. These areas usually experience the largest deflections since they are mostly in the middle of the outer walls. This in turn could raise the failure load.

### 13.1.2 Single Wall Masonry House

- A still water difference of at least 3.75 metres is needed for significant structural damage, below 2-2.5 metres no structural damage seems to occur at all. The actual failure of the house is not expected until an inundation depth of approximately 4-5 m.
- Again, the bore impact seems to cause significant structural damage, failure occurs at as low as 5.5-6% of the total load for the original and door and windows cases and might go up to 9-11% for the inner walls case. That this will happen is not necessarily confirmed by the fact that following the initial impact of the bore, is a quasi-static part. This quasi-static part is estimated to be up to twice the inundation depth of the original bore. Seen the still water results, the bore may not have a depth higher than 2-2.5 metres. Seen that the bore is about 1.50 m in the new approximation, it might very well be possible for a house under these specific circumstances to survive this impact, although some structural damage seems unavoidable.
- The model in DIANA was increased in realism in several steps, adding gaps where normally windows and doors would reside as well as adding inner walls. Overall, the addition of the windows caused no major changes, a small decrease for the static load and a small decrease for the dynamic load, when combined with the inner walls compared to the inner walls

alone. The addition of inner walls, however, had a significant impact on the bore impact case. These increased the maximum failure load with at least 30% and up to potentially 100%.

### 13.1.3 Research questions

The answer to the main research question has already followed from the results of 13.1.1 and 13.1.2. An overview of all sub-questions answers is provided here:

- As determined in chapter 2, the worst possible dyke breach would be a sudden collapse and an entire collapse, creating a gap equal to the height of the dyke. Although this is not very likely, the assumption is made that this will happen since it will cause the highest loads possible.
- Ensuing from this dyke breach is a flood wave, the flow velocity and inundation depth of this flood wave have been determined in chapter 3 and are 10 m/s and 1.50 metres. Note, however, that this is based on a flood level outside the dyke, which is higher than it might get in reality. Furthermore these results themselves might not be fully accurate, see 12.1.
- As determined in chapter 4, the main loads are the hydrostatic water pressure and the dynamic bore impact. Debris, however, might very well be of major significance, but has been left out of the scope of this thesis.
- From the analysis chapter 7, it followed that doors and wall ties might be structural weak points, depending on their orientation and age. The analyses in chapters 10 and 11 showed that the smaller sections of wall between windows or doors are susceptible to larger displacements and cracking due to the lack of support on the sides.
- The analysis in chapter 10 and 11 clearly show the importance of floors with regard to the structural integrity of the house. As wall ties transfer loads in a cavity wall, so do floors in a house, which decreases overall displacements and thus crack widths. The same principle holds for the inner walls which also transfer loads between the outer walls.
- A masonry house at 50 metres from the breach in the situation sketched in this thesis will, most likely, collapse. Although the static water pressure might be coped with, the dynamic bore impact will have caused structural failure, or at the least structural damage, in most cases.
- For this house to survive under the current circumstances, it would need to be a single walled or the cavity walls need to work together. Where the water depth of the bore might already cause structural failure, the velocity increases the damage potential immensely. Therefore, the flow velocity of the bore impact needs to be decreased. This could be achieved for example by normal wave breaking measures. A slower failure of the dyke would also result in a lower initial inundation depth and a lower flow velocity.

## 13.2 Recommendations

In this thesis several assumptions have been made. These lead to the eventual results. From these results, however, it follows that a worst-case scenario is too grim. Therefore, some recommendations are in order to obtain more useful and, perhaps, more realistic results.

- A more realistic analysis is needed to assess the dyke breach and water level behind the dyke. Following this, the flood wave would have to be recalculated to obtain a new inundation depth and flow velocity for the bore impact. This approach could be based on dam break equations.

- The formula and distribution to determine the bore impact require further research. Partially this is already currently being done at the TU Delft.[75]
- In order to improve the accuracy of the model, the strength of the windows and their frames should be determined and modelled. These might provide some support to the adjacent wall sections, increasing their resistance.
- Older house, with basements, usually have the ground floor 30 to 50 cm above the surface. The ground floor would then be able to transfer loads between the walls. This could be modelled to determine what the influence of this would be in the resistance of the house as a whole.
- Older houses have rather high storeys. As is clear from chapter 10 and 11, the floors transfer loads from one wall to another, providing additional strength. Lower storeys could therefore also increase the resistance of the house.
- Instead of modelling the dynamic load as a static load, model the dynamic load over time and space. This might prove very tedious as the distribution and the total force changes over time. Although modelling the load just as dynamic might already make a large difference due to the small time scale of the bore impact.
- Determine whether or not debris would be a leading load case.
- Couple the hydrostatic load with small waves. On a somewhat stable water level, small (wind) waves will also occur, these will increase the loading on the house.
- Although currently not an issue due to the magnitude of the loads, erosion of the soil around the foundation might become leading when the house survives the initial loads.
- In chapter 7 it was determined that there would be little cooperation between the two parts of the cavity wall due to failure of the wall ties. Whether this little cooperation will significantly increase the resistance could be checked. As well as modelling a cavity wall assuming full cooperation and comparing those results to the single wall masonry house.
- Performing actual tests in order to compare the data from the models with measurements in order to extrapolate and determine the actual failure loads of the models. From the current models it is very difficult to determine the actual failure loads.

[75] Chen et al. [58]

# 14 References


[1] 'Roos, W. (June 2003): Damage to buildings'

[2] 'Hoes, O.A.C., Tariq, M.A.U.R. and Van de Giesen, N.C. (September 2014): Online estimation of flood damage in the Netherlands'

[3] 'Pistrika, A.K. and Jonkman, S.N. (February 2009): Damage to residential buildings due to flooding of New Orleans after hurricane Katrina'

[4] 'Kelman, I. and Spence, R. (2004): An overview of flood actions on buildings'

[5] 'Nistor, I., Palermo, D., Nouri, Y., Murty, T. and Saatcioglu, M. (May 2009): Tsunami-Induced Forces on Structures'

[6] 'Wagenaar, D.J., de Bruijn, K.M., Bouwer, L.M. and De Moel, H. (2015): Uncertainty in flood damage estimates and its potential effect on investment decisions'

[7] 'Caraballo-Nadal, N.C., Zapata-López, R.E. and Págan-Trinidad, I. (June 2006): Building Damage Estimation due to Riverine Floods, Storm Surges and Tsunamis: A Proposed Methodology'

[8] 'ASCE (April 2015): ASCE 7 Chapter 6 Tsunami Loads and Effects'

[9] 'Schweckendiek, T., Vrouwenvelder, A.C.W.M., van Mierlo, M.C.L.M., Calle, E.O.F. and Courage, W.M.G. (2008): River System Behaviour Effects on Flood Risk'

[10] 'Chen, X., Hassan, W., Uijttewaal, W., Verwaest, T., Verhagen, H.J., Suzuki, T. and Jonkman, S.N. (2012): Hydrodynamic load on the building caused by overtopping waves'

[11] http://www.makeitfrom.com/ (November 2015)

[12] https://en.wikipedia.org/wiki/Properties_of_concrete (November 2015)

[13] 'Fema P-55 (August 2011): Coastal Construction Manual'

[14] 'Panasyuk, V., Marukha, V. and Sylovanyuk, V. (2014): Injection Technologies for the Repair of Damaged Concrete Structures'

[15] 'van Noort, J.R. (August 2012): Computational Modelling of Masonry Structures'

[16] 'Karoglou, M., Moropoulou, A., Giakoumaki, A. and Krokida, M.N. (June 2004): Capillary rise kinetics of some building materials'

[17] 'Ramsden, J.D. (May 1996): Forces on a Vertical Wall due to Long Waves, Bores, and Dry-Bed Surges'

[18] 'Gómez-Gesteira, M. and Dalrymple, R.A. (March 2004): Using a Three-Dimension Smoothed Particle Hydrodynamics Method for Wave Impact on a Tall Structure'

[19] 'Fujima, K., Achmad, F., Shigihara, Y. and Mizutani, N. (June 2009): Estimation of Tsunami Force Acting on Rectangular Structures'

[20] 'Green, D. W., Winandy, J. E. and Kretschmann, D. E. (1999): Wood handbook – Wood as an engineering material, Chapter 4: Mechanical Properties of Wood'

[21] 'Monier B.V. (May 2013): Keramische dakpannen brochure'

[22] 'Hoogenboom, P.C.J.: 2TM7 Lecture notes'

[23] http://wienerberger.nl/informatie/voorbereiding-maatvoering-metselwerk (July 2017)

[24] 'Morris, M. W. (December 2011): Breaching of Earth Embankments and Dams'

[25] 'Weijers, J., Tonneijck, M. (February 2009): Flood Defences'

[26] 'Zhu, Y. (September 2006): Breach Growth in Clay-Dikes'

[27] 'Battjes, J.A. (April 2002): CT2100 Vloeistofmechanica'

[28] 'Cooker, M.J. and Peregrine, D.H. (1995): Pressure-impulse theory for liquid impact problems'

[29] ‘Peregrine, D.H. (2003): Water-wave impact on walls’
[30] ‘Ramsden, J.D. (1996): Forces on a vertical wall due to long waves, bores and dry-bed surges’
[31] ‘Gomez-Gesteira, M. and Dalrymple, R.A. (2004): Using a three-dimensional smoothed particle hydrodynamics method for wave impact on a tall structure’
[32] ‘Ramachandran, K., Genzalez, R.R., Oumeraci, H., Schimmels, S, Kudella, M., Doorslaer, K., De Rouck, J., Versluys, T. and Trouw, K. (2012): Loading of vertical walls by overtopping bores using pressure and force sensors – A large scale model study’
[33] ‘De Rouck, J., V Doorslaer, K., Versluys, T., Ramachandran, K., Schimmels, S, Kudella, M. and Trouw, K. (2012): Full scale impact tests of an overtopping bore on a vertical wall in the large wave flume (GWK) in Hannover’
[34] ‘Chen, X., Hofland, B., Altomare, C. and Uijttewaal, W. (2014): Overtopping flow impact on a vertical wall on dike crest’
[35] ‘Fujima, K., Achmad, F., Shigihara, Y. and Mizutani, N. (June 2009): Estimation of tsunami force acting on rectangular structures’
[36] ‘Hofland, B. (2017): Impulsive loads of steep bore impact on a vertical wall – theoretical derivations’
[37] ‘Holthuijsen, L.H. (2009): Waves in Oceanic and Coastal Waters’
[38] ‘Battjes, J.A. (April 2002): Stroming in Waterlopen’
[39] ‘Vrijling, J.K., Kuijper, H.K.T., van Baars, S., Bezuyen, K.G., Molenaar, W.F., van der Hoog, C., Hofschreuder, B. and Voorendt, M.Z. (2011): Manual Hydraulic Structures’
[40] ‘Bosboom, J., Stive, J.F. (2013): Coastal Dynamics I’
[41] ‘te Linde, A.H., Bubeck, P., Dekkers, J.E.C., de Moel, H. and Aerts, J.H. (2011): Future flood risk estimates along the river Rhine’
[42] ‘Molenaar, W.F. and Voorendt, M.Z. (2018): Manual Hydraulic Structures’
[43] https://ahn.arcgisonline.nl/ahnviewer/ (August 2018)
[44] http://www.dijkverbetering.waterschaprivierenland.nl/common/projecten/streefkerk-ameide/streefkerk-ameide.html (August 2018)
[45] ‘Ministry of Infrastructure and Water Management (August 2007): Hydraulische Randvoorwaarden primaire waterkeringen’
[46] ‘Schropp, M. (march 2012): Memo aanpassing afvoerverdeling t.b.v. DPRD’
[47] ‘Deltacommissie (1961): Rapport Deltacommissie deel 1’
[48] https://wienerberger.nl/informatie/spouwankers (October 2018)
[49] ‘Green, D.W., Winandy, J.E., Kretschmann, D.E. (1999) Wood handbook: wood as an engineering material.’
[50] ‘Van der Pluijm, R. (April 2009): Eurocode 6, Design of masonry structures’
[51] https://www.engineeringtoolbox.com/concrete-properties-d_1223.html (November 2018)
[52] https://www/omroepzeeland.nl/ (December 2018)
[53] https://www.nemokennislink.nl/ (December 2018)
[54] https://www.iaea.org/ (December 2018)
[55] https://nos.nl (December 2018)
[56] ‘Steenepoorte, K. Ministry of Infrastructure and Water Management (October 2016): De stormvloedkering in de Oosterschelde’
[57] ‘Rots, J.G., Schreppers, G.M.A., Garofano, A., Messali, F. (December 2016): DIANA Validation report for Masonry Modelling’

[58] ‘Chen, X., Hofland, B., Molenaar, W.F., Capel, A., Van Gent, M.R.A. (December 2018): Use of impulses to determine the reaction force of hydraulic structure with an overhang due to wave impact (Draft)’
[59] http://www.abbotbuilding.com/brick-wall-types/ (January 2019)
[60] https://dianafea.com/manuals/d93/Analys/node1.html (January 2019)
[61] ‘Chanson, H. (October 2004): Environmental Hydraulics of Open Channel Flows’

# 15 Lists

## 15.1 List of Figures

## 15.2 List of Tables

## 15.3 List of Symbols

| | | |
|---|---|---|
| $\frac{\partial u}{\partial t}$ | is the time dependent flow acceleration | ($m/s^2$) |
| a | is the height of the crest | (m) |
| a | is the wave amplitude (H/2) | (m) |
| A | is the length of the steel plate next to the latch bolt | (mm) |
| A | is the surface area of the submerged cross-section | ($m^2$) |
| A | is the projected area of the body normal to the flow direction | ($m^2$) |
| A or $A_s$ | is the flow area (B*d) | ($m^2$) |
| $A_{s,s}$ | is the area of the steel active in shear | ($mm^2$) |
| $A_{S,t}$ | is the area of the steel active in tension | ($mm^2$) |
| $A_{w,s}$ | is the area of the wood active in shear | ($mm^2$) |
| $A_{w,srol}$ | is the area of the wood active in rolling shear | ($mm^2$) |
| $A_{w,t}$ | is the area of the wood active in tension | ($mm^2$) |
| b | is the width of the house | (m) |
| b | is the length of the steel plate next to the dead bolt | (mm) |
| B or $B_i$ | is the flow width (at location i) | (m) |
| $b_l$ | Brick length | (mm) |
| $b_t$ | Brick thickness | (mm) |
| $b_w$ | Brick width | (mm) |
| $b_w$ | is the width of the wall | (m) |
| c | is the distance between the bottom and top screw | (mm) |
| c | Is the celerity | (m/s) |
| $C_D$ | is the drag coefficient (see Table 5) | - |
| $c_f$ | is the coefficient of friction | (-) |
| $C_M$ | is the mass coefficient | - |
| $C_{mk}$ | is the coefficient of impact (≈2) | (-) |
| $C_p$ | is the dynamic pressure coefficient | (-) |
| $C_W$ | is the coefficient related to the crest width | (-) |
| d | is the distance between the screw and the side of the frame | (mm) |
| d or $d_i$ | is the inundation/water depth (at location i) | (m) |
| e | is the thickness of the steel plate | (mm) |
| E or $E_c$ | is the young's modulus | ($N/mm^2$) |
| $E_b$ | is the Young's modulus of the brick | ($N/mm^2$) |
| $E_{mt}$ | is the Young's modulus of the mortar | ($N/mm^2$) |
| $E_x$ | is the Young's modulus of the masonry in horizontal direction | ($N/mm^2$) |
| $E_y$ | is the Young's modulus of the masonry in vertical direction | ($N/mm^2$) |
| f | is the width of the screw | (mm) |
| $F_B$ | is the buoyancy force | (N) |
| $f_{cc}$ | is the compressive strength of the concrete after 28 days | ($N/mm^2$) |
| $F_{D,\ distri}$ | is the distributed debris force | (N) |
| $F_{D,\ gen}$ | is the general debris impact force | (N) |
| $F_{D,\ log}$ | is the log and pole debris impact force | (N) |
| $F_{Door}$ | is the minimum force required for punching failure of a non-locked door | (N) |
| $F_{fail,dead}$ | is the force required for tensile failure of the steel plate next to the dead bolt | (N) |
| $F_{fail,latch}$ | is the force required for tensile failure of the steel plate next to the latch bolt | (N) |
| $F_{fail1}$ | is the force required for failure mechanism 1 of the door | (N) |
| $F_{fail2}$ | is the force required for failure mechanism 2 of the door | (N) |

| | | |
|---|---|---|
| $F_{fail3}$ | is the force required for failure mechanism 3 of the door | (N) |
| $F_{fail4}$ | is the force required for failure mechanism 4 of the door | (N) |
| $F_{HD, drag}$ | is the hydrodynamic drag force | (N) |
| $F_{HS}$ | is the hydrostatic force | (N) |
| $F_{Punch, wood}$ | is the force required for the punching failure of wood | (N) |
| Fr | is the Froude number | (-) |
| $F_{S, dyn}$ | is the surge force using a dynamic approximation | (N) |
| $F_{S, stat}$ | is the surge force using a static approximation | (N) |
| $f_{s, wood}$ | is the shear strength of the wood | ($N/mm^2$) |
| $f_{s,steel}$ | is the shear strength of the steel | ($N/mm^2$) |
| $f_{s,wood}$ | is the maximum shear strength of the wood | ($N/mm^2$) |
| $f_{srol,wood}$ | is the rolling shear strength of the wood (≈¼$f_{s,wood}$) | ($N/mm^2$) |
| $f_{t, steel}$ | is the ultimate tensile strength of the steel | ($N/mm^2$) |
| $f_{t,wood}$ | is the tensile strength of the wood perpendicular to the grain | ($N/mm^2$) |
| $F_{W, break, dry}$ | is the breaking wave load on a wall, were the enclosed space behind the wall is dry | (N) |
| $F_{W, break, wet}$ | is the breaking wave load on a wall, were the enclosed space behind has an equal water elevation as the outside | (N) |
| $F_{W, over}$ | is the overtopping wave force | (N) |
| g | is the gravitational constant | ($m/s^2$) |
| g | is the length of the screw | (mm) |
| $G_{xy}$ | is the shear modulus of the masonry | ($N/mm^2$) |
| h | is the actual height of the water against the house | (m) |
| $H_0$ | is a correction factor | (m) |
| $H_b$ | is the wave height | (m) |
| $h_b$ | is the water depth of the bore | (m) |
| $H_{cr}$ | is the height of the capillary rise | (m) |
| $H_e$ | is the equilibrium height, for water at 18°C | (m) |
| $H_i$ | is the energy at location i | (m) |
| $h_i$ | is the water level with respect to the reference plane | (m) |
| $H_L$ | is the depth at one wavelength in front of the wall | (m) |
| $H_m$ | is the average value of the incident wave height near the dyke toe | (m) |
| I | is the area moment of inertia | ($mm^4$) |
| $I_i$ | is the impulse at location i | (N) |
| $j_t$ | Joint thickness | (mm) |
| k | is the wave number of the incoming wave | (1/m) |
| k | is the constant effective stiffness between the debris and the house | (N/m) |
| $K_a$ | is the approach angle correction factor | (-) |
| $K_n$ | is the land-cover correction factor | (-) |
| $K_t$ | is the time-scale correction factor | (-) |
| L | is the wavelength | (m) |
| l | is the length of the cavity | (mm) |
| L | is the horizontal length along the side of the structure | (m) |
| $L_{HL}$ | is the wavelength at depth $H_L$ | (m) |
| $M_b$ | is the modulus of the brick | ($N/mm^2$) |
| $m_c$ | is the mass of the concrete | ($kg/m^3$) |
| $m_D$ | is the mass of the debris impacting the house | (kg) |
| $M_m$ | is the modulus of the masonry | ($N/mm^2$) |
| $M_{mt}$ | is the modulus of the mortar | ($N/mm^2$) |
| $n_c$ | is the Manning's coefficient for actual field conditions | (-) |

| | | |
|---|---|---|
| $Q$ | is the discharge | ($m^3/s$) |
| $Q_i$ | is the discharge at location i | ($m^3$) |
| r | is the mean radius of the capillary | (m) |
| R | is the hydraulic diameter | (m) |
| $R_c$ | is the crest freeboard | (m) |
| $R_u$ | is the maximum wave run-up height for a regular wave on a smooth impermeable slope | (m) |
| $S_0$ | is the bed slope | (-) |
| $S_f$ | is the friction slope | (-) |
| t | is the time during which u occurs | (s) |
| t | is the time of the flood | (s) |
| t | is the time | (s) |
| $t_b$ | is the relative length of the brick in the brick-mortar combination | - |
| $t_c$ | is the time required to reach 2/3 of the equilibrium height | (s) |
| $t_m$ | is the relative length of the mortar in the brick-mortar combination | - |
| $t_u$ | is the time needed to reach the ultimate scour depth | (s) |
| u | is the flow velocity | (m/s) |
| $u_c$ | is the critical velocity for sediment entrainment | (m/s) |
| $u_D$ | is the velocity of the debris | (m/s) |
| $U_i$ | is the flow velocity at location i | (m/s) |
| $u_n$ | is the normal component of the velocity | (m/s) |
| V | is the volume of the submerged section of the house | ($m^3$) |
| v | is the velocity of the wave front | (m/s) |
| x | is the distance in the flow direction | (m) |
| z(t) | is the time-dependent local scour or erosion next to a land based structure | (m) |
| $\Delta t$ | is the impact duration | (s) |
| $\theta$ | is the angle of approach in degrees | (°) |
| $\rho$ | is the density of the water | ($kg/m^3$) |
| $\rho_f$ | is the density of the fluid including suspended solids | ($kg/m^3$) |

# Appendix A. Extended Flood Wave Propagation after the Dyke Breach.

In this appendix the propagation of the flood water will be determined. The assumption regarding the sudden collapse of the dyke and the location data mentioned in the introduction is used to make this determination. In Figure 113 an overview is provided of the flood wave during and after the dyke breach, with the last image being the completely flooded polder. The first schematisation is based on the 'long crested weir equations', the second approximation is done using the method of characteristics and a third approximations is based on a numerical model. Keep in mind that the determinations in this chapter are to determine the first wave of water, not the somewhat stable situation that occurs after a while.

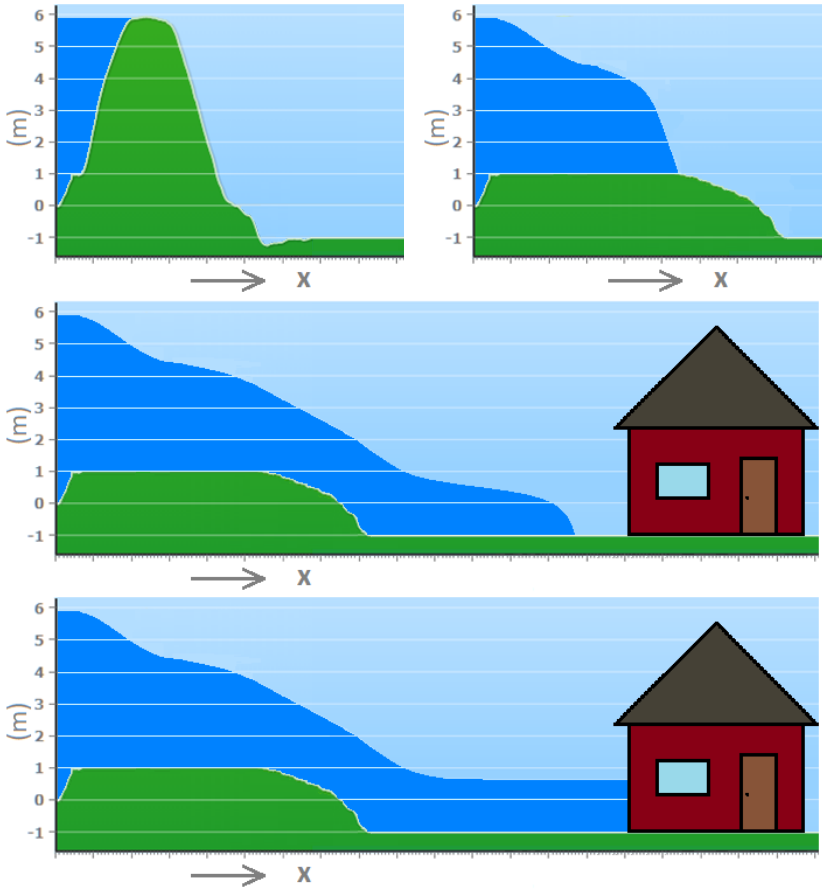


Figure 113 - Overview of the flood wave during and after breaching

## Schematisation of the Breach

In order to determine the velocity and water level shortly after the breach, relations between the velocity and water level before and at the breach are required. To define these, the assumed dimensions of the breach are also required. The breach is therefore schematized as a rectangle with an area equal to the cross-sectional area of the breach, Figure 114. The width of the breach, $B_2$, takes into account the streamlines and represents the actual flow width. In Figure 116 and Figure 117 the locations are provided with a number, (1) before the breach, (2) at the breach and (4) 50 m after the breach. The breach is at the centre of the dyke. Furthermore, two assumptions are made. The first being that the water level, $d_1$, will reach until the dyke crest. The second assumption is that the sill height, a, see Figure 118, is equal to the remaining height of the unprotected outer toe of the dyke. This is at 1.00 NAP, see Figure 115. Usually the height of a, is determined by the toe of the dyke, since the outer protection has not (yet) been removed by the flood water and acts as the edge of the long crested weir. At the chosen location such a protection is not present.

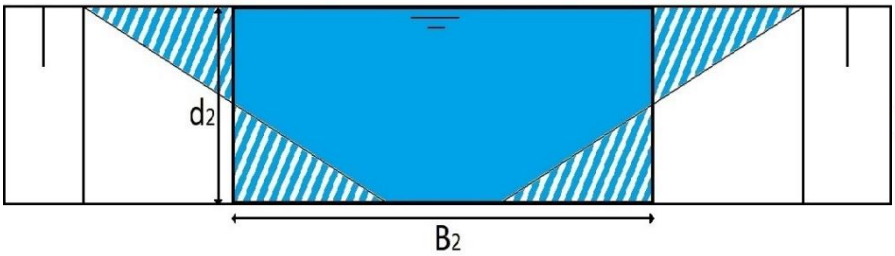


Figure 114 - Approximation of an actual breach schematized as a rectangle

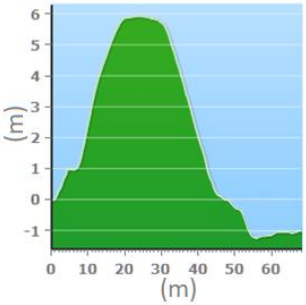


Figure 115 - Cross-section dyke[76] (distorted scale)

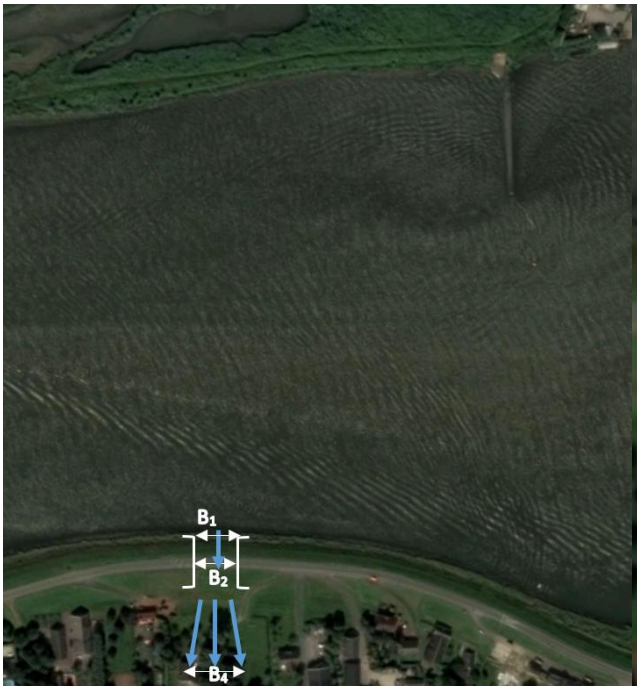


Figure 116 - Top view river and dyke including the breach location

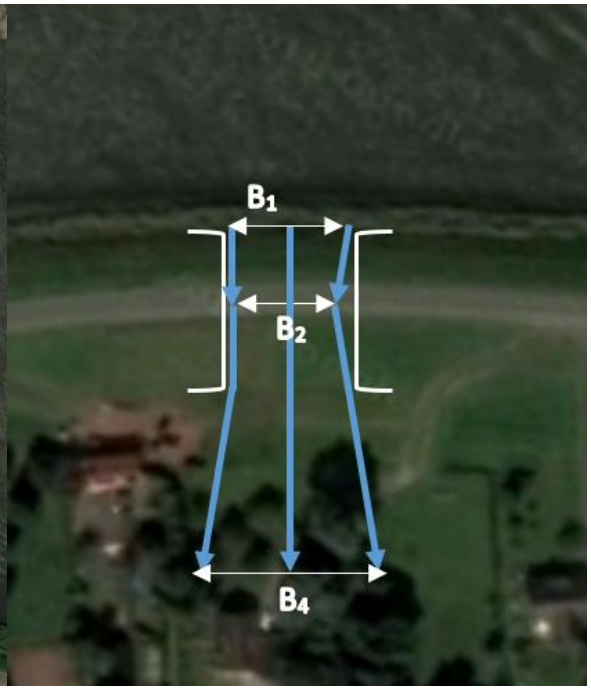


Figure 117 - Top view of the breach, enlarged

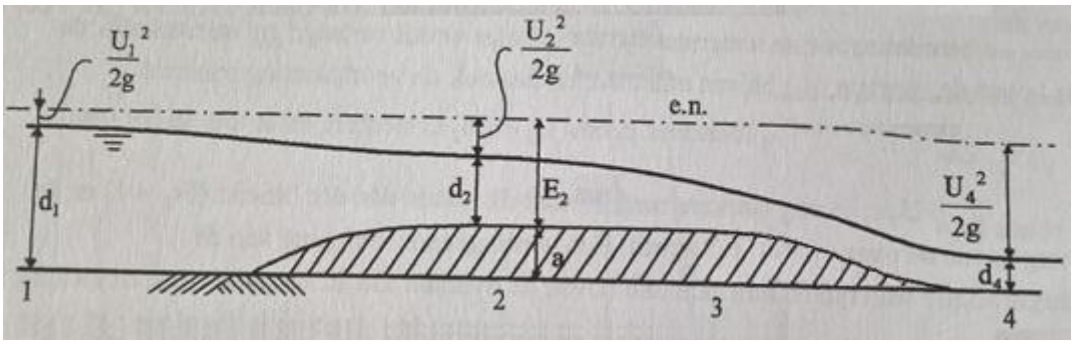


Figure 118 – Long crested weir (Based on[77])

[76] AHN [43]
[77] Battjes [27]

## Long Crested Weir Approximation

As noted before several relations are required to determine all the variables needed. The first relation is the preservation of volume, assuming water as incompressible the volume of the water through each cross-section cannot change. Simply said the discharges at all location must be the same:

$$Q_1 = Q_2 = Q_4$$

Since the discharge is comprised of the velocity, inundation depth and width this can be expanded to:

$$\rightarrow U_1 d_1 B_1 = U_2 d_2 B_2 = U_4 d_4 B_4$$

This can be further simplified since streamlines will have a maximum ratio of 1:6, meaning for every 6 metres travelled from the breach the width on both sides will increase with 1 m. Using streamlines to reduce the width of the breach, $B_1$, it is possible to determine $B_2$ which is equal to $30 - 1 * \frac{45}{2} * \frac{1}{6} = 30 - 3.75 = 26.25$ m. The streamlines are only taken into account on one side due to the direction of the incoming flow. $B_4$ is rewritten as the breach width + x/3. This is based on the assumption that the width at location four will be equal to the width of the breach plus streamlines. Inputting the distance between the toe of the dyke and $B_4$, which is 27.5 metres, this gives the following relation:

$$B_4 = 30 + 2 * \frac{27.5}{6} = 30 + \frac{27.5}{3}$$

$$\rightarrow U_1 d_1 30 = U_2 d_2 26.25 = U_4 d_4 (30 + \frac{27.5}{3})$$

In which:

| | | |
|---|---|---|
| $Q_i$ | is the discharge at location i | ($m^3$) |
| $U_i$ | is the flow velocity at location i | (m/s) |
| $d_i$ | is the water depth at location i | (m) |
| $B_i$ | is the flow width at location i | (m) |

The second relation is the preservation of energy, assuming a smooth transition between location 1 and 2 there will be negligible energy losses. Therefore, the energy level of both cross-sections will be equal. Since there will be turbulence after location 2 this means that the preservation of energy cannot be used to relate location 2 and 4 to one another. The energy level of location 1 and 2 therefore will be the same:

$$H_1 = H_2$$

$$\rightarrow h_1 + \frac{U_1^2}{2g} = h_2 + \frac{U_2^2}{2g}$$

Rewriting $h_1=d_1$ and $h_2=a+d_2$ this becomes:

$$d_1 + \frac{U_1^2}{2g} = a + d_2 + \frac{U_2^2}{2g}$$

In which:

| | | |
|---|---|---|
| $H_i$ | is the energy at location i | (m) |
| g | is the gravitational constant | ($m/s^2$) |
| $h_i$ | is the water level with respect to the reference plane | (m) |
| $d_i$ | is the water depth at location i | (m) |

| | | |
|---|---|---|
| a | is the height of the crest | (m) |

The energy level follows from the Euler equation with the assumption of a gravity potential and a uniform density $\rho$:

$$\rho \frac{D\vec{u}}{Dt} = -\nabla(p + \rho g z)$$

In which $\frac{D}{Dt}$ stands for the moving derivative. Since $h = z + \frac{p}{\rho g}$, in which $z$ is the place head, $\frac{p}{gz}$ the pressure head and $h$ the hydraulic head, this can be rewritten as:

$$\rho \frac{D\vec{u}}{Dt} = -\nabla(\rho g h)$$
$$\rightarrow \frac{D\vec{u}}{Dt} = -g\nabla \mathrm{h}$$

Rewriting the acceleration $\frac{D\overrightarrow{u_s}}{Dt}$ as $\frac{D\overrightarrow{u_s}}{Dt} = \frac{\partial u_s}{\partial t} + u_s \frac{\partial u_s}{\partial s} = \frac{\partial u_s}{\partial t} + \frac{\partial(\frac{u^2}{2})}{\partial s}$, using the assumption of a stationary flow, i.e. no changes in time, $\frac{\partial u_s}{\partial t} = 0$ and rewriting the equation in the direction of the flow this gives:

$$\frac{\partial(\frac{u^2}{2})}{\partial s} = -g \frac{\partial \mathrm{h}}{\partial s}$$
$$\rightarrow \frac{\partial}{\partial s}\left(\frac{1}{2}\frac{u^2}{g} + h\right) = 0$$

This can be read as $\frac{1}{2}\frac{u^2}{g} + h = H$ is constant in the direction of the flow.

The third relation is preservation of impulse. As noted before, between location 2 and 4 there is energy loss in the form of turbulence making it impossible to use preservation of energy. However, when assuming a stationary flow impulse will be equal at both cross-sections.

$$I_2 = I_4$$
$$\rightarrow B_2 * \left(\frac{1}{2}\rho g(a + d_2)^2 + \rho u_2^2 d_2\right) = B_4 * \left(\frac{1}{2}\rho g d_4^2 + \rho u_4^2 d_4\right)$$

In which:

| | | |
|---|---|---|
| $u_i$ | is the flow velocity at location i | (m/s) |
| $d_i$ | is the water depth at location i | (m) |
| $B_i$ | is the flow width at location i | (m) |
| g | is the gravitational constant | ($m/s^2$) |
| a | is the height of the crest | (m) |
| $I_i$ | is the impulse at location i | (N) |
| ρ | is the density of the water | ($kg/m^3$) |

This impulse relation follows from the definition of impulse as mass * velocity for a certain cross-section. Mass, m, can be written as volume * density, this gives:

$$m = V * \rho$$

With the volume, V through the cross-section defined as:

$$V = \iint u_n \, dA$$

Impulse can therefore be written as:

$$\begin{aligned}\vec{I} &= m * \vec{u} \\ &= V * \rho * \vec{u} \\ &= \iint (\rho * u_n * \vec{u}) \, dA \\ &= \iint (\rho u^2 \overrightarrow{e_n}) \, dA\end{aligned}$$

With $\overrightarrow{e_n}$ being the unity vector in the normal direction of the flow. Therefore, impulse in a cross-section is always directed inward, regardless whether or not the velocity is. This means that impulse in a cross-section is similar to pressure, p, in a cross-section, this gives:

$$p = \iint (p\overrightarrow{e_n}) \, dA$$

$$\rightarrow \vec{I} = \iint ((p + \rho u^2)\overrightarrow{e_n}) \, dA$$

In a horizontal flow with a free surface per unit of width this then gives:

$$I = \frac{1}{2}\rho g d^2 + \rho u^2 d$$

Since the widths of the cross-sections might not be equal:

$$I = B * \left(\frac{1}{2}\rho g d^2 + \rho u^2 d\right)$$

These relations give a total of 12 variables, of which $\rho, g, B_1, B_2 \; and \; B_4$ are assumed to be known. The remaining 3 required variables are $d_1, d_2 \; and \; a$. Assuming critical flow at location two, $d_2 = 2 * \frac{1}{2}\frac{{U_2}^2}{g} = \frac{{U_2}^2}{g}$, combining this with the worst-case scenario, the water up to the edge of the dyke, and $d_1$ = 6.8m, after which it collapses and a=2, the remaining variables are determined using the following maple script:

```
>
restart :
a := 2 :
g := 9.81 :
rho := 1000 :
B1 := 1 :
B2 := 1 :
B4 := 1 :
d1 := 6.8 :
h1 := d1 − a :
h2 := d2 :
h4 := d4 − a :
```

>
$$Q1 := U1 \cdot d1 \cdot B1 :$$
$$H1 := \left( h1 + \frac{U1^2}{2 \cdot g} \right) \cdot B1 :$$
$$Q2 := U2 \cdot d2 \cdot B2 :$$
$$I2 := \left( \frac{1}{2} \cdot \mathrm{rho} \cdot g \cdot (a + d2)^2 + \mathrm{rho} \cdot U2^2 \cdot d2 \right) \cdot B2 :$$
$$H2 := \left( h2 + \frac{U2^2}{2 \cdot g} \right) \cdot B2 :$$
$$d2 := \frac{U2^2}{g} :$$
$$Q4 := U4 \cdot d4 \cdot B4 :$$
$$I4 := \left( \frac{1}{2} \cdot \mathrm{rho} \cdot g \cdot d4^2 + \mathrm{rho} \cdot U4^2 \cdot d4 \right) \cdot B4 :$$
$$H4 := \left( h4 + \frac{U4^2}{2 \cdot g} \right) \cdot B4 :$$

>
$$eq1 := solve(\{Q1 = Q2, Q2 = Q4, H1 = H2, I2 = I4, U1 > 0, U2 > 0, U4 > 0, d4 > 0, d4 < d1, H4 < H2\}, \{U1, d4, U2, U4\}) :$$

### Baseline Weir

The script is first run with unit values for the width the get a first approximation:

$$\{U1 = 3.031967858, U2 = 5.869946879, U4 = 3.195528232, d4 = 6.451947829\}$$

This result indicates sub critical flow and fits with the situation where the polder has almost fully flooded.

Redoing the calculation using the actual widths provided no results at all.

### Submerged Baseline Weir

Since the first approximation using unit values provided a result which did not fit the assumption of critical flow at location two. The calculation is rerun without the relation between $d_2$ and $u_2$. This has been replaced by an approximation of $u_1$=1.5 m/s. Since the polder is almost flooded the height difference has decreased, see Figure 119, and with it the flow velocity.

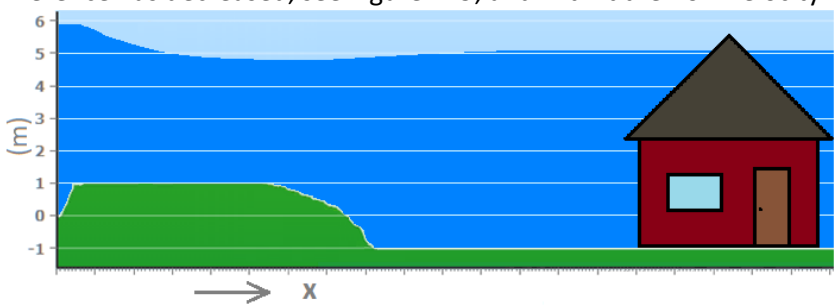


Figure 119 - Submerged Weir situation when the polder is almost fully flooded

The results for this 1 meter wide submerged baseline weir are:

Table 17 - Flow velocities and depth for the submerged baseline weir

| | | |
|---|---|---|
| $U_2$ | 2.183 | (m/s) |
| $U_4$ | 1.505 | (m/s) |
| $d_2$ | 4.672 | (m) |
| $d_4$ | 6.777 | (m) |

## Area Filling Approximation

Due to the unfortunate situation of the lack of a result from the weir equations that fits with the super critical flow situation that occurs immediately after the breach, the flow velocity and depth need to be determined in a different manner. To determine the flow velocity a method of filling an area is used. Simply said, an area behind the dyke is filled with the flood water until a certain height. Dividing the horizontally travelled distance with the time required to do this, provides the flow velocity. After determining the flow, only an approximation of the water depth is needed to determine the flow velocity.

### Input

To determine the flow, the 'long crested weir' equations are used. Based on the assumption that there should be critical flow[78], we know that $d_2 = \frac{2}{3} * H_2 = \frac{2}{3} * H_1$. The initial velocity at location one at the moment of breaching, $U_1$ is set to 0, the water is still stationary. This means that $d_2 = \frac{2}{3} * 4.8 = 3.2\ m$ and $U_2 = \sqrt{d_2 * g} = 5.6\ m/s$ and $q = 17.93\ m^3/s$.

Next, an approximation of the width at location 2 and location 4, $B_2$ and $B_4$ respectively, is required. To determine this, the breach width of 30 meters is used, see paragraph 2.4. Using streamlines to reduce the width of the breach, these streamlines will have a ratio of 1:6, meaning for every 6 metres travelled from the breach the width on both sides will increase with 1 m. Therefore $B_2$ is determined to be equal to $30 - 1 * \frac{45}{2} * \frac{1}{6} = 30 - 3.75 = 26.25$ m. The streamlines are only taken into account on one side due to the direction of the incoming flow. The flow, Q, is thus $17.93 * 26.25 = 470.7\ m^3/s$.

$B_4$ is rewritten as the breach width + x/3. This is based on the assumption that the width at location four will be equal to the width of the breach plus streamlines. Therefore, with a distance of x metres behind the foot of the dyke this width increases by x/3.

### Calculations

The calculations are performed using Maple. First the volume is determined, which is dependent on the distance, x. This is then rewritten to be dependent on the time, t. Differentiating the distance to the time provides the flow velocity, the first plot. Rewriting this back to the distance provides the second plot.

```
> restart: d := 1.5: Q := 17.93·26.25:
>
  V := d/6·x^2 + 30/1·d·x:
  eq1 := t = V/Q:
  xall := solve(eq1, x):
  x := xall[1]:
  u := diff(x, t):

> plot(u, t = 0..50);
```

[78] Paul Visser

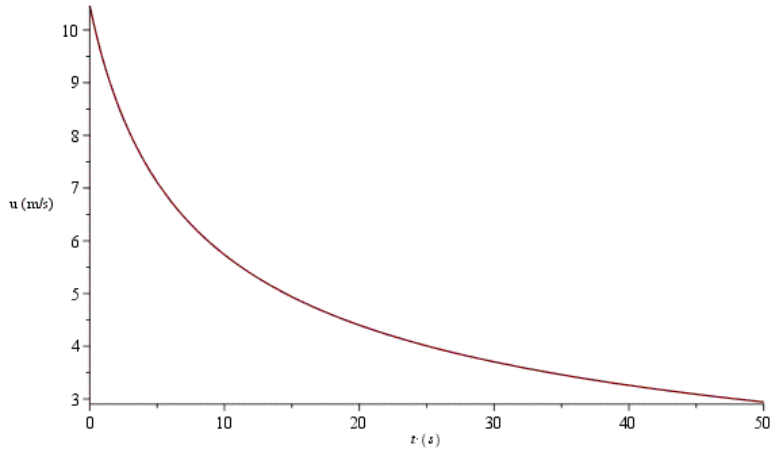


> $Vx := \frac{d}{6} \cdot xx^2 + \frac{30}{1} \cdot d \cdot xx : \; t := \frac{Vx}{Q} : \; ux := u :$

> $plot(ux, xx = 0..100);$

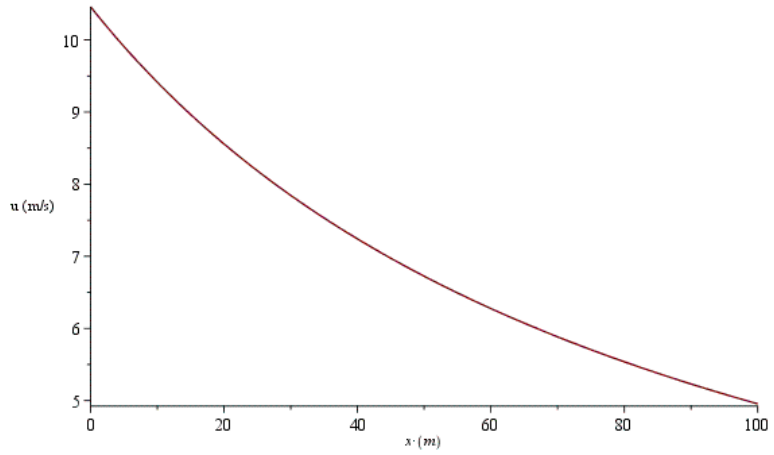


## RESULTS

Considering that in actuality the water depth will have decreased after the flood wave enters the polder, a lower limit for the velocity follows from assuming that the water depth remains the same, 3.2 m. This provides the minimum flow velocities as in Table 18. For the location of the house, at a distance of 27.5 meters behind the dyke, this minimum flow velocity is 3.75 m/s.

**Table 18 - Flow velocity for a water depth of 3.2 m**

| Distance, x (m) | Minimum Flow Velocity (m/s) |
|---|---|
| 10 | 4.41 |
| 20 | 4.01 |
| 30 | 3.68 |
| 40 | 3.39 |
| 50 | 3.15 |

The numeric approximation provides a water depth of approximately 1.5 m at the location of the masonry house. When changing the water depth in the method used above to the numeric result of 1.5 m, the results of Table 19 are obtained. For the location of the house the flow velocity would then now be 8.01 m/s.

Table 19 - Flow velocity for a water depth of 1.5 m

| Distance, x (m) | Minimum Flow Velocity (m/s) |
|---|---|
| 10 | 9.41 |
| 20 | 8.56 |
| 30 | 7.84 |
| 40 | 7.24 |
| 50 | 6.72 |

## METHOD OF CHARACTERISTICS[79]

The 'long crested weir' approximation did not provide the results as expected and the area filling approximation is a rough approximation, heavily based on the assumed water depth of the wave front. Therefore another approximation is used, the method of characteristics.

The method of characteristics is used to solve systems of differential equations. This mathematical technique can be used on the Saint-Venant equations to determine the wave characteristics of a dyke breach wave. Expressed in terms of the water depth d, the continuity equation is:

$$\frac{\partial d}{\partial t} + \frac{A}{B}\frac{\partial u}{\partial x} + u\frac{\partial d}{\partial x} + \frac{u}{B}\left(\frac{\partial A}{\partial x}\right)_{d=constant} = 0$$

In which:

| | | |
|---|---|---|
| d | is the water depth | (m) |
| t | is the time | (s) |
| A | is the flow area, B*d | ($m^2$) |
| B | is the flow width | (m) |
| u | is the flow velocity | (m/s) |
| x | is the distance in the flow direction | (m) |

The dynamic equation is:

$$\frac{\partial u}{\partial t} + u\frac{\partial u}{\partial x} + g\frac{\partial d}{\partial x} + g(S_f - S_0) = 0$$

In which:

| | | |
|---|---|---|
| g | is the gravitational constant | ($m/s^2$) |
| $S_f$ | is the friction slope | (-) |
| $S_0$ | is the bed slope | (-) |

[79] Chanson [61]

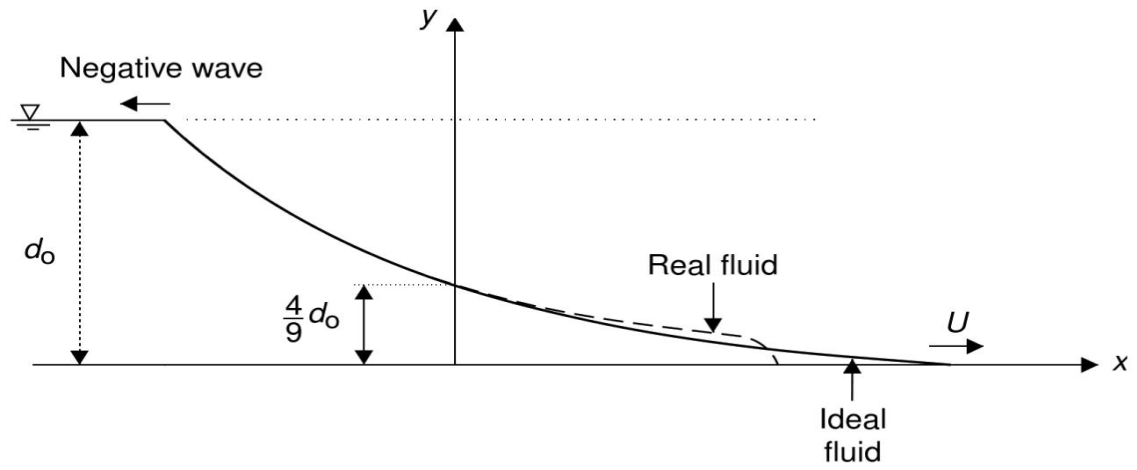


Figure 120 - Dyke Breach Wave on a dry horizontal bed (Based on [80])

The immediate dyke breach causes a negative wave to propagate upstream and a positive wave to propagate downstream, see Figure 120. The celerity of this wave is for an irregular channel equal to $c = \sqrt{g(\frac{A}{B})}$ in which A is the cross-section of the flow and B is the width of the free surface. For a dyke breach wave over a dry horizontal bed the positive wave travels with a speed of $u + 2c$ and the negative wave travels with a speed of $u - 2c$. In this u is the flow velocity.

The velocity of the wave front, v, of this dyke breach wave equals:

$$v = 2c_0 = 2\sqrt{gd_0}$$

In which $c_0$ is the initial negative wave celerity and $d_0$ is the initial water depth.

Based on the parameters from 3.1 this would provide a velocity of:

$$v = 2\sqrt{9.81 * 4.8} = 13.7\ m/s$$

With the velocity of the wave front determined, the actual height of the wave needs to be determined as well. This can be done using the inverse slope of a backward characteristic of the wave front. Since the initial backward characteristic is a straight line, the inverse slope is a constant:

$$\frac{dx}{dt} = u - c = 2c_0 - 3c$$

Integration gives the profile of the water surface for a certain time, thus t is constant. This provides the free surface profile between the negative wave front and the wave front:

$$\frac{x}{t} = 2\sqrt{gd_0} - 3\sqrt{gd} \qquad \text{for } -\sqrt{gd_0} \leq \frac{x}{t} \leq 2\sqrt{gd_0}$$

However, this cannot be used to accurately determine the depth of the wave front, since it is implicitly assumed to be 0, see Figure 120.

### Numerical Approximation

Although the method of characteristics was able to provide an approximation of the velocity of the wave front, it did not succeed in providing a depth of said wave front. Therefore a third, numerical,

[80] Chanson [61]

approximation is used. This numeric approximation is a courtesy of Svašek Hydraulics and calculated using Finel2D. This provided the following results:

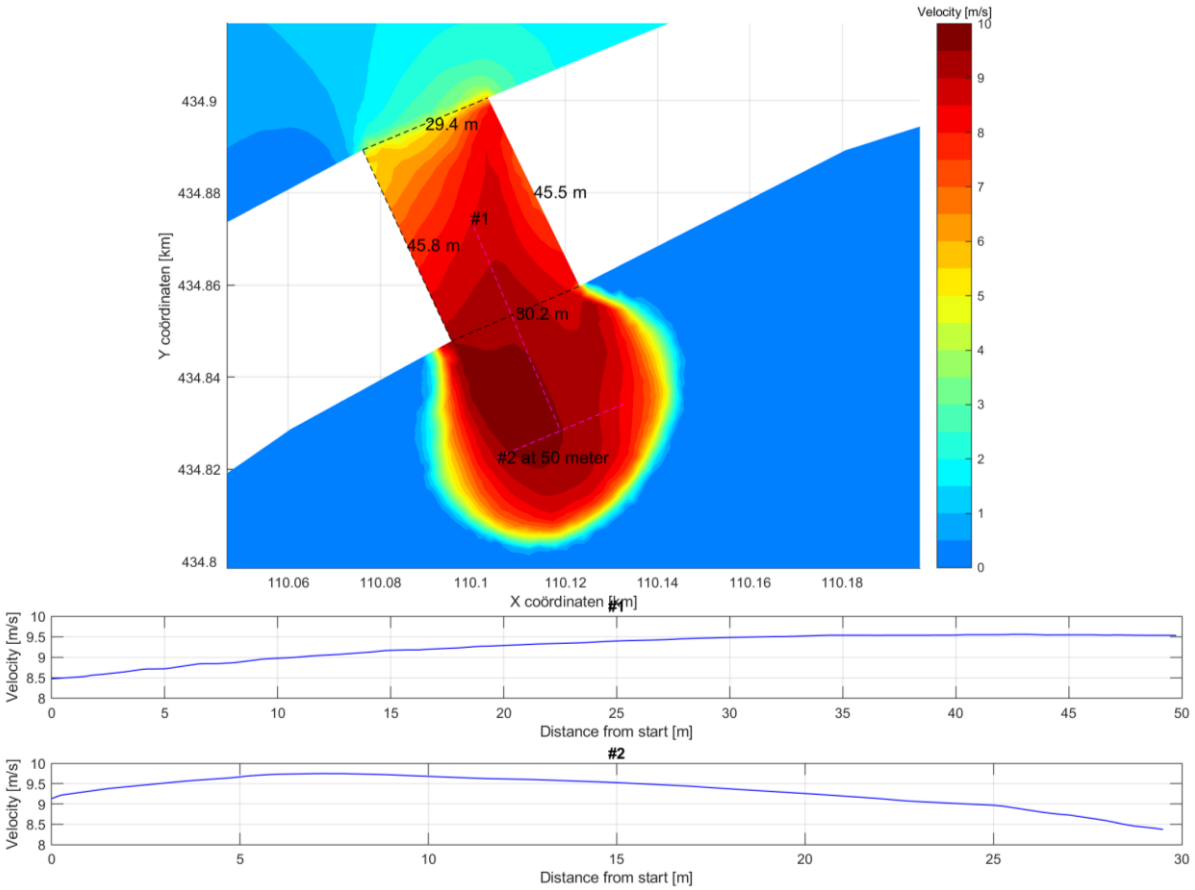


Figure 121 - Numerical approximation of the flow velocity near the breach[81]

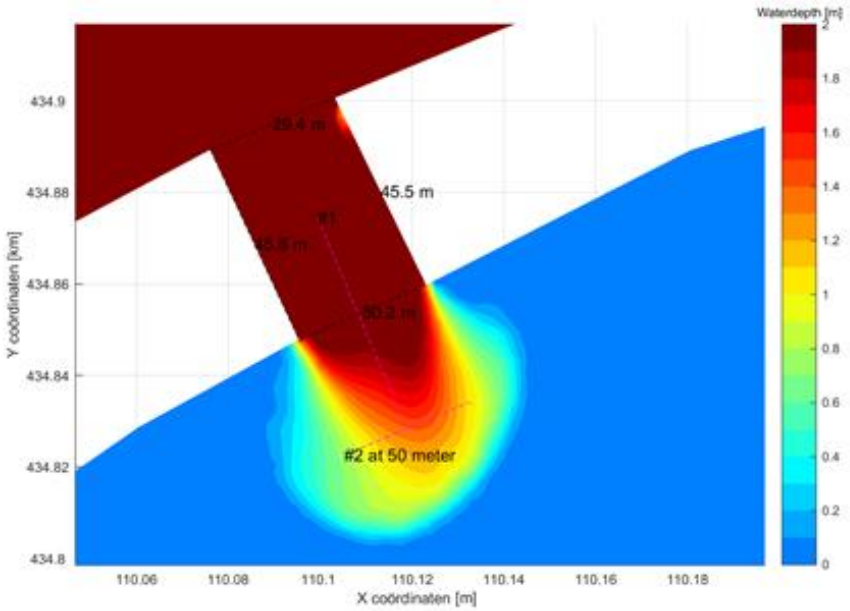


[81] Finel2D provided by Svašek Hydraulics

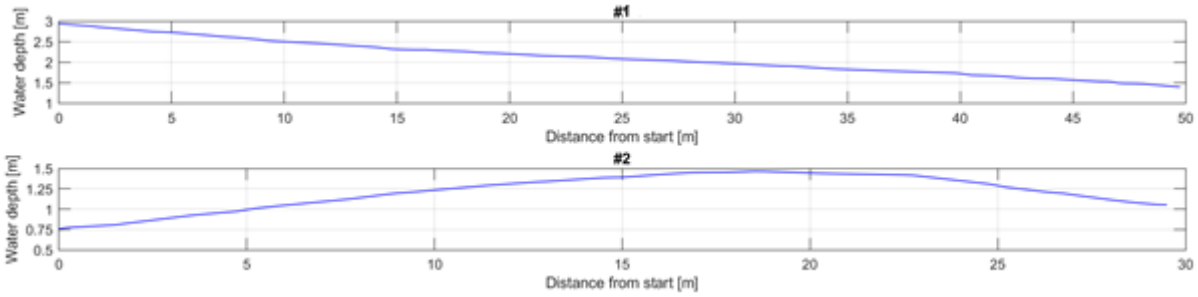


Figure 122 - Numerical approximation of the water depth near the breach, part 2[82]

The numerical approximation predicts a flow velocity of about 9.5 m/s and a water depth of approximately 1.5 m at the location of the house, 50 meter behind the centre of the breach. Since this model has not been fully calibrated for the situation used in this thesis, this is a rough first approximation.

## CONCLUSIONS

The result from the baseline weir do not match the expectations for the situation shortly after the breach. The result that did follow belonged to the situation in which the polder has almost been fully flooded. Since the assumption of critical flow at location two used to obtain this result is not valid in the new situation, a recalculation is done using a submerged weir and a decreased flow due to the decreased height difference.

Neither of those provided a somewhat accurate approximation of the water depth and flow velocity shortly after the breach. Therefore another approximation was done to obtain a minimum flow velocity combined with a maximum water depth of 3.2 meters. At the location of the masonry house, 27.5 meters behind the dyke, the minimum flow velocity would then be 3.75 m/s. When the water depth is changed to 1.5 m, similar to the result from the numeric approximation, the flow velocity at the masonry house is 8.01 m/s.

This results is, however, heavily based on the assumed water depth of the wave front. Therefore another approximation is done using the method of characteristics. Although unable to provide an accurate water depth of the wave front, an approximation of the velocity of the wave front can be obtained. This approximation is:

$$v = 2c_0 = 2\sqrt{gd_0} = 2\sqrt{9.81 * 4.8} = 13.7\ m/s$$

Finally also the results of a numeric approximation show a water depth of about 1.5 m at the location of the breach combined with a flow velocity of around 9.5 m/s.

Due to the differences in the results further research is necessary. Based on all these results, a water depth of 1.5 m and a flow velocity of 10 m/s is used to calculate the dynamic load.

[82] Finel2D provided by Svašek Hydraulics

# Appendix B. Current Model Approach

In this appendix the approach to determine the damage, used by the current models, is shortly discussed. This damage can be divided into several categories, buildings, crops, infrastructure and loss of human lives. These categories can experience direct or indirect damage, direct damage being damage directly caused by the flood, such as the destruction of a building. Indirect damage is damage as a consequence of the flood and occurs before and after the flood, for example evacuation costs or the time required to repair buildings or roads[83].

### DAMAGE CURVES

To determine the damage to one of these categories, models use damage curves. A damage curve relates the load at a certain location to the damage. These loads are almost always the inundation depth, often also the duration and sometimes the flow velocity, others are used but more scarcely. The damage curve is based on either data from previous floods and/or case study data from models. Using standardised types for the categories one can determine the damage of an entire area, by selecting the standardised type most closely to the actual type. This can for example be a type of crop but also a type of road or building. With this it is then possible to determine the total damage of this area and doing so for all categories, thus for the entire flooded area.

However, this is not a very precise method for determining the damage to a single specific building, road etc., the reason this method is still fairly accurate is because it works with averages. Therefore, if you have a large enough flooding and thus a large amount of these specific buildings, roads etc., the results will still be quite accurate.

Since every building, road, etc. is different, it is difficult to determine the exact resistance and thus damage of a single specific building, road etc. Even more so considering all the different factors that determine the resistance and damage. Working with averages is therefore a way to minimise this problem. A way to minimise the uncertainty even further is to increase the amount of types used in each category, this will allow a more precise matching of the actual buildings to the building types used in the model. This however means more damage curves are needed as well.

Some examples of damage curves are shown in Figure 123.

[83] Hoes et al. [2]

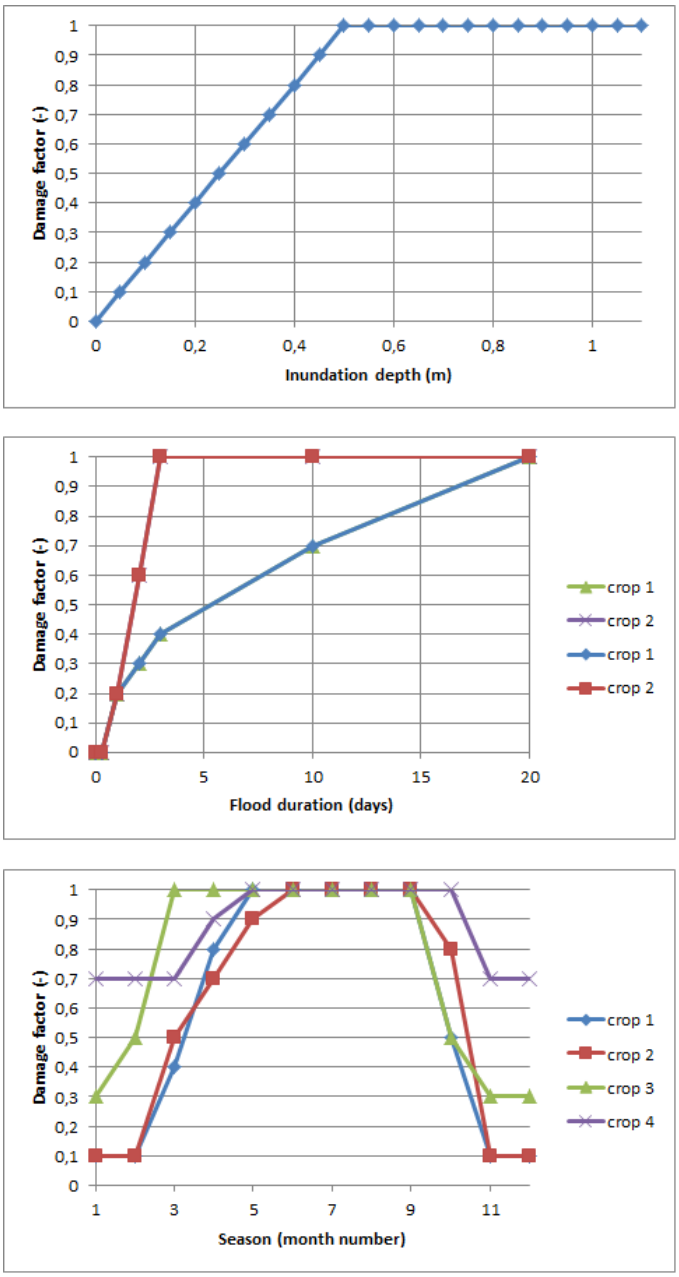


Figure 123 - Examples of damage curves

## Overview of current models

There are quite a number of models to predict the damage due to a flood event, some are specific for a certain area or type of event. An overview of several models is given in Table 20.[84,85] There are also a number of studies done to determine the damage to buildings due to a flood event, Table 21 gives an overview of several of these studies which take more than just the inundation depth into account.[86] The difference between these models and studies is that the models try to estimate the total damage caused by a flood whereas the studies are more focused on just the damage to

[84] Hoes et al. [2]
[85] Wagenaar et al. [6]
[86] Kelman et al. [4]

buildings. From the dates it is clearly visible that the current trend is to design a complete model, not just look at the individual parts of such a model.

Table 20 - Several damage estimation models

| Model name | Year | Parameters | Short description |
|---|---|---|---|
| **GIS** | 2002 | Flood depth | GIS is an Australian model that evaluates flood migration and floodplain development from an economic point of view for riverine floods. |
| **AIR** | 2008 | Flood depth<br>Duration<br>Recovery period | Air is a company which made a model for Germany as well as Great-Britain to price and underwrite the risks for floods. It takes riverine and pluvial flooding into account. |
| **HAZUS** | 2006 | Flood depth<br>Duration<br>Recovery period<br>season | HAZUS is a fairly complete model with stage damage curves for buildings, infrastructure and crops. |
| **AGDAM** | 1985 | Flood depth<br>Duration<br>Recovery period<br>Season | AGDAM is an American model specifically set up to calculate the damage to crops due to riverine floods. |
| **Adapt** | 2010 | Flood depth<br>Duration<br>Recovery period<br>Season | Adapt is a model for riverine floods that evaluates adaption methods with an integrated decision tool. Again, a rather complete model which considers buildings, infrastructure and crops. |
| **HOWAD-PREVENT** | 2012 | Flood depth<br>Duration | HOWAD-PREVENT is a model that evaluates pluvial flood damage to buildings. |
| **HIS-SSM** | 2003 | Flood depth | HIS-SSM is very general model by the Dutch ministry of Public works, which predicts damage and casualties of coastal and riverine floods. |
| **Loss estimation model** | 2003 | Velocity | The Loss estimation model is designed by Tokyo University and calculates the losses for buildings infrastructure and crops. |
| **A new damage** | 2003 | Flood depth | A new damage index is a very specialised model which calculates the replacement value of buildings. |
| **MCM** | 2005 | | MCM is a British model based on a systematic expert judgement approach. A hypothetical building is divided into small elements, which are checked individually. |
| **FLEMO** | 2008 | | FLEMO is a German flood damage model founded on date from the Elbe floods in 2002 and includes a high and low estimate. |
| **Rhine Atlas** | 2012 | | Rhine Atlas is also a German model founded on expert judgement and data from another, earlier, damage database called HOWAS |

Table 21 - Several damage estimation studies

| Study | Year | Parameters | Short description |
|---|---|---|---|
| **Beck et al.** | 2002 | Flood depth<br>Velocity | Luxembourgian study of the flood risk and vulnerability of river basins. |
| **Black** | 1975 | Flood depth<br>Velocity | American study on flood proofing rural structures. |
| **CH2M Hill** | 1974 | Flood depth<br>Velocity | American study on the potential flood damage of the Willamette river system. |
| **Smith** | 1991 | Flood depth<br>Velocity (optional) | Australian study on the implications for loss assessment of extreme floods and dam failure inundation. |
| **Islam** | 1997 | Flood depth<br>Duration<br>Velocity<br>Salinity | Study on the impacts of flooding and assessment methods in urban areas of Bangladesh. |
| **Kato and Torii** | 2002 | Flood depth<br>Sediment depth<br>Duration | Japanese study to the damages to general properties due to a storm surge in Japan. |
| **Sangrey et al.** | 1975 | Flood depth<br>Velocity | American study evaluating the impact of structurally interrupted flood plain flows. |
| **Smith and Greenaway** | 1994 | Flood depth<br>Velocity<br>Wave height | Australian study providing a damage assessment and emergency planning for Mackay, Queensland due to a tropical storm. |
| **Torterotot et al.** | 1992 | Flood depth<br>Duration | French study providing an analysis of individual real-time responses to flooding and the influence on damage to households. |

### Conclusions

Current models experience problems with accurately determining the loads and resistances in both size and location and relating those to a specific damage amount. The newer models partially counter this by increasing the number of parameters taken into account, thus increasing the physical accuracy of the model when determining the damage curves. Furthermore, they also use an increasing amount of different types in each category, i.e. a greater variety of buildings, crops, roads etc., which also increases the model's accuracy. And finally, they also decrease the size of the grid to be able to determine the loads more accurately, of course this was not possible before due to lack of computing power. A problem remains however, the amount of actual observations with which these models can be calibrated. This problem will persist, since similar flood events are not a very common occurrence.

# Appendix C. Hydraulic boundaries Streefkerk

The dyke and hinterland level are determined to be 5.8m NAP and -1.0m NAP[87]. Which would mean a possible difference of 6.8m. This is supported by the finished improvements in the area[88]. The current water level taken into account is however significantly lower, approximately 3.5m NAP[89].

To check of this would fit with historical data, a Q-h curve has been determined for the closest possible location, Hagestein, see Figure 124. In order to get the best fit possible a known high-water event from the past was chosen, the winter of 1993. Using the average of the trendlines of the rising and subsiding water a water level of 6.8m was found for Hagestein with the maximum discharge of about 4000 $m^3/s$[90]. Of course, this needs to be corrected to obtain the correct water level at Streefkerk. Therefore, the difference between Hagestein and another measuring location, Schoonhoven, during the high-water event was extrapolated to Streefkerk. This difference was 2.5m over 25km which meant that the difference at Streefkerk should approximately be 3.3m. Subtracting this from the previously calculated 6.8m NAP the previously found value of 3.5m NAP appears again. This should therefore be the maximum water level to occur at Streefkerk during high water without any other influences.

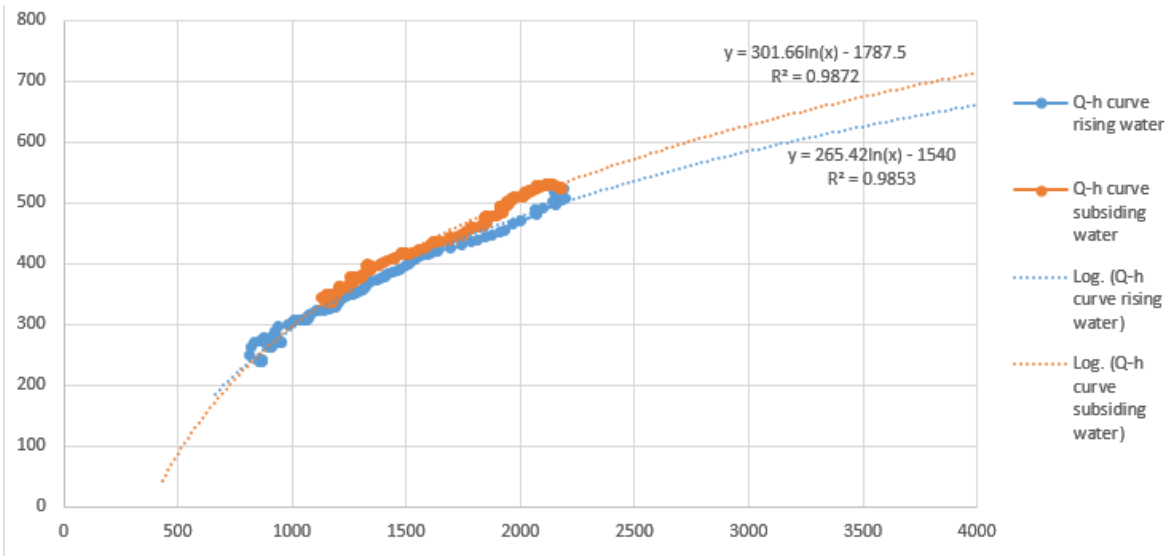


Figure 124 - Q-h curve river Lek winter 1993 at Hagestein

[87] AHN [43]
[88] Waterschap Rivierenland [44]
[89] Ministry of Infrastructure and Water Management [45]
[90] Schropp [46]

# Appendix D. Door Schematisations

Doors are essentially also plates, however they are hinged on one side, have one or more rigid point connections on the opposing side and are not connected on the top and bottom. A door can swing two ways, towards the inside and towards the outside. This has a large effect on their resistance against a water load, a door that opens against the load has the benefit that the door is supported around the edges by the frame, making failure less likely. Since it is impossible to know the orientation of every door, the weakest option is governing. Doors are therefore presumed to all swing towards the inside and only have one point connection at the height of the handle, the latch bolt. If the door is locked there are 2 or more point connections, this will also increase the resistance, especially if they are divided over the height of the door.

Since the presumed door is now hinged on one side and connected with a single point on the other side, whether or not the door will be able to resist the load comes down to whether or not the point connection is able to cope with the load. This load is transferred through the door to the latch bolt and onward to the door frame. The strength of this point can be determined, this is possible for a wide variety of materials, such as wood, aluminium and plastic. For a pre-1930 Dutch masonry house the material used to construct the door frame is assumed to be wood, spruce to be more precise. In order to transfer the load from the latch bolt to the frame a steel plate is placed on top of the wooden frame. Dried spruce has a maximum shear strength of approximately 8 N/mm$^2$ and a tensile strength perpendicular to the grain of approximately 2.5 N/mm$^2$. The ultimate tensile strength of the steel depends on the steel type and is chosen to be 400 N/mm$^2$ to make some example calculations. In Figure 125 an impression is given of the punching failure of such a connection.

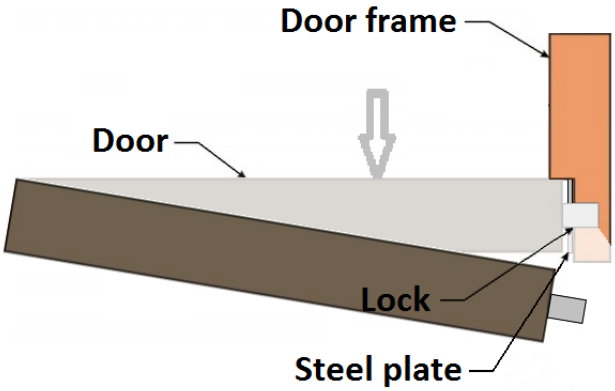


Figure 125 - Punching failure of a door/frame connection

### Failure mechanisms

To calculate the minimum force required for the failure of the connection, several failure mechanisms have been determined. Depending on the specific dimensions of the lock, the governing mechanism can be determined.

- The first failure mechanism is the tensile failure of the steel plate next to the latch (and dead) bolt. No possible shear failure of the wood is included as to get a bottom approximation.
- The second failure mechanism is a kind of punching failure. The wood next to the screws is pushed out by the screws causing the entire steel plate to disconnect and thus failure of the connection.
- The third failure mechanism is linked to the second. However now not the wood next to the screws is pushed out, but the entire section between the top and bottom screw is pushed out as a whole.

- The fourth and final failure mechanism is failure of the screws connecting the steel plate to the frame.

Figure 126 - Steel plate on the wooden door frame

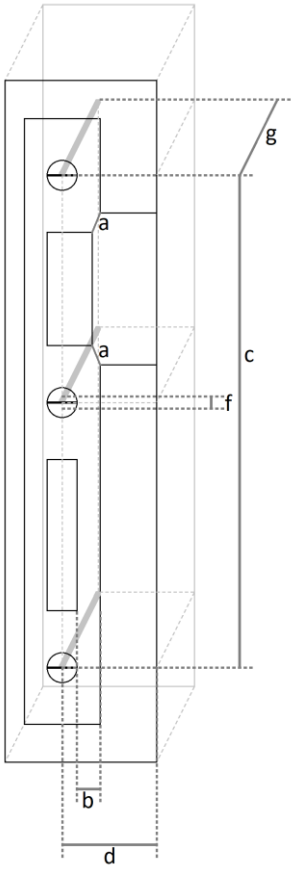


Figure 127 - Lock schematisation

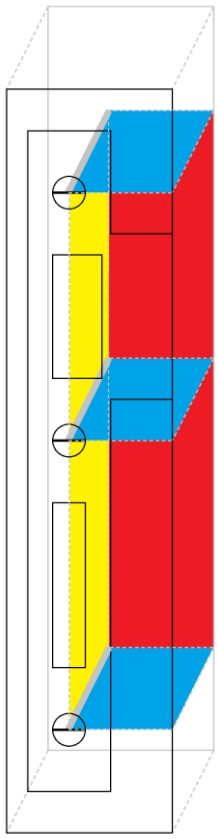

Figure 128 - Failure areas of the wooden door frame

Figure 127 shows the different dimensions of the lock and its related parts. Figure 128 shows the different areas of failure for the wooden frame, the blue areas are active in maximum shear, the red areas are active in rolling shear and the yellow areas are active in tension perpendicular to the grain.

Based on the four failure mechanisms and the dimensions from Figure 127 and Figure 128, resistance formulas can be made.

- For the steel plate to fail the strike plate near the latch bolt has to fail. This consists of two parts with equal length, a. The cross-section depends on the thickness of the steel plate which is assumed to be 'e'. The resistance of this mechanism is then:

$$F_{fail,latch} = A_{s,t} * f_{t,steel} = 2 * a * e * f_{t,steel}$$

If the door is locked another component needs to be added which is the part of the steel that fails due to the dead bolt:

$$F_{fail,dead} = A_{s,t} * f_{t,steel} = 2 * b * e * f_{t,steel}$$

The total for the first failure mechanism then is:

$$F_{fail1} = F_{fail,latch} + F_{fail,dead} = 2 * (a + b) * e * f_{t,steel}$$

| | | |
|---|---|---|
| $F_{fail,latch}$ | is the force required for tensile failure of the steel plate next to the latch bolt | (N) |
| $F_{fail,dead}$ | is the force required for tensile failure of the steel plate next to the dead bolt | (N) |

| | | |
|---|---|---|
| $F_{fail1}$ | is the force required for failure mechanism 1 of the door | (N) |
| $A_{S,t}$ | is the area of the steel active in tension | ($mm^2$) |
| $f_{t,\ steel}$ | is the ultimate tensile strength of the steel | ($N/mm^2$) |
| A | is the length of the steel plate next to the latch bolt | (mm) |
| e | is the thickness of the steel plate | (mm) |
| b | Is the length of the steel plate next to the dead bolt | (mm) |

- The area that is pushed out by the screws depends on the width, f, and length, g, of the screws, assuming that the screws push over their entire length against the wood. Furthermore, the kind of failure within the wood and its direction also influence the resistance. The resistance of the second mechanism is:

$$F_{fail2} = 3 * \left(A_{w,s} * f_{s,wood} + A_{w,srol} * f_{srol,wood}\right)$$
$$= 3 * \left(2 * d * g * f_{s,wood} + d * f * \frac{1}{4} * f_{s,wood}\right)$$
$$= \frac{3}{4} * d * f_{s,wood} * (8 * g + f)$$

| | | |
|---|---|---|
| $F_{fail2}$ | is the force required for failure mechanism 2 of the door | (N) |
| $A_{w,s}$ | is the area of the wood active in shear | ($mm^2$) |
| $f_{s,wood}$ | is the maximum shear strength of the wood | ($N/mm^2$) |
| $A_{w,srol}$ | is the area of the wood active in rolling shear | ($mm^2$) |
| $f_{srol,wood}$ | is the rolling shear strength of the wood (≈¼$f_{s,wood}$) | ($N/mm^2$) |
| d | is the distance between the screw and the side of the frame | (mm) |
| g | is the length of the screw | (mm) |
| f | Is the width of the screw | (mm) |

- Similar to the previous mechanism this resistance also depends on the length of the screws, g, as well as the kind of failure and direction within the wood. The rolling shear strength is approximately ¼ of the maximum shear strength. For the third mechanism the resistance is:

$$F_{fail3} = A_{w,s} * f_{s,wood} + A_{w,srol} * f_{srol,wood} + A_{w,t} * f_{t,wood}$$
$$= 2 * d * g * f_{s,wood} + d * c * \frac{1}{4} * f_{s,wood} + g * c * f_{t,wood}$$
$$= \frac{1}{4} * d * f_{s,wood} * (8 * g + c) + g * c * f_{t,wood}$$

| | | |
|---|---|---|
| $F_{fail3}$ | is the force required for failure mechanism 3 of the door | (N) |
| $A_{w,t}$ | is the area of the wood active in tension | ($mm^2$) |
| $f_{t,wood}$ | is the tensile strength of the wood perpendicular to the grain | ($N/mm^2$) |
| c | Is the distance between the bottom and top screw | (mm) |

- The final and fourth mechanism depends solely on the width of the screws. Again, extra resistance will likely be provided by the wood, but none is taken into account to get a bottom approximation. This leads to the following resistance:

$$F_{fail4} = 3 * \left(A_{s,s} * f_{s,steel}\right)$$
$$= 3 * \left(\frac{1}{4} * \pi * f^2 * f_{s,steel}\right)$$

| | | |
|---|---|---|
| $F_{fail4}$ | is the force required for failure mechanism 4 of the door | (N) |
| $A_{s,s}$ | is the area of the steel active in shear | ($mm^2$) |
| $f_{s,steel}$ | is the shear strength of the steel | ($N/mm^2$) |

### DOOR RESISTANCE CALCULATIONS

In order to do some example calculations for the resistance of a door lock, first all the variables need to be known. These variables are the dimensions of the lock, the properties of the wooden frame and the properties of the steel plate. See Table 22 for the assumed values of these properties.

Table 22 - Properties for example calculations door resistance

| **a** | **10** | **(mm)** |
|---|---|---|
| **b** | 6 | (mm) |
| **c** | 160 | (mm) |
| **d** | 25 | (mm) |
| **e** | 1 | (mm) |
| **f** | 4 | (mm) |
| **g** | 40 | (mm) |
| $\mathbf{f_{t,\,steel}}$ | 400 | ($N/mm^2$) |
| $\mathbf{f_{s,steel}}$[91] | $\approx (1/\sqrt{3})*f_{t,steel} = (1/\sqrt{3})*400 \approx 231$ | ($N/mm^2$) |
| $\mathbf{f_{s,wood}}$ | 8 | ($N/mm^2$) |
| $\mathbf{f_{srol,wood}}$ | $\approx ¼*f_{s,wood} = ¼*8 = 2$ | ($N/mm^2$) |
| $\mathbf{f_{t,wood}}$ | 2.5 | ($N/mm^2$) |

Using these values, the resistance of the four failure mechanisms is:

$$F_{fail1} = 2 * a * e * f_{t,steel} = 2 * 10 * 1 * 400 = 8000\ N$$

$$F_{fail2} = \frac{3}{4} * d * f_{s,wood} * (8 * g + f) = \frac{3}{4} * 25 * 8 * (8 * 40 + 3) = 48450\ N$$

$$F_{fail3} = \frac{1}{4} * d * f_{s,wood} * (8 * g + c) + g * c * f_{t,wood}$$

$$= \frac{1}{4} * 25 * 8 * (8 * 40 + 160) + 40 * 160 * 2 = 36800\ N$$

$$F_{fail4} = 3 * \left(\frac{1}{4} * \pi * f^2 * f_{s,steel}\right) = \frac{3}{4} * \pi * 4^2 * 231 = 8708\ N$$

From the chosen simplifications and values the failure of the lock would be due to tensile failure of the plate near the lock. The resistance of the lock would thus be at least 8.0 kN. Which is comparable to an inundation depth of 1.49 m for a door of 0.8 m width. This does not take into account the lever action of the door itself. The top of the door will in reality function as the rotation point of a lever with the resistance of the lock and the force of the water acting on that lever. If the resulting force of the water acts below the lock, this will have a negative effect on the resistance and if it acts above, there will be a positive effect.

[91] Von Mises in the case of pure shear stress

# Appendix E. Extended Preliminary Calculations to Masonry-Water interaction

## General Information for the Preliminary Calculations

To get an idea of how the masonry house responds to the loads, a single wall of the house is loaded and evaluated with some hand calculations. Only a small section of the wall, see Figure 129, is used undergoing a hydrostatic load and the self-weight of the house. To ease the calculations, the wall has been simplified into 2 large bricks connected with 1 layer of mortar at the breaking point. This breaking point has been assumed to be at the same location as the point of maximum bending.

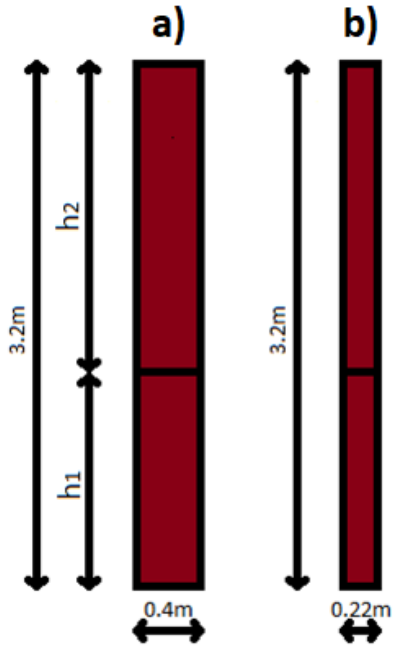


Figure 129 - Front view and side view of the small wall section

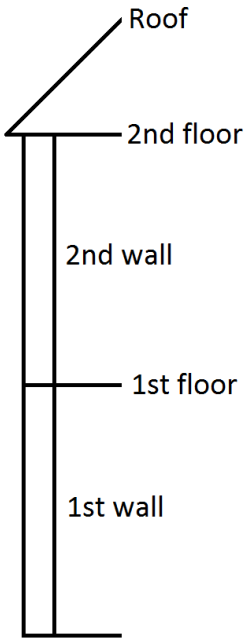


Figure 130 - Overview of the house

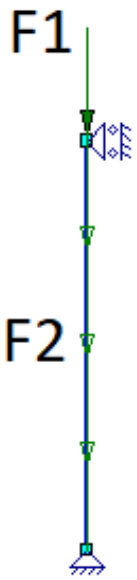


Figure 131 - Self-weight loads of the wall section

Since not all assumed dimensions are clear from Figure 129 and Figure 130, some additional information is required. The effective length for the floors working on the wall section is assumed to be 4 m. Since the roof is under a 45° angle, the effective length of the roof assumed to work on this section of wall is then 4*√2 m. Using the properties from chapter 6 the force corresponding to the self-weight of the 1st wall, $F_1$, can be determined. The self-weight corresponding to the rest of the house, $F_2$, can be determined after assumptions regarding the roof weight are made. The woodwork supporting the roof is assumed to be equal to the weight of a normal wooden floor and the weight of the ceramic roofing tiles is assumed to be 500 N/m².[92] $F_1$ is the load on top of the 1st wall, $F_2$ is the distributed load of the 1st wall, see Figure 131.

[92] Monier B.V. [21]

$$F_1 = 1st\ floor + 2nd\ wall\ + 2nd\ floor\ + roof$$
$$= (0.65\ kN/m^2 + 0.5\ kN/m^2) * 0.4m * 4m$$
$$+ 3.96\ kN/m^2 * 0.4m * 3.2m$$
$$+ (0.65\ kN/m^2 + 0.5\ kN/m^2) * 0.4m * 4m$$
$$+ (0.65\ kN/m^2 + 0.5\ kN/m^2) * 0.4m * 4m + 4m * \sqrt{2} * 0.4m * 0.5\frac{kN}{m^2}$$
$$= 1.84\ kN + 5.0688\ kN + 1.84\ kN + 2.97\ kN = 11.72\ kN$$

$$F_2 = 3.96\ kN/m^2 * 0.4m = 1.584\ kN/m$$

### Moment Capacity Calculation

For the first and second approach, the moment capacity was derived from the maximum moment and the load on top of the wall using a linear elastic stress distribution. In order to determine the moment capacity more clearly for the third approach, a stress distribution for concrete under tension has been examined[93]. Using the trendline plotted through that stress distribution, a linear approximation for the elastic part, the non-elastic part as well as for the non-elastic (partially) cracked part was determined. This was done by equalising the surface areas of the trendline and the linear approximation.

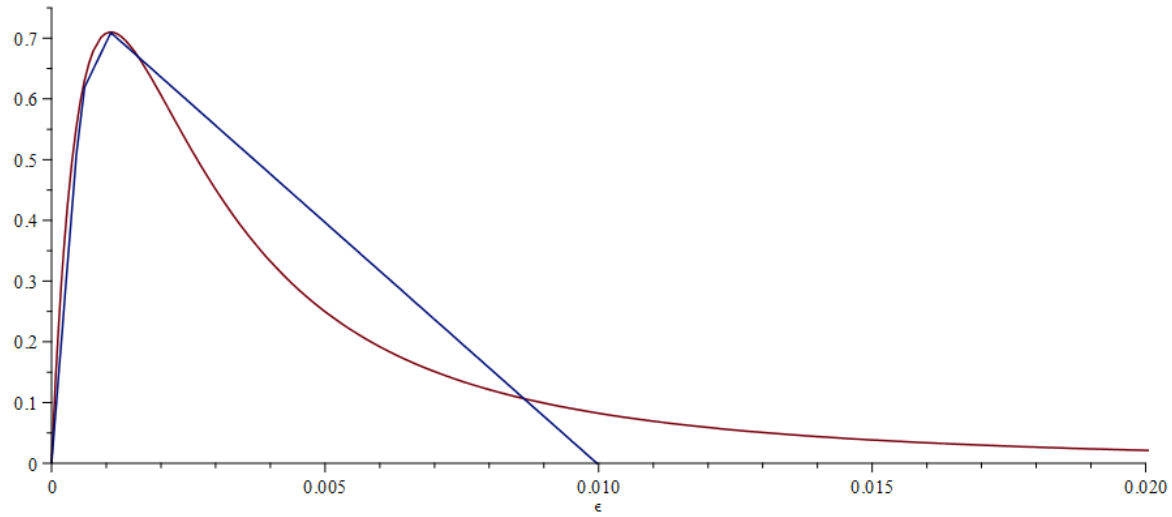


Figure 132 - Stress distribution for tension from the trendline as well as the linear approximations

```
> restart;
> sigma := epsilon/d·exp(a·epsilon/d + 1/(b + c·epsilon/d)):
>
  a := -74.8:
  b := 0.120:
  c := 16.0:
  d := 1:
  sigma2 := sigma·1.1/maximize(sigma):
  plot(sigma2, epsilon = 0..0.03)
```

[93] 2TM7 Lecture notes, figuur 5 and figuur 6 [22]

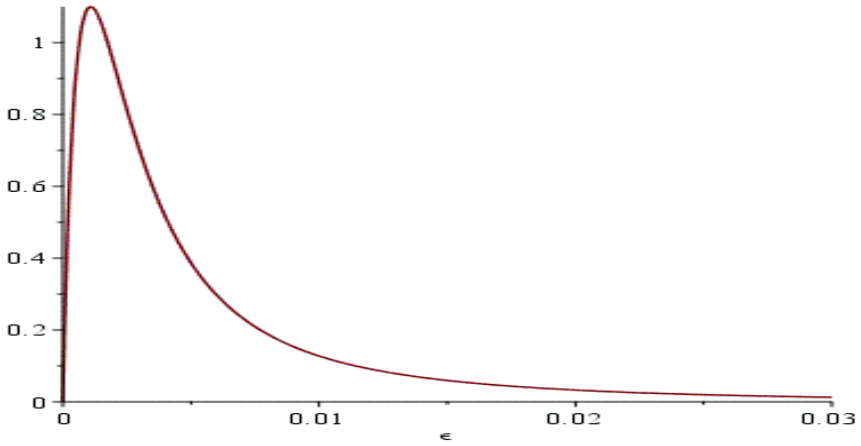


> $int(sigma2, \text{epsilon} = 0..0.05, numeric)$ :

> $s := 0.0010835056$ : $\text{delta} := \dfrac{\dfrac{1.45}{\left(\frac{7}{6}\right)}}{0.5 \cdot s}$ :

>
$y1 := \text{delta} \cdot \text{epsilon}$ :
$y2 := \dfrac{\text{delta}}{6} \cdot \text{epsilon} + \dfrac{1.45}{\left(\frac{7}{5}\right)}$ :
$y3 := -\text{delta} \cdot \left(\dfrac{1}{14.057}\right) \cdot \text{epsilon} + 1.45 + \text{delta} \cdot \left(\dfrac{1}{14.057}\right) \cdot s$ :

> $y4 := y1 \cdot \text{Heaviside}(0.5 \cdot s - \text{epsilon}) + y2 \cdot \text{Heaviside}(s - \text{epsilon}) - y2 \cdot \text{Heaviside}(0.5 \cdot s - \text{epsilon}) + y3 \cdot \text{Heaviside}(\text{epsilon} - s)$ :

> $plot(\{y4, \text{sigma}\}, epsilon = 0..0.03)$

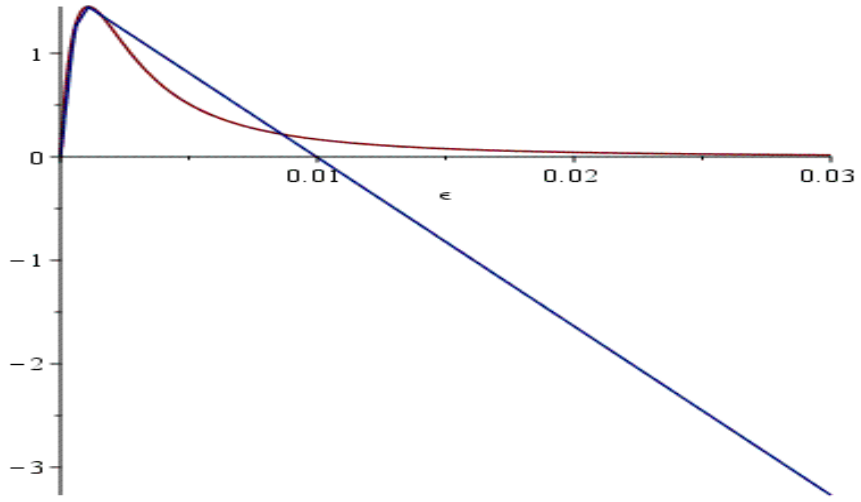


> $o := solve(y3 = 0, \text{epsilon})$ :
$app := int(y4, \text{epsilon} = 0..o)$ :
$fact := int(\text{sigma}, \text{epsilon} = 0..0.03, numeric)$ :

The linear approximations in the non-elastic part were then scaled to match the maximum tensile strength of the mortar, 0.71 N/mm$^2$, and the distance from the test setup to the actual distance

between the cracks in the wall. This distance is one brick plus two times half a joint = 50 + 2*½*12.5 = 62.5 mm[94], which gives the final linear approximations.

Using these three linearized parts of the stress distribution it is possible to determine the stress distribution for all different crack lengths, assuming the compression part is always in the linear elastic stage. Crack length has been determined as the length after reaching the maximum tensile strength of the mortar.

Calculates the stress distribution in the cross-section of a wall given the maximum tensile force at the end of the first linear part, c1, the maximum compressive force, b and the distance where compression changes into tension,g. The stress distribution is based on the crack width.

$$> c1 := \frac{6}{7} \cdot 0.71 :$$

$$b := -3.4451 :$$

$$g := 46.3529 :$$

$$k := -\frac{c1 \cdot g}{b} + g;$$

$$\mathrm{a} := \frac{(\mathrm{k} - \mathrm{g}) \cdot 5}{3} + g;$$

$$N := -0.1908 \cdot 220 :$$

$$k := 54.54106597$$

$$a := 59.99984328$$

$$> y1 := \frac{(c1 - b)}{k} \cdot x + b :$$

$$y2 := \frac{c1}{6(a - k)} \cdot x + c1 - \frac{(c1 \cdot k)}{6 \cdot (a - k)} :$$

$$y3 := -\frac{35 \cdot c1}{328 \cdot (k - g)} \cdot x + \frac{7}{6} \cdot c1 + \frac{35 \cdot c1}{328 \cdot (k - g)} \cdot a :$$

$$> y\_4 := int(y1, x) :$$

$$y\_5 := int(y2, x) :$$

$$y\_6 := int(y3, x) :$$

$$L := solve(y3 = 0, x) :$$

$$> y4 := y1 \cdot \mathrm{Heaviside}(k - x) + y2 \cdot \mathrm{Heaviside}(\mathrm{a} - x) - y2 \cdot \mathrm{Heaviside}(k - x) + y3 \cdot \mathrm{Heaviside}(x - a) - y3 \cdot \mathrm{Heaviside}(x - L) :$$

$$> plot(y4, x = 0..220)$$

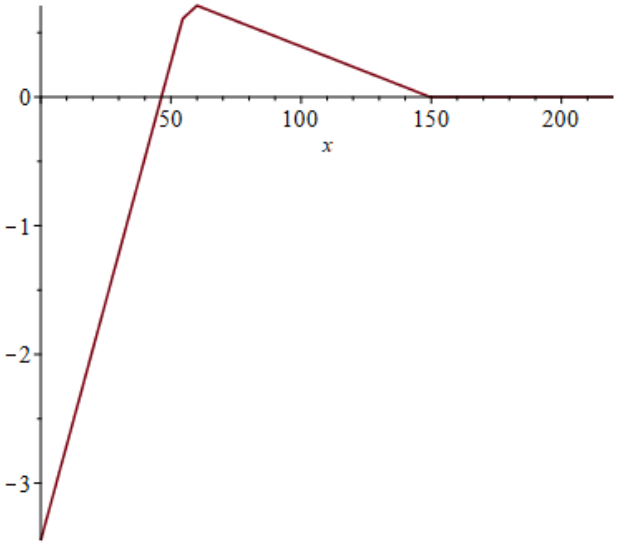


[94] Wienerberger [23]

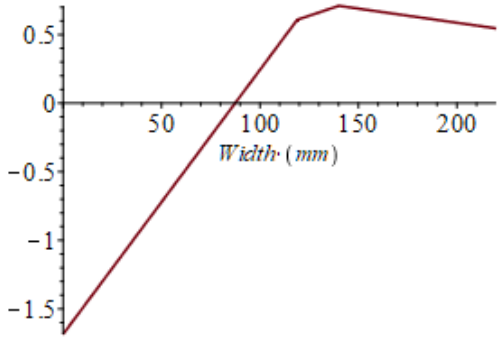


Figure 133 - Stress distribution (N/mm²) for a crack length of 80 mm

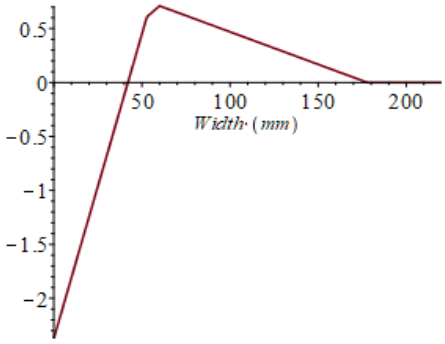


Figure 134 - Stress distribution (N/mm²) for a crack length of 160 mm

From these stress distributions the moment capacity of the cross-section has been determined by multiplying the areas under the distribution with the width of the wall and the distance to the point where compression changes to tension. This leads to a moment capacity distribution dependent on the crack length. The values for N follow from the self-weight of the wall divided by the assumed width of the wall, 400 mm. Depending on the location on the wall this value changes.

```
digits
%Formulating variables
w=400.00;             %width of the wall
N = -0.1908*220;      %self-weight, dependent on the position on the wall
                       (bottom 0.1908, top 0.1332, interpolate for the rest
                       middle at about 0.1656)
c1 = 6/7*0.71;        %maximum tensile stress linear part
E = 6700;             %young's modulus of the mortar
n = 0;                %counter for the number of iterations of b
error = 0.0050;       %allowed error for the total stress

%Initial values to start the loop
b_I = -1.3000;        %maximum compressive stress
g_I = 110;            %distance until sign change
k_I = 176;            %distance during which the stress is linear

%Parametric solutions
syms a b k g x        %a stands for the crack length, b for the maximum
                       compressive stress, k for the distance during which the
                       stress is linear, g stands for the distance until sign
                       change and x stands for relative position along the
                       brick.
y1 = (c1-b)*x/k+b;   %linear stress distribution
y3 = -35*c1*x/(328*(k-g))+(7/6)*c1+35*c1*a/(328*(k-g)); %cracked and
                       decreasing stress distribution
gFunc = matlabFunction(solve(y1 == 0, x)); %@(b,k)
h2Func = matlabFunction(solve(y3 == 0, x)); %@(a,g,k)

%Removing the symbolic variables for the rest of the code
clearvars a b k g x


%Formulating matlab functions
%stress distributions
y1 =@(b,k,x)  (c1-b)*x/k+b;                          %linear stress distribution
y2 =@(a,k,x)  c1*x/(6*(a-k))+c1-c1*k/(6*(a-k));      %cracked but still active
                                                     stress distribution
y3 =@(a,k,g,x)  -35*c1*x/(328*(k-g))+(7/6)*c1+35*c1*a/(328*(k-g));    %cracked
                                                     and decreasing stress
                                                     distribution
```

```
%integrals of the stress distributions
y4 =@(b,k,x)  (1/2)*(c1-b)*x^2/k+b*x;                    %area under the linear stress
                                                         distribution
y5 =@(a,k,x)  (1/2)*c1*x^2/(6*a-6*k)+c1*x-c1*k*x/(6*a-6*k); %area under the
                                                         cracked but still active
                                                         stress distribution
y6 =@(a,k,g,x)  -(35/2)*c1*x^2/(328*k-328*g)+(7/6)*c1*x+35*c1*a*x/(328*k-
                                                         328*g); %area under the
                                                         cracked and  decreasing stress
                                                         distribution

%Declare initial values for starting the loop after declaring the functions
b = b_I;
g = g_I;
k = k_I;
%Preallocate for speed
aVec = 220:-0.1:0.1;
Num_a = numel(aVec);
Mtot=zeros(1,Num_a);
atot=Mtot;
xtot=Mtot;
btot=Mtot;
htot=Mtot;
Wcrtot=Mtot;
etot=Mtot;

for q = 1:Num_a
    a = aVec(q);
    eq14 = 1;
    while abs(eq14)>error
        g = gFunc(b,k);
        h = min(220,h2Func(a,g,k));
        k = g + 3/5*(a-g);

        eq10 = y4(b,k,g);                    %stress area of the compression
        eq11 = y4(b,k,k)-eq10;               %stress area of the linear part of
                                              tension
        eq12 = y5(a,k,a)-y5(a,k,k);          %stress area of the non-linear
                                              tension part
        eq13 = y6(a,k,g,h) - y6(a,k,g,a);    %stress area of the cracked
                                              tension part
        eq14 = eq10+eq11+eq12+eq13-N;        %Sum of all stress areas minus the
                                              self-weight

        %Iterating b until eq14 is approximately zero.
        if eq14>50
            b = b-1;
        elseif eq14>5
            b = b-0.1;
        elseif eq14>0.5
            b = b-0.01;
        elseif eq14>0.1
            b = b-0.001;
        elseif eq14>error
            b = b-0.0001;
        elseif eq14<-15
            b = b+0.1;
        elseif eq14<-5
            b = b+0.01;
        elseif eq14<-0.1
            b = b+0.001;
        elseif eq14<-error
            b = b+0.0001;
        end
        n = n+1;
    end
```

```
%Stresses (N/mm)
equ = eq10;
equ2 = eq11;
equ3 = y2(a,k,k)*(a-k);
equ4 = y2(a,k,(1/2*(k+a)))*(a-k)-equ3;
equ5 = y3(a,k,g,h)*(h-a);
equ6 = y3(a,k,g,(1/2*(h+a)))*(h-a)-equ5;

%Forces generated by these stresses (N)
F1 = equ*w;
F2 = equ2*w;
F3 = equ3*w;
F4 = equ4*w;
F5 = equ5*w;
F6 = equ6*w;

%Moments generated by the forces (kNm)
M1 = -(2/3)*g*F1/10^6;
M2 = F2*(2/3*(k-g))/10^6;
M3 = F3*(1/2*(k+a)-g)/10^6;
M4 = F4*(1/3*(k+2*a)-g)/10^6;
M5 = F5*(1/2*(h+a)-g)/10^6;
M6 = F6*(1/3*(h+2*a)-g)/10^6;

M = M1+M2+M3+M4+M5+M6;


Mtot(q)=M;
atot(q)=a;
xtot(q)=abs(a-220);
btot(q)=b;
htot(q)=h;
Wcrtot(q)=(50+12.5)*(-b/E)*220/g;     %crack width mm
etot(q)=Wcrtot(q)*1200/220;

end
plot(xtot, Mtot)
[Mmax, Mloc] = max(Mtot);
aMmax = atot(Mloc);
```

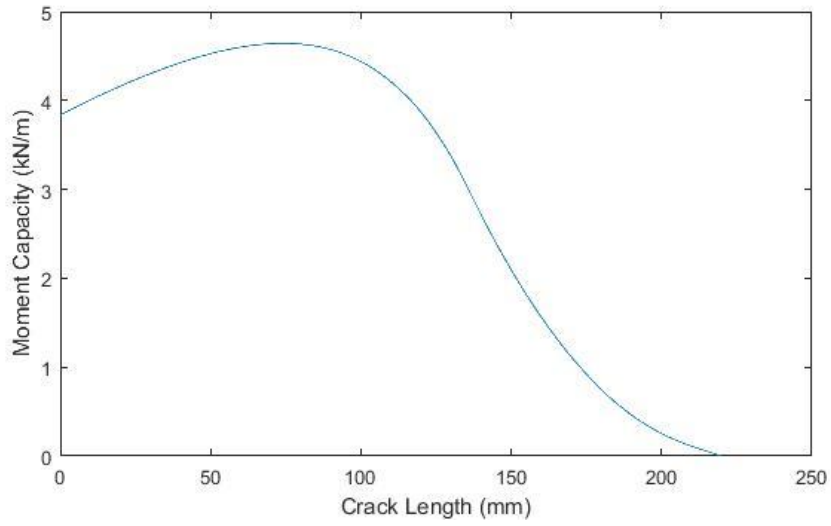


Figure 135 - Moment capacity distribution at the bottom of the wall

A remark has to be made regarding Figure 135 and the maximum compressive stress. When the crack length reaches 214 mm, the maximum compressive stress reaches 15 N/mm$^2$, any results after are

therefore not accurate anymore. In reality when this point is reached not only the tension part but also the compression part of the cross-section will start to fail.

Furthermore, the maximum moment capacity in this cross-section is 4.64 kN/m, while the moment capacity when the maximum tensile strength is reached is 3.84 kN/m and the moment capacity at the end of the elastic stage is at most 3.30 kN/m. The maximum moment capacity at the bottom thus increases with respectively 20.8% and 40.6%.

Table 23 - Moment capacities under different circumstances at the bottom, field and top location

| | Bottom (kN/m) | Field (at a height of 1.4 m) (kN/m) | Top (kN/m) |
|---|---|---|---|
| $M_{max}$ | 4.6430 | 4.5210 | 4.3724 |
| $M_{ftmax}$ | 3.8374 | 3.6849 | 3.5008 |
| $M_{el}$ | 3.2978 | 3.1284 | 2.9244 |

## First Approach to Masonry-Water Interaction

The first approach assumes no resistance at the top and bottom of the 1st wall, i.e. a hinged connection and only one load type, a hydrostatic load, $F_3$, Figure 136 shows these features.

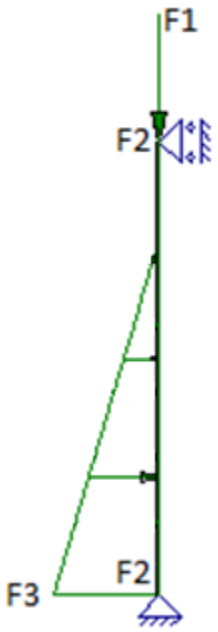


Figure 136 - Side view of the model including the hydrostatic load

### Hydrostatic Load

The hydrostatic load, $F_3$, was determined using a hydrostatic distribution. This gives the following forces:

$$F_3 = 0.5 * \rho * g * b * h^2$$
$$= 0.5 * 1.000 * 9.81 * 0.4 * h^2$$
$$= 1.962 * h^2\ kN$$

At the breaking point, the stresses can be determined which can then be compared to the material properties to determine whether or not failure occurred. In order to swiftly run several inundation depths, different values of h, a simple elastic 1D MatrixFrame model is used, see Figure 136. Since MatrixFrame does not have the material properties for masonry, concrete with a tensile strength closest to masonry is used, C12/15. This gives the following results for the hydrostatic loads:

**Table 24 - Mmax and Sigmatmax due to the hydrostatic load**

| h (m) | Mmax (kNm) | sigmatmax (N/mm²) |
|---|---|---|
| 0.5 | 0.07 | -0.162 |
| 1.0 | 0.49 | -0.027 |
| 1.5 | 1.45 | 0.275 |
| 1.97 | 2.85 | 0.712 |
| 2.0 | 2.96 | 0.746 |
| 2.5 | 4.95 | 1.365 |
| 3.0 | 7.27 | 2.086 |
| 3.2 | 8.25 | 2.390 |

$Sigma_{tmax}$ is negative for h<1 m since there is no tensile stress in the cross-section yet. The maximum tensile force of the mortar is 0.71 N/mm², so for h>1.97 m cracking occurs. Since the material is brittle and the supports are hinged it seems logical to assume that once a tensile crack occurs, this will lead to failure. Since the area transferring the tensile load will decrease and thus the stress on the remaining part will increase. For this to be true an entirely linear stress distribution is required. However, a higher load is transferable, due to the change in the stress distribution. This has been calculated above in the moment capacity calculation.

### NOTES

The situation where the first cracks supposedly appear correspond with a deflection of the wall of about 0.4mm according to MatrixFrame. Using the Young's modulus of masonry from chapter 6 and the fact that the tensile strength has just been reached three scenarios might be possible. The first option is that the entire wall is seen as elastic and will crack at the point of maximum bending when the tensile strength is exceeded. The second option is that the joint will have to cope with the deformation and will crack is soon as the tensile strength is reached. The 3rd option is the intermediate solution where only a part of the wall is active.

The three scenarios give 3 different results. Using the tensile strength and Young's modulus, the strain should be 0.0001642, this leads to an elongation or crack width of 0.525mm for scenario 1 and 0.002mm for scenario 2. However, based on the deflection of 0.4mm and the terminology as in Figure 140, the crack width should be 0.11mm, the strain for scenario 1, 0.00003438 and 0.0088 for scenario 2. This then gives tensile forces of 0.23 N/mm$^2$ and 58.96 N/mm$^2$ respectively. Both clearly do not match the expected 1.1 N/mm$^2$, therefore scenario 3 comes into view. To match the strain to the tensile force of 1.1 N/mm$^2$ only a part of the wall could be active, which can be directly determined from the previous results since the relations are linear. This leads to an active section of 0.67m, just over 20% of the entire wall.

This problem arises due to the difference between the MatrixFrame model and the assumed 2-brick model.

What happens after the first crack? Due to the deformation of the wall, the parts resting on the wall will be lifted. However, the entire building on top of the wall is already taken into account. Perhaps the side walls can lead to an extra loading on top of the wall. Assuming a 45° angle and the 4 m of effective length, the extra area of the side wall that can be taken into account is 20 $m^2$ on each side on the wall, which corresponds to 3.96 $kN/m^2$*20 $m^2$ = 79.2 kN. There are however other factors to take into account such as, this effect is localised to the sides of the wall and by decreasing the load on the side walls, the side walls are more prone to cracking themselves.

Finally, the assumed stress distribution was linear, whether this is true and what this will mean for the maximum load the wall can carry will be discussed later.

## Second Approach to Masonry-Water Interaction

The assumptions made considering a hinged connection at the top and bottom of the wall were not realistic, at the bottom the wall is connected to the foundation and at the top to a floor and a roof or another wall in this case. This means the connections are more rigid than assumed in the first approach. Therefore, a second estimation has been made assuming a rigid connection at the top and bottom, see Figure 137, using the same hydrostatic, the following results were obtained, see Table 25.

In Figure 139 the moment distribution at h=2.5 m can be seen. This clearly shows that the maximum moment is at the left (bottom) connection, this is therefore the dominant location and value.

Table 25 - Mmax and sigmatmax due to the hydrostatic load

| h (m) | Mmax (kNm) | sigmatmax ($N/mm^2$) |
|---|---|---|
| 0.5 | 0.07 | -0.17 |
| 1.0 | 0.47 | -0.05 |
| 1.5 | 1.32 | 0.22 |
| 1.97 | 2.49 | 0.58 |
| 2.0 | 2.58 | 0.61 |
| 2.12 | 2.92 | 0.71 |
| 2.5 | 4.11 | 1.08 |
| 3.0 | 5.76 | 1.59 |

Figure 137 - Second model, rigid at the top and bottom

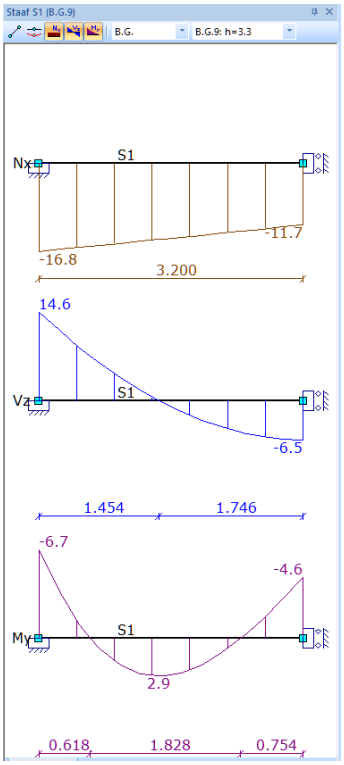


Figure 138 - Force distribution due to the hydrostatic load with an inundation depth of h=3.3 m

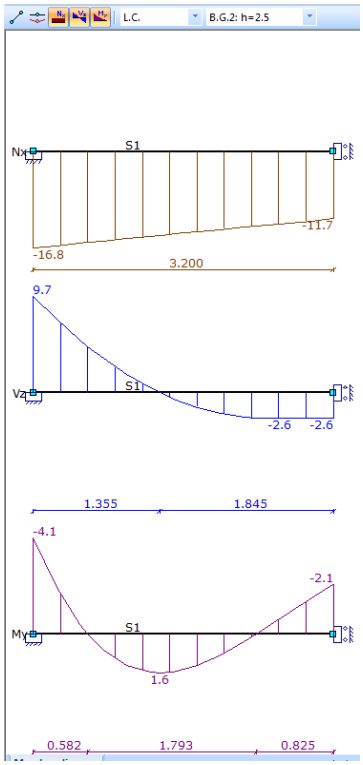


Figure 139 - Force distribution due to the hydrostatic load with an inundation depth of h=2.5 m

## Conclusions

As can be seen from Table 25, the maximum inundation depth that can be withstood increased slightly with the assumption of rigid connections at the top and bottom. The location of the maximum moment also moves to the bottom of the wall. Although the moment distribution changed significantly in value, it did not in shape, the differences between hinged and rigid are small based on their impact on when first crack occurs.

For the hinged connection equilibrium is no longer possible after the moment capacity of the cross-section has been reached which therefore determines the failure load. The rigid connection will be able to withstand at least that load and fail at or before the moment capacity is reached at all three locations, field, top and bottom. This moment capacity appeared to be about 2.9 kNm, see Table 24 and Table 25 and was reached at the third, field, location at h=3.3 m, see Figure 138. The accompanying moment at the top and bottom however grossly exceed the moment capacity, making this an unrealistic upper value for the failure load.

## Third Approach to Masonry-Water Interaction

### Plastic Hinge Model Calculation

The scenarios used in the first and second approach are not completely realistic, thus a more realistic situation will be discussed in this section assuming three plastic hinges. The first two hinges are located at the bottom and top of the wall, the third plastic hinge is assumed to be at the location of the maximum field moment.

The same MatrixFrame model as in the second approach has been used, however now when the moment capacity, $M_{max}$, of the cross-section is reached, a plastic hinge will appear. This will allow for a redistribution of the forces.

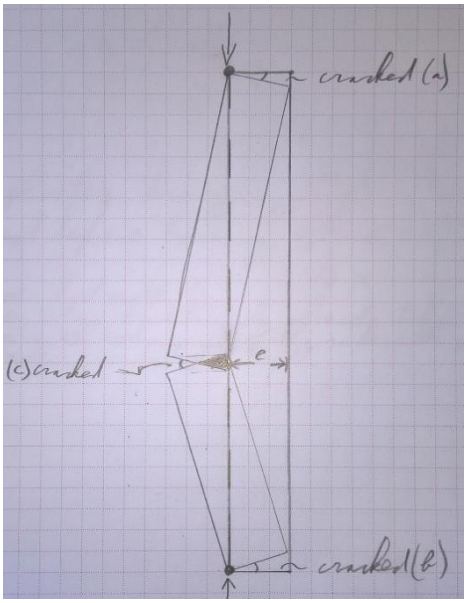


Figure 140 - More realistic situation with three plastic hinges

### Plastic Model Calculations

To determine in what order and when these hinges will appear several steps were taken. First the actual moment capacity of the cross-sections was determined, starting at $M_{el}$ after which some plastic deformation occurs and $M_{ftmax}$ is reached. Second the load was increased in order to find the location of the first hinge. After finding the first hinge the load was increased to find the second hinge whilst lowering the resistance of the first hinge in order to prevent the moment at that location from being greater than $M_{ftmax}$. When hinge two was found the same procedure was followed as before to find the third hinge, only now both existing hinges were prevented from being greater than $M_{ftmax}$. The load at which hinge three appears is when deflections start to increase and the extra moment capacity will be utilised. After the maximum moment capacities, $M_{max}$, are reached equilibrium is no longer possible and failure will occur.

Using the new moment capacities, the following distributions for the hydrostatic load have been obtained, with h being the inundation depth. First without any plastic hinges, next with plastic hinges at the bottom and finally with plastic hinges at the bottom and top. The values of the springs representing the plastic hinges are indicated below the figures.

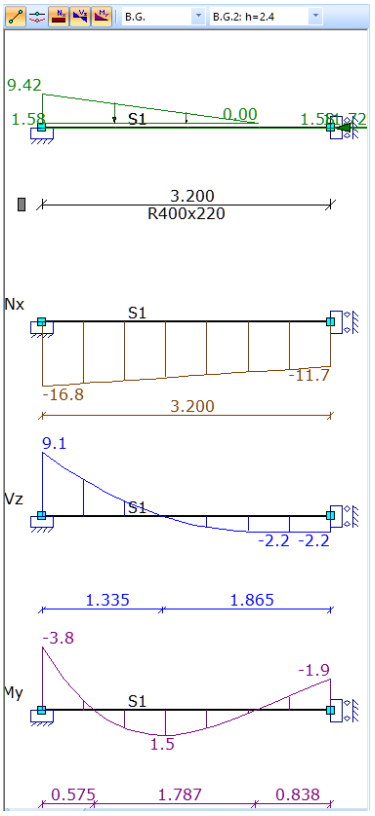


No springs

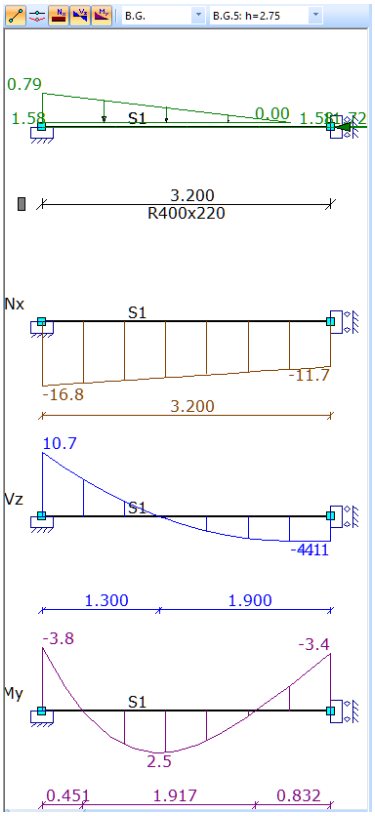


Bottom: 40.000 kNm*rad

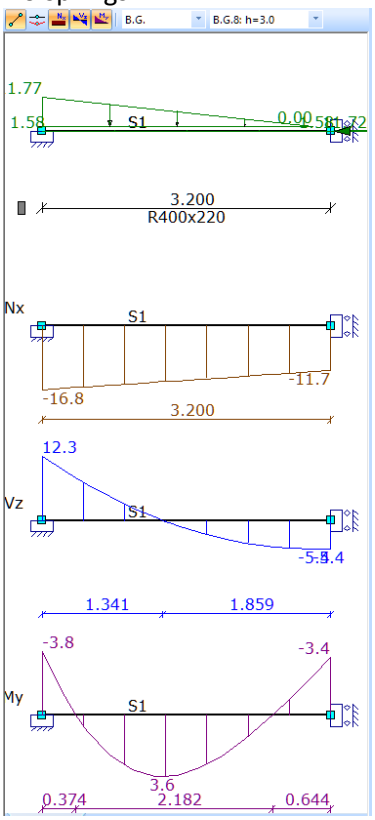


Bottom: 16.500 kNm*rad
Top: 26.000 kNm*rad

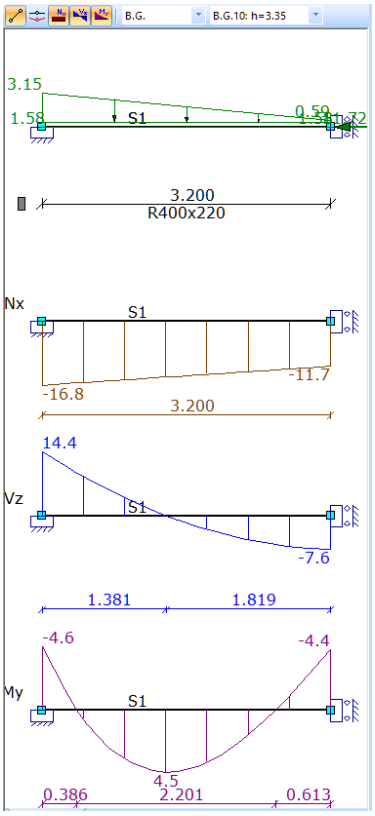


Bottom: 16.500 kNm*rad
Top: 25.000 kNm*rad

**Figure 141 - Moment distribution when the first, second and third plastic hinge occur and when failure occurs**

The first plastic hinge appears at h = 2.4 m, the second at h = 2.75 m and the third at h = 3.0 m, then the load can increase untill h = 3.35 m before failure occurs. Compared to the previous paragraphs

the load increases due to the increased moment capacity. The load at which failure occurs also increases slightly, due to the higher maximum moment capacity. Previously this was reached at or before h = 3.3 m and with the higher maximum moment capacity this value is increased to an inundation depth of 3.35 m.

### Plastic Hinge Hand Calculation

Instead of using a computer program it is also possible to do the plastic hinge calculation by hand. Using the sign conventions as seen in Figure 142 and Figure 143 the following equations can be derived:

$$h = 3.2\ m = h_1 + h_2$$

$$\delta\theta_1 = \frac{h_2}{h_1} * \delta\theta_2 \ \rightarrow\ \delta\theta_2 = \frac{h_1}{h_2} * \delta\theta_1$$

$$\delta A = 0 = -Mp_1 * \delta\theta_1 - Mp_2 * \delta\theta_1 - Mp_2 * \delta\theta_2 - Mp_3 * \delta\theta_2 + F_1 * \delta\theta_2 * \left(\frac{1}{3} * (h_1 - h_3) + h_2\right) + F_2 * \delta\theta_1 * \frac{1}{3} * h_1 + F_3 * \delta\theta_1 * \frac{1}{2} * h_1$$

$$\rightarrow 0 = -Mp_1 * \delta\theta_1 - Mp_2 * \left(\delta\theta_1 - \frac{h_1}{h_2} * \delta\theta_1\right) - Mp_3 * \frac{h_1}{h_2} * \delta\theta_1 + F_1 * \frac{h_1}{h_2} * \delta\theta_1 * \left(\frac{1}{3} * (h_1 - h_3) + h_2\right) + F_2 * \delta\theta_1 * \frac{1}{3} * h_1 + F_3 * \delta\theta_1 * \frac{1}{2} * h_1$$

$$\rightarrow 0 = \delta\theta_1 * \left(-Mp_1 - Mp_2 * \left(1 + \frac{h_1}{h_2}\right) - Mp_3 * \frac{h_1}{h_2} + F_1 * \frac{h_1}{h_2} * \left(\frac{1}{3} * (h_1 - h_3) + h_2\right) + F_2 * \frac{1}{3} * h_1 + F_3 * \frac{1}{2} * h_1\right)$$

$$\rightarrow Mp_1 + Mp_2 * \left(1 + \frac{h_1}{h_2}\right) + Mp_3 * \frac{h_1}{h_2} = F_1 * \frac{h_1}{h_2} * \left(\frac{1}{3} * (h_1 - h_3) + h_2\right) + F_2 * \frac{1}{3} * h_1 + F_3 * \frac{1}{2} * h_1$$

$$F = \frac{1}{2} * \rho * g * b * h^2, with\ \rho = 1000 \frac{kg}{m^3}, g = 9.81 \frac{m}{s^2}, and\ b = 0.4\ m$$

$$\rightarrow F = 1.962 * h^2$$

$$F_1 = 1.962 * (h_3 - h_1)^2$$

$$F_2 = 1.962 * {h_1}^2$$

$$F_3 = 3.924 * h_1 * (h_3 - h_1)$$

$$\rightarrow Mp_1 + Mp_2 * \left(1 + \frac{h_1}{h_2}\right) + Mp_3 * \frac{h_1}{h_2} = 1.962 * \left((h_3 - h_1)^2 * \frac{h_1}{h_2} * \left(\frac{1}{3} * (h_1 - h_3) + h_2\right) + \frac{1}{3} * {h_1}^3 + {h_1}^2 * (h_3 - h_1)\right)$$

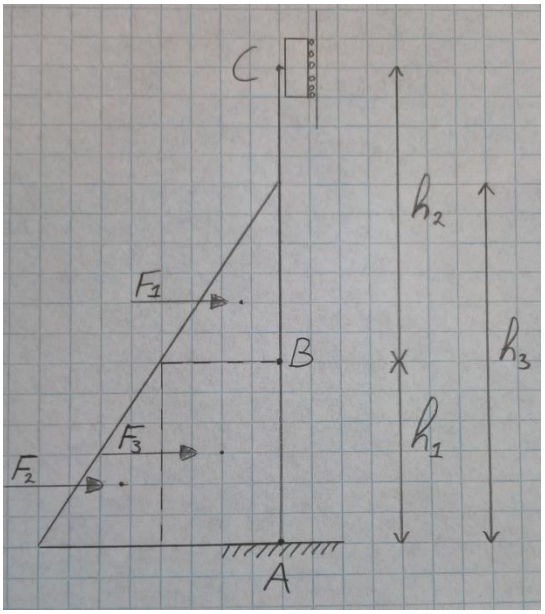


Figure 142 - Sign convention plastic hinge hand calculation

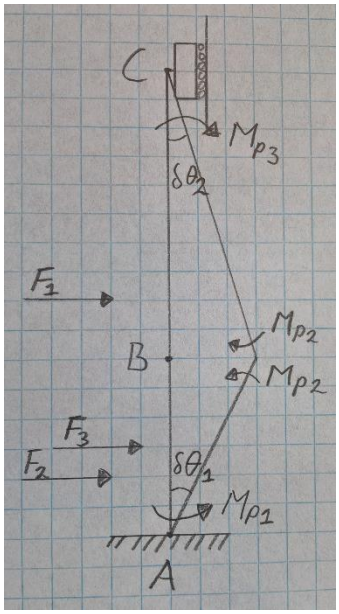


Figure 143 - Sign convention plastic hinge hand calculation

From the unknowns left in the final equation, $Mp_1$, $Mp_2$ and $Mp_3$ can be determined using the obtained moment capacity. The only thing needed to be able to solve this equation is a relation between $h_3$ and one of the other h. Assuming point B is at the location of the maximum field moment it is possible to calculate $h_1$ for the inundation depth, $h_3$, using the MatrixFrame model from the previous paragraphs. After plotting these values in a graph, a trendline can be drawn through these values to provide the relation needed, see Figure 144. This relation will however only be valid for $0<h_3<4.5$ m.

-

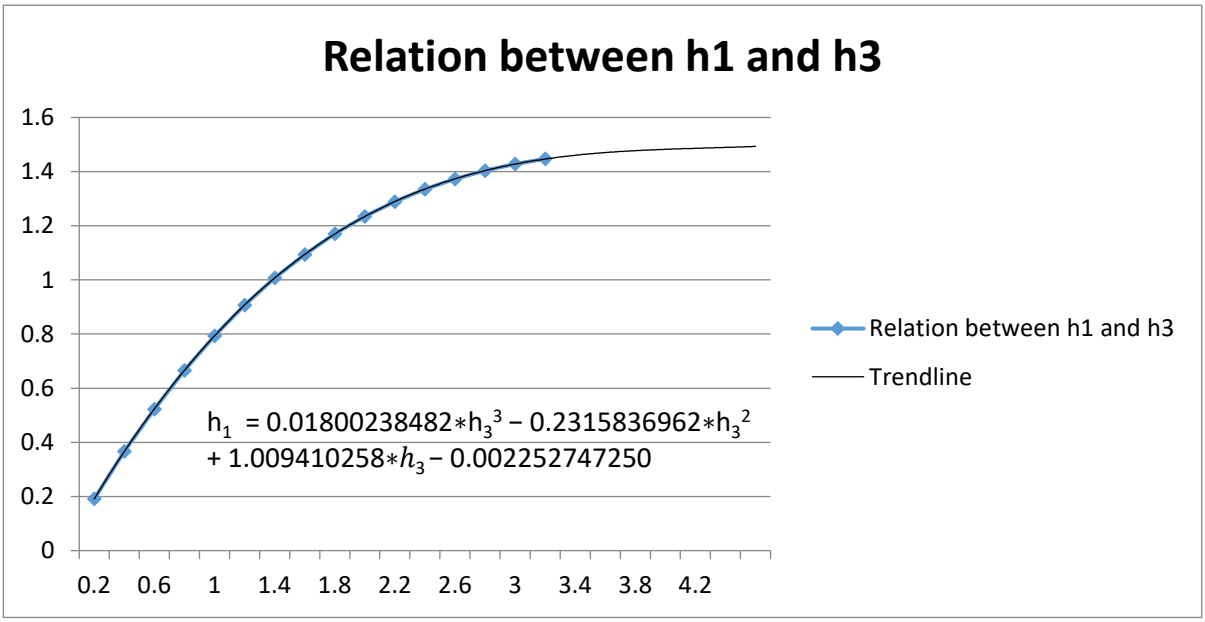


Figure 144 - Relation between $h_1$ and $h_3$

Since the remaining formula is rather unpleasant to work out by hand, Maple is used to solve the equation.

```
> restart;
```

Calculates the water level at which the plastic moments are reached.
Adjust Mp1, Mp2 en Mp3 and possibly the relation between h1 and h3

Plastic moments:

> $Mp1 := 3.8374 : \ Mp2 := 3.6849 : \ Mp3 := 3.5008 :$

Calculations according to the derived equations:

> $F := 1.962 \cdot \left( (h3 - h1)^2 \cdot \left( \frac{h1}{h2} \cdot \left( \frac{1}{3} \cdot (-h3 + h1) + h2 \right) \right) + \frac{1}{3} \cdot h1^3 + h1^2 \cdot (h3 - h1) \right) :$

> $M := Mp1 + Mp2 \cdot \left( 1 + \frac{h1}{h2} \right) + Mp3 \cdot \left( \frac{h1}{h2} \right) :$

>

$h := h1 + h2 = 3.2 :$
$eq := M = F :$
$eq2 := h1 = -0.0004603125\, h3^5 + 0.0054708125\, h3^4 - 0.0043752500\, h3^3$
$\quad - 0.1930415675\, h3^2 + 0.9830384415\, h3 + 0.0028479301 :$
$y := -0.0000001473 \cdot (h3 \cdot 5)^5 + 0.0000087533 \cdot (h3 \cdot 5)^4 - 0.0000350020 \cdot (h3 \cdot 5)^3$
$\quad - 0.0077216627 \cdot (h3 \cdot 5)^2 + 0.1966076883 \cdot (h3 \cdot 5) + 0.0028479301 :$

$plot(y, h3 = 0..5)$

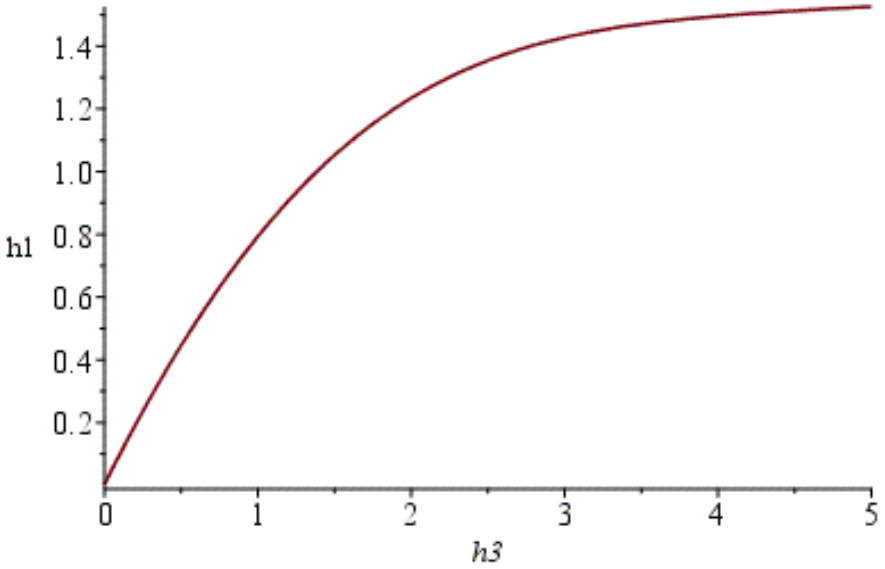


Solving previous equations:

> $s := solve(\{eq, eq2, h, h1 > 0, h2 > 0, h3 > 0\}, \{h1, h2, h3\}) :$

> $s[1]; s[2]; s[3]; s[4]; s[5]; s[6]; s[7]; s[8]; s[9];$

Assigning the proper values for h1, h2 and h3:

> $assign(s[1]); h1; h2; h3$

This gives the following results:

$\{h1 = 0.9243134551, h2 = 2.275686545, h3 = 7.673085466\}$
$\{h1 = 1.461243945, h2 = 1.738756055, h3 = 3.367577160\}$

These results have been narrowed down since when $h_3$ rises the load approaches a uniform distribution, for which $h_1$ is 1.6 m. This means $h_1$ cannot be greater than 1.6 m. Furthermore, for any plastic hinge to occur an inundation depth, $h_3$, of well above 2.0 m is needed, which means an $h_1$ of

more than 1.2 m. This means $h_1$ should be between 1.2 and 1.6 m, only one of the results fits these criteria. Thus $h_1$ = 1.4612 m, $h_2$ = 1.7388 m and $h_3$ = 3.3676 m.

Rerunning the calculation again with the moment capacity before any major deformations take place, $M_{ftmax}$, where $Mp_1$ = 3.8374 kNm, $Mp_2$ = 3.6849 kNm, $Mp_3$ = 3.5008 kNm, gives the following results:

$$\{h1 = 1.430754873, h2 = 1.769245127, h3 = 3.027582352\}$$
$$\{h1 = 0.6547316630, h2 = 2.545268337, h3 = 7.949664521\}$$

Applying the same conditions as before gives $h_1$ = 1.4308 m, $h_2$ = 1.7692 m and $h_3$ = 3.0276 m.

## CONCLUSIONS

When comparing the first model calculations with the later plastic calculations there are some relatively big differences. These can be largely contributed to the difference in the stress distributions and model schematisations. Since the first and second approach lack a certain degree of realism, the focus will be on the results of the third approach, both computer and hand calculations.

In order to properly compare both plastic hinge calculations they were done for $M_{max}$ and $M_{ftmax}$. The results are almost the same, for $M_{ftmax}$, $h_3$ = 3.35 m compared to $h_3$ = 3.37 m. And for $M_{max}$, $h_3$ = 3.0 m while the hand calculation gives $h_3$ = 3.03 m. The difference can be explained by the lack of accuracy in the model calculation, $h_3$ is accurate within about 0.05m, while the hand calculation gives a result with an accuracy of several decimals. Besides that, the changing circumstances between the model and hand calculation cause small differences such as the relation between $h_1$ and $h_3$ which changes due to the deformations of the cross-sections. And lastly the use of C12/15 as a representative for the properties of masonry. Since both different methods independently give similar results, the results can be taken as fairly accurate.

From this it follows that from the moment the first crack appears the next cracks follow rather quickly but quite some margin is left before the failure load is reached. This means that although failure will be quick and sudden, there is a distinct warning period, which unfortunately will not be visible to the naked eye since the cracks are too small.

# Appendix F. Masonry Properties Calculations[95]

The masonry properties have been calculated using the values from Table 26.

**Table 26 - Brick and Mortar Properties**

| | | | |
|---|---|---|---|
| **Young's modulus brick** | $E_b$ | 6000 | ($N/mm^2$) |
| **Young's modulus mortar** | $E_{mt}$ | 6600 | ($N/mm^2$) |
| **Joint thickness** | $j_t$ | 10 | (mm) |
| **Brick thickness** | $b_t$ | 50 | (mm) |
| **Brick length** | $b_l$ | 220 | (mm) |
| **Brick width** | $b_w$ | 100 | (mm) |

The Young's moduli and shear modulus of the masonry can be determined by[96]:

$$\frac{1}{M_m} = \frac{t_b}{M_b} + \frac{t_m}{M_{mt}}$$

In which:

| | | |
|---|---|---|
| $M_m$ | is the modulus of the masonry | ($N/mm^2$) |
| $M_b$ | is the modulus of the brick | ($N/mm^2$) |
| $M_{mt}$ | is the modulus of the mortar | ($N/mm^2$) |
| $t_b$ | is the relative length of the brick in the brick-mortar combination | - |
| $t_m$ | is the relative length of the mortar in the brick-mortar combination | - |

The shear moduli are 0.4 times the respective Young's moduli. This leads to the moduli as in Table 27.

**Table 27 - Masonry Moduli**

| | | | |
|---|---|---|---|
| **Young's modulus masonry in horizontal direction** | $E_x$ | 6024 | ($N/mm^2$) |
| **Young's modulus masonry in vertical direction** | $E_y$ | 6092 | ($N/mm^2$) |
| **Shear modulus masonry** | $G_{xy}$ | 2423 | ($N/mm^2$) |

The mass density can be determined from the respective density of the bricks and mortar and their respective volume in the masonry. This gives a mass density of about 1800 $kg/m^3$.[97]

The angle between the stepped diagonal crack and the bed-joint follows from the thickness of the joint and brick divided by the width of the brick and joint times a half.

$$\alpha = \tan^{-1}\left(\frac{(b_t + j_t)}{0.5 * (b_l + j_t)}\right)$$

This leads to an angle of 27.55°.

For the factor to strain at compressive strength, the default value of 4 has been used. This would mean with $n = \frac{E*\varepsilon_{peak}}{f_c} = 4, E \approx 6060\ N/mm^2 + and\ f_c = 14.2\ N/mm^2$ that $\varepsilon_{peak} \approx 0.0094$, which is realistic.

[95] The remaining properties come from Van Noort, J.R. Table 6.2 [15]
[96] Van Noort, J.R. [15]
[97] Roos, W. [1]

# Appendix G. Head-Joint Failure Types[98]

There are four different kinds of head-joint failure that the engineering masonry model offers, these are:

- Head-joint failure not considered
- Direct input head-joint tensile strength
- Diagonal stair-case cracks
- Tensile strength head-joint defined by friction

Since head-joint failure is expected to occur, the first option is not adequate. In order to determine the difference between the other three, besides their theoretical differences, a model in DIANA is run with the different kinds of head-joint failure to determine the difference and what causes them. From that and the theory it is then possible to determine to most appropriate head-joint failure type.

The simplest of the three options is the direct input head-joint tensile strength. Especially, since in principle the head-joint tensile strength is equal to the bed-joint tensile strength and this head-joint tensile strength is the only added variable. Therefore, no additional information is required. Theoretically seen besides failure in the direction normal to the bed-joint and shear-failure, cracking and crushing is also considered in the direction normal to the head-joint. Diagonal cracks are still not considered.

Next is the diagonal stair-case cracks, it does not require a direct input for the head-joint tensile strength, but it does require and angle for the diagonal cracks in the wall. This angle is determined by the dimensions of the brickwork, since it usually follows the joints in the wall. Information about the brickwork is therefore required to properly use this option. Compared to the previous option, head-joint failure is now considered to be a part of the diagonal stair-case cracks. The tensile strength of these diagonal cracks is calculated from the user defined bed-joint tensile strength, the frictional shear stress and the diagonal stair-case crack angle. Failure due to compression is only considered in the direction normal to the bed-joint.

The last option is the tensile strength head-joint defined by friction, this option requires the angle is mentioned above as well as a minimum tensile strength for the head-joint. If this information is not available and zero is chosen, some areas of the wall will crack very early. Although those cracks are small, they do not depict the actual situation accurately. Theoretically seen the tensile strength is calculated from the friction shear stress in the bed-joint. The effect of high overburden load can be considered in this mode. Similar to the direct input head-joint tensile strength, the cracking and crushing in the direction normal to the head-joint is considered.

## HEAD-JOINT MODEL TESTS

The theory mentioned above is confirmed by the tests performed in DIANA. Five different tests have been run, one for the direct input, one for the diagonal stair-case cracks and 3 for the tensile strength head-joint defined by friction. The results of the direct input and the tensile strength head-joint defined by friction are the same of the minimum strength of the head-joint is the same as the tensile strength in the direct input. Since the minimum strength of the head-joint is unknown only the direct-input or the diagonal stair-case cracks are thoroughly compared.

[98] Rots et al. [57]

The results are in the following figures for the last point where convergence was achieved, note that a stress of $7.1*10^5$ is equal to the tensile strength of the masonry. Layer 1 is located at the inside of the wall, layer 7 on the outside of the wall. Overall as expected the stresses and strains of both options match fairly well, some differences in magnitude can be observed where the diagonal stair-case cracks have to higher stresses, strains and therefore also larger crack widths. The largest difference can be observed between Figure 145 and Figure 146, with the presence of the diagonal strains. The lack of cracks for the direct input potion in Figure 162 and Figure 164 in the centre of the wall follows from the stresses, which are just below the tensile strength of the masonry.

Seen the minor differences the diagonal stair-case cracks option is used for the rest of the computations. The slightly large values make it the safer option and the added diagonal cracks are of larger importance in the inner walls and side walls of the house.

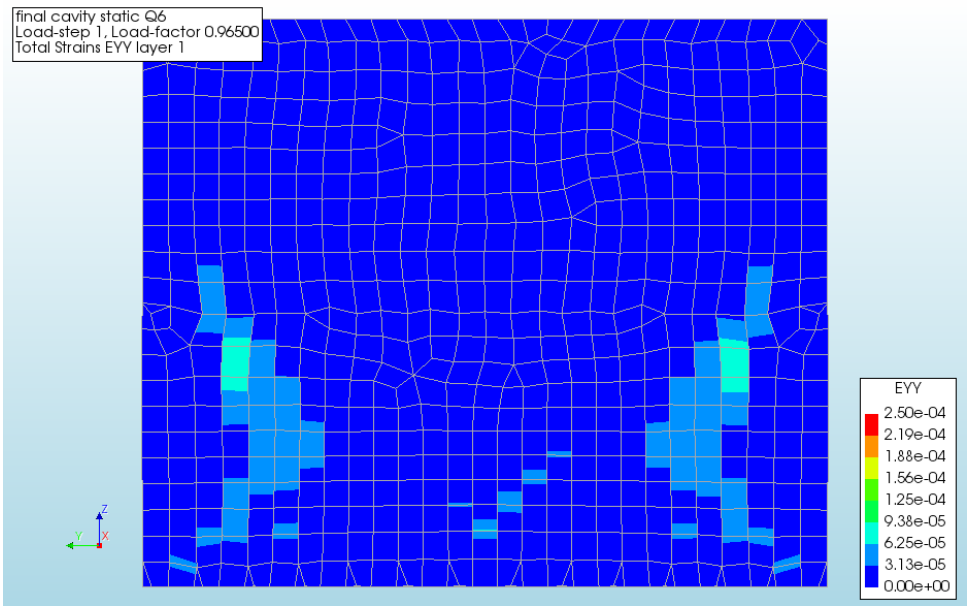


Figure 145 - Strain EYY from layer 1 with an inundation depth of 1.5m for the diagonal option

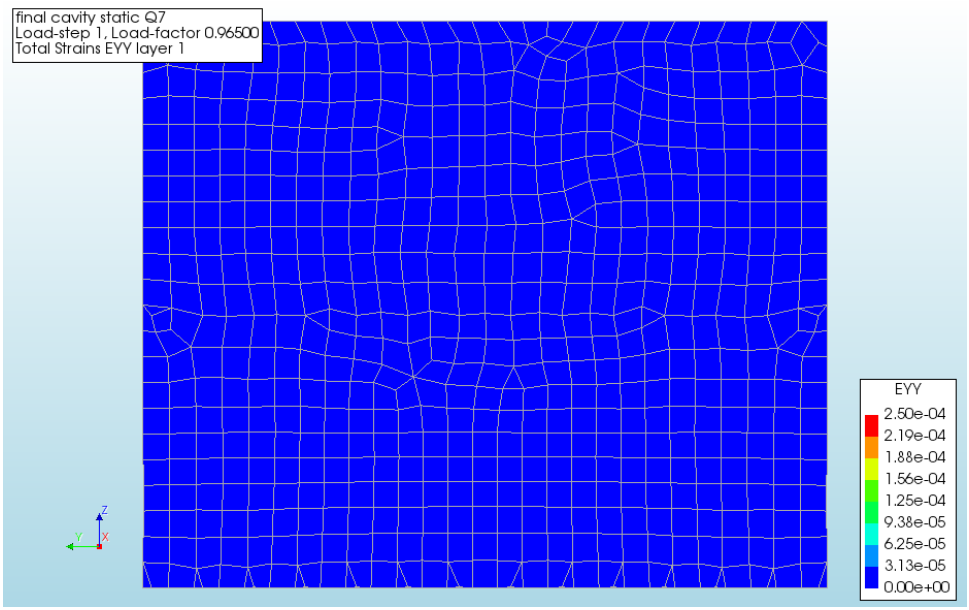


Figure 146 - Strain EYY from layer 1 with an inundation depth of 1.5m for the direct input option

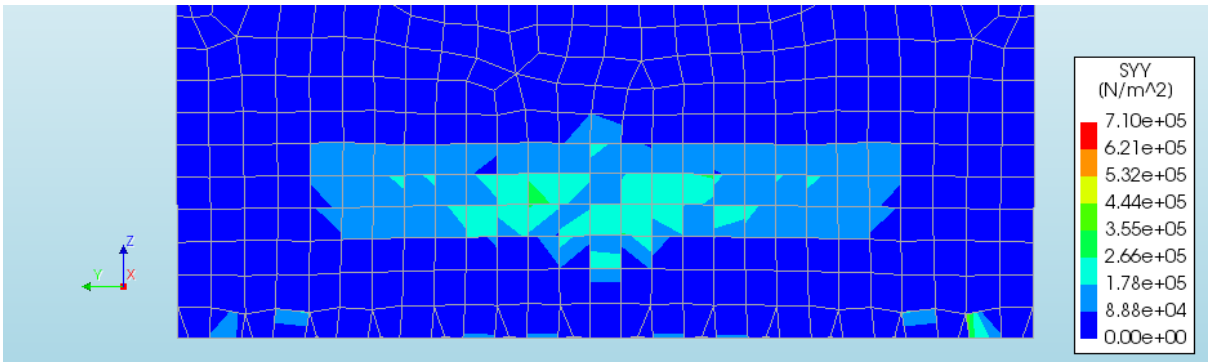


Figure 147 - Stress SYY for layer 1 with an inundation depth of 1.5m for the diagonal option

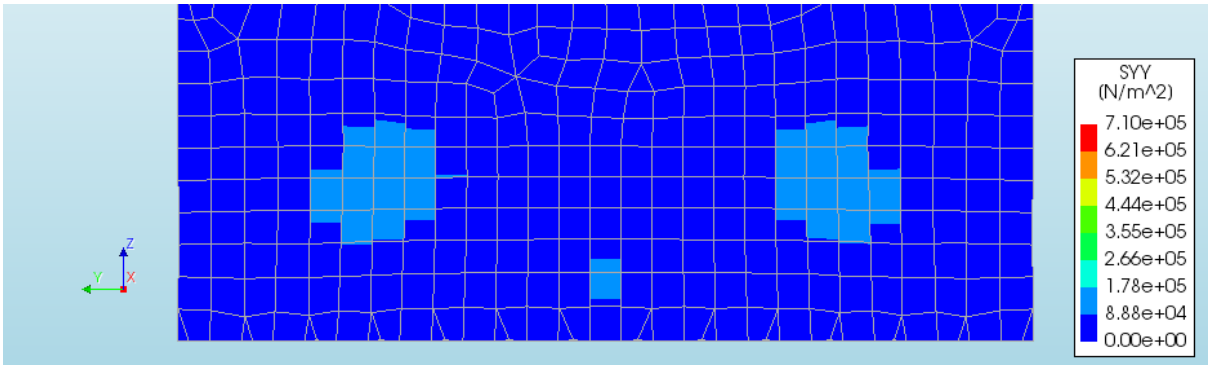


Figure 148 - Stress SYY for layer 1 with an inundation depth of 1.5m for the direct input option

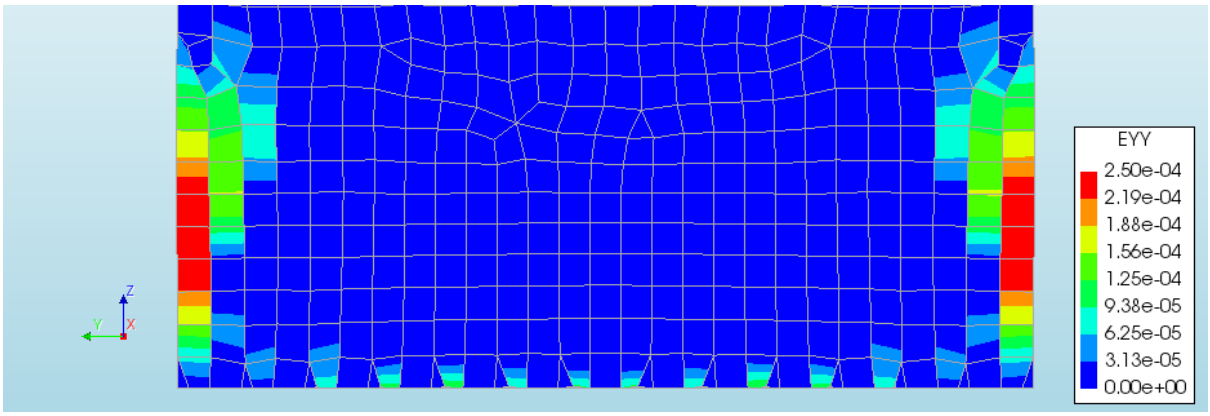


Figure 149 - Strain EYY from layer 7 with an inundation depth of 1.5m for the diagonal option

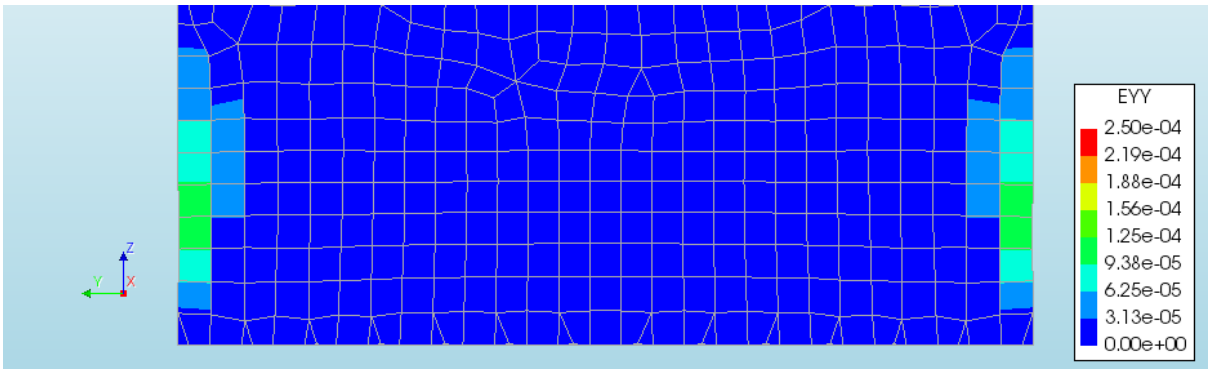


Figure 150 - Strain EYY from layer 7 with an inundation depth of 1.5m for the direct input option

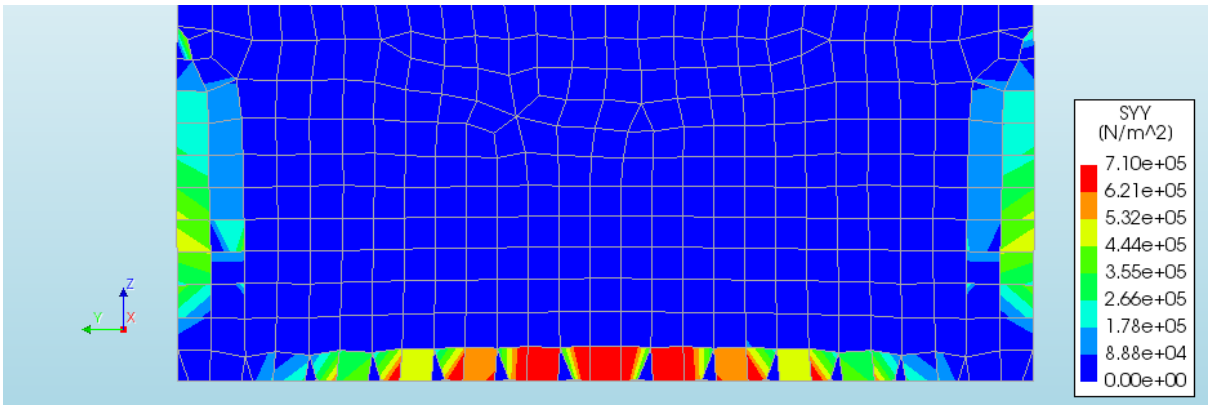


Figure 151 - Stress SYY from layer 7 with an inundation depth of 1.5m for the diagonal option

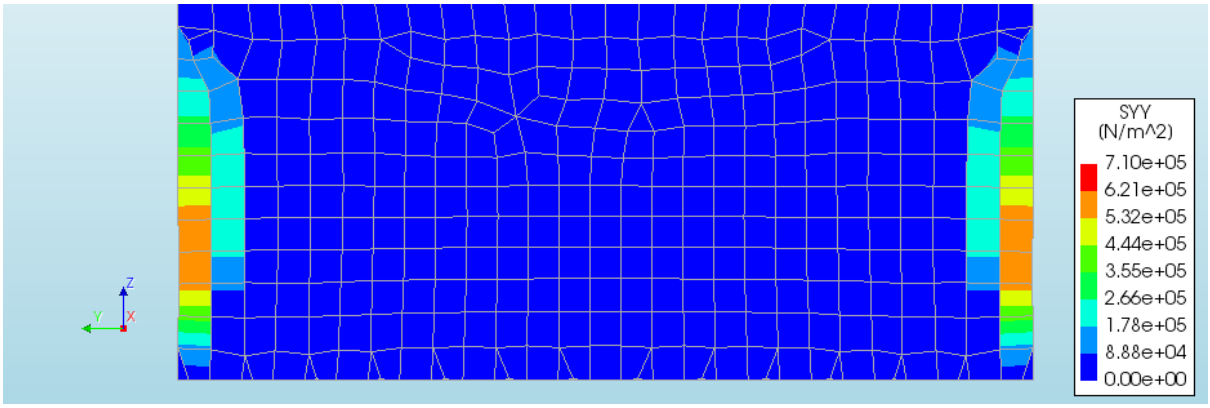


Figure 152 - Stress SYY from layer 7 with an inundation depth of 1.5m for the direct input option

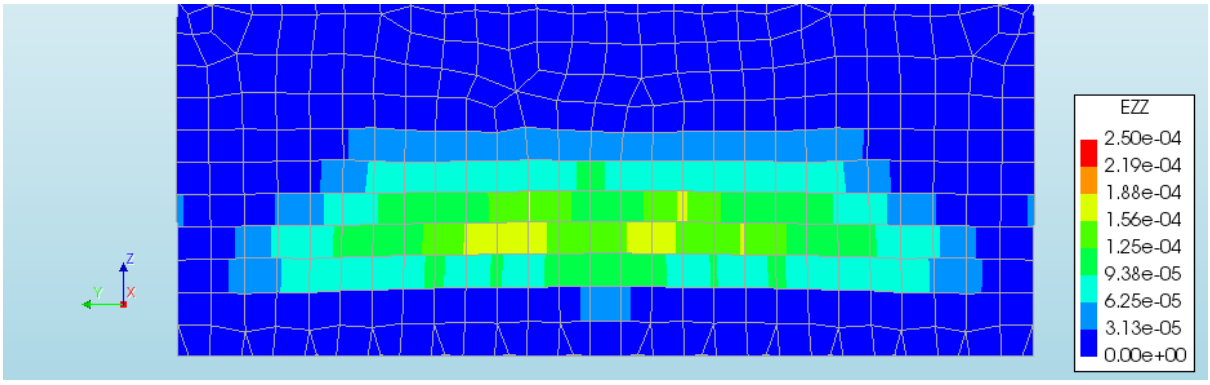


Figure 153 - Strain EZZ from layer 1 with an inundation depth of 1.5m for the diagonal option

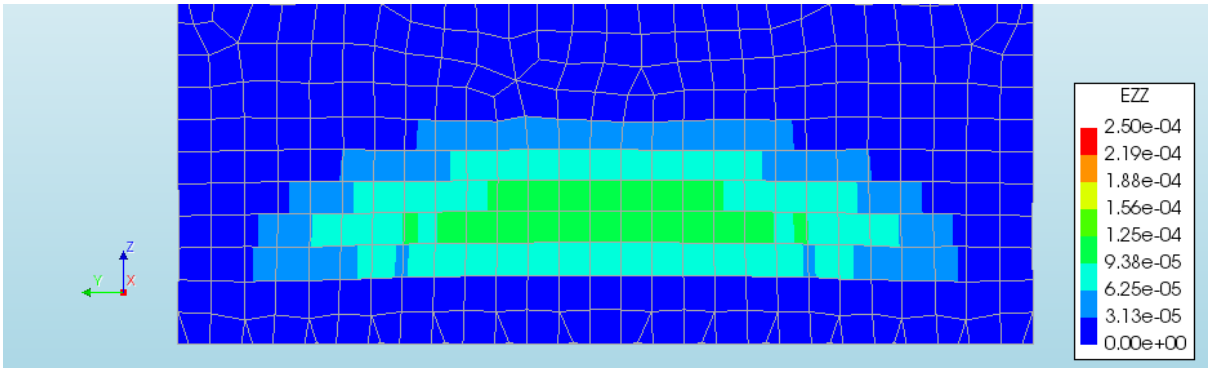


Figure 154 - Strain EZZ from layer 1 with an inundation depth of 1.5m for the direct input option

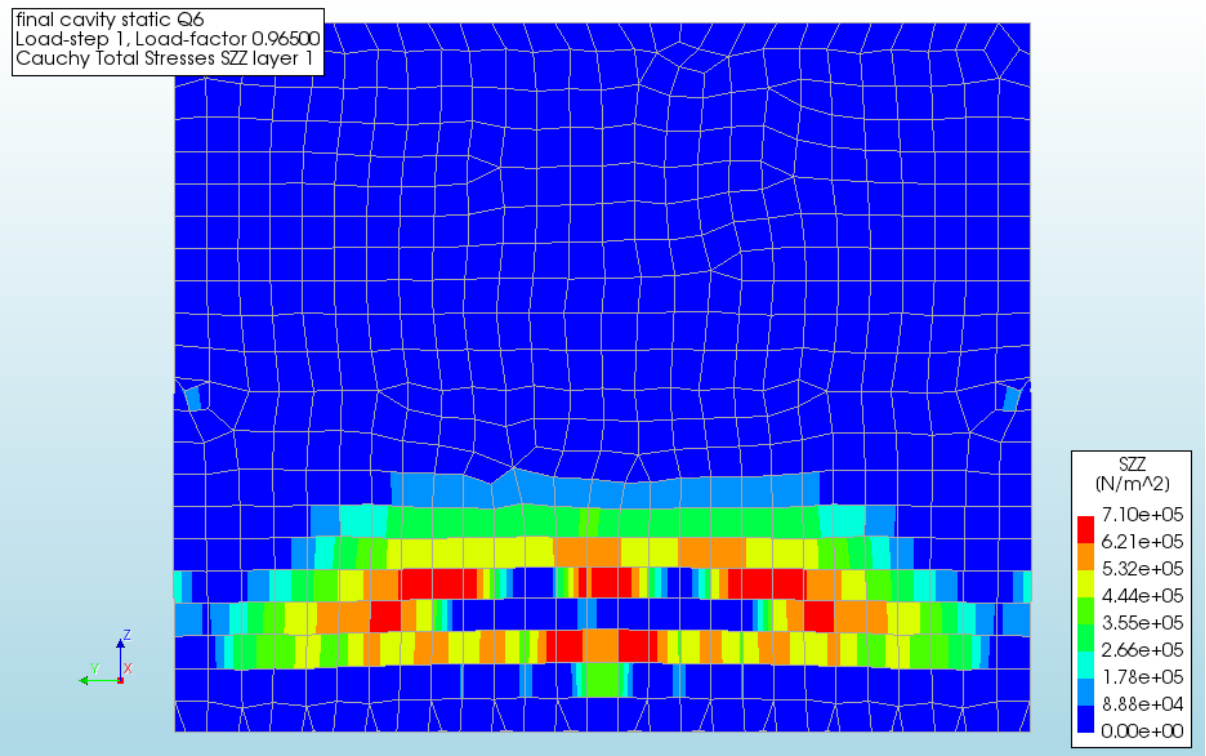


Figure 155 - Stress SZZ from layer 1 with an inundation depth of 1.5m for the diagonal option

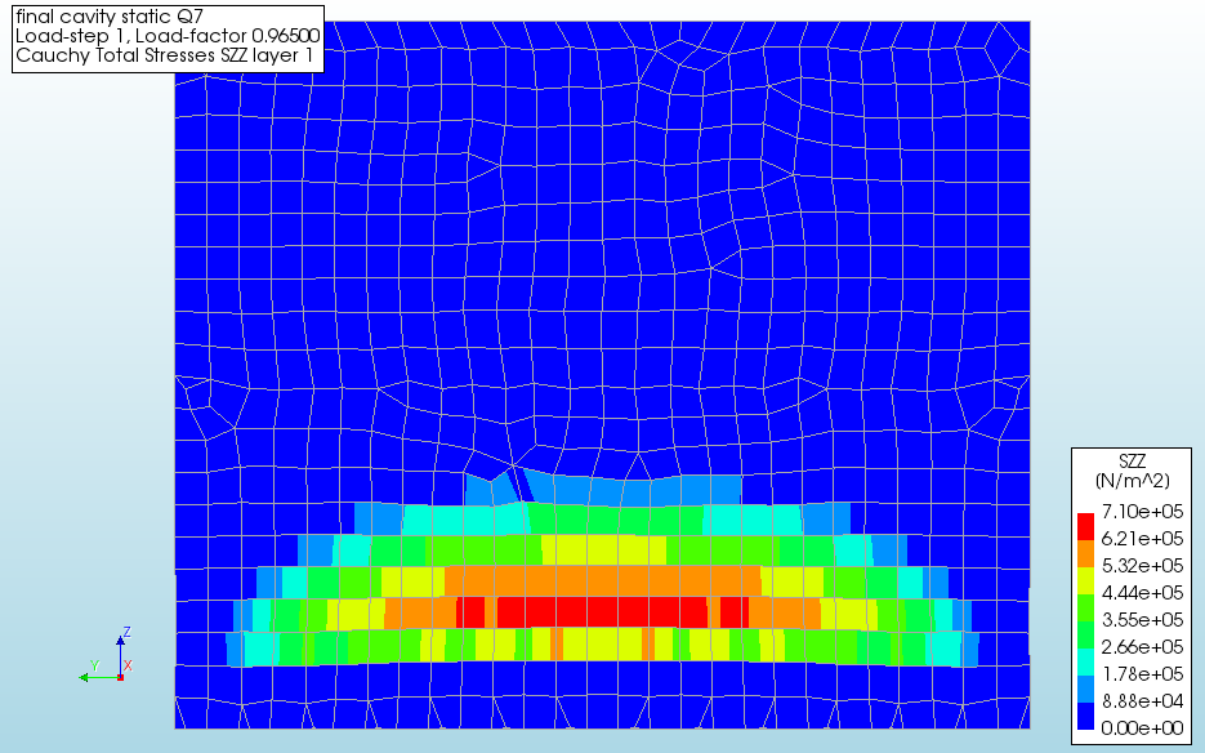


Figure 156 - Stress SZZ from layer 1 with an inundation depth of 1.5m for the direct input option

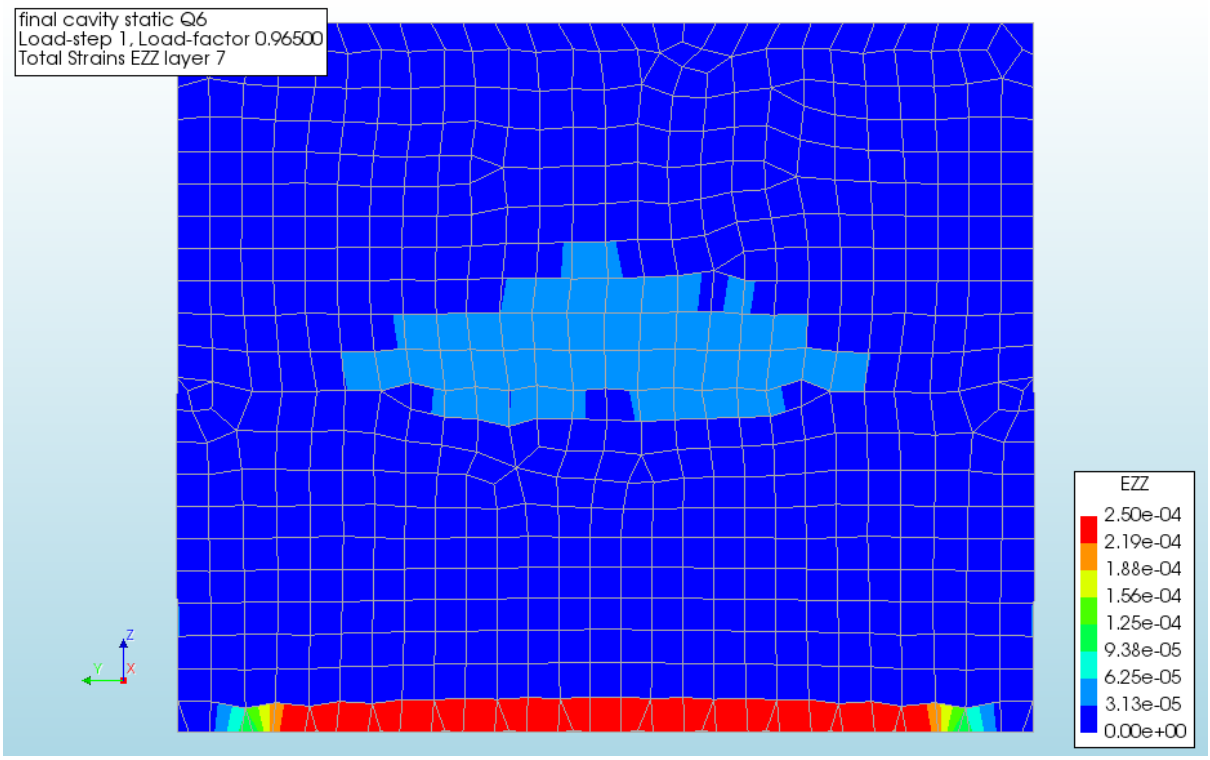


Figure 157 - Strain EZZ from layer 7 with an inundation depth of 1.5m for the diagonal option

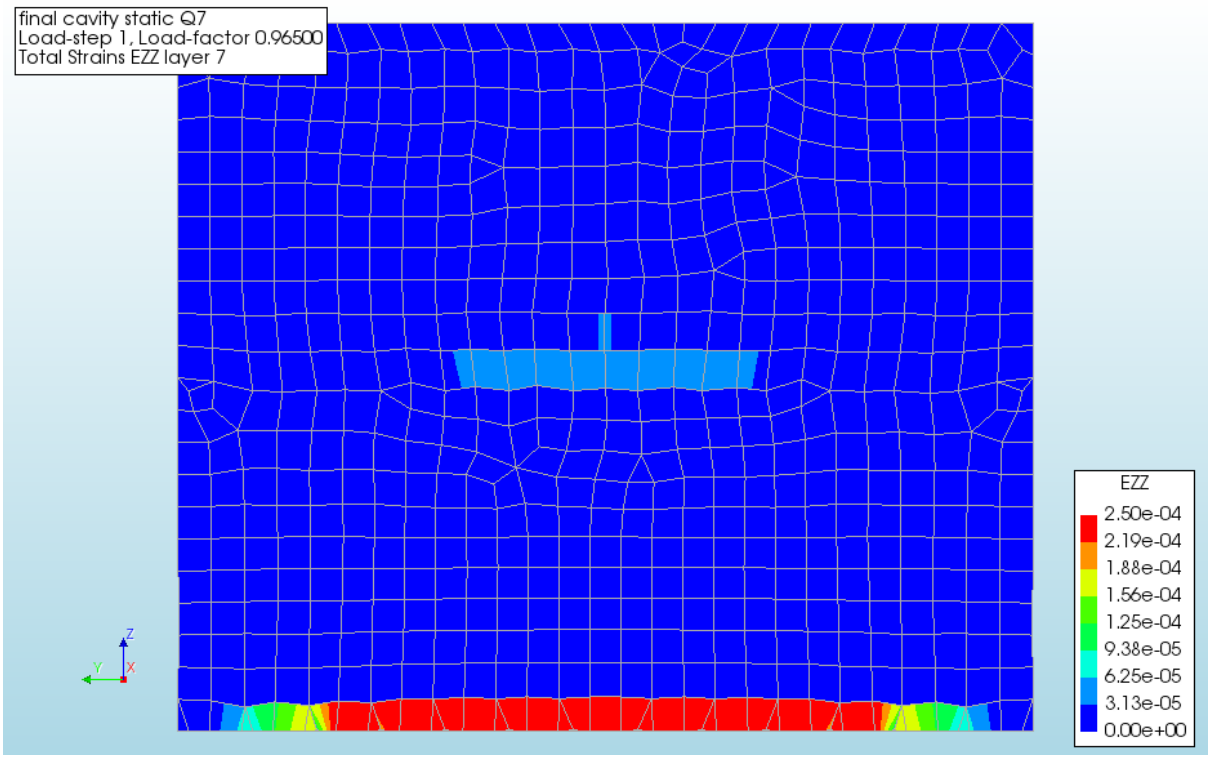


Figure 158 - Strain EZZ from layer 7 with an inundation depth of 1.5m for the direct input option

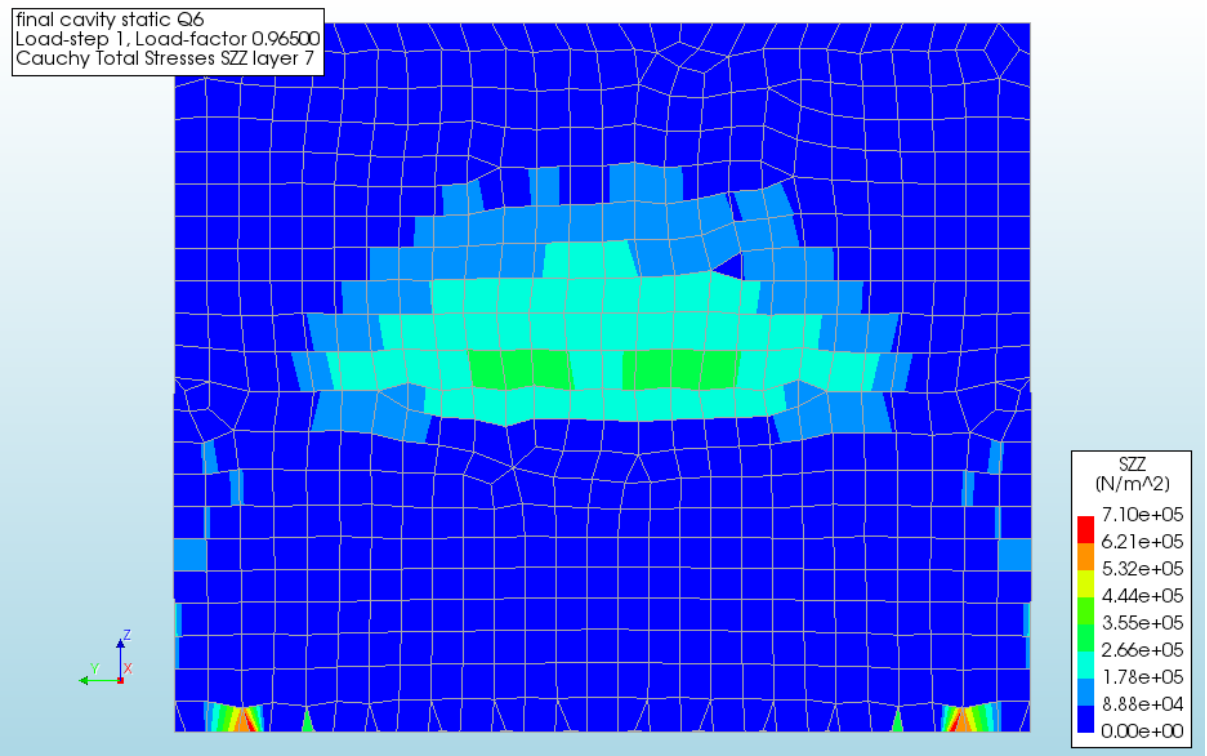


Figure 159 - Stress SZZ from layer 7 with an inundation depth of 1.5m for the diagonal option

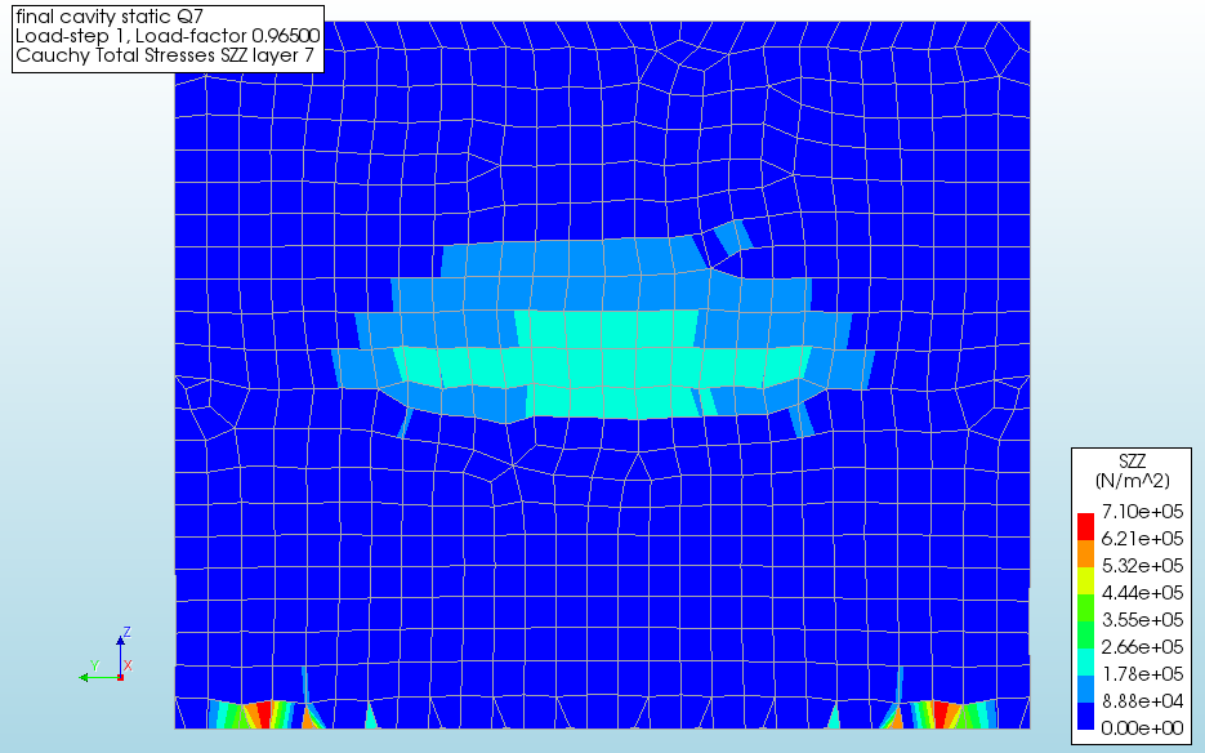


Figure 160 - Stress SZZ from layer 7 with an inundation depth of 1.5m for the direct input option

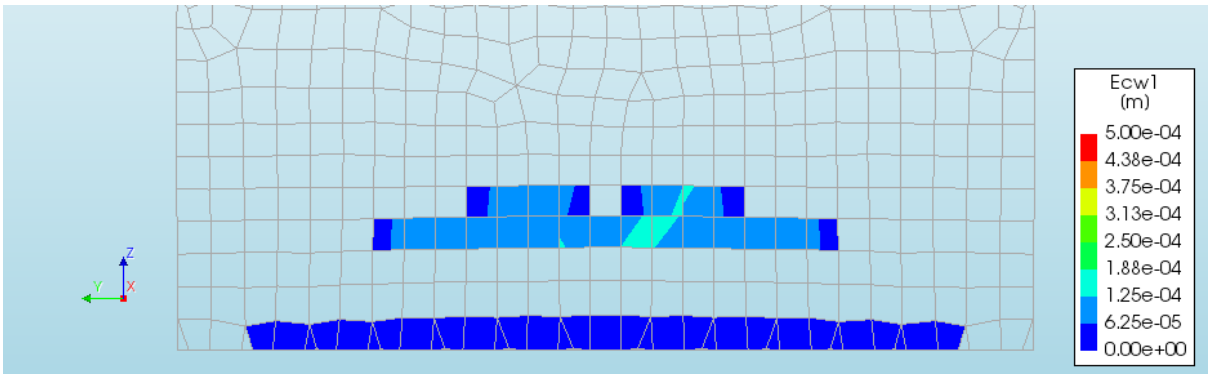


Figure 161 - Crack widths ECW 1 from layer 1 with an inundation depth of 1.5m for the diagonal option

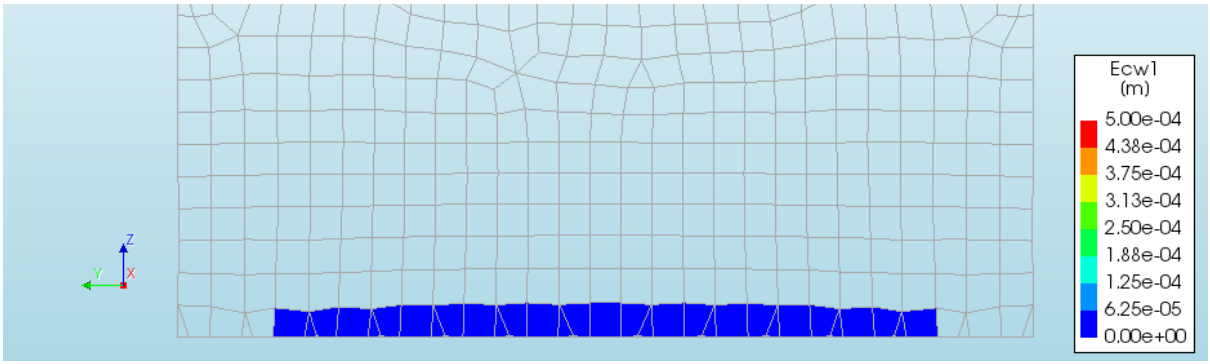


Figure 162 - Crack widths ECW 1 from layer 1 with an inundation depth of 1.5m for the direct input option

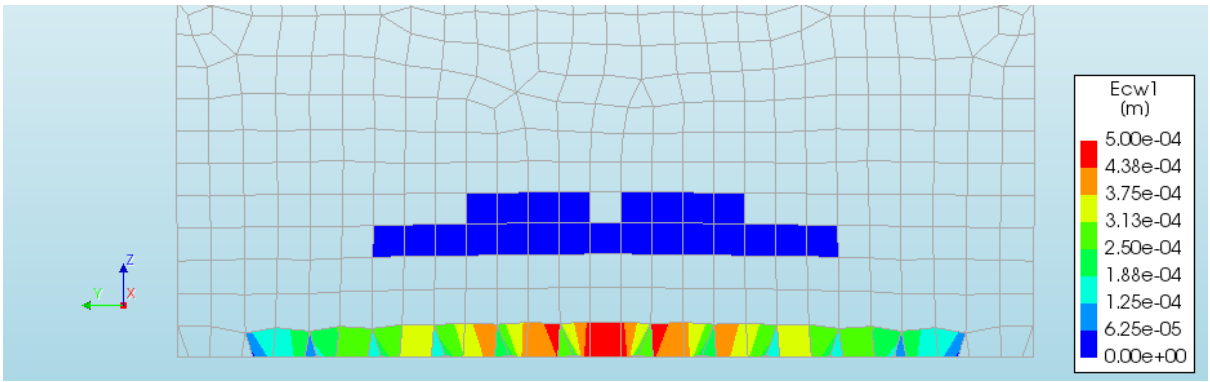


Figure 163 - Crack widths ECW 1 from layer 7 with an inundation depth of 1.5m for the diagonal option

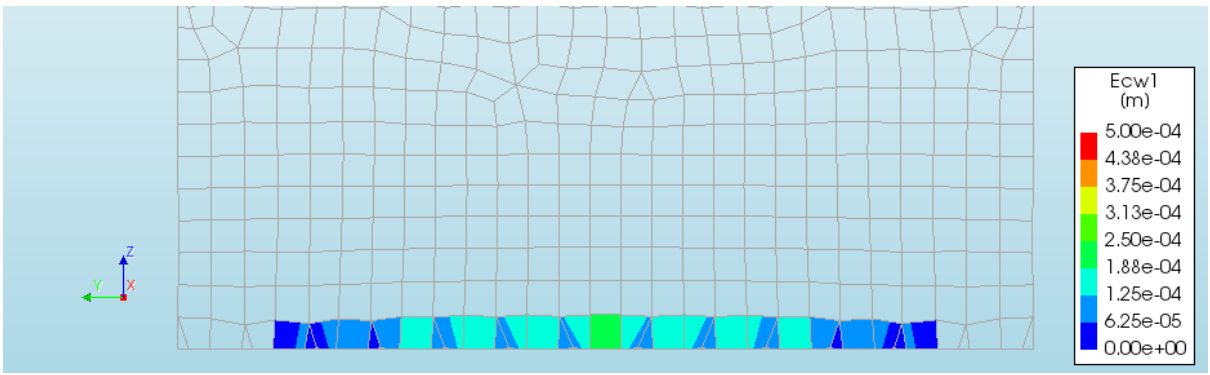


Figure 164 - Crack widths ECW 1 from layer 7 with an inundation depth of 1.5m for the direct input option

# Appendix H. Thickness Integration Points

In order to perform a non-linear analysis more than the 3 integration points normally used, are needed. To determine which amount suffices, several tests with 5, 7, 9 and 11 integration points have been run for the Single Wall Masonry House under the static load.

From these results the last converted step has been taken, step 27, which corresponds with an approximate inundation depth of 2.7 m. Next the stresses, SYY and SZZ, have been taken of a single wall. From these stresses the average of the absolute percentage change and the average of the normal percentage change has been taken. This is done for the step from 5 to 7 integration points, 7 to 9 integration points and 9 to 11 integration points. Besides the loaded sections of the wall, the majority of the nodes will experience very low stresses. These are of course very perceptible to relatively large changes. Therefore, a threshold has been taken, a minimum stress which should be present in a node for it to be taken into account in the average. The higher this threshold, the smaller the difference between the different amounts of integration points becomes.

Table 28 - Averages of the stresses with the threshold at 1 N/m²

| Absolute | 5->7 | 7->9 | 9->11 |
|---|---|---|---|
| Szz start | 17.4% | 36.0% | 43.2% |
| Szz end | 28.1% | 56.0% | 31.5% |
| Syy start | 82.7% | 52.0% | 96.0% |
| Syy end | 23.8% | 37.0% | 43.5% |
| Average | 38.0% | 45.3% | 53.5% |

| Normal | 5->7 | 7->9 | 9->11 |
|---|---|---|---|
| Szz start | 8.6% | 1.8% | -22.8% |
| Szz end | 7.8% | 1.4% | -3.7% |
| Syy start | 17.2% | 2.0% | -3.8% |
| Syy end | 45.4% | 1.3% | -9.9% |
| Average | 19.7% | 1.6% | -10.0% |

Table 29 - Averages of the stresses with the threshold at 10 N/m2

| Absolute | 5->7 | 7->9 | 9->11 |
|---|---|---|---|
| Szz start | 22.0% | 17.8% | 24.5% |
| Szz end | 25.3% | 26.2% | 26.6% |
| Syy start | 50.9% | 44.8% | 61.9% |
| Syy end | 20.3% | 28.7% | 39.9% |
| Average | 29.6% | 29.4% | 38.2% |

| Normal | 5->7 | 7->9 | 9->11 |
|---|---|---|---|
| Szz start | 1.4% | 1.9% | -0.5% |
| Szz end | 6.4% | 1.0% | 0.3% |
| Syy start | 12.3% | -7.0% | -5.7% |
| Syy end | 41.8% | -0.9% | -10.1% |
| Average | 15.5% | -1.2% | -4.0% |

Table 30 - Averages of the stresses with the threshold at 100 N/m2

| Absolute | 5->7 | 7->9 | 9->11 |
|---|---|---|---|
| Szz start | 15.6% | 15.5% | 15.7% |
| Szz end | 16.0% | 18.8% | 15.8% |
| Syy start | 39.6% | 37.5% | 46.1% |
| Syy end | 17.4% | 23.2% | 32.1% |
| Average | 22.2% | 23.8% | 27.4% |

| Normal | 5->7 | 7->9 | 9->11 |
|---|---|---|---|
| Szz start | 1.5% | -1.4% | 0.7% |
| Szz end | 6.7% | 1.2% | -0.3% |
| Syy start | 5.5% | -5.6% | -3.9% |
| Syy end | 16.9% | -0.5% | -8.4% |
| Average | 7.6% | -1.6% | -3.0% |

Table 31 - Averages of the stresses with the threshold at 1000 N/m2

| Absolute | 5->7 | 7->9 | 9->11 |
|---|---|---|---|
| Szz start | 11.6% | 10.9% | 11.9% |
| Szz end | 11.1% | 13.2% | 10.7% |
| Syy start | 26.0% | 25.4% | 31.0% |
| Syy end | 13.0% | 13.0% | 15.5% |
| Average | 15.4% | 15.6% | 17.3% |

| Normal | 5->7 | 7->9 | 9->11 |
|---|---|---|---|
| Szz start | 0.3% | -1.4% | -0.1% |
| Szz end | 5.5% | 0.4% | -0.7% |
| Syy start | 3.9% | 0.1% | 1.7% |
| Syy end | 5.1% | 1.3% | -0.6% |
| Average | 3.7% | 0.1% | 0.1% |

From Table 28, Table 29, Table 30 and Table 31 it can be concluded that there will remain rather significant differences when increasing the amount of integration points when averaging the absolute percentage changes. However, when just the average is taken from the percentage changes an increase in accuracy can be seen from 5 to 7 integration points, from 7 to 9 and from 9 to 11 integration points this difference is much smaller.

Overall the observed patterns between the different amounts of integration points, are very similar, see Figure 165, Figure 166, Figure 167 and Figure 168. Some minor differences can be observed, mainly again for the difference between 5 and 7 integration points. This confirms the results from the averages.

The conclusion therefore is that 7 integration points will suffice for the non-linear calculations done in this thesis. All calculations are thus done using 7 integration points for the thickness of the walls.

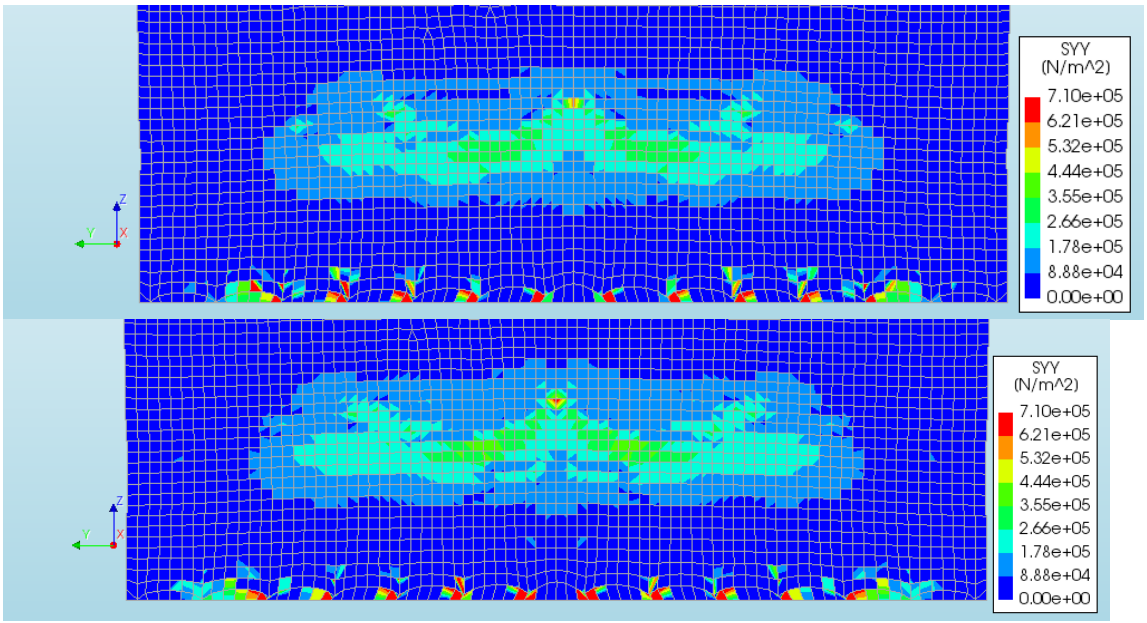


Figure 165 - Stress, SYY, for the first layer, for 5 (top) and 7 (bottom) integration points

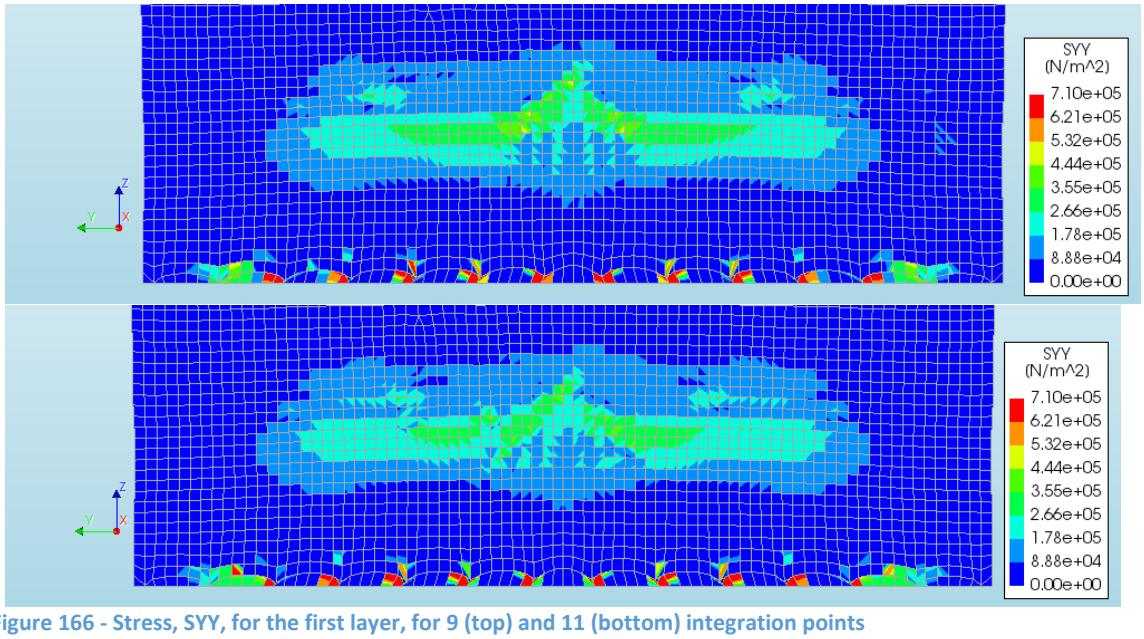


Figure 166 - Stress, SYY, for the first layer, for 9 (top) and 11 (bottom) integration points

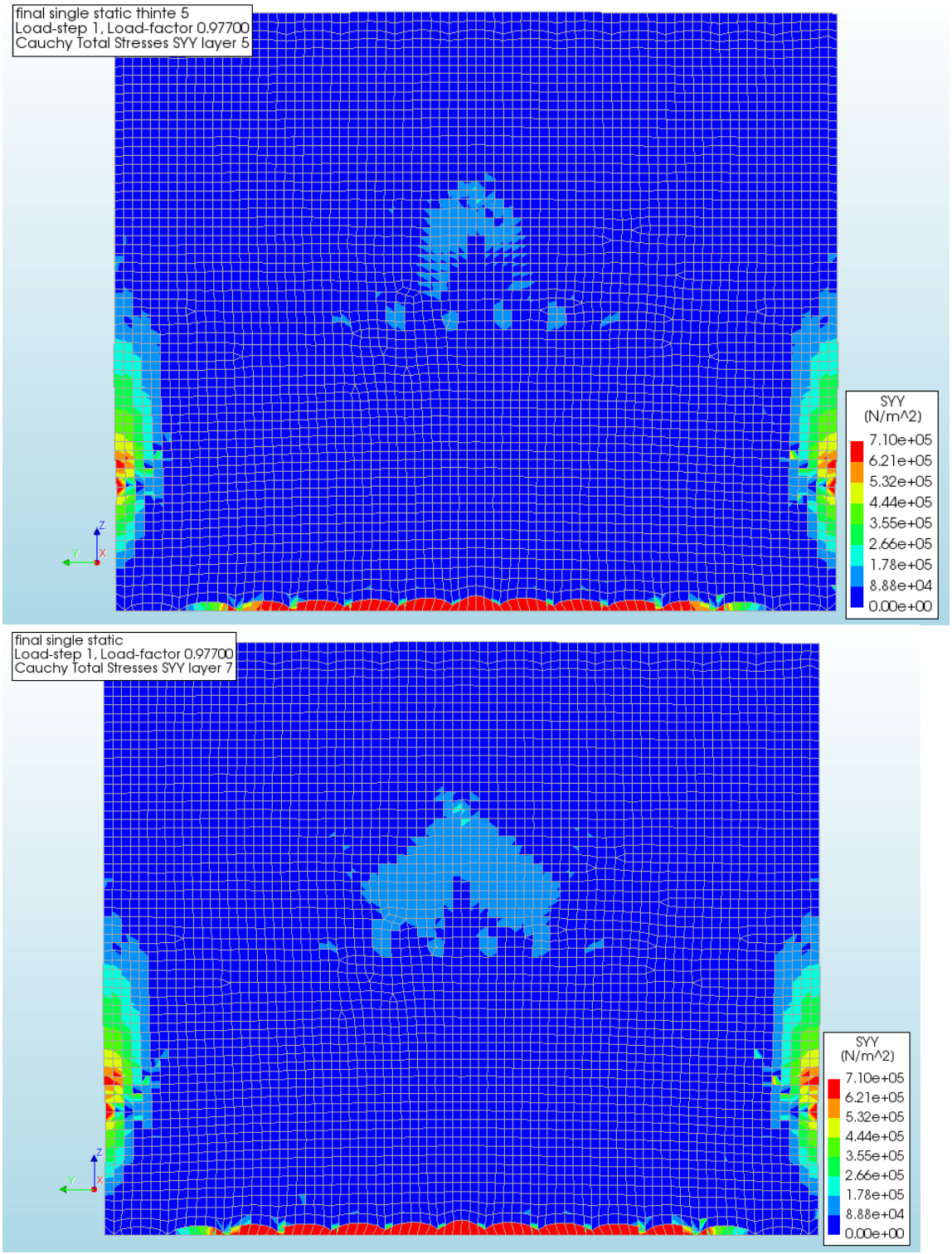


Figure 167 - Stress, SYY, for the last layer, for 5 (top) and 7 (bottom) integration points

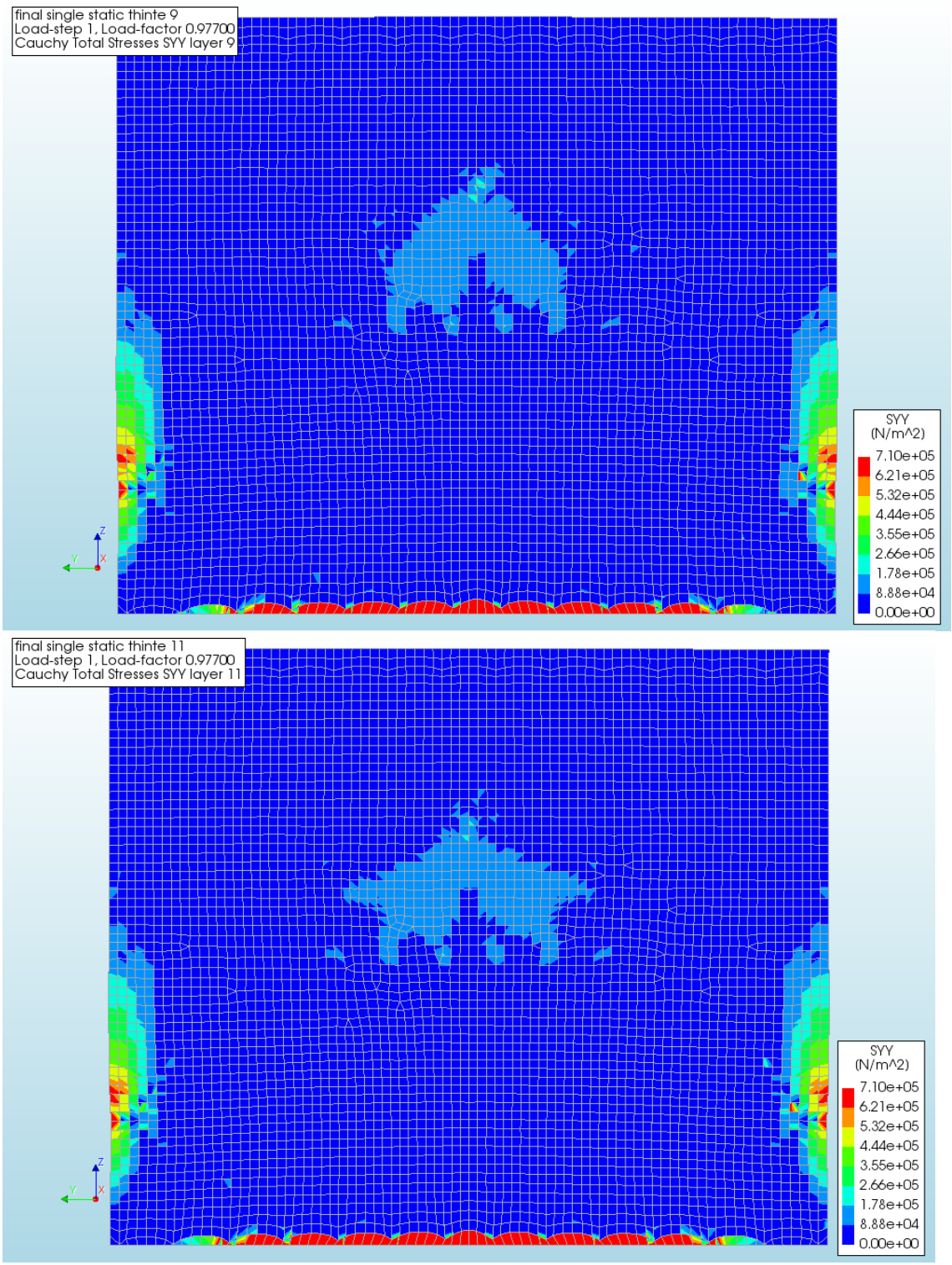


Figure 168 - Stress, SYY, for the last layer, for 9(top) and 11 (bottom) integration points

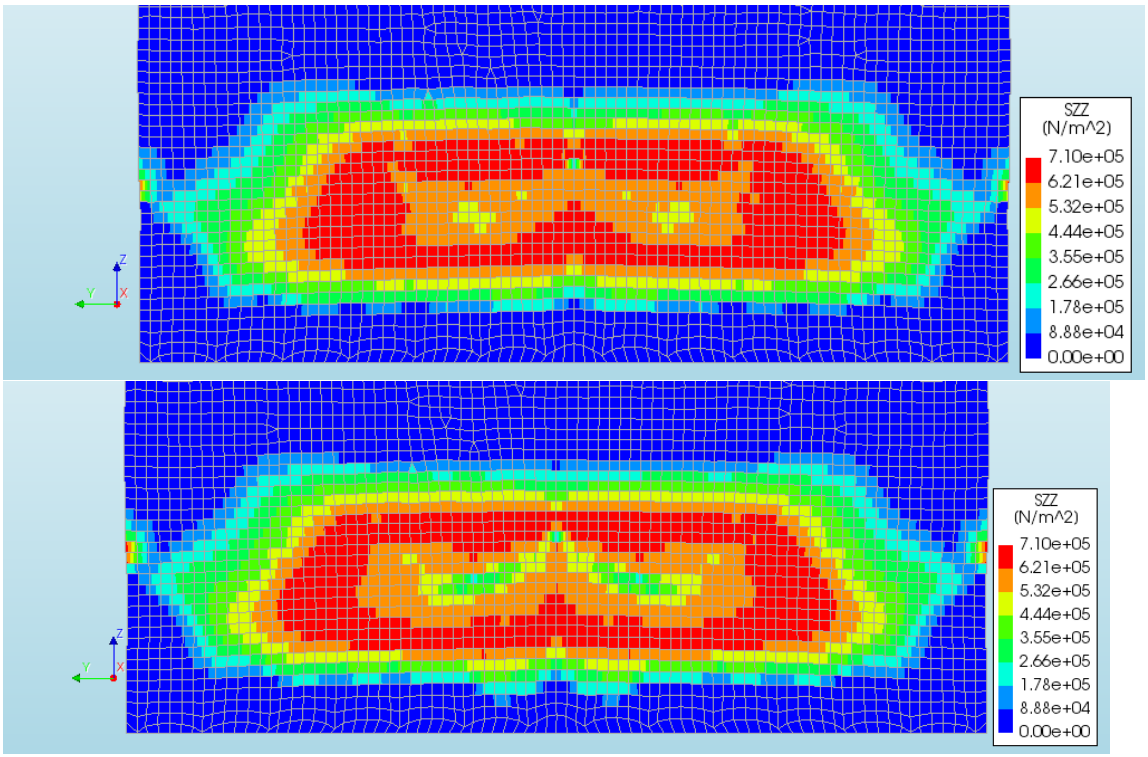


Figure 169 - Stress, SZZ, for the first layer, for 5 (top) and 7 (bottom) integration points

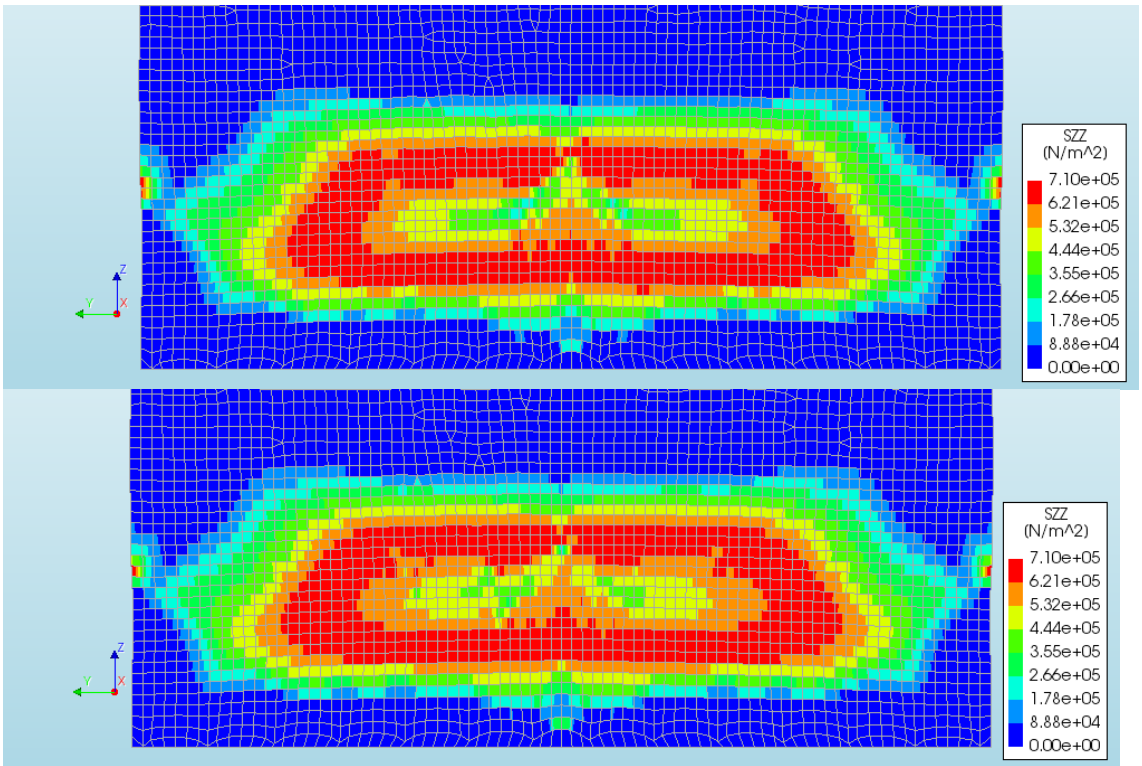


Figure 170 - Stress, SZZ, for the first layer, for 9 (top) and 11 (bottom) integration points

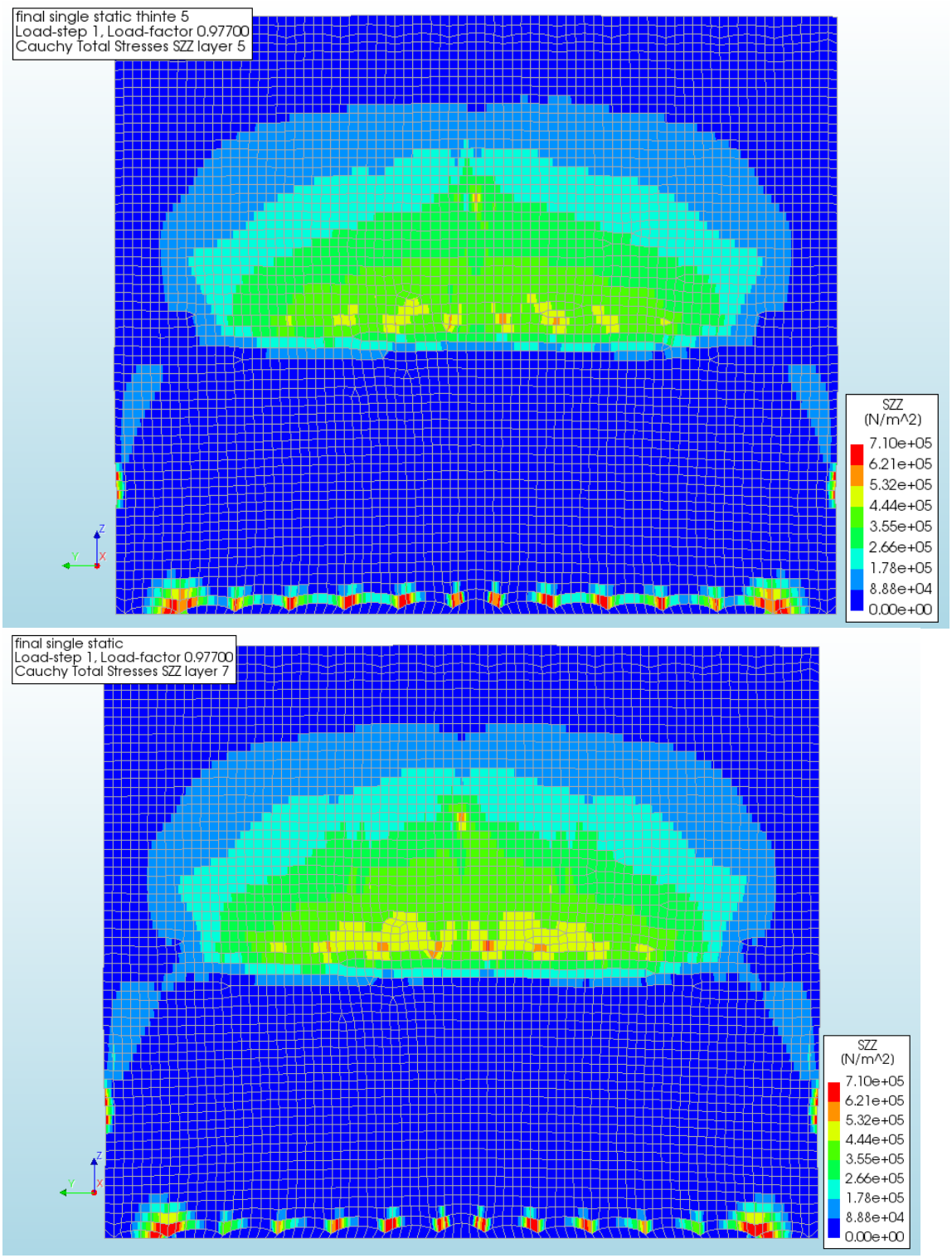


Figure 171 - Stress, SZZ, for the last layer, for 5 (top) and 7 (bottom) integration points

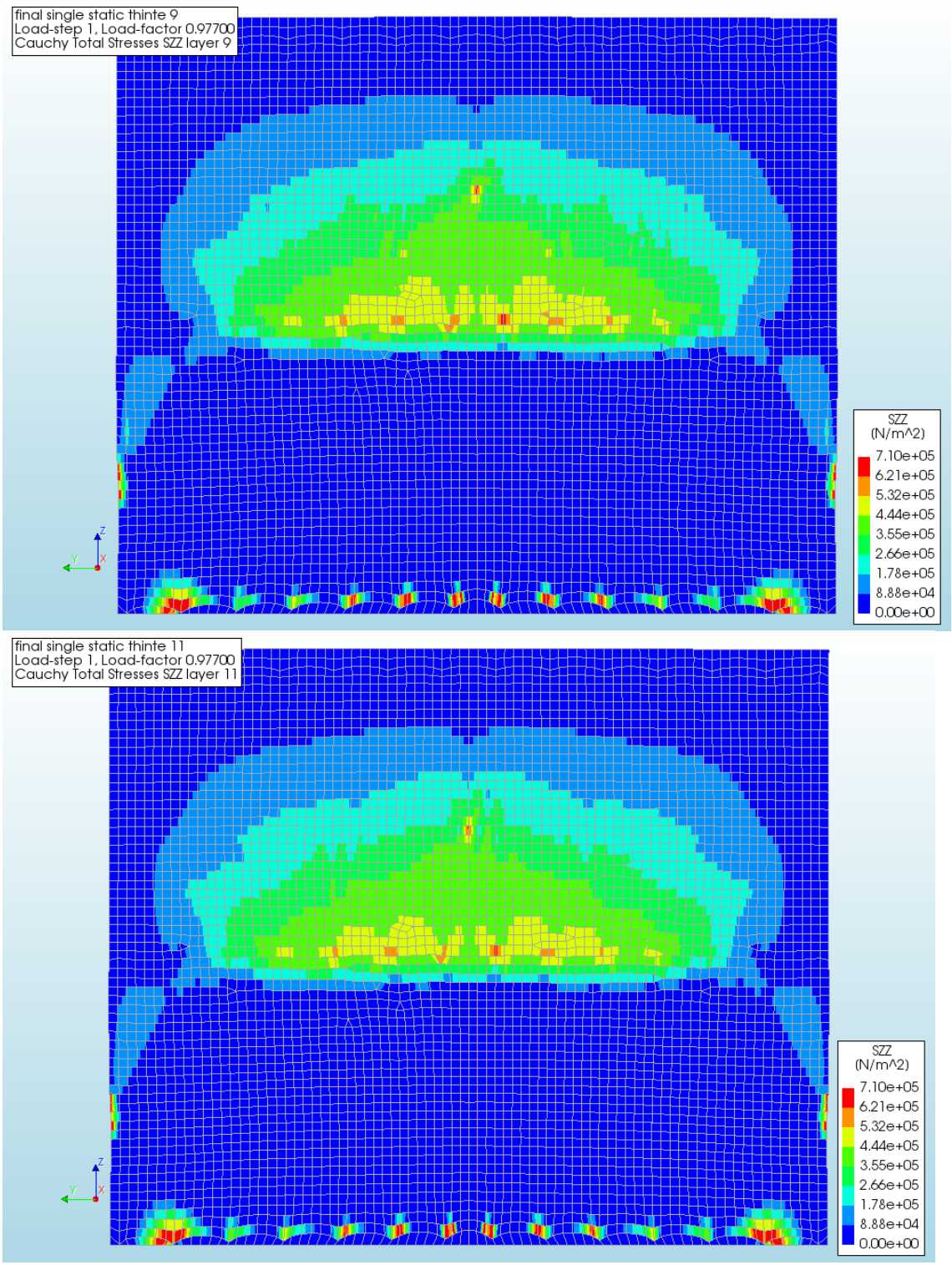


Figure 172 - Stress, SZZ, for the last layer, for 59 (top) and 11 (bottom) integration points

# Appendix I. Diana Calculations of a Masonry House with a Cavity Wall, Extended

The DIANA calculations have been split into 2 main groups. The first group is the calculations regarding a masonry house with a cavity wall, those are treated in this chapter. The second group regards the calculations of a masonry house with a single wall.

Next the calculation will increase in detail, first only the foundation, outer walls and floors are modelled. One by one, extra details will be added, door and windows, inner walls and a combination of both.

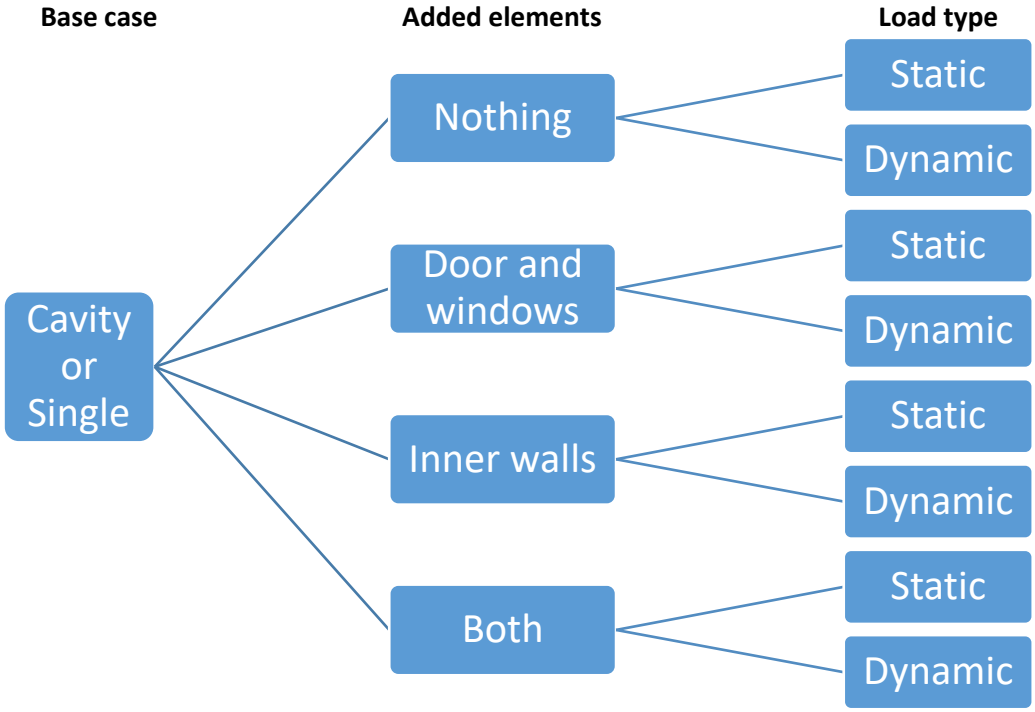


Figure 173 - Overview of the different cases

In order to preserve the accuracy of the figures the legend is not the same for all displacements and crack widths. Patterns would otherwise not be visible, therefore keep an eye on the legend when comparing figures. Furthermore only 1 wall is displayed in the figures to keep the results as clear and readable as possible. If not stated otherwise the displacement at a certain point is the maximum displacement of the wall. The crack widths are displayed at two points, the inside of the wall, layer 1, and the outside of the wall, layer 7. Lastly, the error mentioned to indicate the trustworthiness of the results, is the relative displacement variation, of course, smaller is better.

## Masonry House

The simplest model, the masonry house with a cavity wall.

### Static

The single cavity wall house has been loaded with a rising water level until it failed. The first cracks started at an inundation depth of approximately 1.0 m. This corresponds with the second-last green dot in Figure 174. The load then still increases and failure occurs between approximately 2.0 and 2.5 m. The maximum displacement of the walls at the three points are respectively 0.65 mm, 3.0 mm and 11.2 mm. Even though those last results are reasonably inaccurate, since convergence did not

occur and the error was 0.547, they are used to show the patterns that do occur. The errors due to convergence not being met, will be discussed at each point.

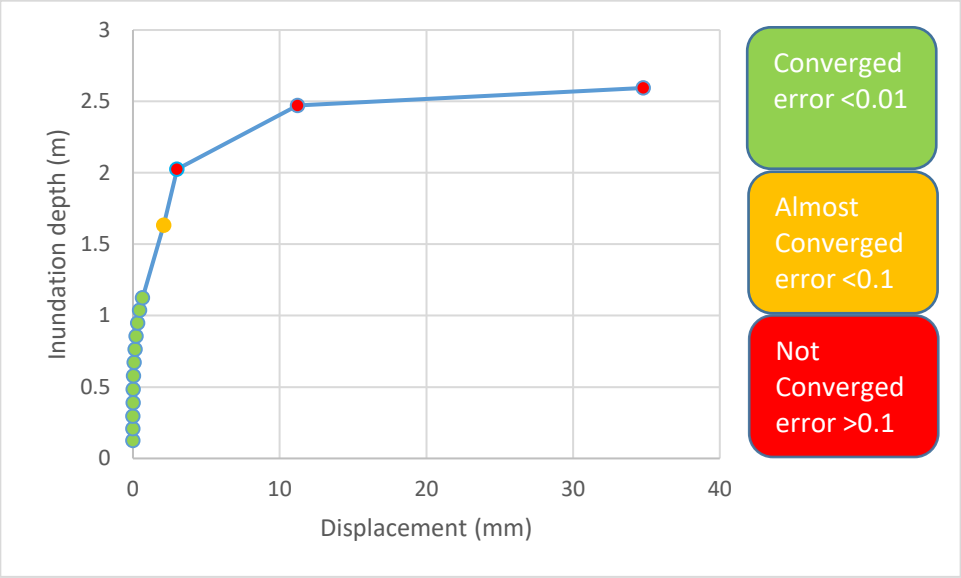


Figure 174 - Inundation depth vs Displacement of the Cavity Wall Masonry House due to the static load

Figure 175 and Figure 176 show the displacements of the house. As is especially visible in Figure 176 there is a sharp bend in the displacements, the locations of the cracks.

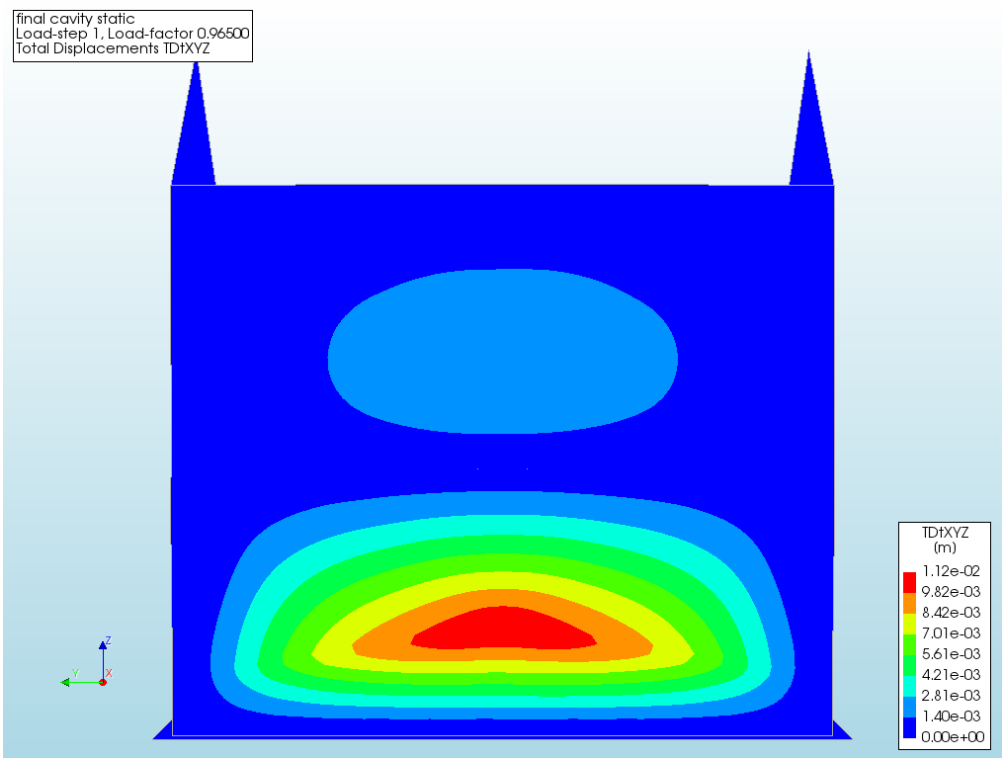


Figure 175 - Displacement of the Cavity Wall Masonry House due to the static load, 2.5 m, front view

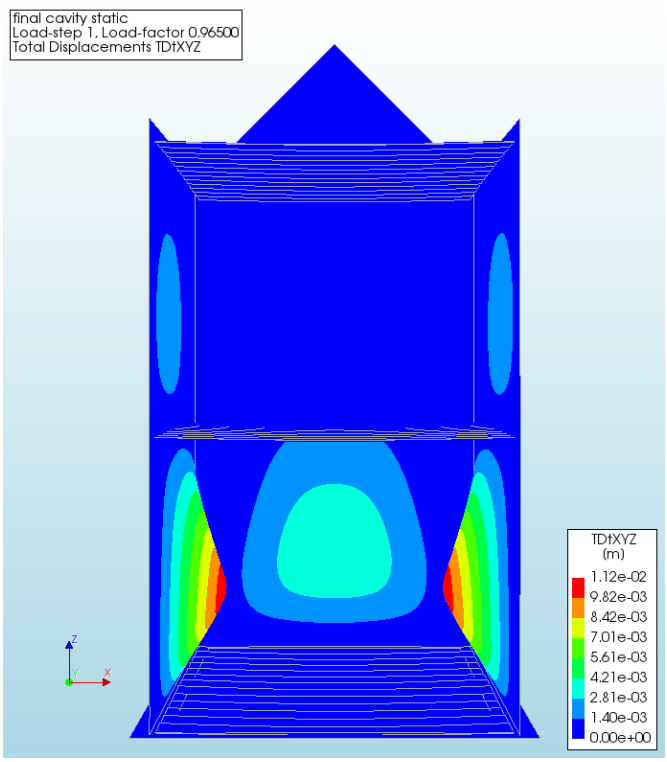


Figure 176 - Displacement of the Cavity Wall Masonry House due to the static load, 2.5 m, side view

Figure 177 shows the crack widths at the inside of the wall, here there are cracks at the middle of the wall which are up to several millimetre. Figure 178 shows the crack widths at the outside of the wall, the cracks here are located at the bottom and are also up to several millimetre. Notice that the upper part of the wall has also started to crack. This fits with the deflections seen in Figure 175 and Figure 176.

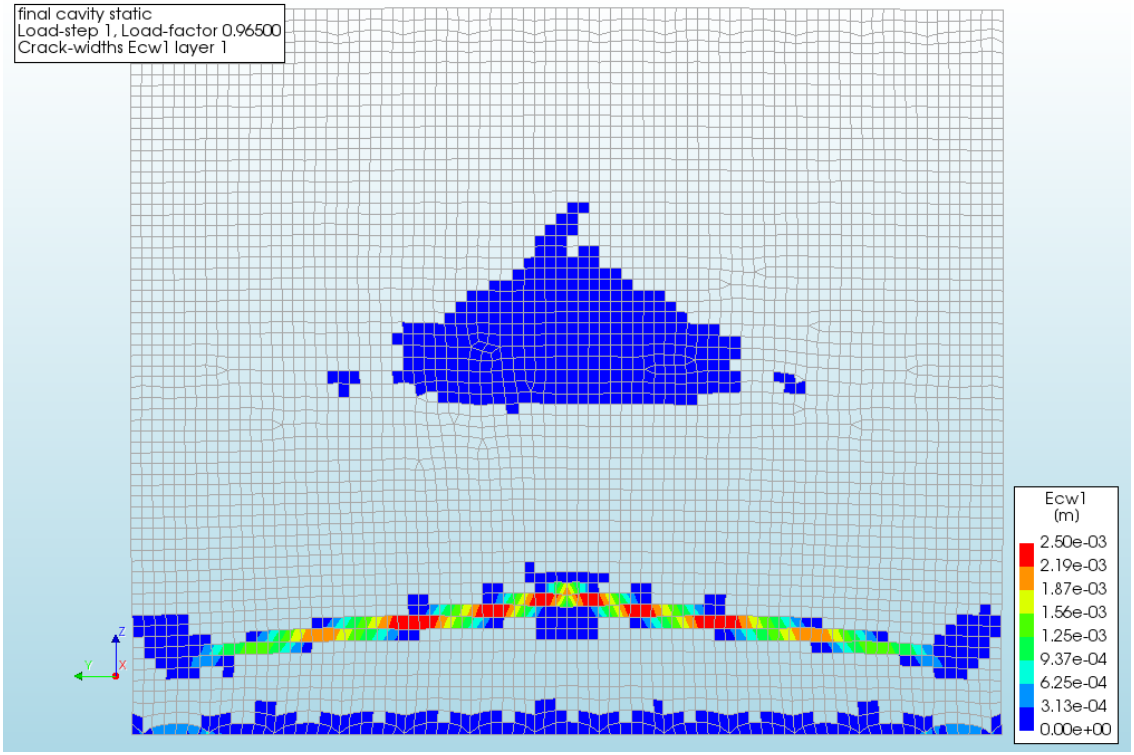


Figure 177 - Crack widths of the Cavity Wall Masonry House due to the static load, 2.5 m, front view layer 1

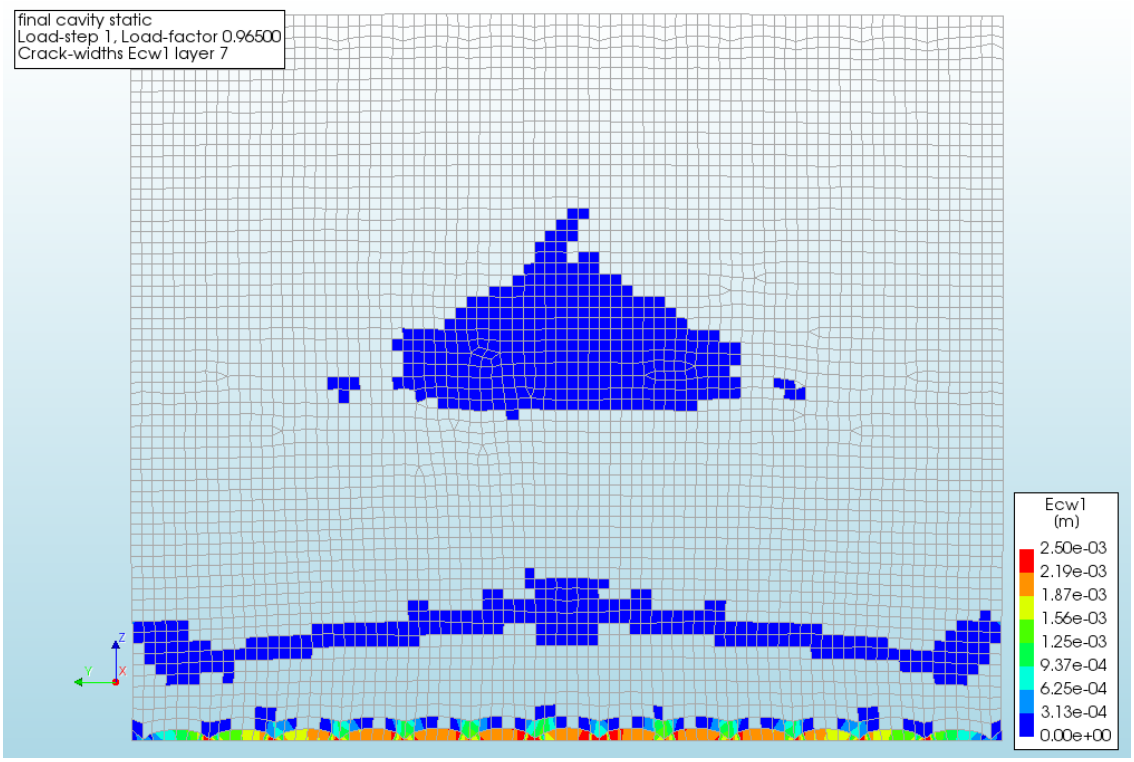


Figure 178 - Crack widths of the Cavity Wall Masonry House due to the static load, 2.5 m, front view layer 7

The cracking locations and relative sizes fit well with the expected results from the preliminary calculations from chapter 8. The largest moments where at the bottom, causing the first and largest cracks to be situated there. Next follows the middle of the wall, since in the calculations performed here, the wall is not restricted by the first floor. It is thus able to rotate, decreasing the stresses, strains and thus crack widths at that location.

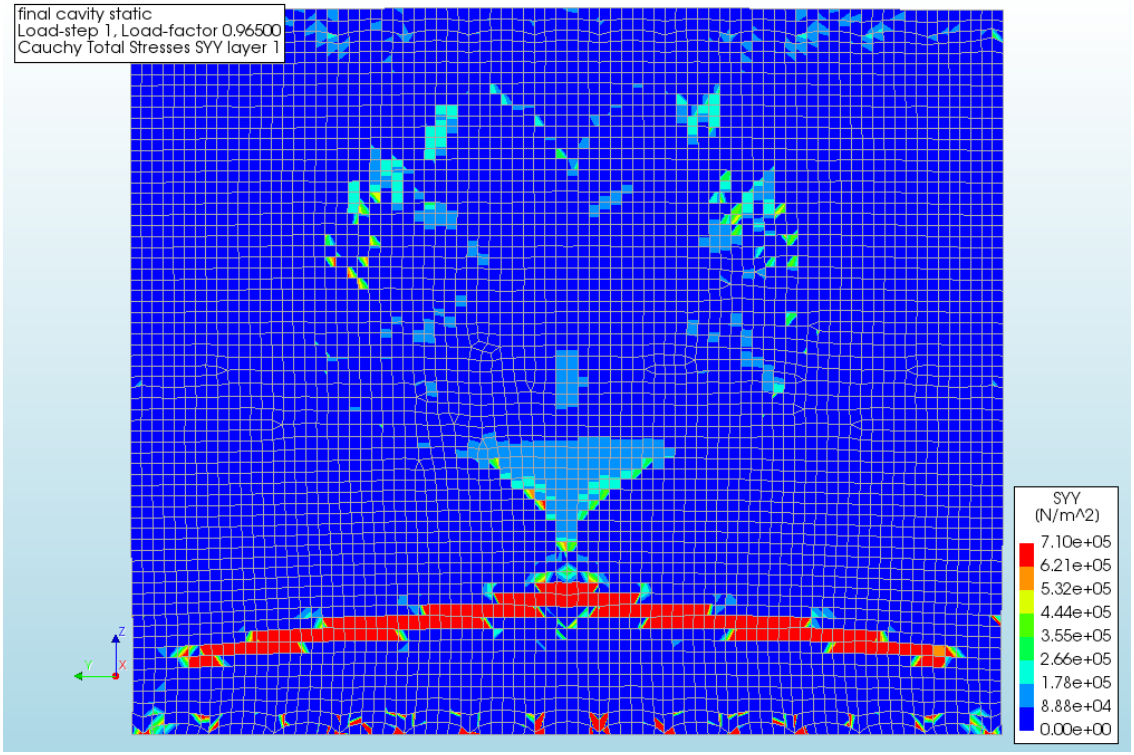


Figure 179 - Stress SYY of the Cavity Wall Masonry House due to the static load, 2.5 m, front view layer 1

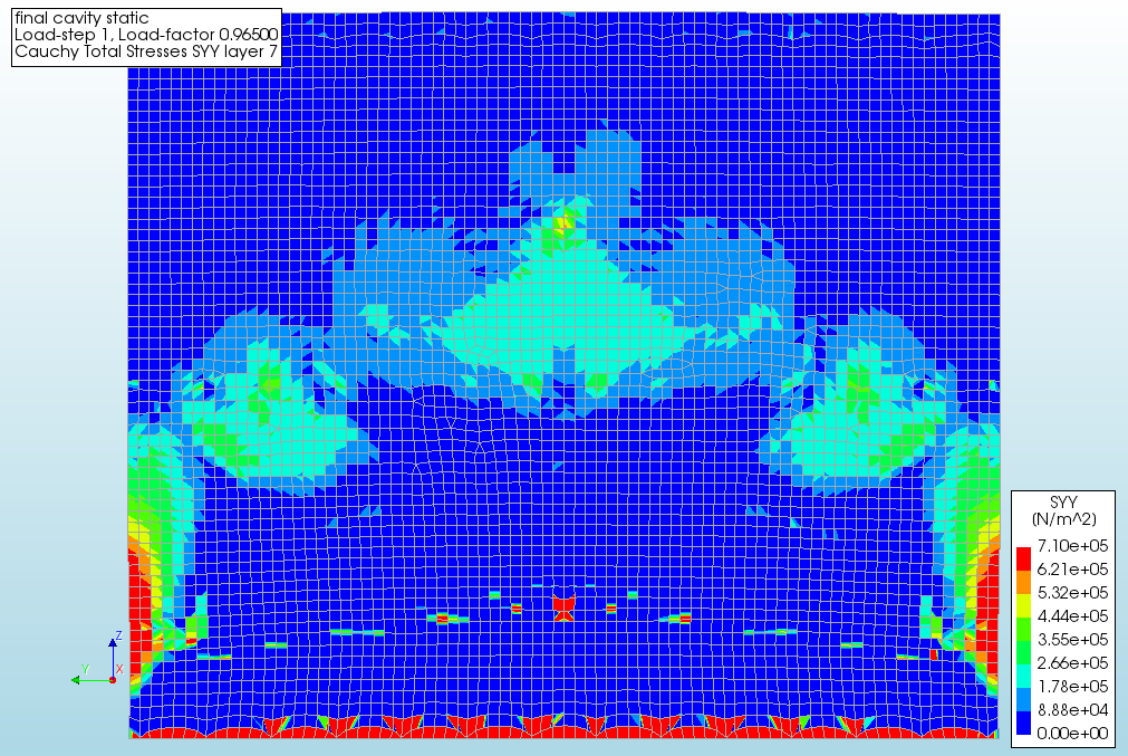


Figure 180 - Stress SYY of the Cavity Wall Masonry House due to the static load, 2.5 m, front view layer 7

In order to verify the crack widths, the stresses have been visualised for the YY and ZZ directions. The legends have been scaled as such that they match the tensile strength of the masonry, dark red therefore indicates cracks. The cracks at the inside, see Figure 177 match the stresses well, see Figure 179 and Figure 181. The same goes for the cracks at the outside, Figure 178, and the stress there, Figure 180 and Figure 182. Notice the gap in the stresses in Figure 181 and Figure 182 is where the cracks are largest. The cracks prevent the transfer of stresses in the Z-direction. Furthermore, some small peaks are visible in the different figures which can be contributed to the lack of convergence. The overall patterns are very similar to the observed patterns in Appendix J which increases their credibility.

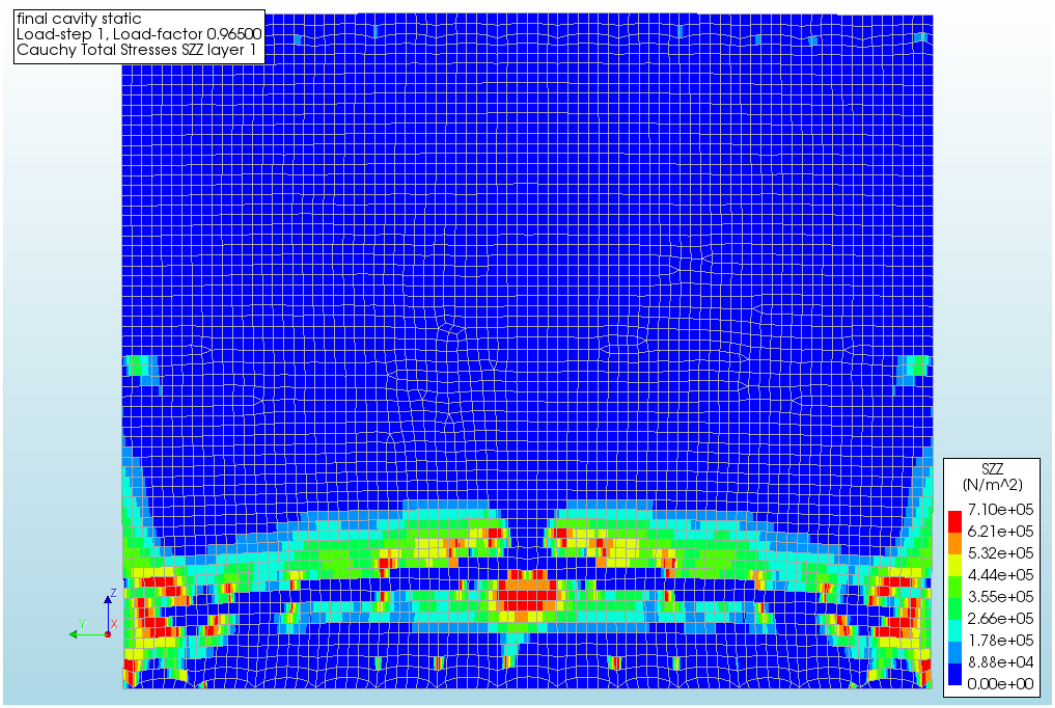


Figure 181 - Stress SZZ of the Cavity Wall Masonry House due to the static load, 2.5 m, front view layer 1

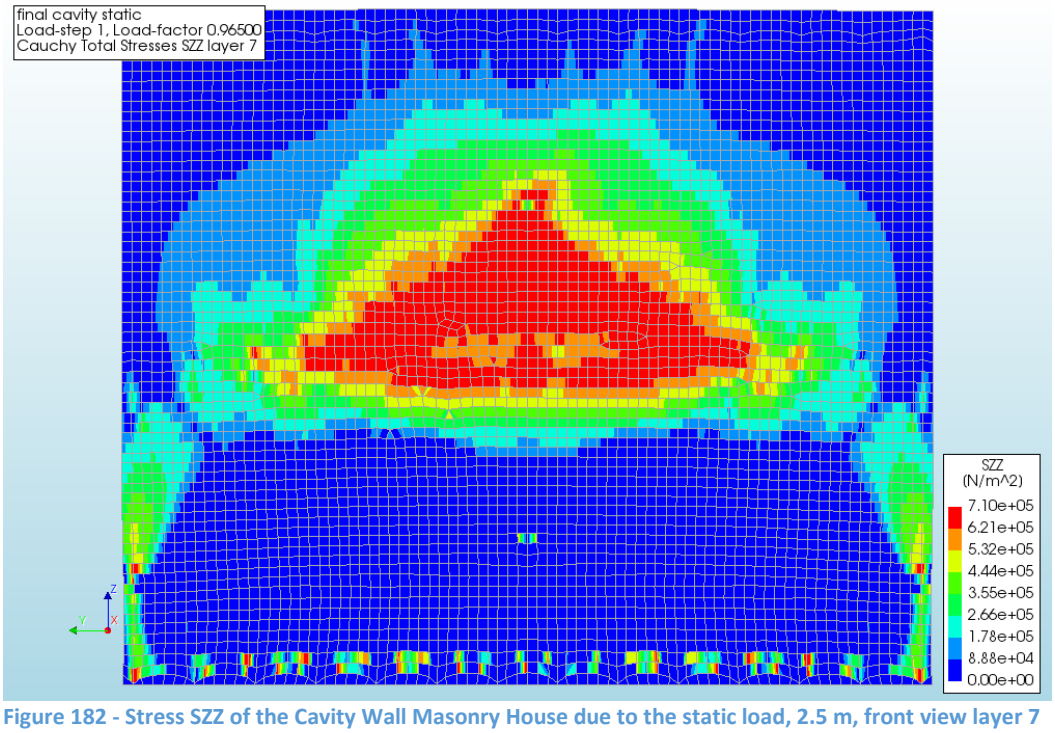


Figure 182 - Stress SZZ of the Cavity Wall Masonry House due to the static load, 2.5 m, front view layer 7

### Dynamic

The masonry house has been loaded with the dynamic load case as defined in Appendix K. Convergence only occurred until 0.7% of the actual load, the maximum deflection at that point was 1.0 mm, see Figure 183. No convergence is reached for the next steps up to the final 'Almost Converged' step at 1.8% of the load. The error, however, of this final 'Almost Converged' step is 0.021. The results are, therefore, still fairly accurate. Failure seems to occur between this 1.8% and 2.0% of the total load.

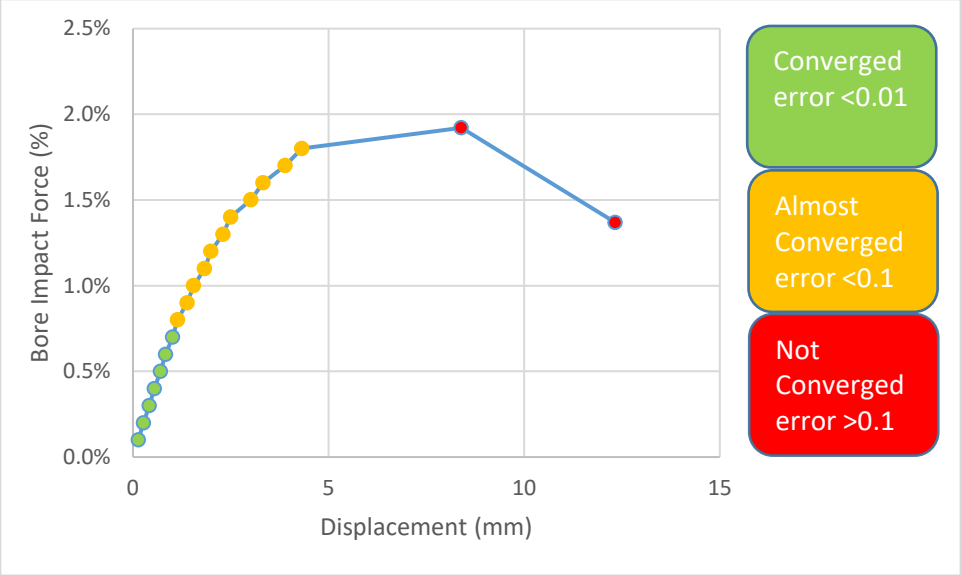


Figure 183 - Bore Impact Force vs Displacement of the Cavity Wall Masonry House due to the dynamic load

Figure 184 and Figure 185 show the displacement of the house at 1.8% of the dynamic load. As can be seen the entire ground floor wall is deformed and via the first floor causes the second wall to deform as well. The second wall provides some additional strength to the first wall in this way.

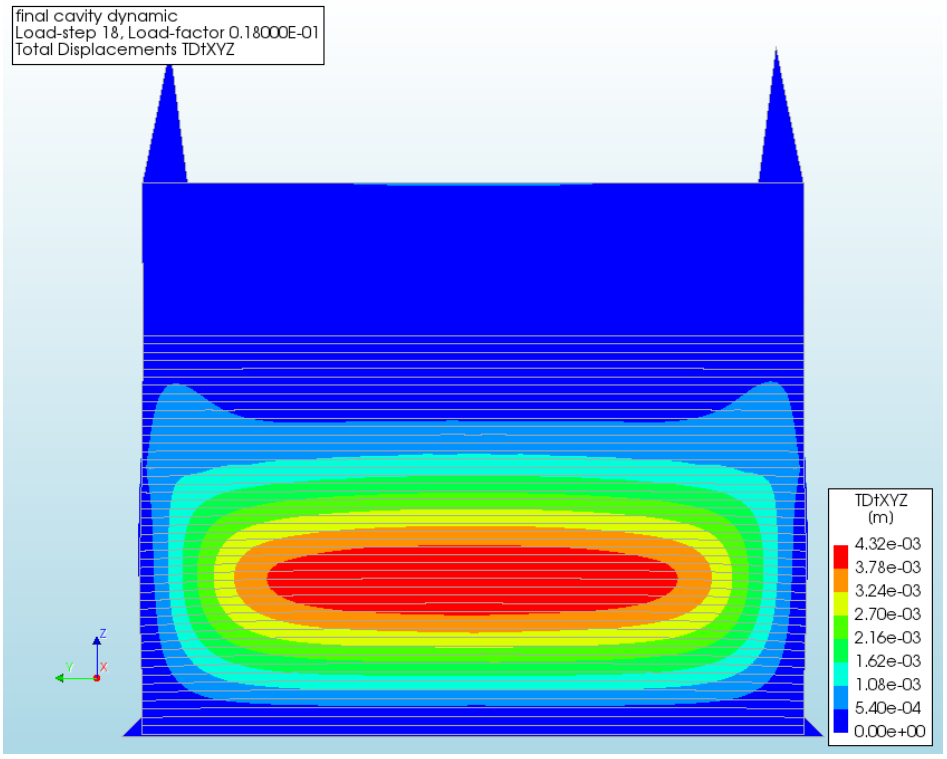


Figure 184 - Displacement of the Cavity Wall Masonry due to the dynamic load at 1.8%, front view

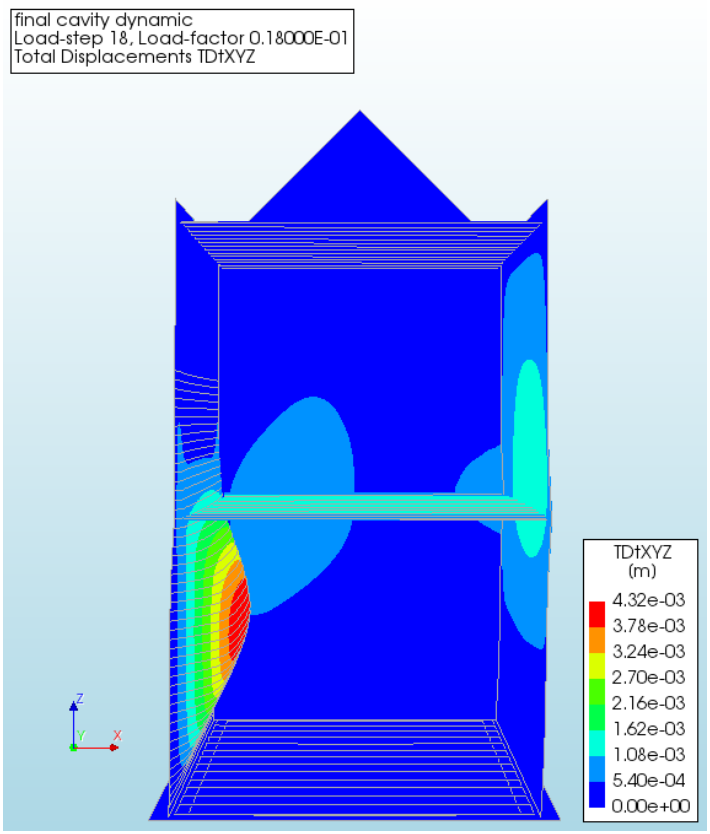


Figure 185 - Displacement of the Cavity Wall Masonry House due to the dynamic load at 1.8%, side view

Although the magnitude of the displacements is not yet very large, only 4-5mm, significant cracks have already formed. Figure 186 and Figure 187 show the crack widths which already reach beyond 1 millimetre. As expected, the largest cracks are located at the bottom, followed by the middle and the top of the ground floor.

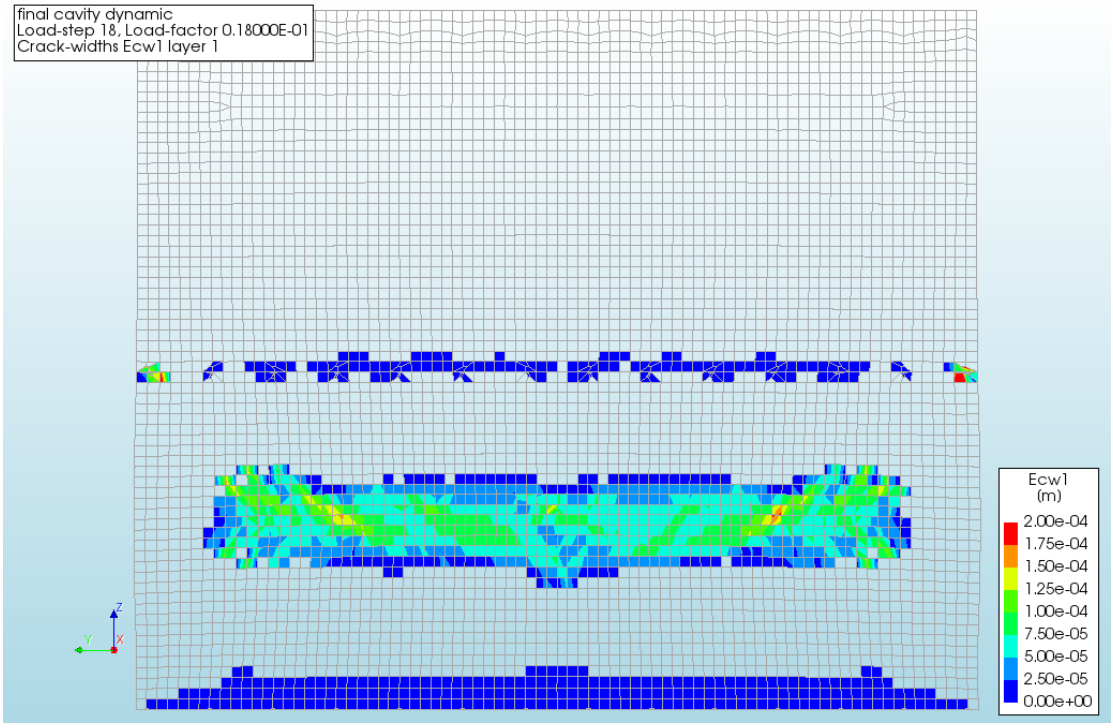


Figure 186 - Crack widths of the Cavity Wall Masonry House due to the dynamic load at 1.8%, front view layer 1

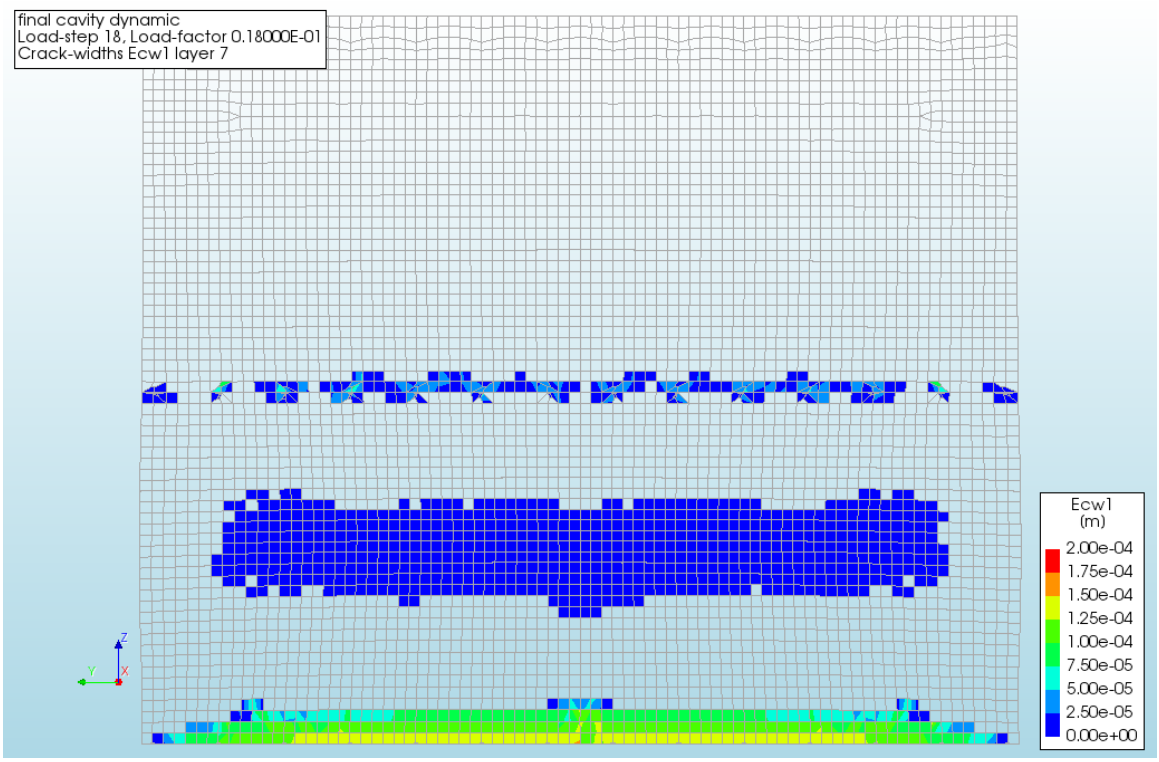


Figure 187 - Crack widths of the Cavity Wall Masonry House due to the dynamic load at 1.8%, front view layer 7

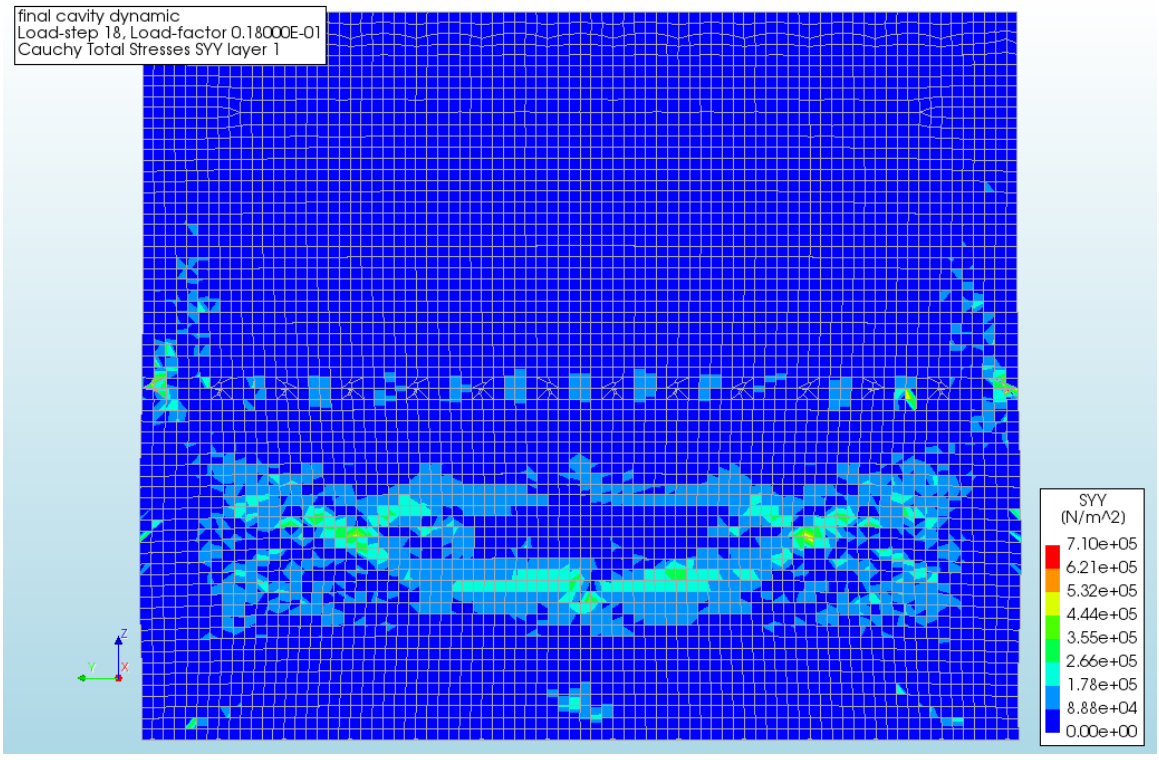


Figure 188 - Stress SYY of the Cavity Wall Masonry House due to the dynamic load at 1.8%, front view layer 1

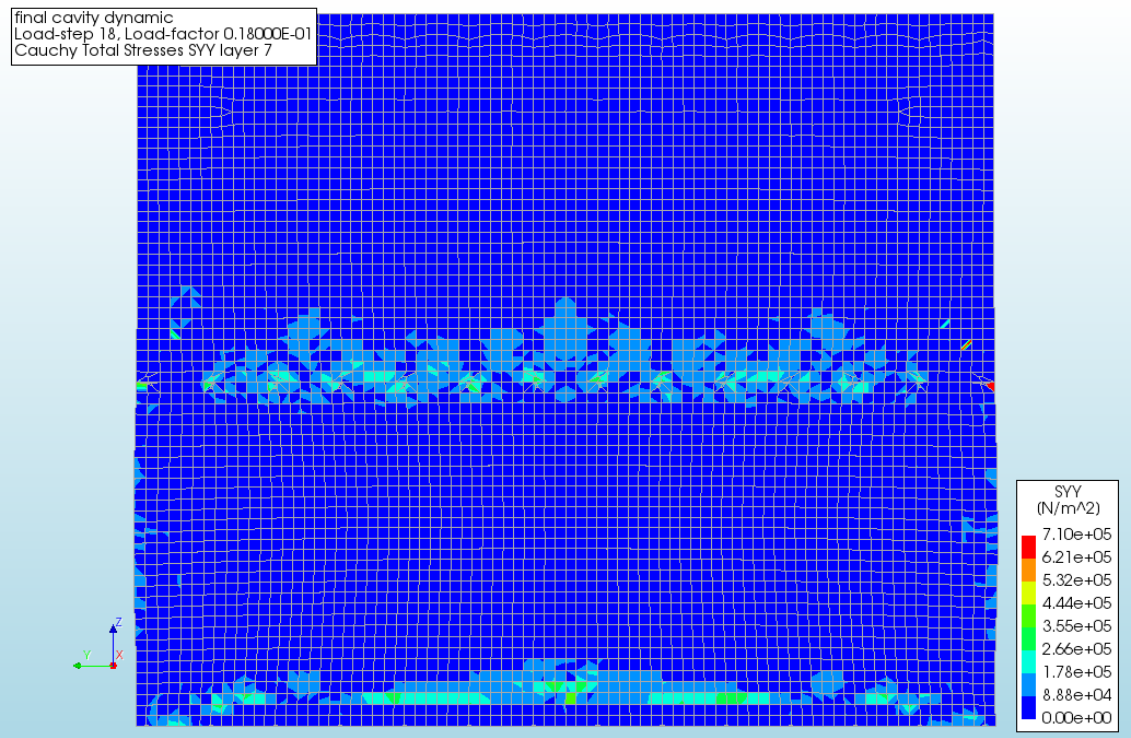


Figure 189 - Stress SYY of the Cavity Wall Masonry House due to the dynamic load 1.8%, front view layer 7

To verify the crack widths again the stresses have been visualised for the YY and ZZ directions. The legends have been scaled as such that they match the tensile strength of the masonry, dark red therefore indicates cracks. The cracks locations at the inside, Figure 186, match the stresses at the inside fairly well, see Figure 188 and Figure 190. The same holds for the outside of the wall, see Figure 187, Figure 189 and Figure 191. Notice how there are no tensile stresses in ZZ direction at the location with somewhat larger crack widths. Due to those cracks, no tensile stresses can be transferred anymore.

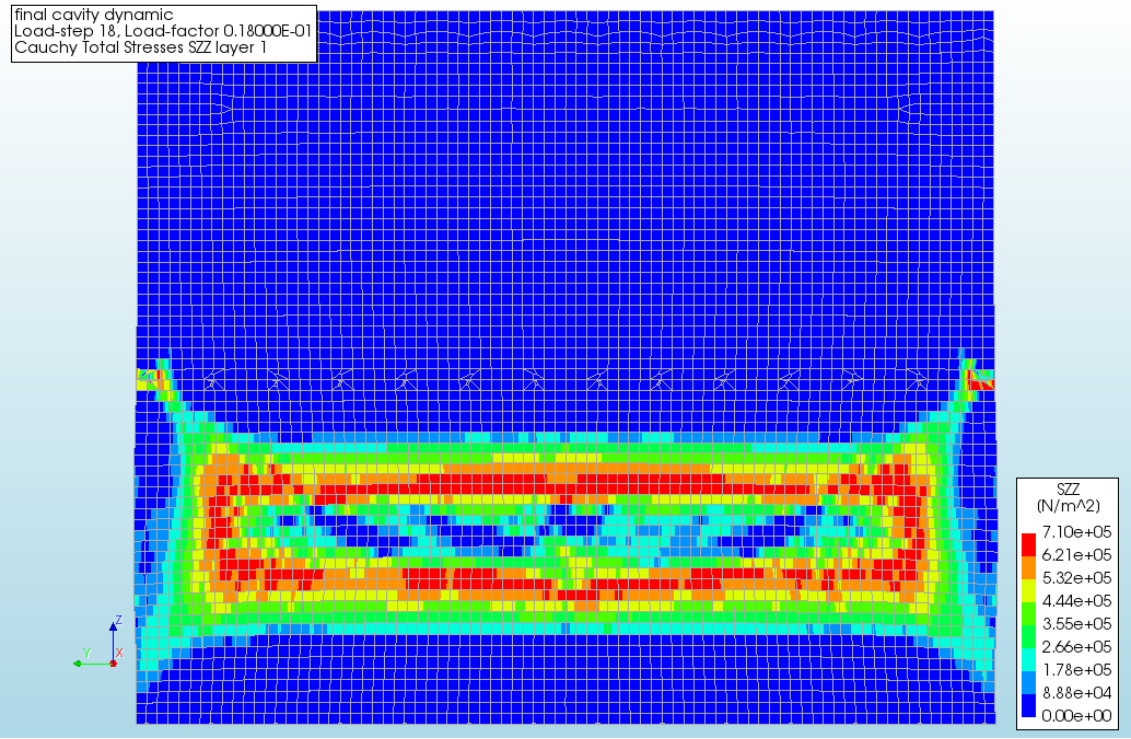


Figure 190 - Stress SZZ of the Cavity Wall Masonry House due to the dynamic load at 1.8%, front view layer 1

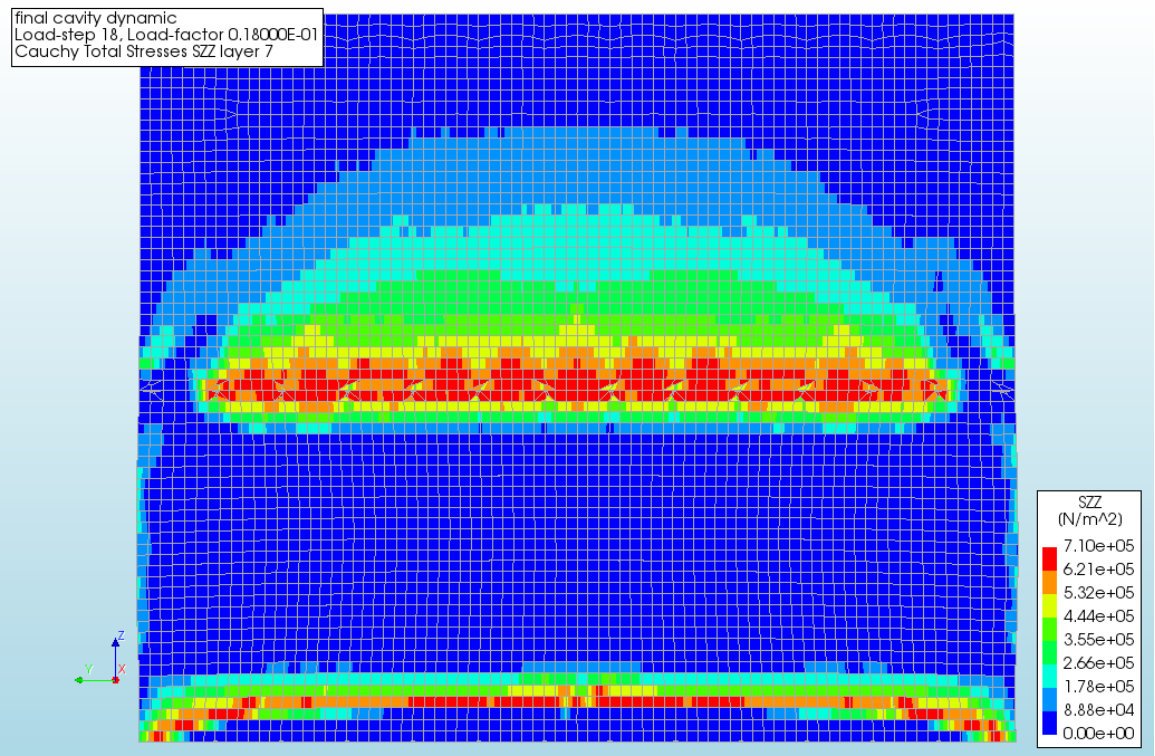


Figure 191 - Stress SZZ of the Cavity Wall Masonry House due to the dynamic load at 1.8%, front view layer 7

## Masonry House with Door and Windows

Increasing the complexity and realism of the model a little, door and windows are added as holes in the walls. The removal of these section from the walls is expected to cause a decrease in the resistance, since smaller sections of the wall will have to carry the same load.

### Static

Loaded with a rising water level, see Figure 192, first damage occurred at an inundation depth of approximately 1.75 m. The load then increases until collapse, which occurs between an inundation depth of 2.35-2.85 m. This corresponds with the second and third 'Not Converged' steps in Figure 192. However, since the wanted cracking and deformation patterns already occur at the first 'Not Converged' step, this first step, with an error of 0.155, is used. Although there is a lack of accuracy, the cracking and deformation patterns overall are fairly accurate. These patterns are not yet visible in the last 'Converged' step. Due to the lack of accuracy it is not possible to determine whether or not a decrease has taken place in the resistance compared to the previous static case.

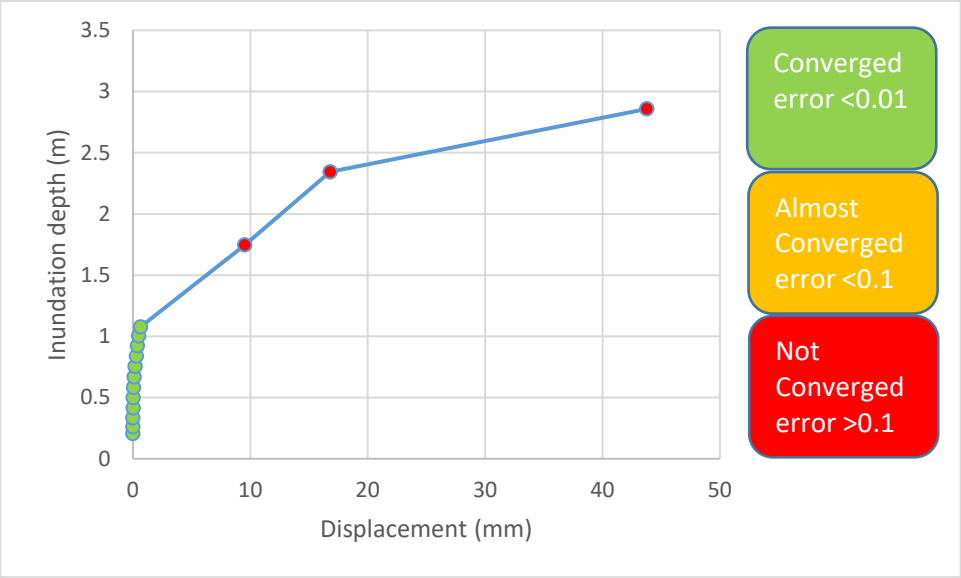


Figure 192 - Inundation depth vs Displacement of the Cavity Wall Masonry House with Door and Windows due to the static load

Figure 193 and Figure 194 show the displacements of the house. As expected, the largest displacements are near the large window and the section of wall between this large window and the smaller window. At the inundation depth of these two figures there is already damage to the wall below the large window. With increasing depth, the displacements follow the same pattern until the section between the two windows cracks and collapses.

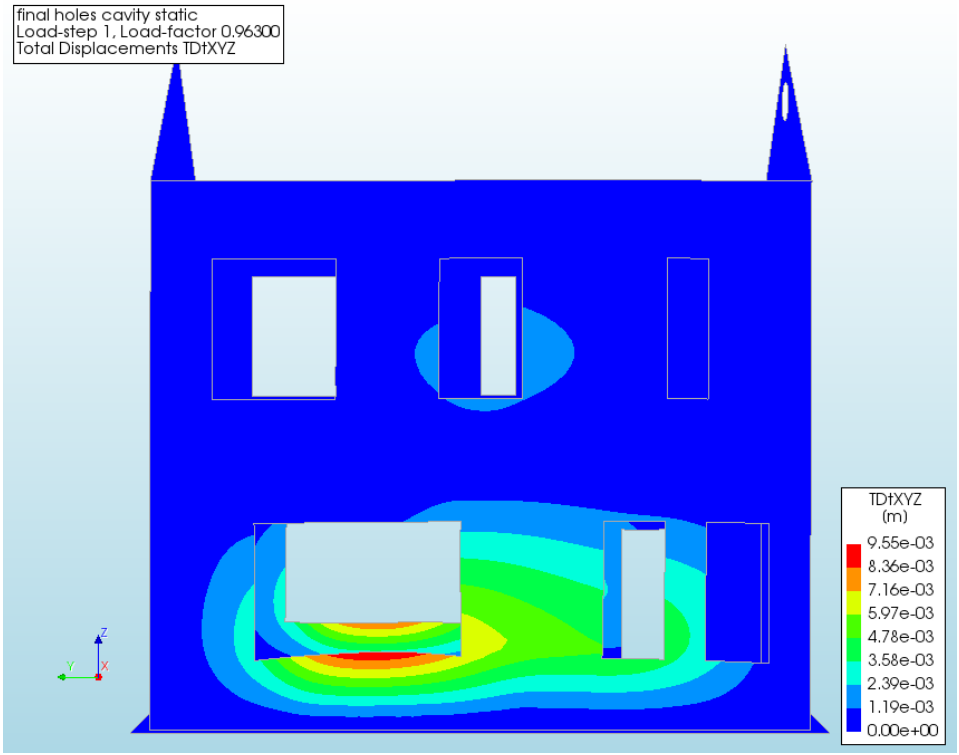


Figure 193 - Displacement of the Cavity Wall Masonry House with Door and Windows due to the static load, 1.75 m, front view

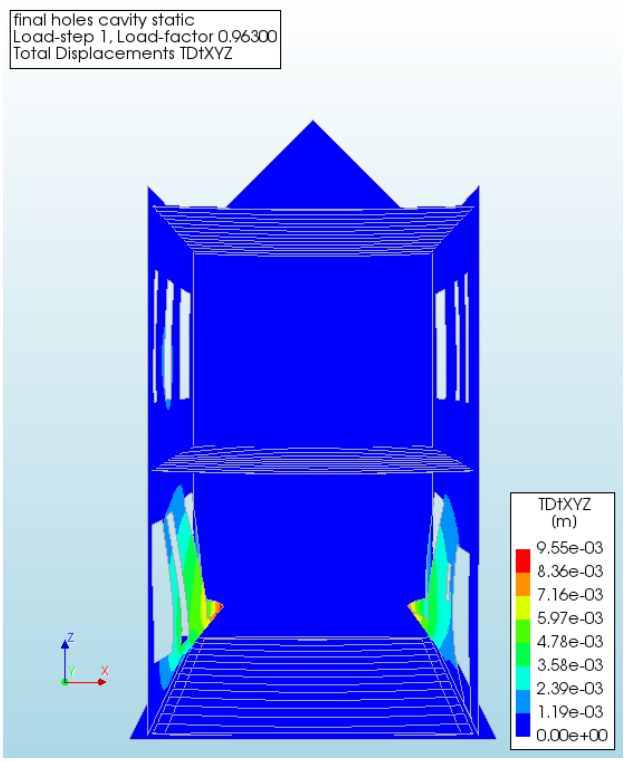


**Figure 194 - Displacement of the Cavity Wall Masonry House with Door and Windows due to the static load, 1.75 m, side view**

As mentioned before, the cracking patterns are already visible in Figure 195 and Figure 196. As expected, the cracks are mainly located at the bottom of the wall and near the windows. Especially the wall section between the large and small window is vulnerable since it carries a large part of the house and receives no extra out of plane support. With increasing depth, the magnitude of the cracks and displacement increases and the wall breaks and collapses.

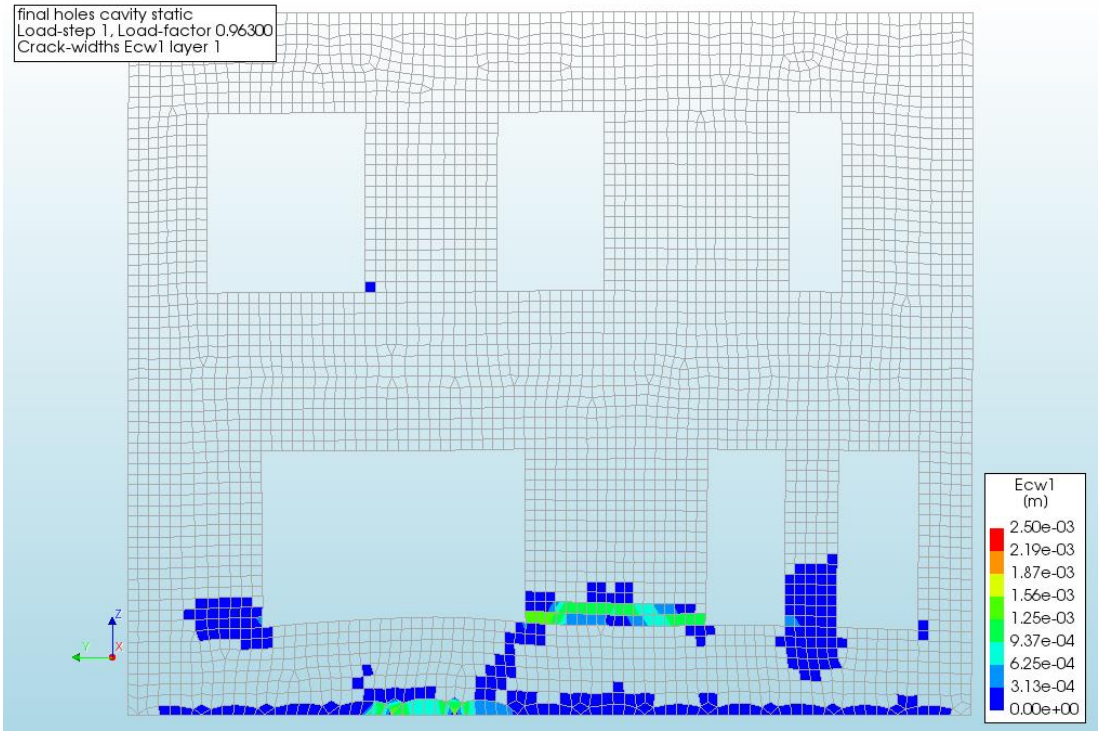


**Figure 195 - Crack widths of the Cavity Wall Masonry House with Door and Windows due to the static load, 1.75 m, front view layer 1**

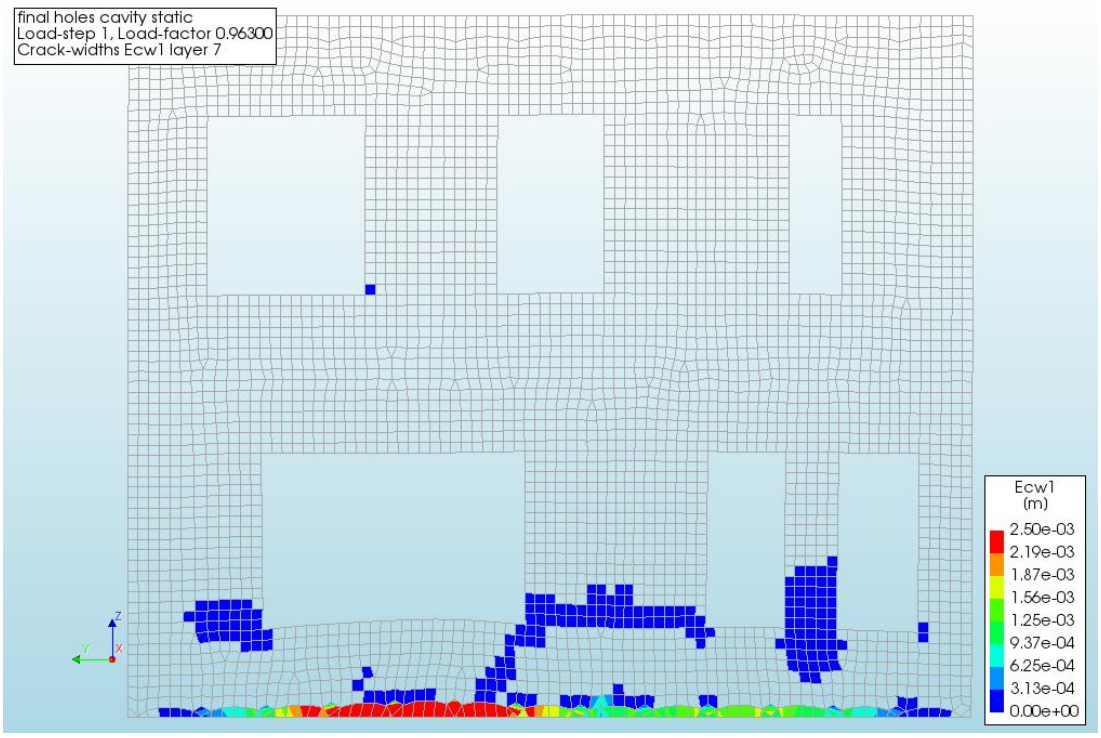


**Figure 196 - Crack widths of the Cavity Wall Masonry House with Door and Windows due to the static load, 1.75 m, front view layer 7**

### DYNAMIC

Loaded with the dynamic load, the displacement increased until collapse at about 1.6% of the total dynamic load, see Figure 197. The displacement and cracking patterns are already visible at the last 'Almost Converged' step. The error of this last 'Almost Converged' step is 0.029, which makes those results still fairly accurate. As expected the total load slightly decreased compared to the previous dynamic case.

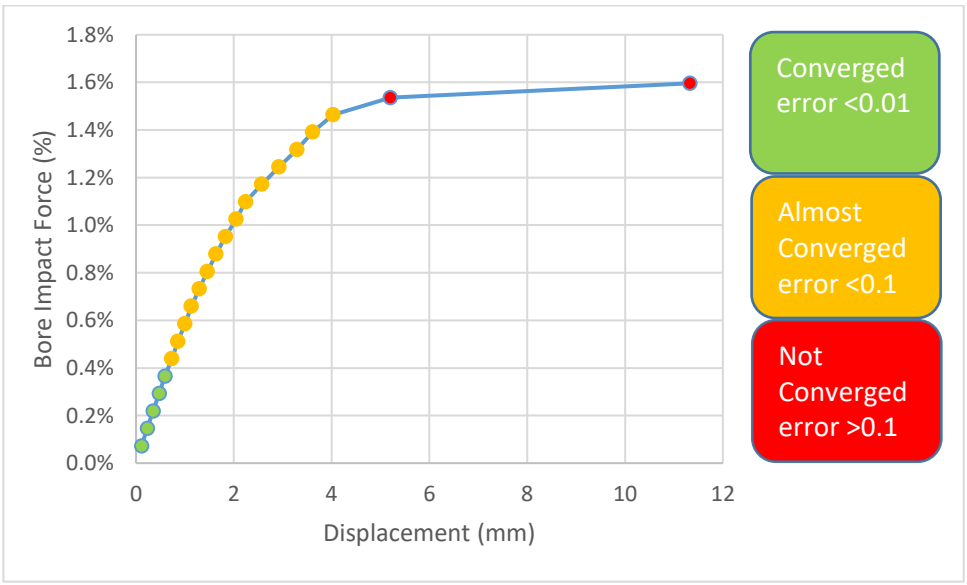


**Figure 197 - Bore Impact Force vs Displacement of the Cavity Wall Masonry House with Door and Windows due to the dynamic load**

Figure 198 and Figure 199 show these aforementioned displacement patterns. As in the previous case, the first floor causes a cooperation between the front and back wall. This effectively decreases the affected height of the wall to only the ground floor. Similar to the static case in the previous

paragraph, the wall section between the large and small window experiences the largest displacements. This is also the section that will fail, thus causing the house to collapse. Due to the load acting higher on the wall, the displacements beneath the large window are much lower than for the static case.

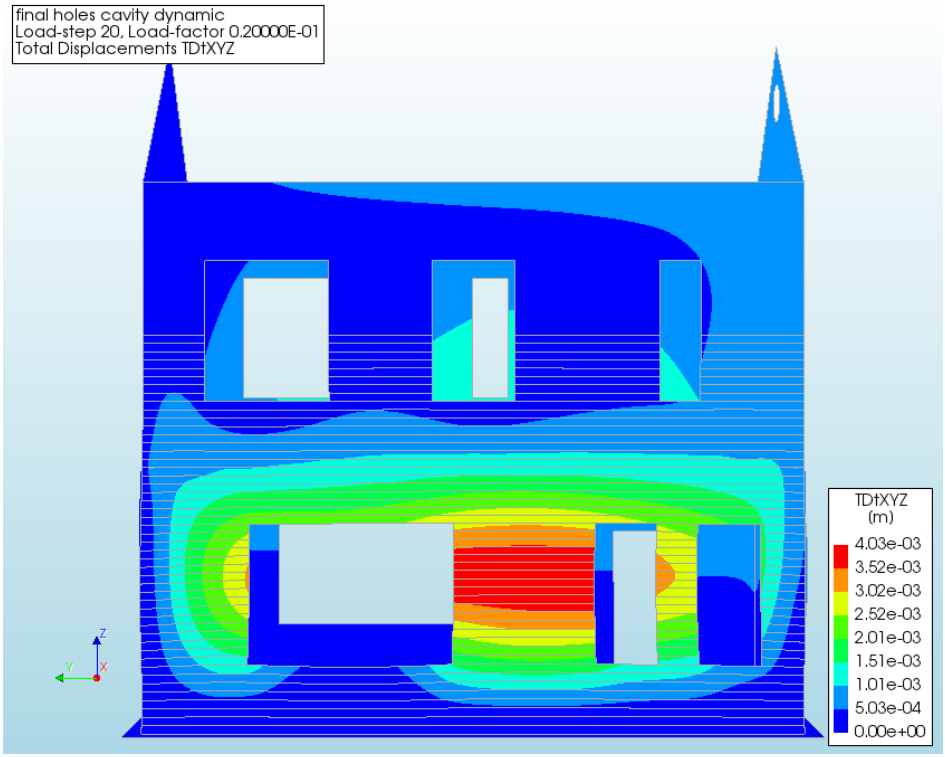


**Figure 198 - Displacement of the Cavity Wall Masonry House with Door and Windows due to the dynamic load at 1.46%, front view**

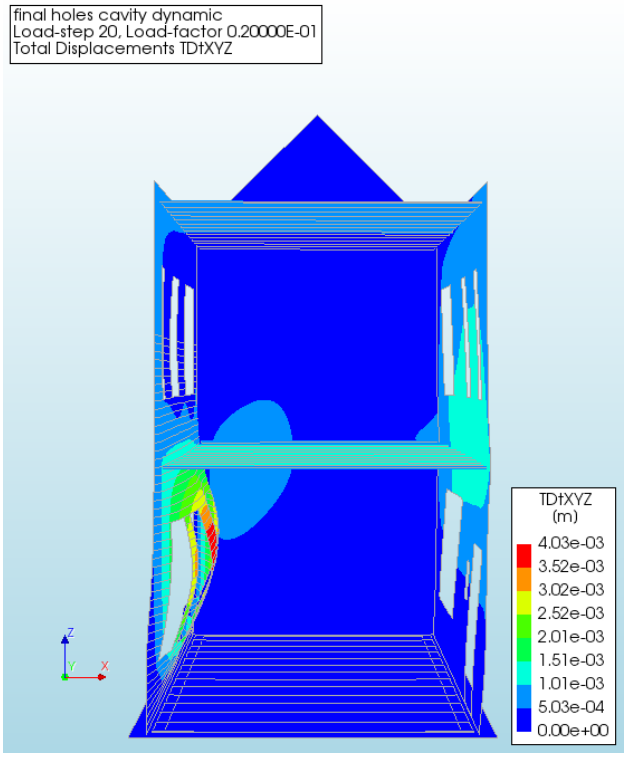


**Figure 199 - Displacement of the Cavity Wall Masonry House with Door and Windows due to the dynamic load at 1.46%, side view**

As was with the displacements, the image sketched in the previous paragraph is also visible for the crack widths. However, the cracks at the inside are now even more clearly mainly situated at this wall section between the large and small window. The cracks at the outside, at the bottom, have also moved to match these more pronounced displacements of that wall section.

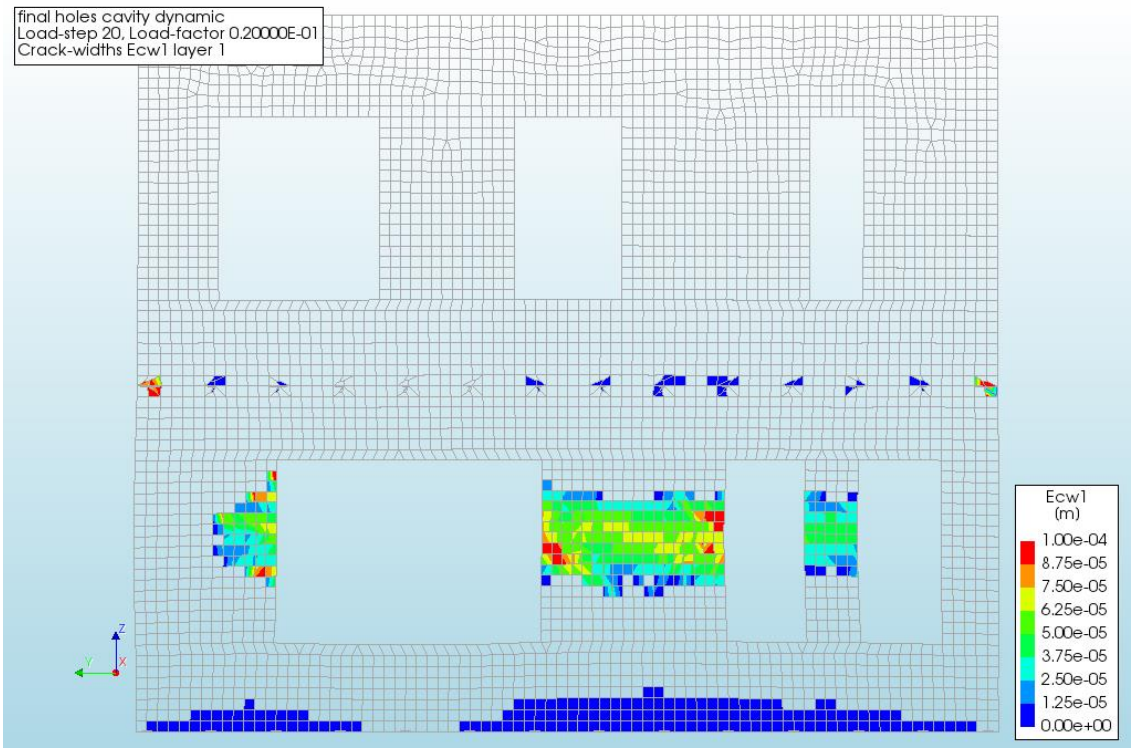


**Figure 200 - Crack widths of the Cavity Wall Masonry House with Door and Windows due to the dynamic load at 1.46%, front view layer 1**

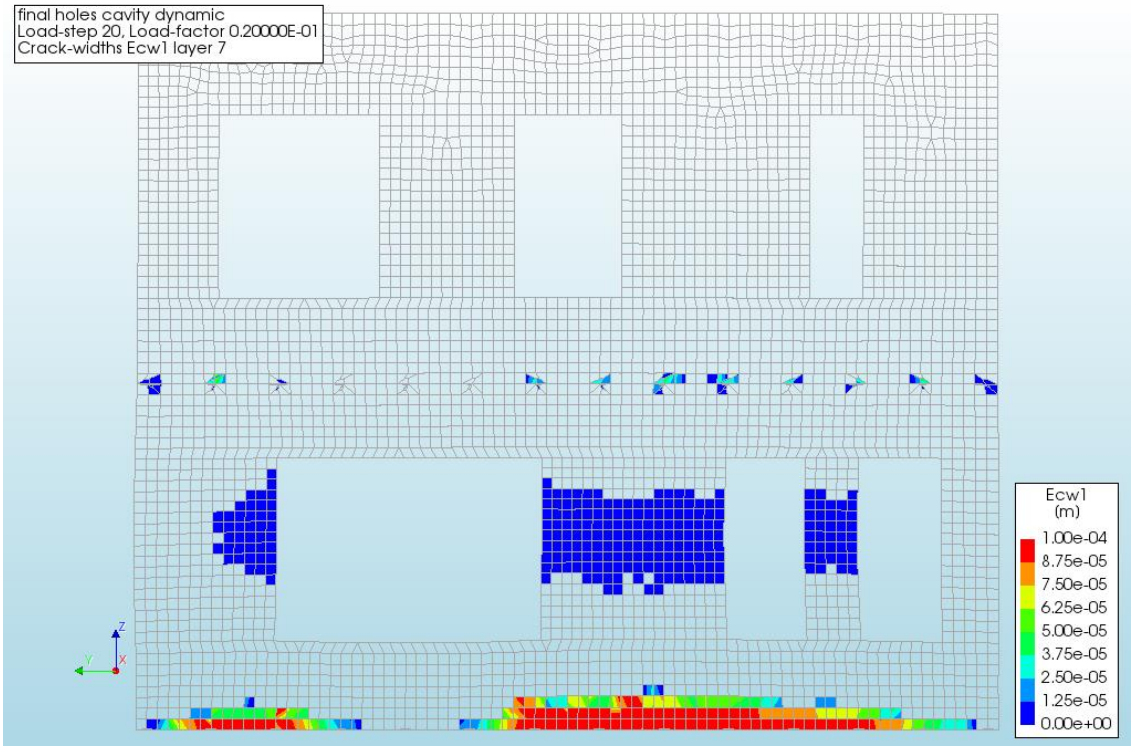


**Figure 201 - Crack widths of the Cavity Wall Masonry House with Door and Windows due to the dynamic load at 1.46%, front view layer 7**

## Masonry House with Inner Walls

Again, the complexity is increased, compared to the first, simple model, inner walls have been added. These should provide some out of plane support to the front walls and thus increase their resistance.

### Static

Again, the model has been loaded with a rising water level. The final 'Almost Converged' step, see Figure 202, already clearly shows the locations of the displacements and cracks. The error of the final 'Almost Converged' step is 0.089, which makes those results still reasonably accurate, especially regarding the patterns. When comparing Figure 202 to Figure 174, there is hardly an increase in the maximum inundation depth. Although the inner wall does provide out of plane support, the remaining width of the wall is still sufficient to cause similar results. Since this remaining width is still large than the width of the side walls, the front wall is still leading.

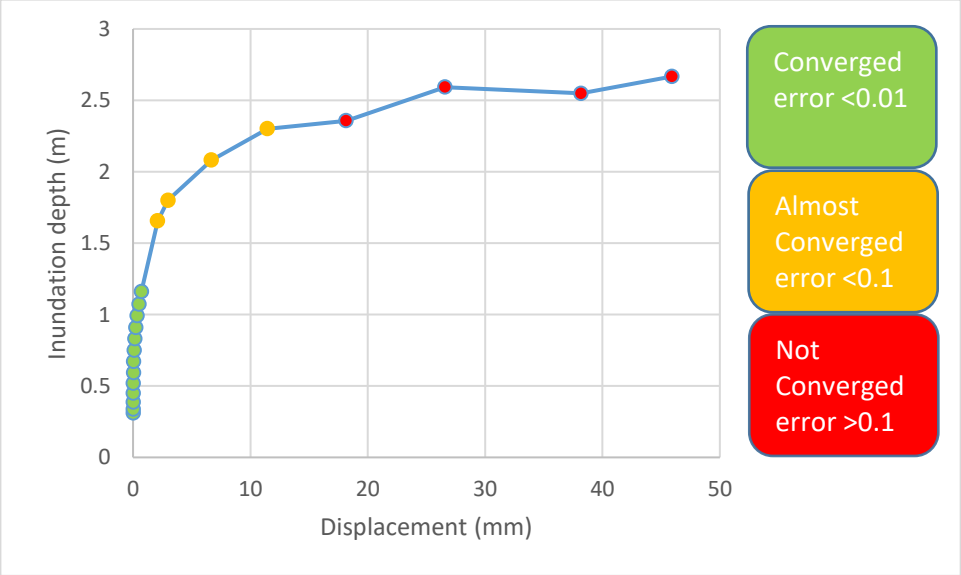


**Figure 202 - Inundation depth vs Displacement of the Cavity Wall Masonry House with Inner Walls due to the static load**

Figure 203 and Figure 204 show the displacements of the house. Notice the, now, small difference between the front, back and side wall. As mentioned above the main difference with Figure 175 is the width of the displacement field.

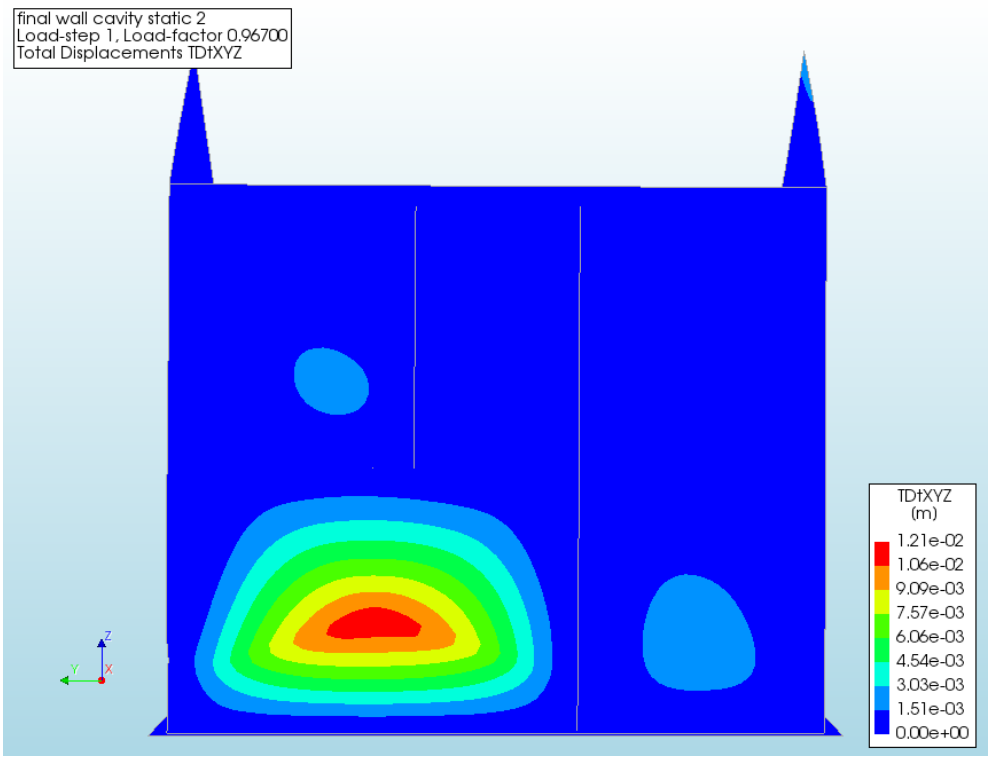


Figure 203 - Displacement of the Cavity Wall Masonry House with Inner Walls due to the static load, 2.3 m, front view

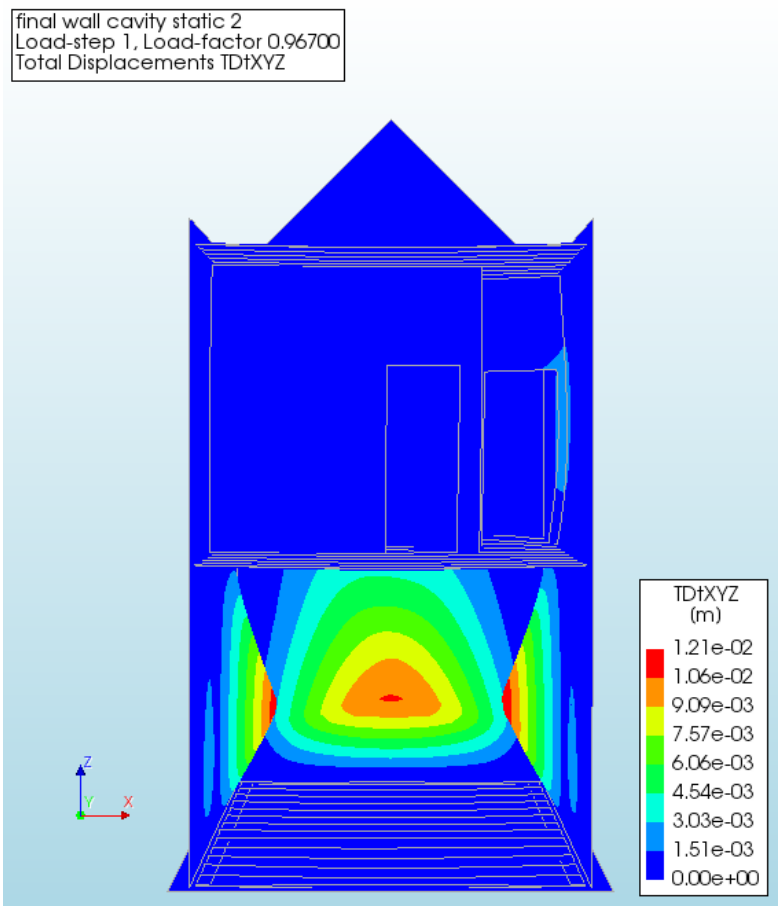


Figure 204 - Displacement of the Cavity Wall Masonry House with Inner Walls due to the static load, 2.3 m, side view (without the ground floor inner wall)

As expected from the results above, the cracking patterns and crack widths are again very similar. The only difference being the relocation of these patterns to the smaller section of the wall, see Figure 177 and Figure 178 compared to Figure 205 and Figure 206.

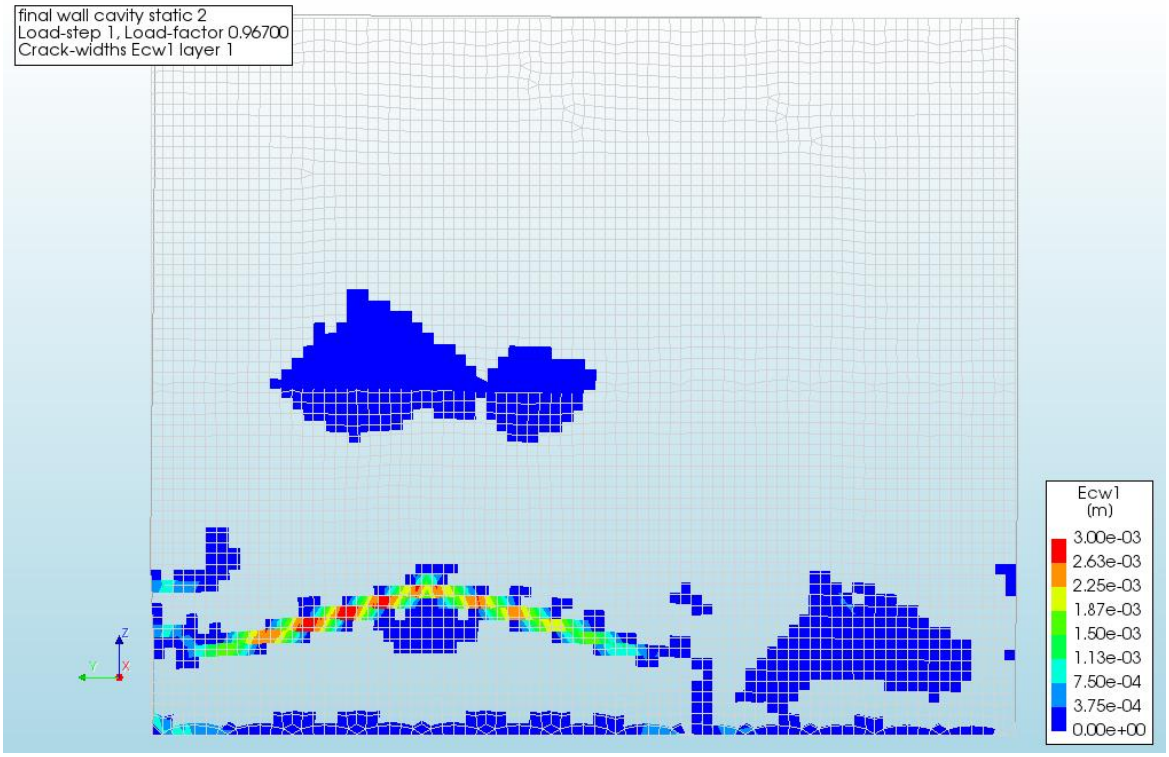


Figure 205 - Crack widths of the Cavity Wall Masonry House with Inner Walls due to the static load, 2.3 m, front view layer 1

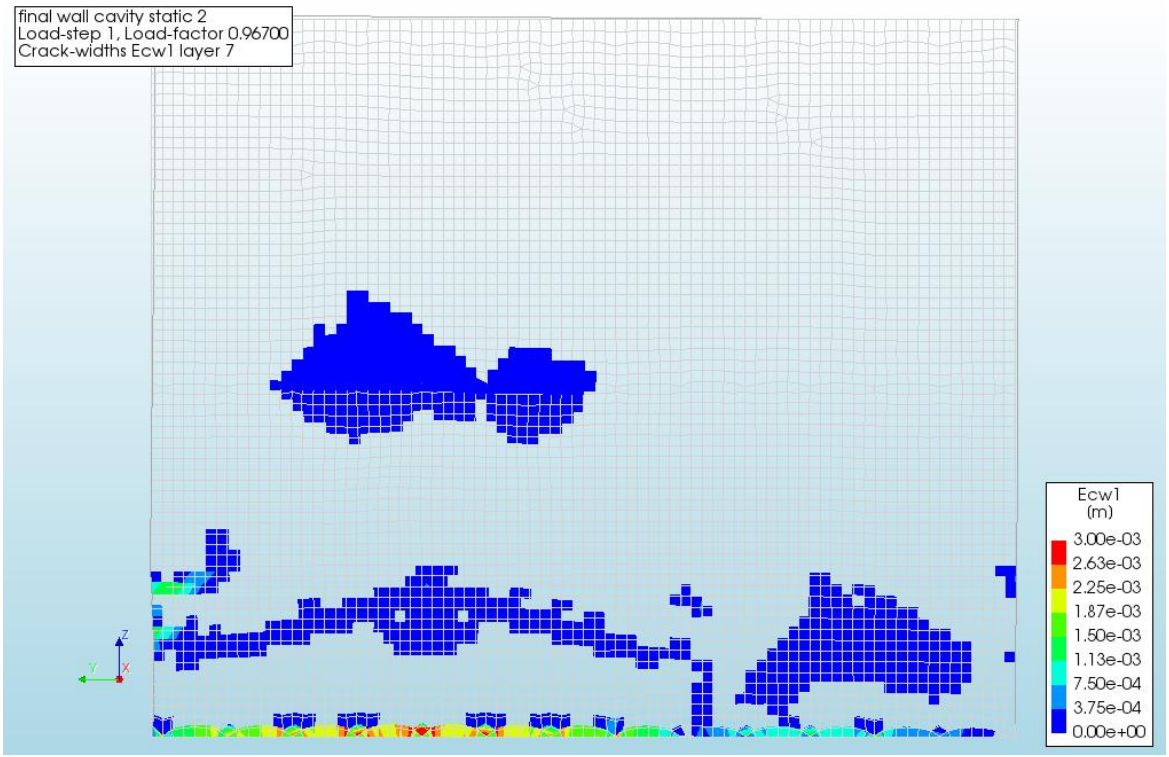


Figure 206 - Crack widths of the Cavity Wall Masonry House with Inner Walls due to the static load, 2.3 m, front view layer 7

### DYNAMIC

The model is now loaded with the dynamic load until failure. Compared to first dynamic, a small increase in resistance is expected due to the inner walls. The last 'Almost Converged' step already matches this expectation, see Figure 207 and Figure 183. The house then proceeds to fail, but due to the inaccuracy of the results, the exact load could not be determined. The error of the final 'Almost Converged' step is 0.035, which makes those results still fairly accurate. The error of the following two steps, however, are 0.568 and 0.159 respectively. The expected failure load is expected to be between 2.25-2.75% of the total dynamic load.

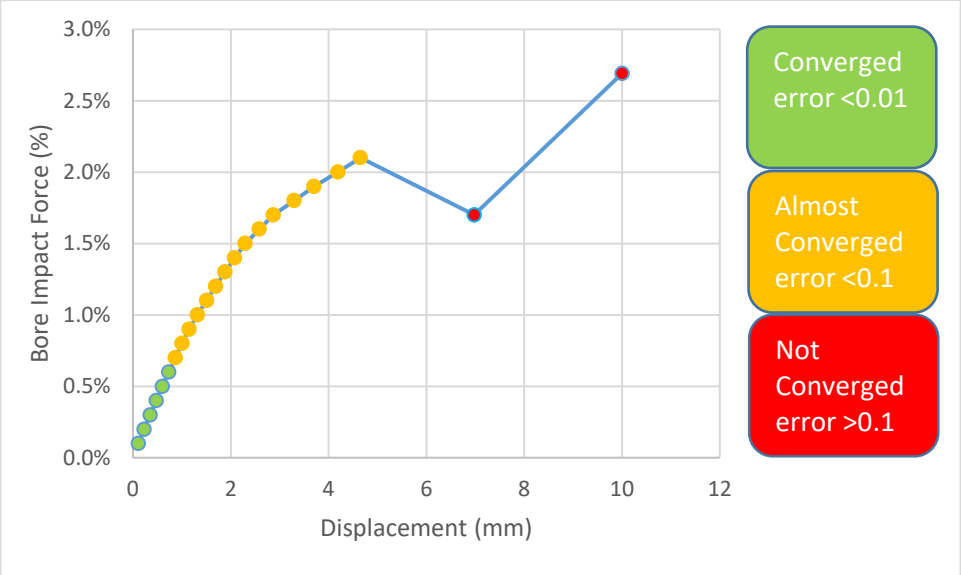


**Figure 207 - Bore Impact Force vs Displacement of the Cavity Wall Masonry House with Inner Walls due to the dynamic load**

The displacement fields of Figure 208 and Figure 209 are similar to the displacement fields of the first static and dynamic case as well as the inner walls static case. This was to be expected after the results of the inner walls static case. Although, now there is an increase in the resistance or a decrease in the displacement, depending on the point of view. A similar displacement is reached however the load is approximately 0.3% higher, see Figure 184 and Figure 208. This increase is about 15% with respect to the previous case.

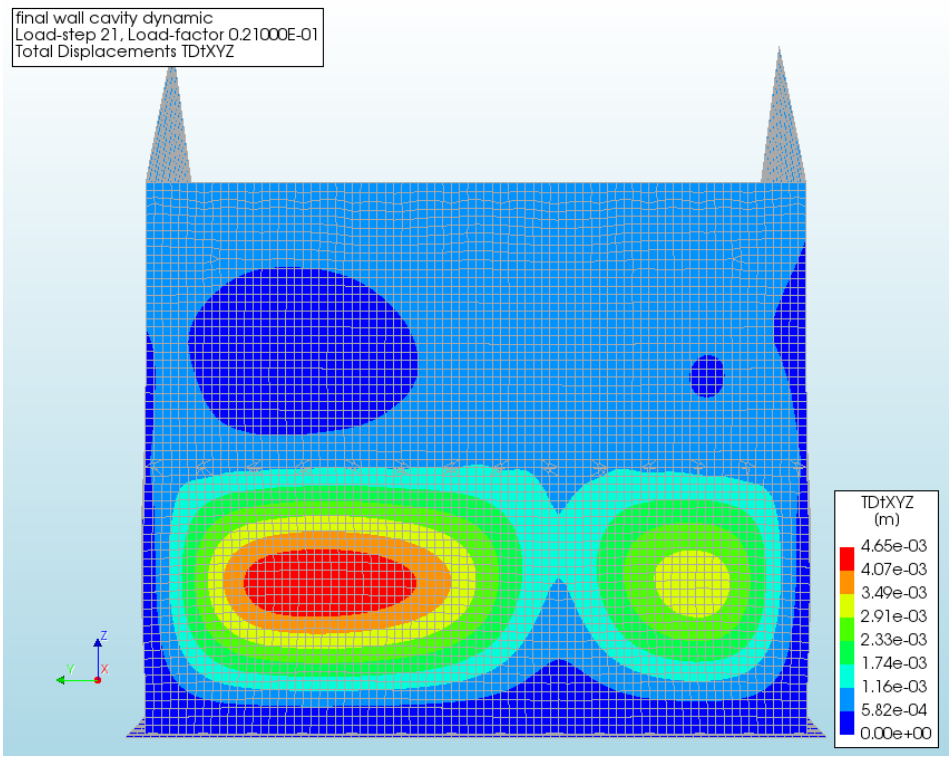


Figure 208 - Displacement of the Cavity Wall Masonry House with Inner Walls due to the dynamic load, at 2.1%, front view

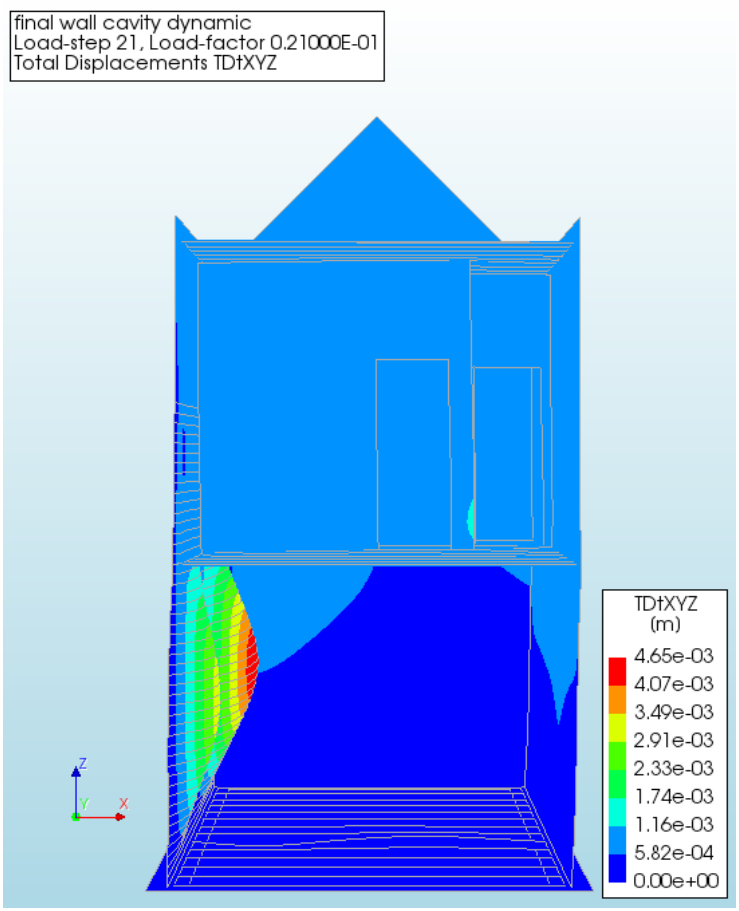


Figure 209 - Displacement of the Cavity Wall Masonry House with Inner Walls due to the dynamic load, at 2.1%, side view (without the ground floor inner wall)

The cracking patterns and widths, as expected, bare the same resemblance as the displacements. Again, the largest cracks are located at the bottom of the wall, now divided into two sections. Next the cracks in the middle of the ground floor wall follow. Both already reach values larger than 1/10 millimetre. Finally, there are cracks at the top of the ground floor where the wall is supported by the first floor.

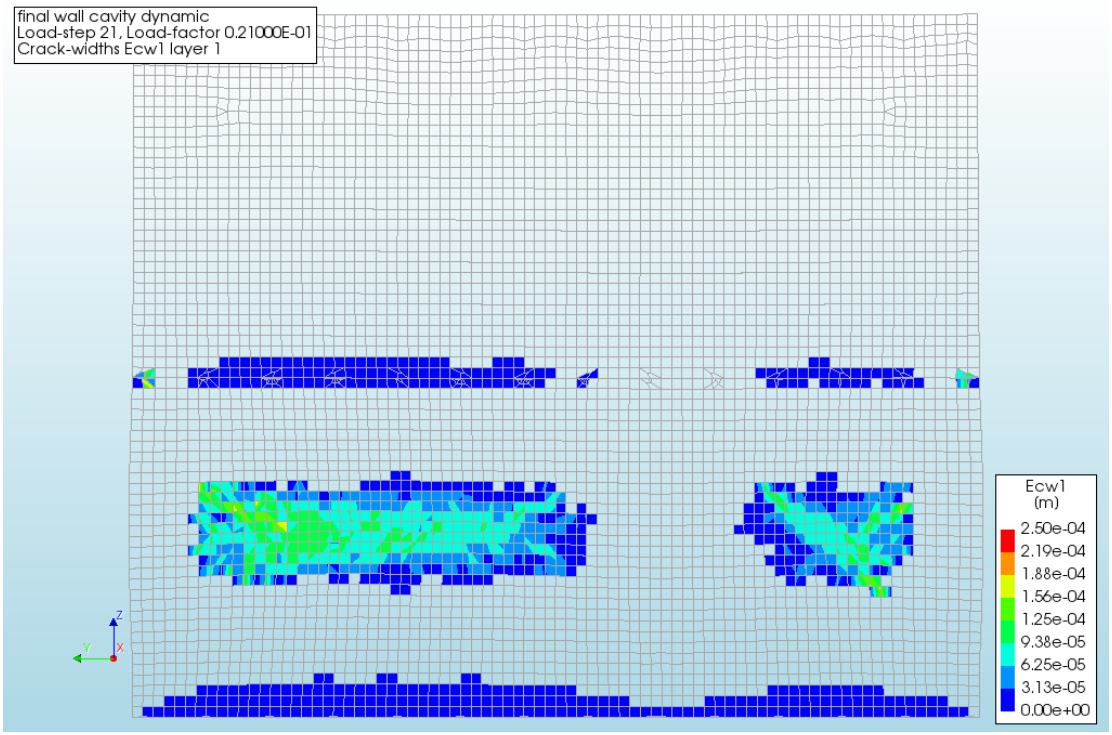


**Figure 210 - Crack widths of the Cavity Wall Masonry House with Inner Walls due to the dynamic load, at 2.1%, front view layer 1**

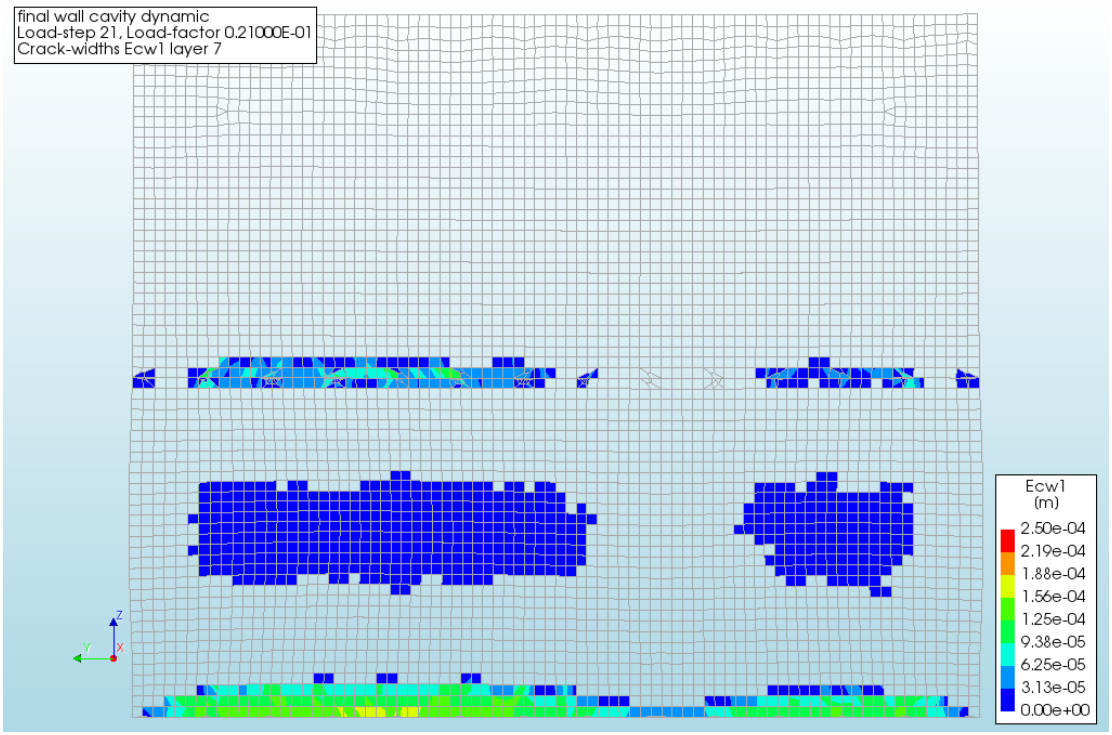


**Figure 211 - Crack widths of the Cavity Wall Masonry House with Inner Walls due to the dynamic load, at 2.1%, front view layer 7**

## Masonry House with Door, Windows and Inner Walls

The final model combines both the door and windows as well as the inner walls. Whether or not this will cause an increase or decrease in the resistance compared to the first two cases, is difficult to determine. One measure seems to increase the resistance, while the other decreases the resistance.

### Static

Here there are two situations to be shown, the point where first damage occurs and the point where structural collapse occurs.

For first damage the last 'Almost Converged' step from Figure 212is used. The error of the final 'Almost Converged' step is 0.086, which makes those results still reasonably accurate.

For the point where structural collapse occurs, the last 'Not Converged' step of Figure 93 is used. The error of this 'Not Converged' step is 0.638, which makes those results not very accurate at all. However, the inaccuracy mainly seems to follow for a significant part from the large deflections at the large living room window and the side wall, see Figure 217. This side wall experiences at this point a load due to an inundation depth of approximately 6.3 m compared to the 3.4 for the front wall.

The side wall fails at an earlier load step but at a higher load, ~4-5 m, between the first and second 'Not Converged' step in Figure 214. These have an of 0.185 and 0.312 respectively, which is not very accurate. The results are, however, significantly higher than those for the front wall, that the front wall is leading.

With regard to the first static case, damage near the large window seems to occur at the same time. Collapse however seems to increase from about 2.5 m to 3.4 m.

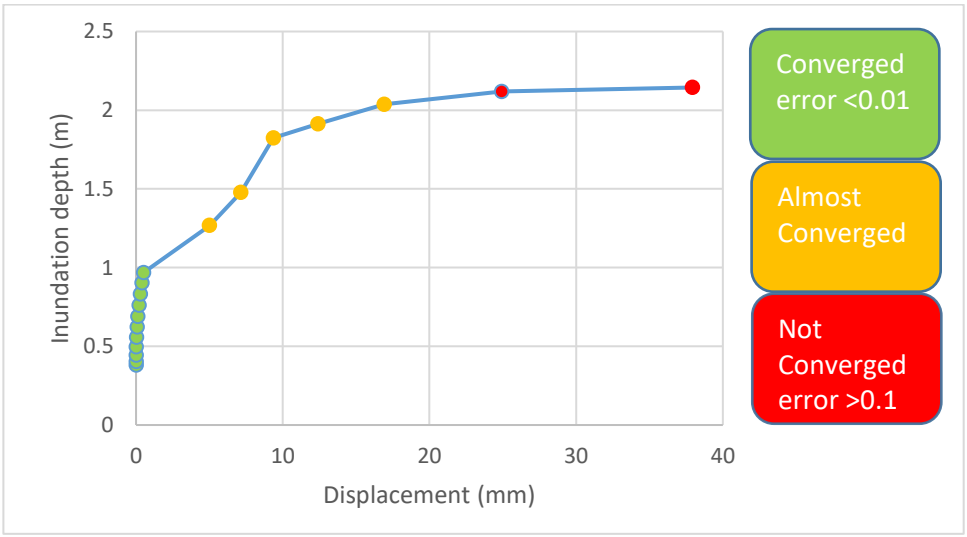


Figure 212 - Inundation depth vs Displacement of the Cavity Wall Masonry House with Door, Windows and Inner Walls due to the static load, entire wall

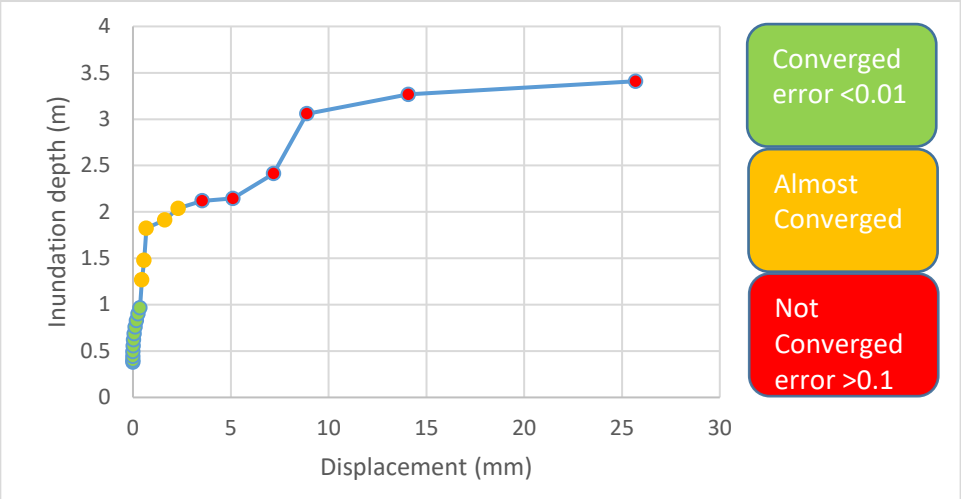


Figure 213 - Inundation depth vs Displacement of the Cavity Wall Masonry House with Door, Windows and Inner Walls due to the static load, section of the wall

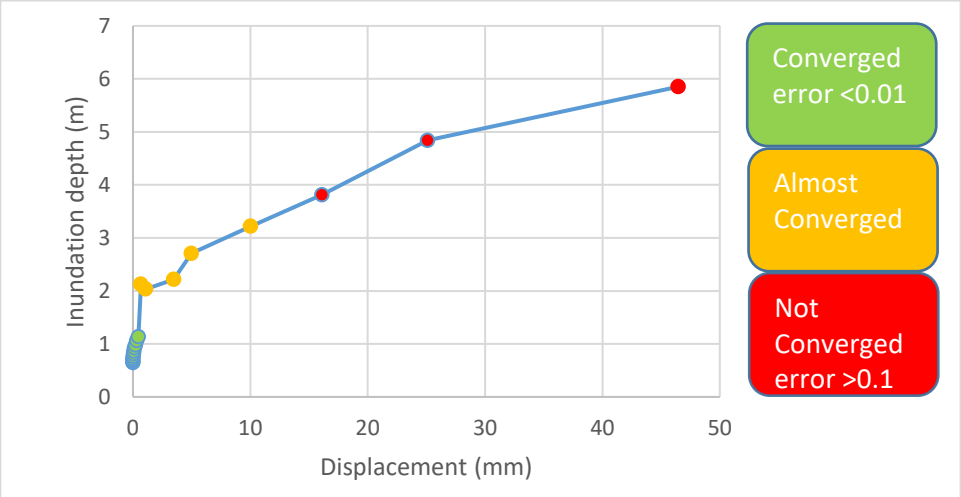


Figure 214 - Inundation depth vs Displacement of the Cavity Wall Masonry House with Door, Windows and Inner Walls due to the static load, side wall

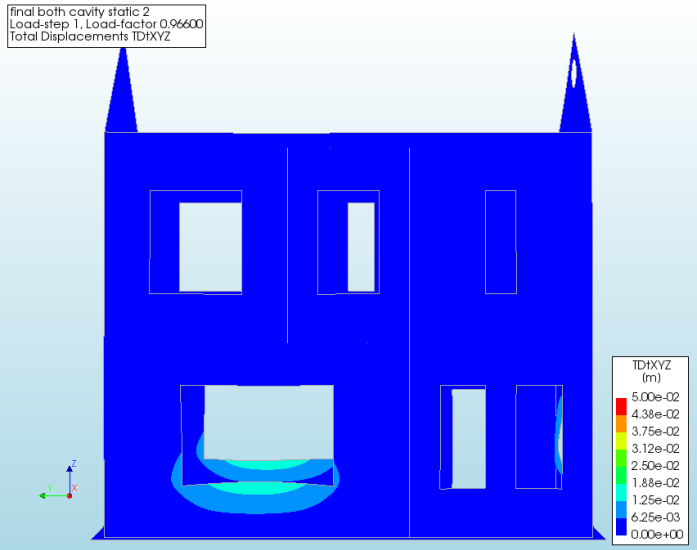


Figure 215 - Displacement of the Cavity Wall Masonry House with Door, Windows and Inner Walls due to the static load, 2.0 m, front view

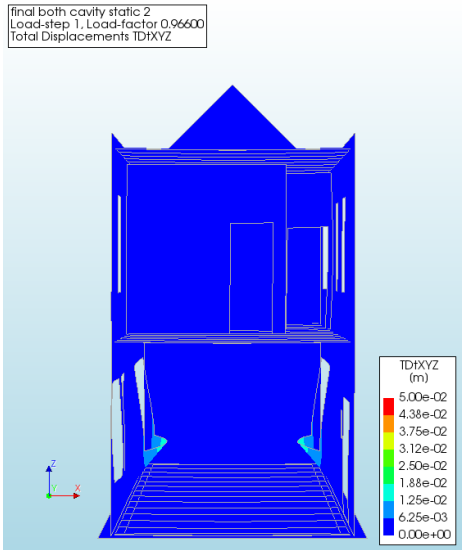


Figure 216 - Displacement of the Cavity Wall Masonry House with Door, Windows and Inner Walls due to the static load, 2.0 m, side view (without the ground floor inner wall)

Figure 215 until Figure 218 show the displacements related to the aforementioned points. The large deflections around the large living room window are clearly visible. These cause the first damage, but do not endanger the building with regard to collapse. With increasing inundation depth, the displacement of other parts of the house start to increase. This continues until the wall segment between the two windows, Figure 217, and the side wall, Figure 218, cannot cope with the load anymore and crack, followed with collapse.

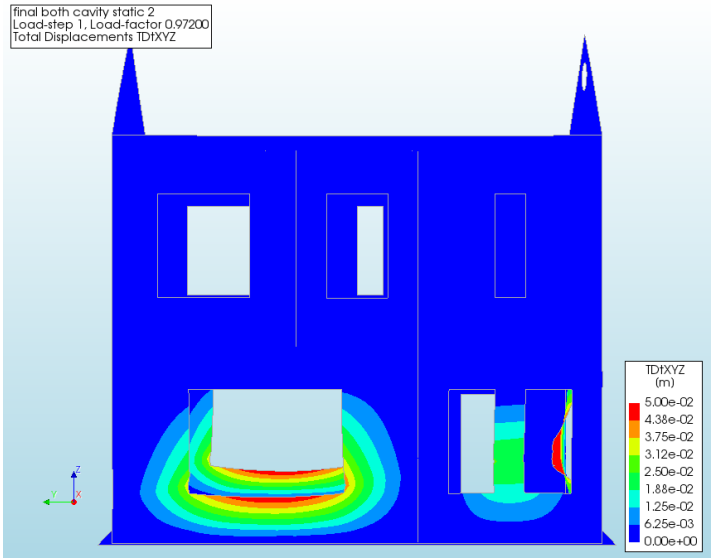


Figure 217 - Displacement of the Cavity Wall Masonry House with Door, Windows and Inner Walls due to the static load, 3.4 m, front view

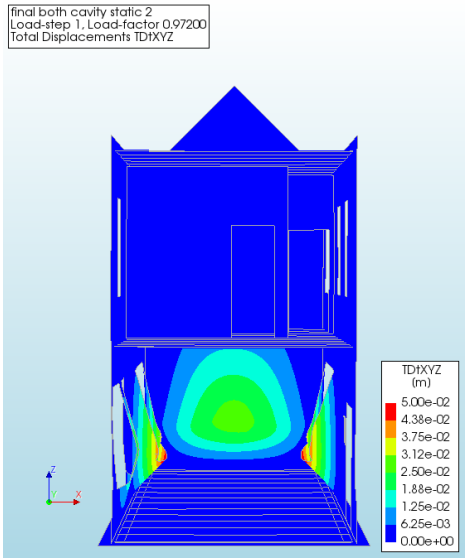


Figure 218 - Displacement of the Cavity Wall Masonry House with Door, Windows and Inner Walls due to the static load, 3.4 m, side view (without the ground floor inner wall)

The crack widths show similar results as the displacements. Cracks are already present at an inundation depth of 2.0 m, mainly at the section near the large window, see Figure 219 and Figure 220.

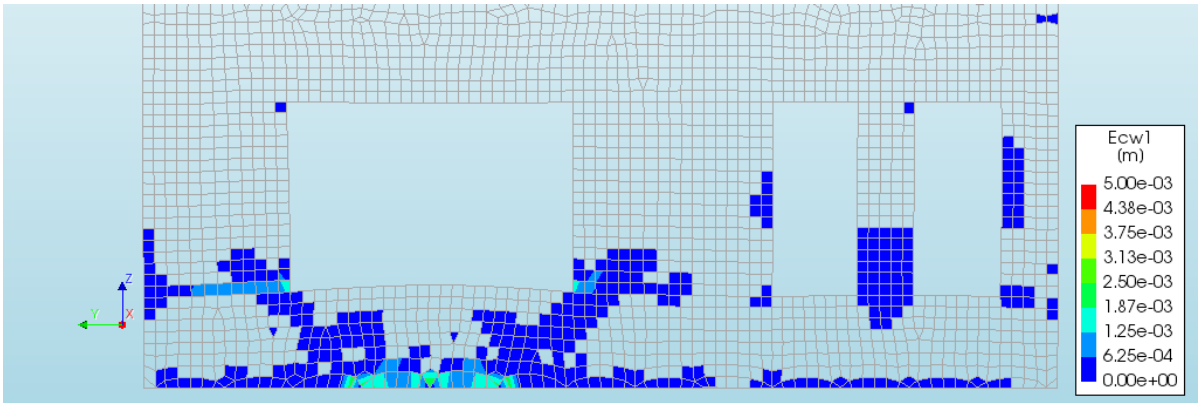


Figure 219 - Crack widths of the Cavity Wall Masonry House with Door, Windows and Inner Walls due to the static load, 2.0 m, front view layer 1

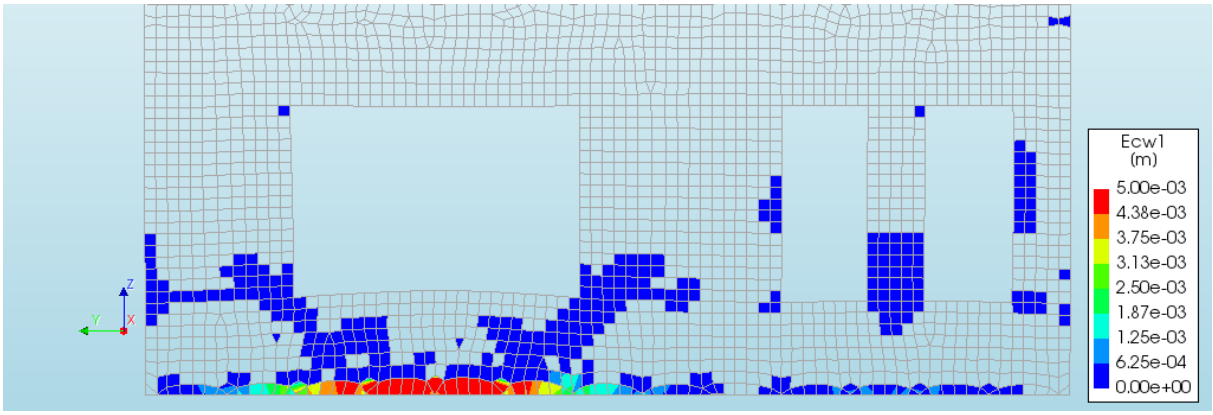


Figure 220 - Crack widths of the Cavity Wall Masonry House with Door, Windows and Inner Walls due to the static load, 2.0 m, front view layer 7

Figure 221 and Figure 222 show the inaccuracy around the large window, with cracks in all directions. However, near the wall section between the two small windows, the crack at the bottom, middle and top are clearly visible. Combined with the magnitude of the displacements, these indicate collapse of this wall section.

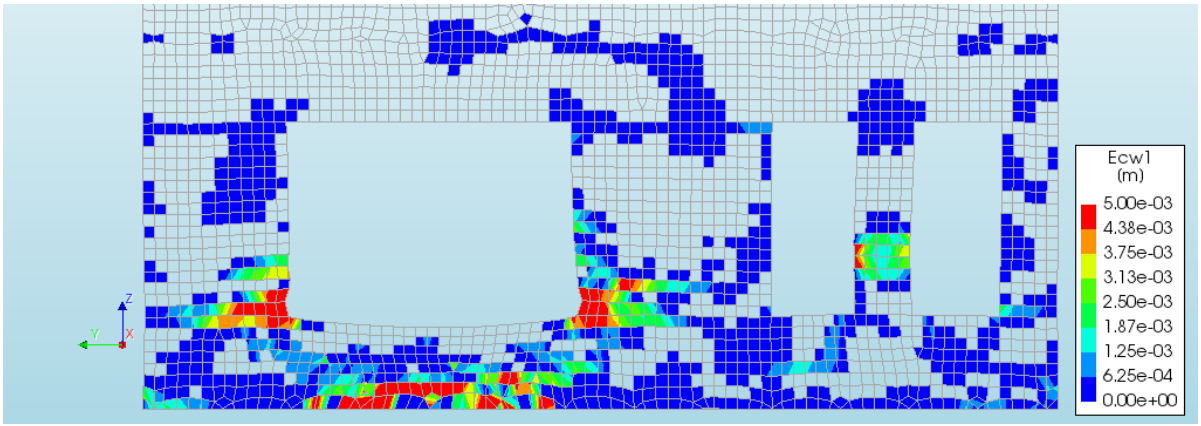


Figure 221 - Crack widths of the Cavity Wall Masonry House with Door, Windows and Inner Walls due to the static load, 3.4 m, front view layer 1

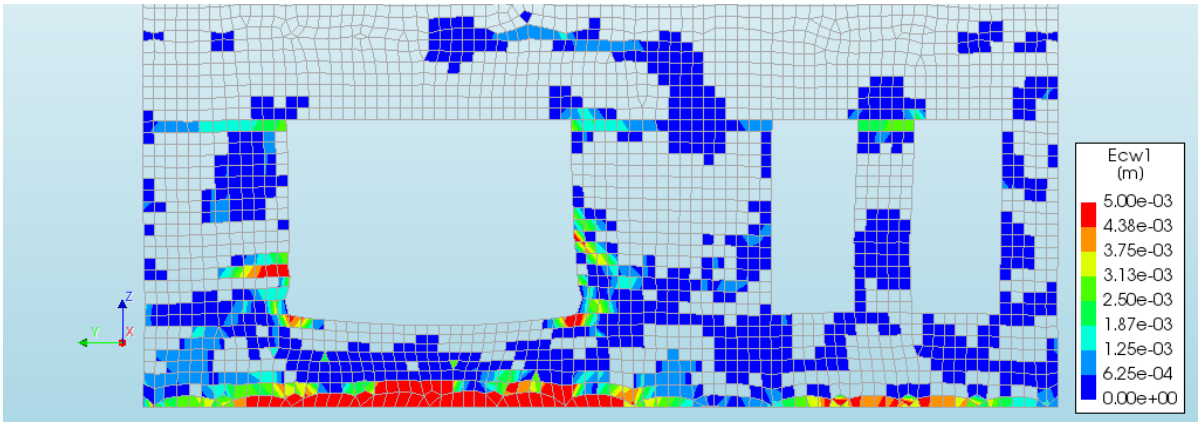


Figure 222 - Crack widths of the Cavity Wall Masonry House with Door, Windows and Inner Walls due to the static load, 3.4 m, front view layer 7

### DYNAMIC

Again, the model is loaded with the dynamic load until failure. The error of the final 'Almost Converged' step is 0.034, which makes those results still fairly accurate. The next step has an error of 0.238, which makes it much less trustworthy. The actual maximum load is therefore somewhat difficult to determine, it is expected to be between 2.0-2.5% of the total dynamic load. This makes it weaker than the case with just the inner walls, but stronger than both the other cases.

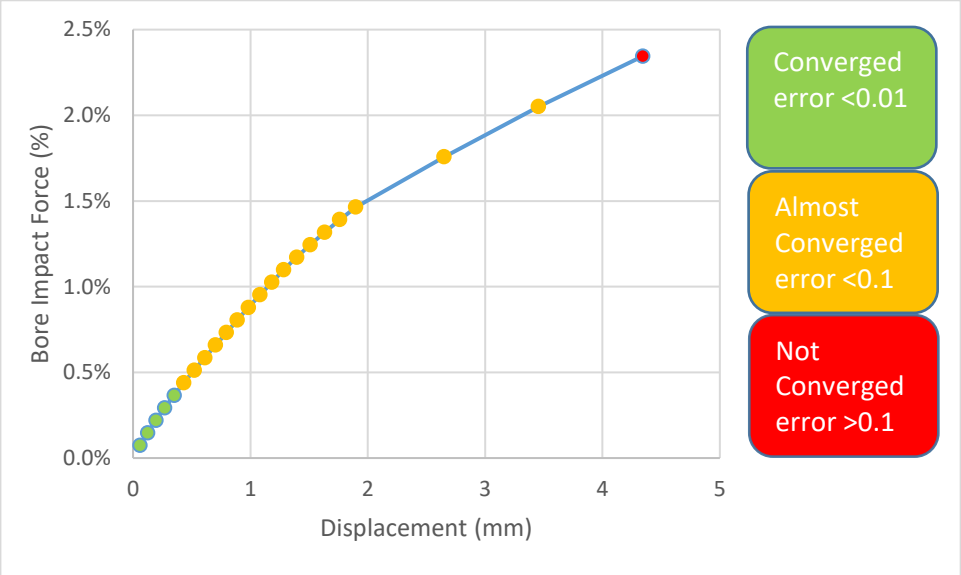


Figure 223 - Bore Impact Force vs Displacement of the Cavity Wall Masonry House with Door, Windows and Inner Walls due to the dynamic load

The displacement fields of Figure 224 and Figure 225 are, as expected, similar to the inner walls dynamic case. However, there is a large window now at the location where the largest displacements previously were. The maximum displacement is thus at the edge of this large window.

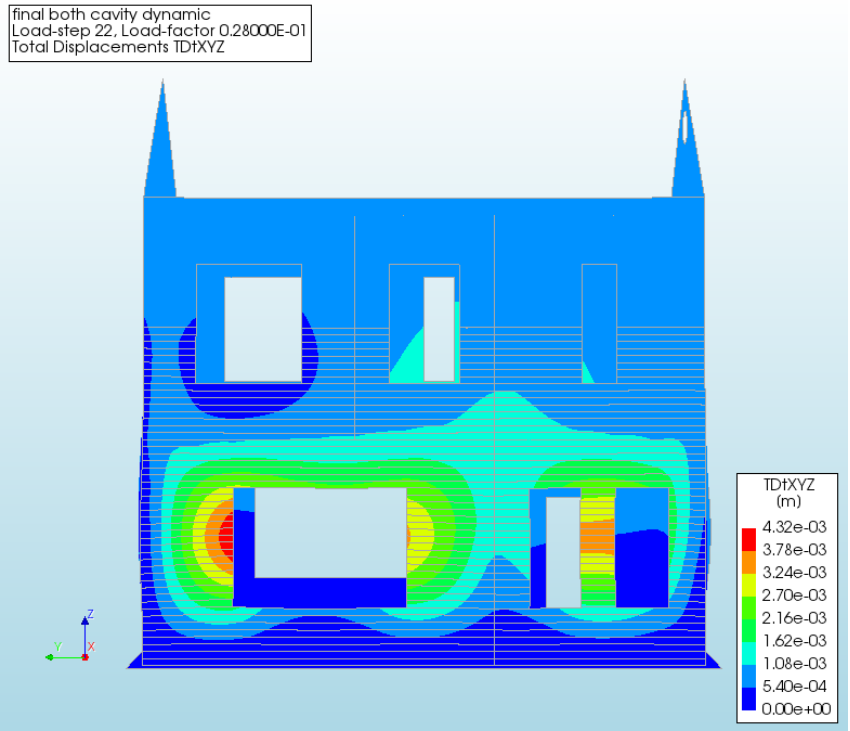


Figure 224 - Displacement of the Cavity Wall Masonry House with Door, Windows and Inner Walls due to the dynamic load, at 2.05%, front view

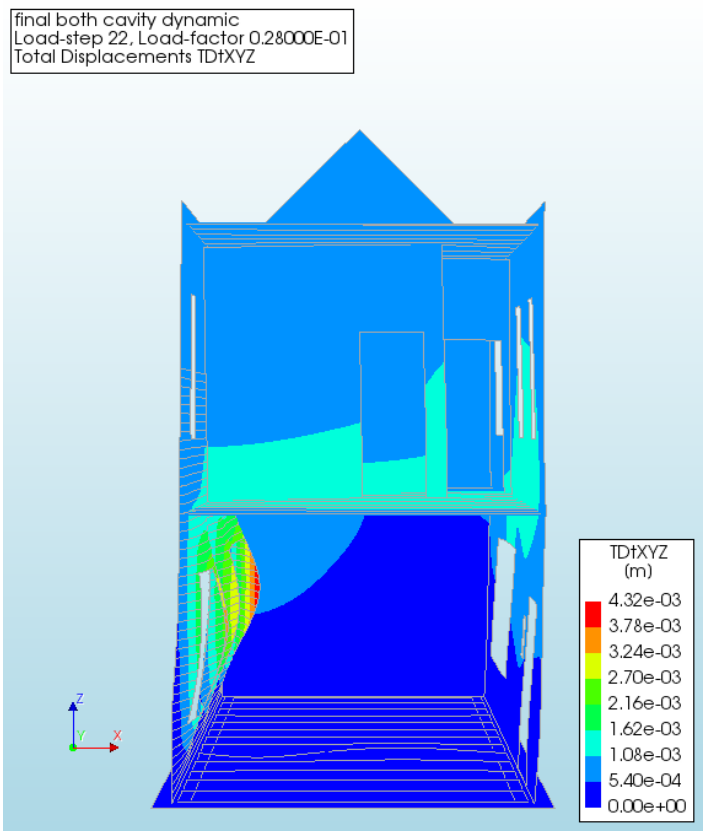


Figure 225 - Displacement of the Cavity Wall Masonry House with Door, Windows and Inner Walls due to the dynamic load, at 2.05%, side view (without the ground floor inner wall)

The cracking patterns and widths also follow the expectations. On the outside at the bottom and near the top of the ground floor, cracks of several tenth of a millimetre. On the inside cracks in the middle of the wall at the edges of the windows.

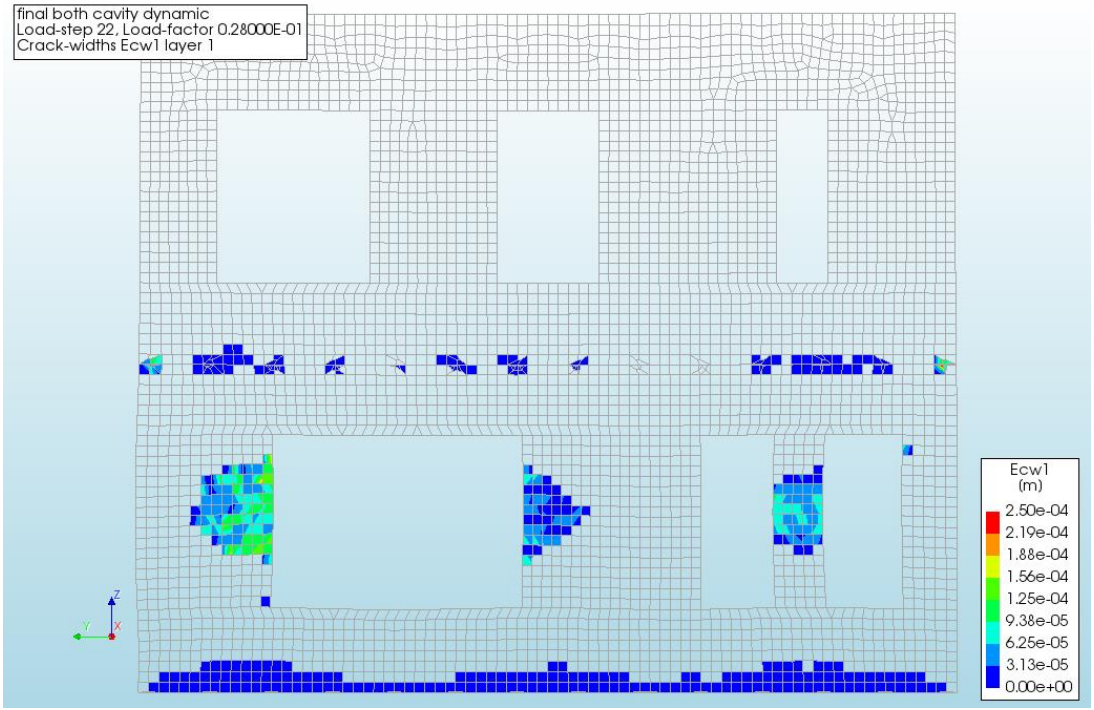


Figure 226 - Crack widths of the Cavity Wall Masonry House with Door, Windows and Inner Walls due to the dynamic load, at 2.05%, front view layer 1

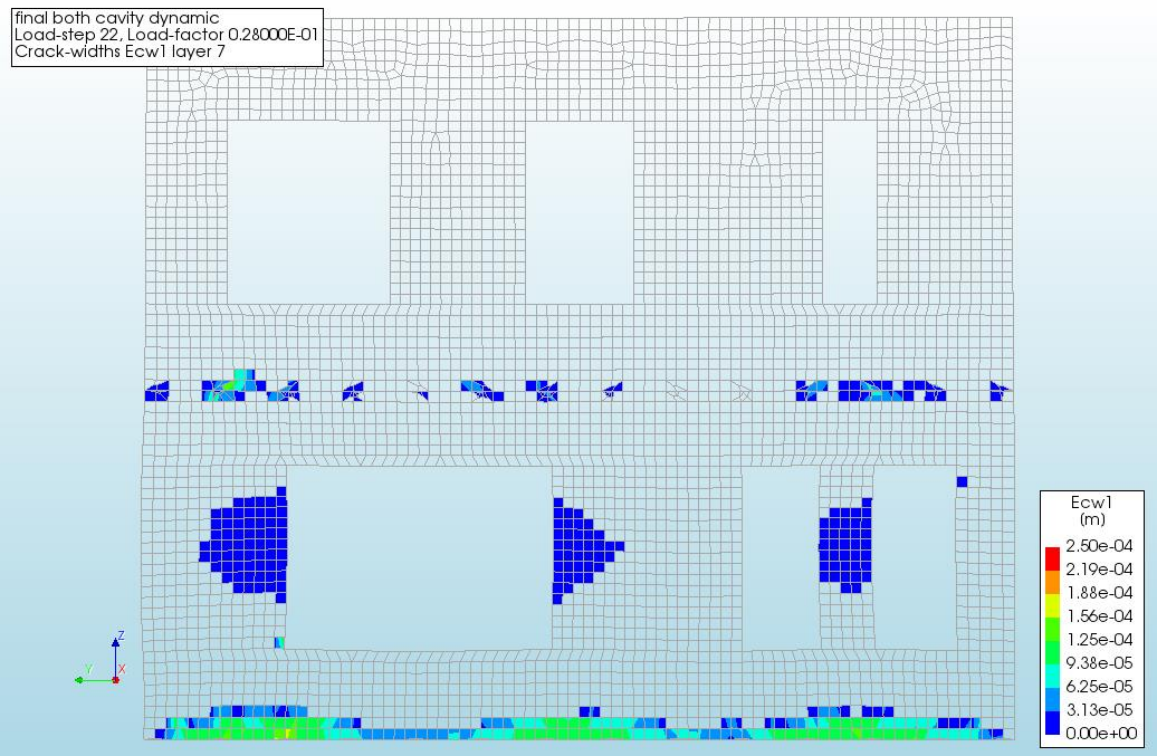


Figure 227 - Crack widths of the Cavity Wall Masonry House with Door, Windows and Inner Walls due to the dynamic load, at 2.05%, front view layer 7

## CONCLUSIONS

Four different cases have been investigated for the dynamic and static load. Each case added some complexity and realism to the original model, windows, door and inner walls. These changes also caused differences in the results.

Table 32 - Summary of the estimated failure loads of the Cavity Wall Masonry House

| | Failure load static (m) | Failure load dynamic (%) |
|---|---|---|
| **Original** | 2.0-2.5 | 1.8-2.0 |
| **Door and Windows** | 2.35-2.85 | 1.5-1.6 |
| **Inner Walls** | 2.4-2.6 | 2.25-2.75 |
| **Door, Windows and Inner Walls** | 3.2-3.6 | 2.0-2.5 |

Table 32 shows for the static load that each extra element raises the failure load, increases the accuracy or does both. Especially the combination of door, windows and inner walls increases the failure load tremendously.

For the dynamic load this is not the case, the introduction of door and windows causes a decrease of the failure load. The inner walls do cause a significant increase of the failure load but decrease the accuracy. Combining both, an increase of the failure load compared to the original case is observed at the cost of accuracy.

These results seem partially contradictory, an increase in one case is coupled with a decrease in another and vice versa. Where the door and windows caused a decrease in the maximum load for the dynamic load, there was an increase for the static load. The inner walls caused an increase in the maximum load for both loads. However, for the static load, the increase is only marginal, whereas for the dynamic load the increase is 20-40%. The combined case, door, windows and inner walls caused

an increase with regard to the starting case, no door, windows and inner walls, for both loads. For the dynamic load however, there was a decrease with regard to just the inner walls.

The most logical conclusion for these phenomena, is the height at which the loads act on the house. The door and especially the windows are located at the same height as the maximum dynamic load. The maximum static load however is at the bottom of the wall, and therefore is less affected by these door and windows. The inner walls have a larger effect on the dynamic load for the same reason.

# Appendix J. Diana Calculations of a Masonry House with a Single Solid Wall, Extended

As mentioned in chapter 10, the DIANA calculations have been split into 2 main groups. The first group is the calculations regarding a masonry house with a cavity wall, those are treated in chapter 10. The second group regards the calculations of a masonry house with a single wall, treated in this chapter.

Next the calculation will increase in detail, first only the foundation, outer walls and floors are modelled. One by one, extra details will be added, door and windows, inner walls and a combination of both.

In order to preserve the accuracy of the figures the legend is not the same for all displacements and crack widths. Patterns would otherwise not be visible, therefore keep an eye on the legend when comparing figures. Furthermore only 1 wall is displayed in the figures to keep the results as clear and readable as possible. If not stated otherwise the displacement at a certain point is the maximum displacement of the wall. The crack widths are displayed at two points, the inside of the wall, layer 1, and the outside of the wall, layer 7. Lastly, the error mentioned to indicate the trustworthiness of the results, is the relative displacement variation, of course, smaller is better.

## Masonry House

A variation on the simplest model, the masonry house with a single wall.

### Static

The single solid wall house has been loaded with a rising water level until it failed. The first cracks started at an inundation depth of approximately 2.0 m. This corresponds with the last green dot before the first orange dot in Figure 228. The last point of convergence is at an inundation depth of about 3.2 m. The load then still increases until approximately 3.6 m, where the convergence criteria is almost met, the error is 0.061. The wall is definitely cracked at this stage and therefore this point is used for the figures in this paragraph. The maximum deflection of the wall at 2.0 m, 3.2 m and 3.6 m inundation depth are respectively 0.65 mm, 1.78 mm and 4.69 mm. Failure of the wall is most likely to occur between an inundation depth of 4-5 m.

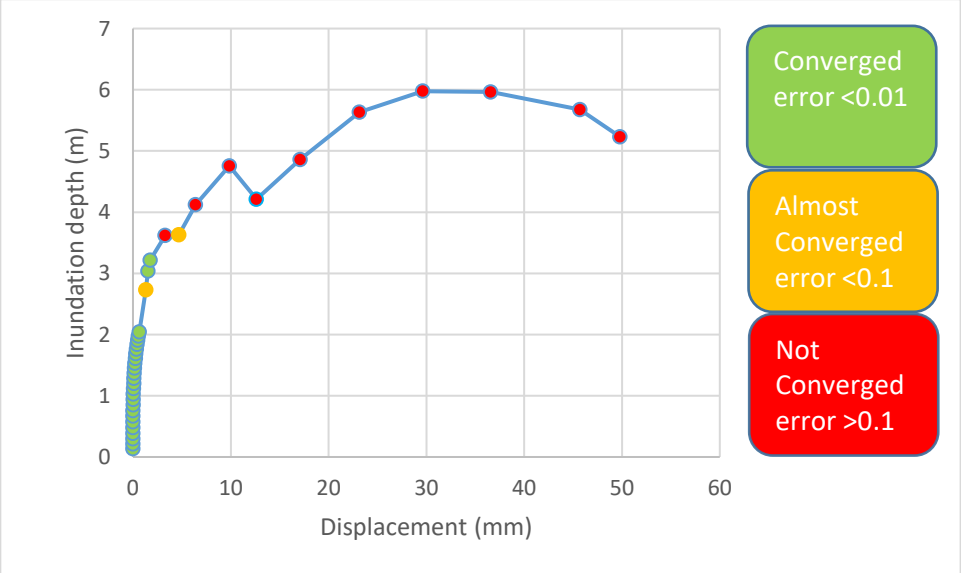


Figure 228 – Inundation depth vs Displacement of the Single Wall Masonry House due to the static load

Figure 229 and Figure 230 show the displacements of the house for all parts. The deflection of the floors is still high compared to the deflection of the walls, which is due to their self-weight and the relatively small deflection overall. Pattern wise they are nearly identical to Figure 175 and Figure 176.

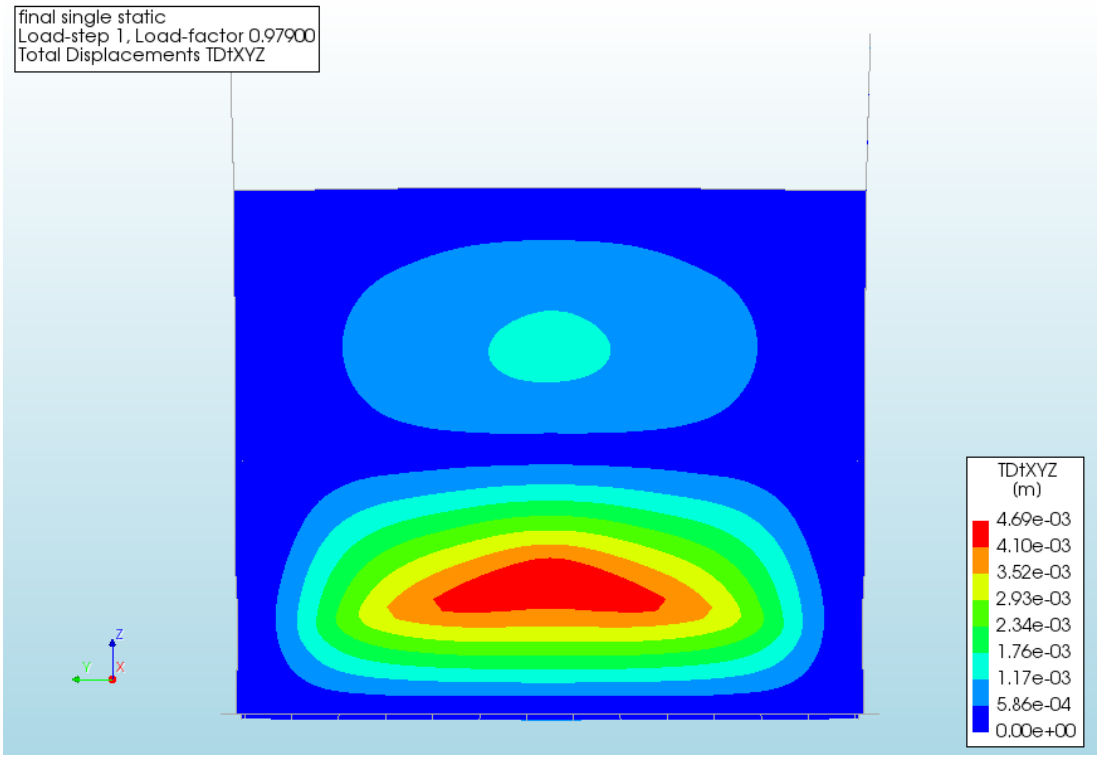


Figure 229 - Displacement of the Single Wall Masonry House due to the static load, 3.6 m, front view

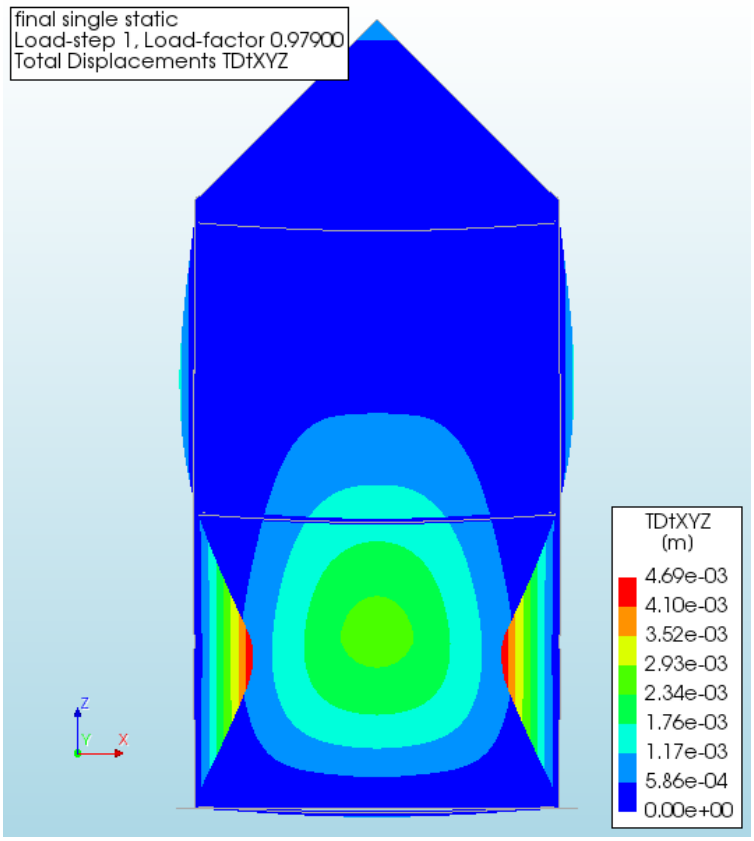


Figure 230 - Displacement of the Single Wall Masonry House due to the static load, 3.6 m, side view

Figure 231 shows the crack widths at the inside of the wall, here there are cracks at the middle of the wall which are up to several millimetre. Figure 232 shows the crack widths at the outside of the wall, the cracks here are located at the bottom and are also up to several millimetre. Notice that the upper part of the wall has also started to crack. This fits with the deflections seen in Figure 229 and Figure 230. These patterns are as expected and are nearly identical to Figure 177 and Figure 178.

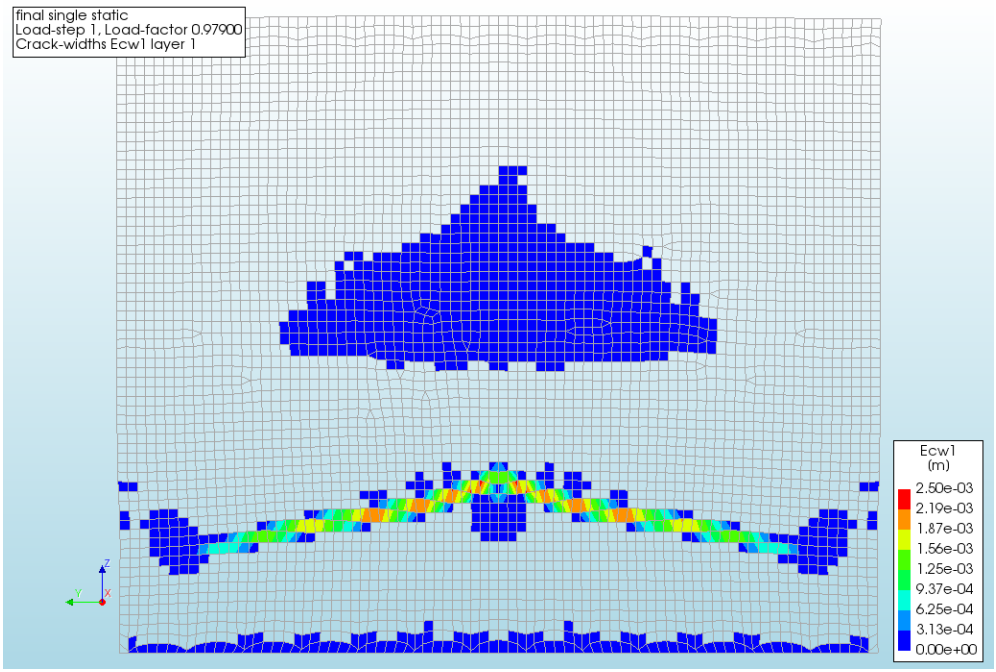


Figure 231 - Crack widths of the Single Wall Masonry House due to the static load, 3.6 m, front view layer 1

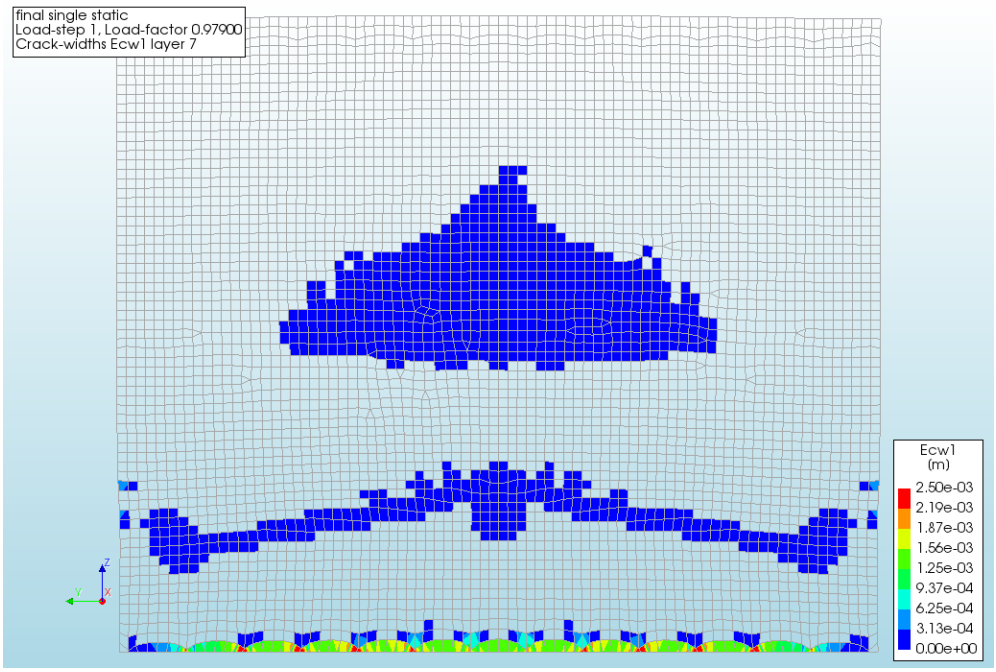


Figure 232 - Crack widths of the Single Wall Masonry House due to the static load, 3.6 m, front view layer 7

The cracking locations and relative sizes fit well with the expected results from the preliminary calculations from chapter 8. The largest moments where at the bottom, causing the first and largest cracks to be situated there. Next follows the middle of the wall since in the calculations performed here, the wall is not restricted by the first floor and is thus able to rotate decreasing the stresses, strains and thus crack widths at that location.

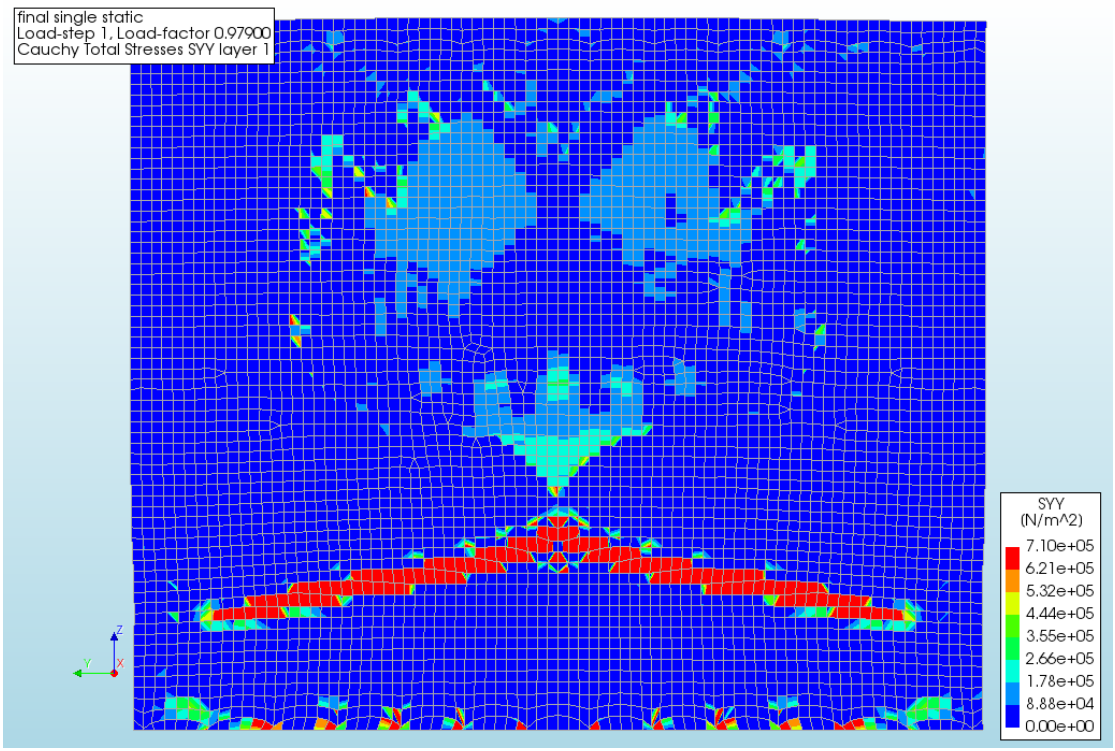


Figure 233 - Stress SYY of the Single Wall Masonry House due to the static load, 3.6 m, front view layer 1

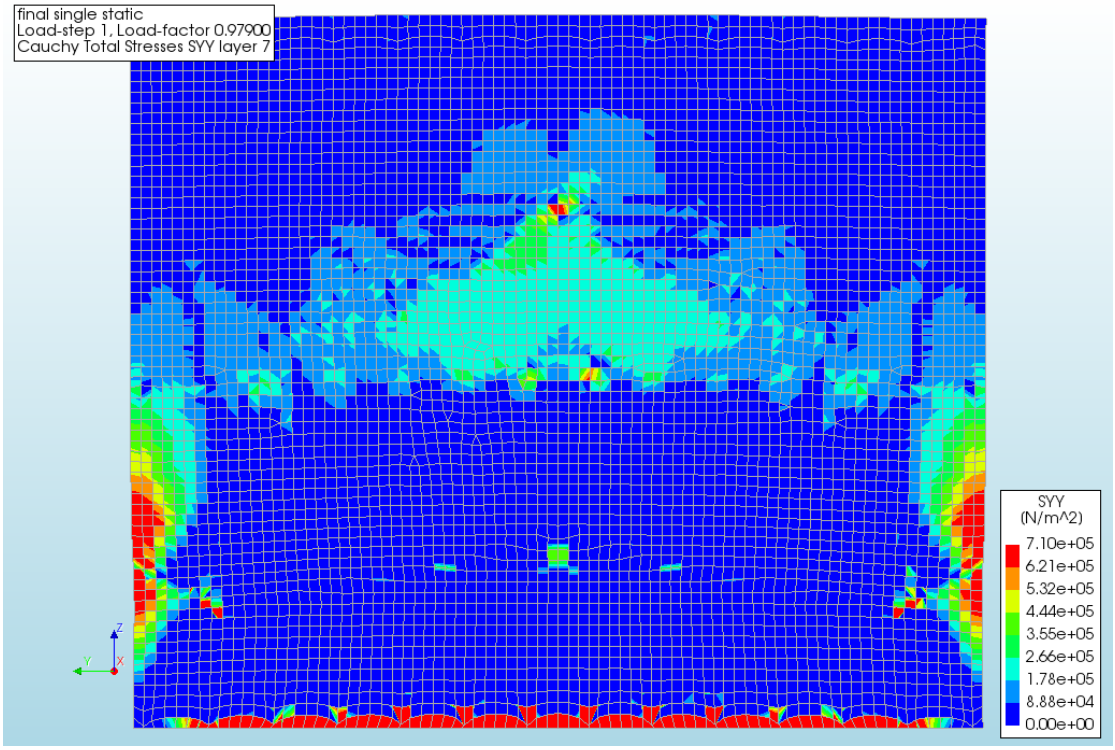


Figure 234 - Stress SYY of the Single Wall Masonry House due to the static load, 3.6 m, front view layer 7

In order to verify the crack widths, the stresses have been visualised for the YY and ZZ directions. The legends have been scaled as such that they match the tensile strength of the masonry, dark red therefore indicates (starting) cracks. The cracks at the inside, see Figure 231 match the stresses well, see Figure 233 and Figure 235. Notice the gap in Figure 235 caused by the cracks so no stresses can be transferred anymore. The same goes for the cracks at the outside, Figure 232, and the stress

there, Figure 234 and Figure 236. All stresses are nearly identical to their counterparts in the first cavity static case.

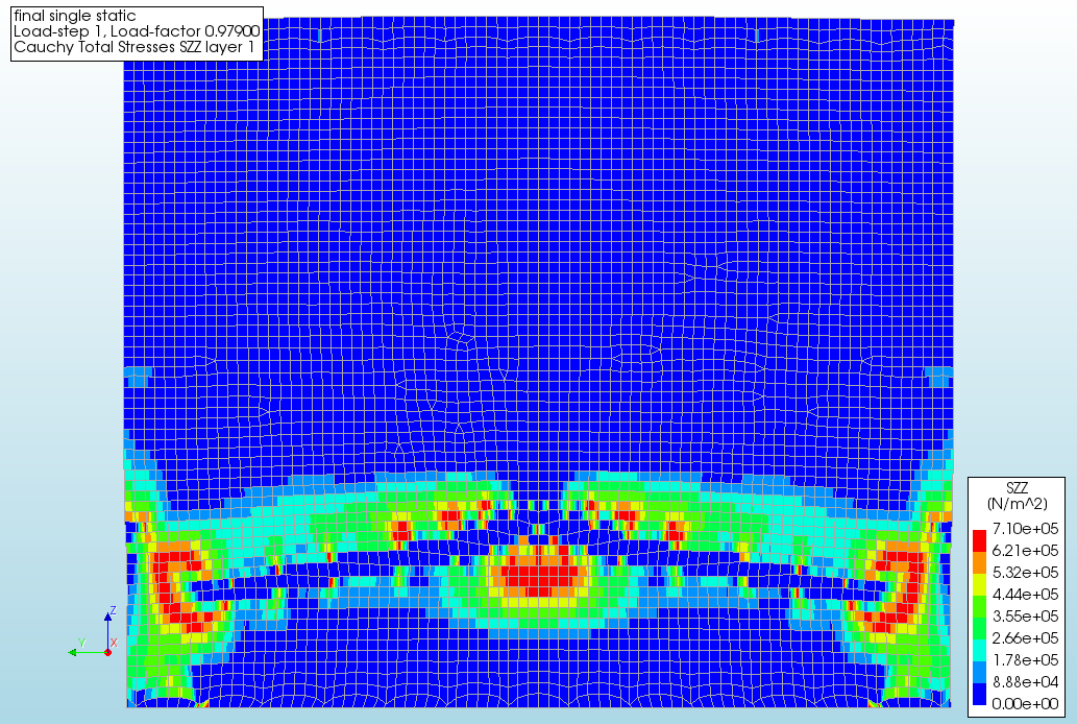


Figure 235 - Stress SZZ of the Single Wall Masonry House due to the static load, 3.6 m, front view layer 1

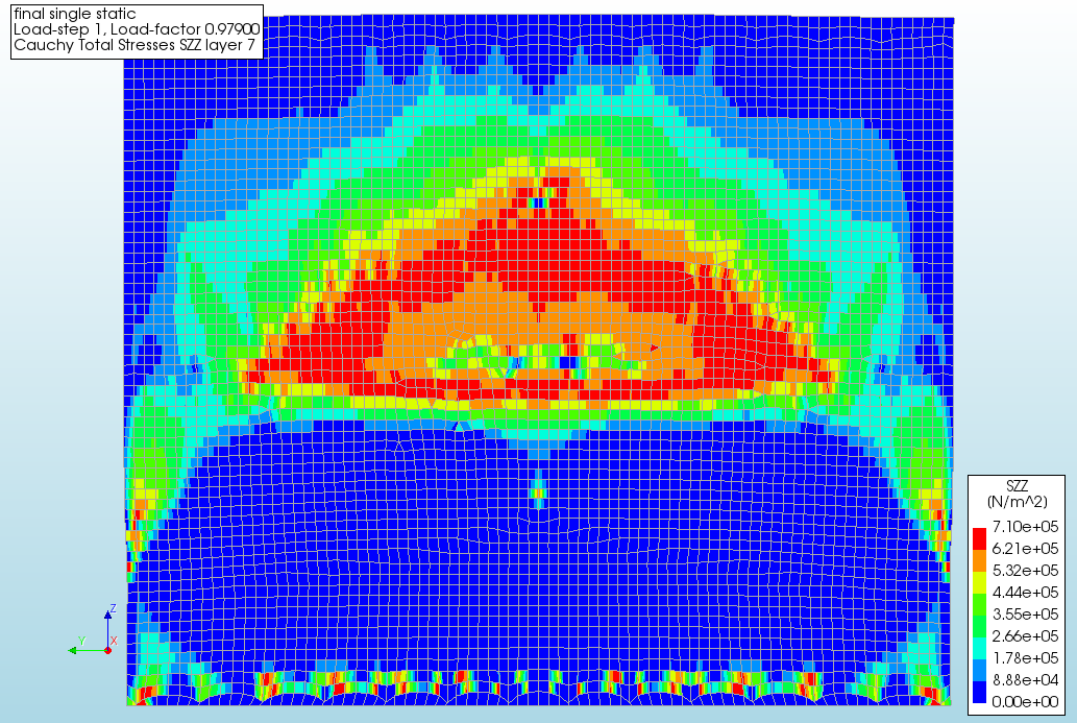


Figure 236 - Stress SZZ of the Single Wall Masonry House due to the static load, 3.6 m, front view layer 7

### Dynamic

The single wall masonry house has been loaded with the dynamic load case. As was the case for the first cavity dynamic case, convergence only occurred for a small part of the steps. Most of the following steps however were very close to the convergence criterion. The first 'Not Converged' step indicates the point where the first major cracks appear, at the bottom of the wall. The load then increases until not only the bottom of the ground floor wall crack, but also the middle and top. This happens at the second 'Not Converged' step, with an error of 0.102. Although the error is significant, the previous steps do support its credibility and displacement and cracking patterns are somewhat better visible in this step than in previous steps. Collapse has not yet occurred at this point, but is expected to have occurred at approximately 5.5-6% of the total dynamic load. Although this cannot be said certainly due to the increased model inaccuracies.

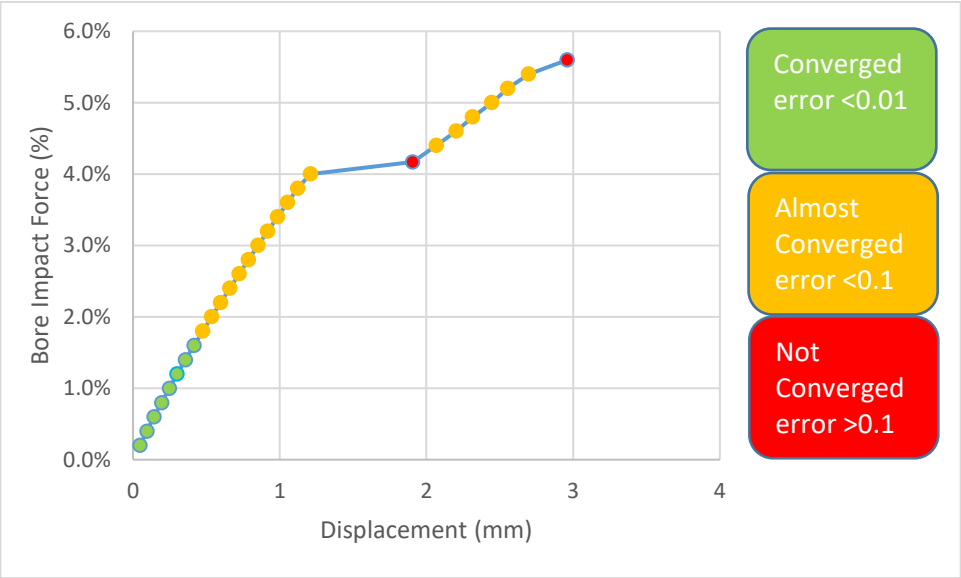


Figure 237 - Bore Impact Force vs Displacement of the Single Wall Masonry House due to the dynamic load

Figure 238 and Figure 239 show the displacement of the single wall masonry house at 5.6% of the dynamic load. These show still a large degree of cooperation between the front and back wall. With increased loading, patterns more like Figure 184 and Figure 185 are expected, where the front ground floor wall experiences the main displacements.

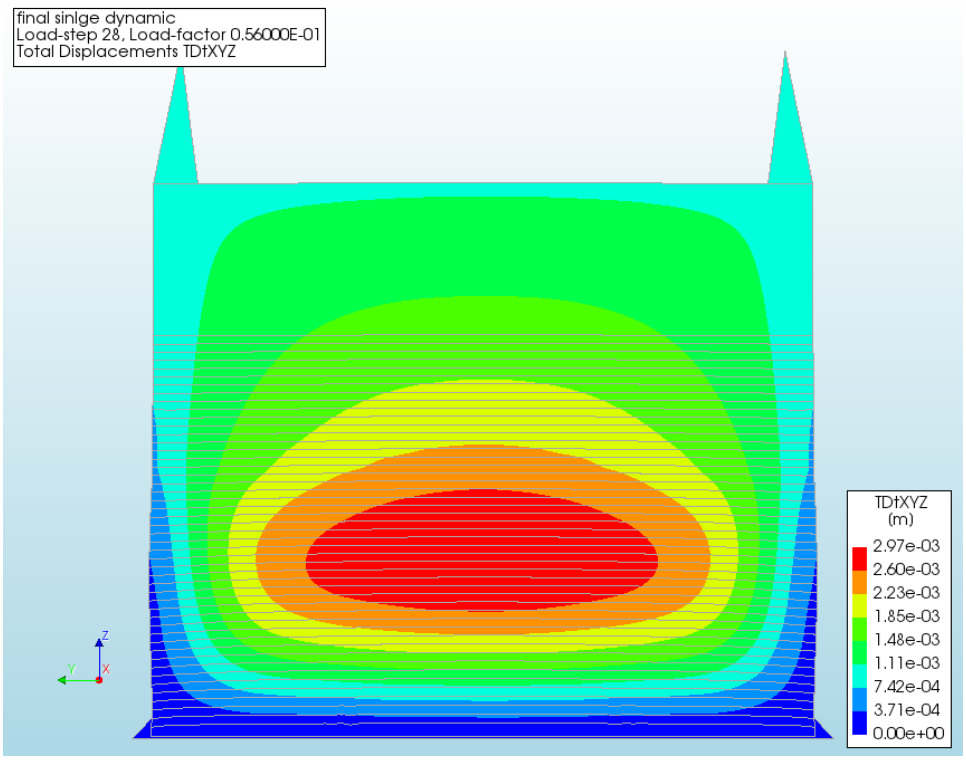


Figure 238 - Displacement of the Cavity Wall Masonry due to the dynamic load at 5.6%, front view

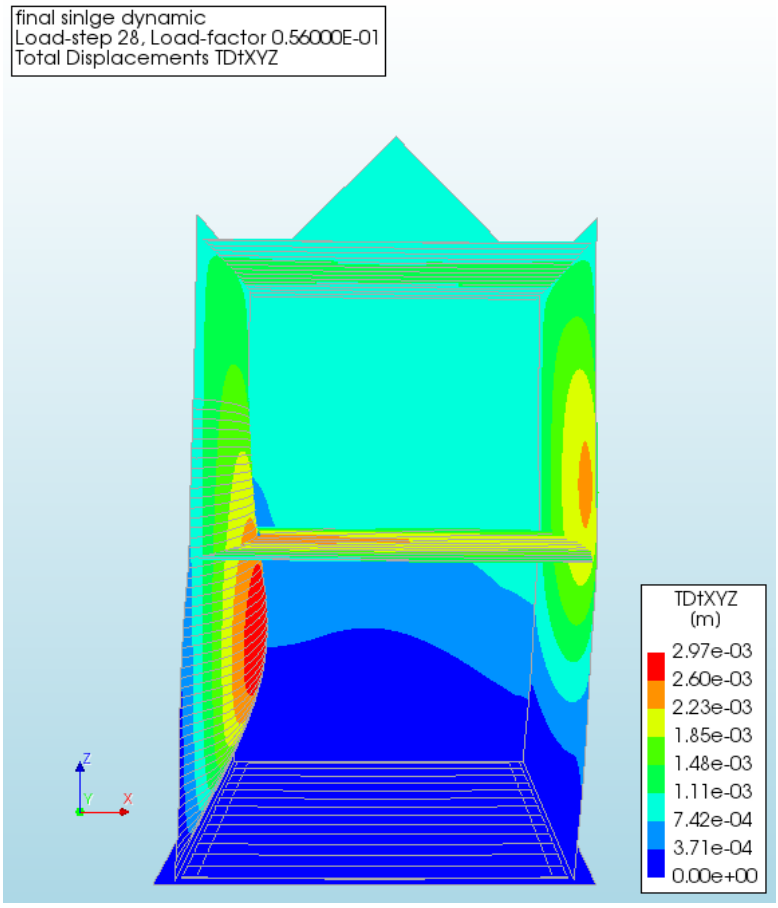


Figure 239 - Displacement of the Cavity Wall Masonry due to the dynamic load at 5.6%, side view

The patterns of the crack widths in Figure 240 and Figure 241 follow the expectations. However, there is still a distinct difference in the size of the crack widths. This fits with the wall not yet having completely cracked, the cracks at the bottom are still far larger than the crack at the middle of the ground floor wall. Cracks at the top of the ground floor wall are not yet present.

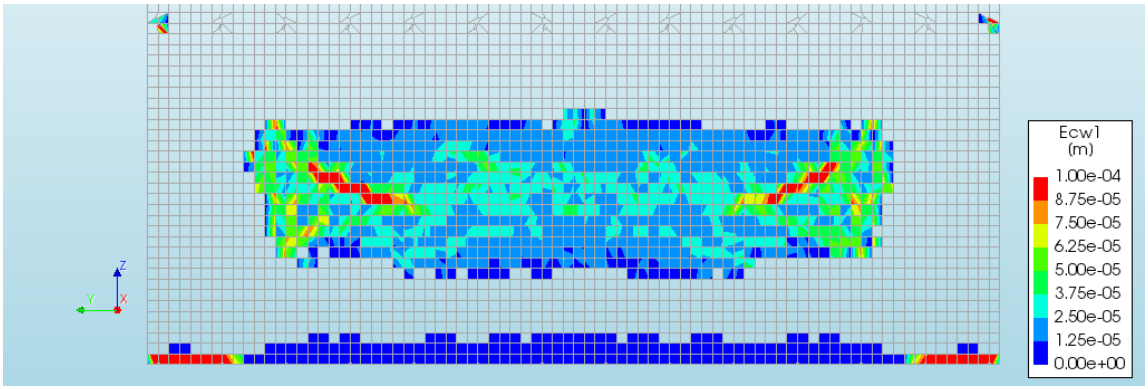


Figure 240 - Crack widths of the Cavity Wall Masonry due to the dynamic load at 5.6%, front view layer 1

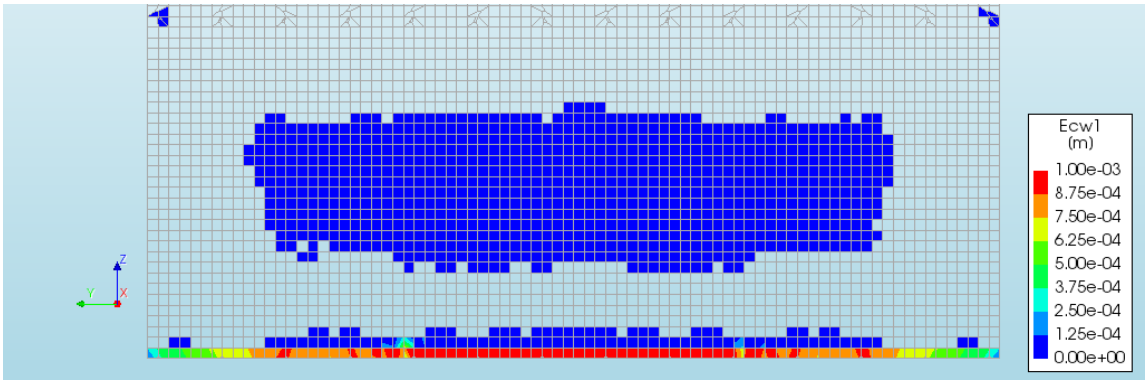


Figure 241 - Crack widths of the Cavity Wall Masonry due to the dynamic load at 5.6%, front view layer 7

The situation of the crack widths is supported by the stresses, the patterns match well, as was expected. The highest stresses are at the bottom and middle of the ground floor wall. The stresses near the top of the ground floor wall are not yet causing cracks, see the difference between Figure 191 and Figure 245.

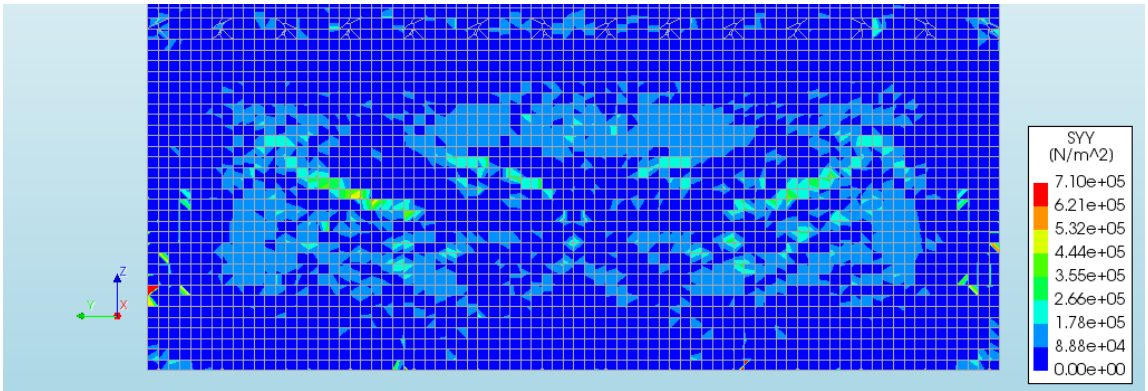


Figure 242 - Stress YY of the Cavity Wall Masonry due to the dynamic load at 5.6%, front view layer 1

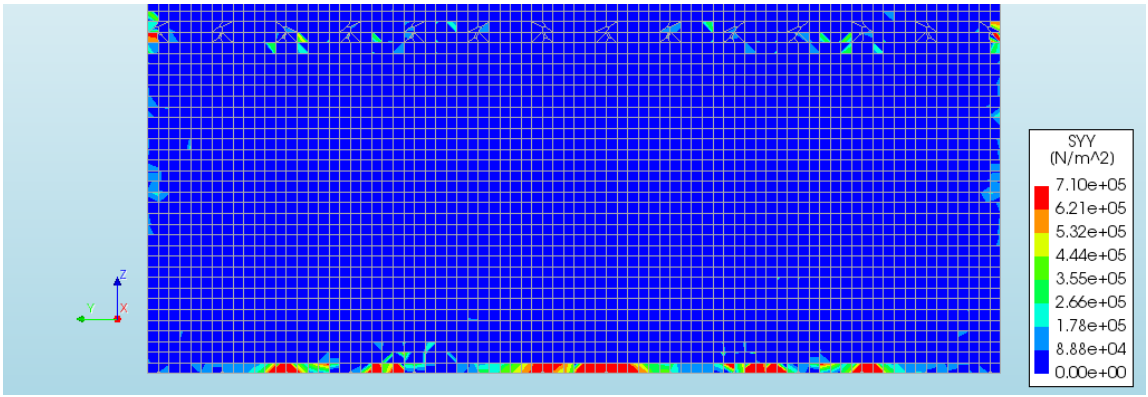


Figure 243 - Stress YY of the Cavity Wall Masonry due to the dynamic load at 5.6%, front view layer 7

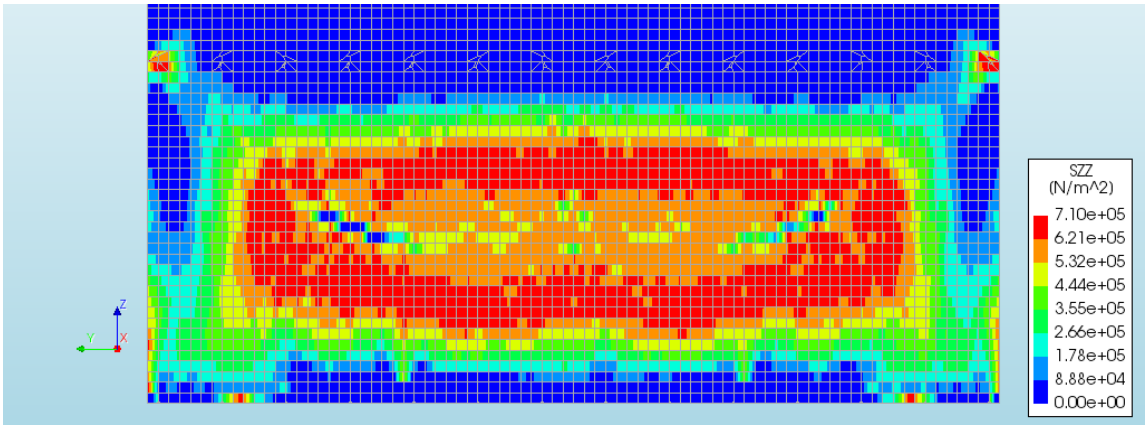


Figure 244 - Stress ZZ of the Cavity Wall Masonry due to the dynamic load at 5.6%, front view layer 1

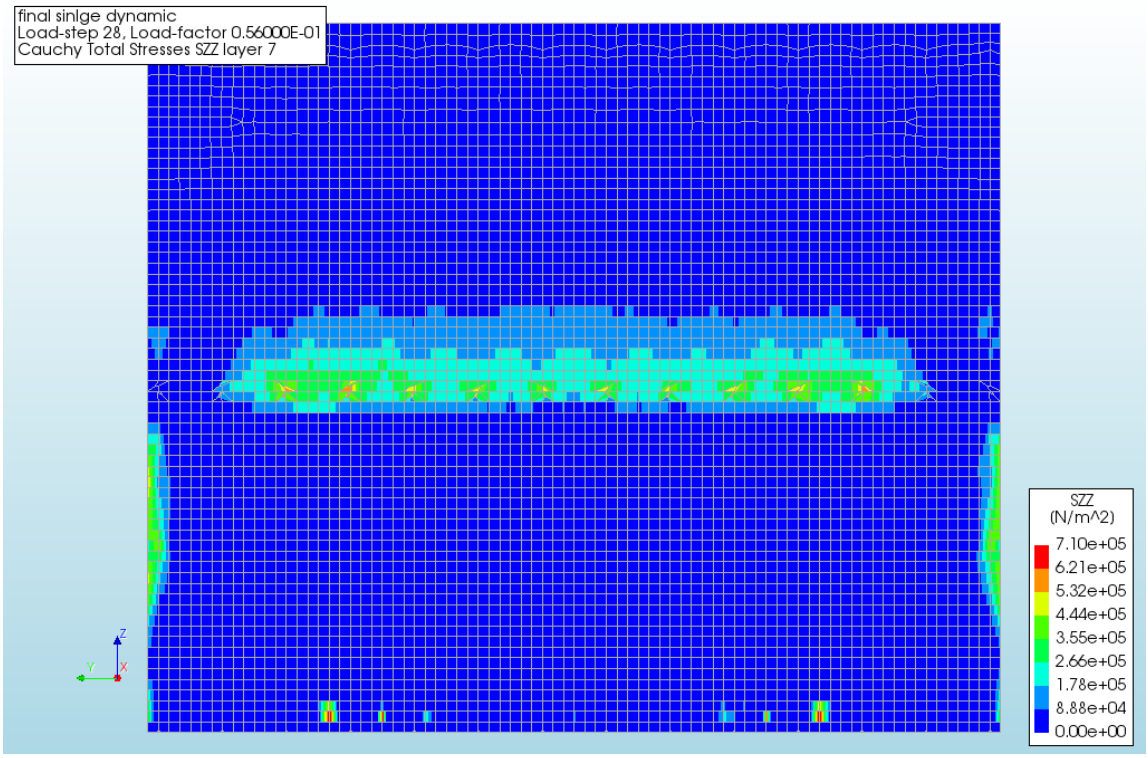


Figure 245 - Stress ZZ of the Cavity Wall Masonry due to the dynamic load at 5.6%, front view layer 7

## Masonry House with Door and Windows

Increasing the complexity and realism of the model a little, door and windows are added as holes in the walls. The removal of these section from the walls is expected to cause a decrease in the resistance, since smaller sections of the wall will have to carry the same load.

### Static

Loaded with a rising water level, see Figure 246, the single wall masonry house experiences the first damage at an inundation depth of approximately 2.5 m. The load then increases until collapse, which occurs between an inundation depth of 3.75-4.6 m. This large margin follows from the lack of accuracy in the results at those points. For the displacement and cracking patterns, the first point in this margin, the first 'Not Converged' step is used. This step has an error of 0.162, which makes it still somewhat accurate.

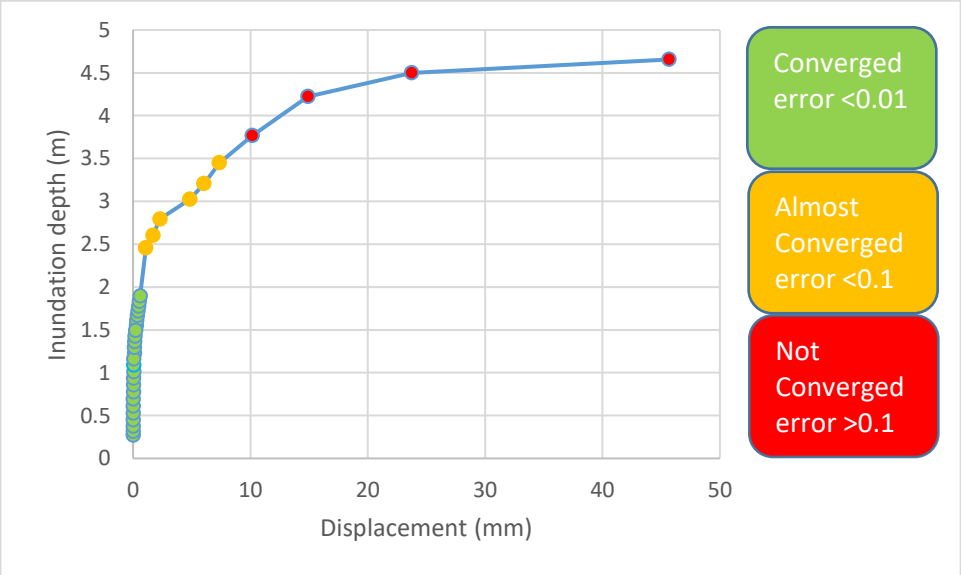


**Figure 246 - Inundation depth vs Displacement of the Single Wall Masonry House with Door and Windows due to the static load**

Figure 247 and Figure 248 show the displacements of the house. Contrary to the cavity wall, the largest displacements are now not located at the bottom of the largest window, see also Figure 193. This lack of local failure also partially explains the improved overall accuracy of the results from this model compared to the model from the cavity door and windows static case. For the increased inundation depths, the displacement patter remains similar, although the displacement of the first floor decreases, relatively. This fits with increased cracking near the top of the ground floor.

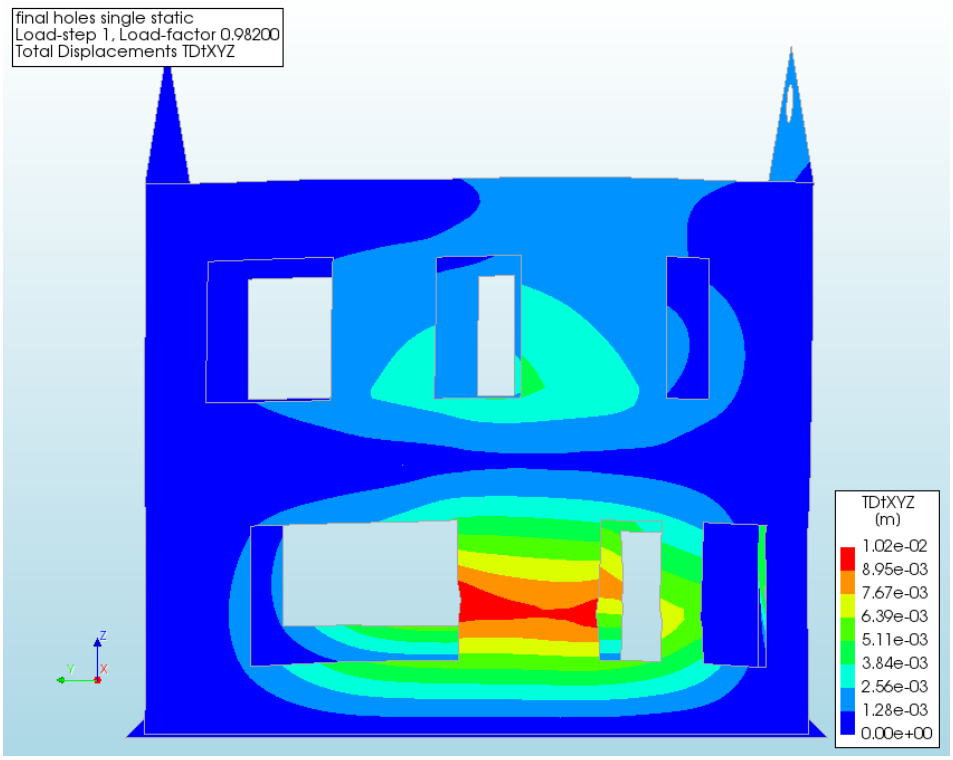


**Figure 247 - Displacement of the Single Wall Masonry House with Door and Windows due to the static load, 3.75 m, front view**

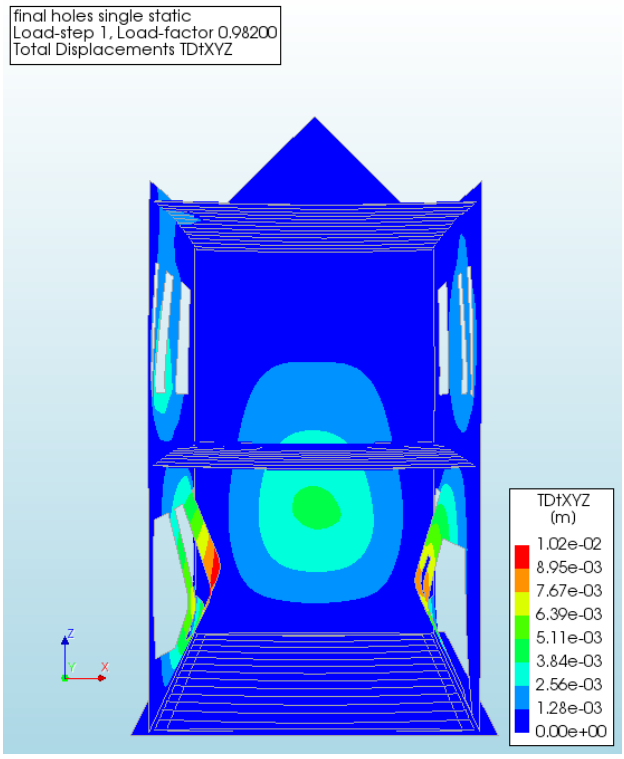


**Figure 248 - Displacement of the Single Wall Masonry House with Door and Windows due to the static load, 3.75 m, side view**

The cracking patterns from Figure 249 and Figure 250 differ from previous patterns due to the presence of significant crack widths at the first floor. This follows from the displacement of this first floor as a consequence of the ground floor displacement. As expected, the largest cracks are at the bottom of this ground floor, followed by the cracks in the middle and finally the cracks at the first

floor. As with the displacements, these first floor crack will decrease relatively as the cracks at the top of the ground floor appear. When this happens the ground floor starts to fail and so will the house as a whole.

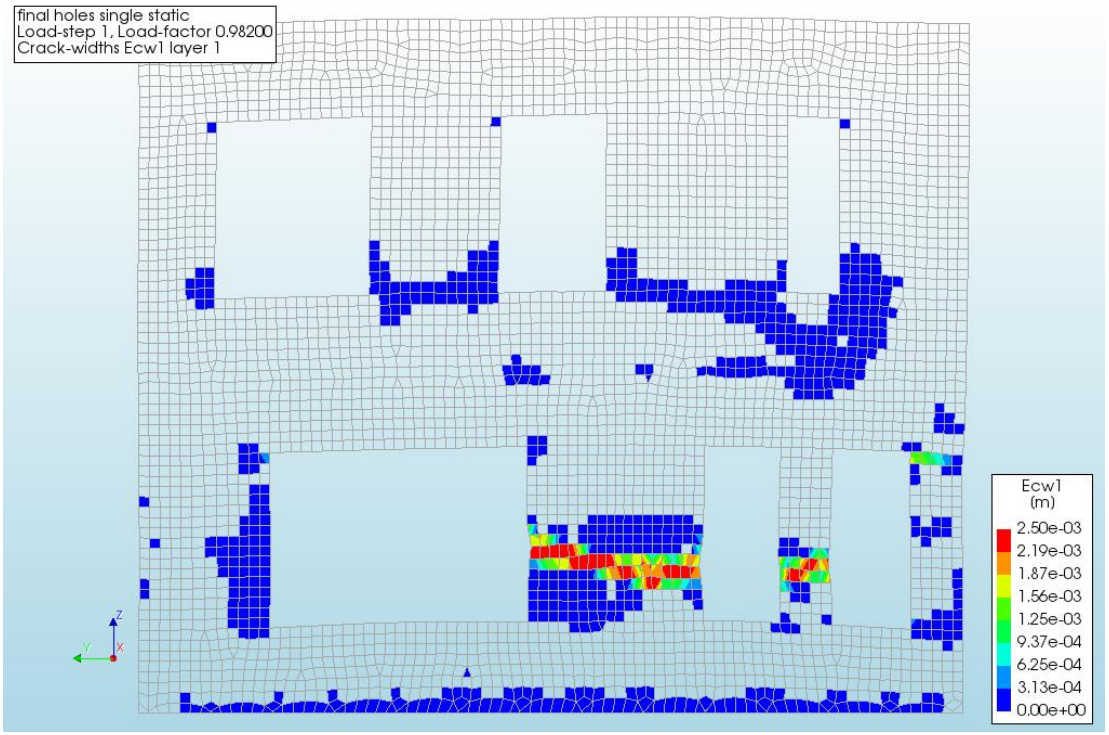


**Figure 249 - Crack widths of the Single Wall Masonry House with Door and Windows due to the static load, 3.75 m, front view layer 1**

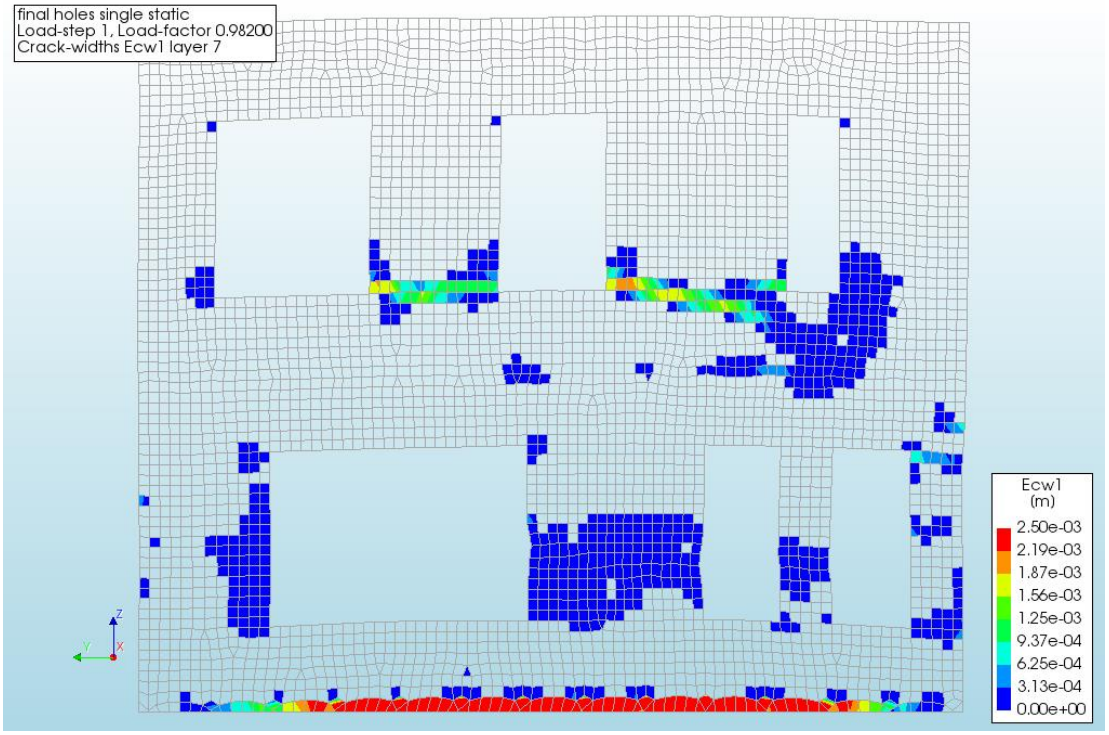


**Figure 250 - Crack widths of the Single Wall Masonry House with Door and Windows due to the static load, 3.75 m, front view layer 7**

## DYNAMIC

Loaded with the dynamic load, the displacement increased until failure occurred. The exact point of failure is difficult to determine as the last 'Almost Converged' step still has not fully cracked at any location. The cracking patterns and overall displacement pattern are already visible at this step, which has an error of 0.048. This makes these results still fairly accurate. With increased cracking the failure load will most likely be around 5.5-6%.

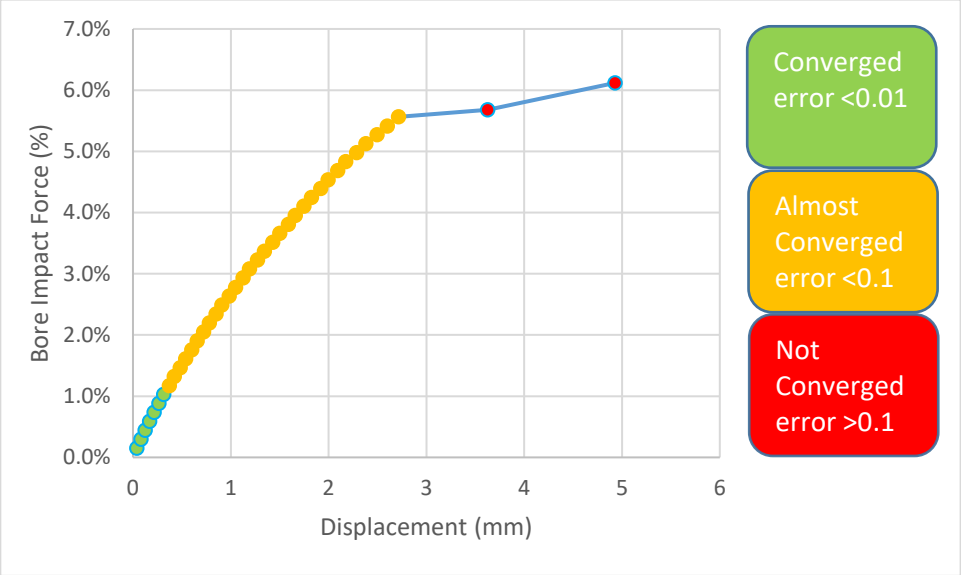


**Figure 251 - Bore Impact Force vs Displacement of the Single Wall Masonry House with Door and Windows due to the dynamic load**

Figure 252 and Figure 253 show the displacement field. As mentioned above, the wall has not yet fully cracked at any location. This is visible in the displacement pattern, which is still rather smooth, higher up on the wall and there is considerable cooperation between the front and back wall. With increased loading these will change, the displacement will have sharp bends at the crack location, be lower on the wall due to these crack areas and the back wall can provide less support relatively seen.

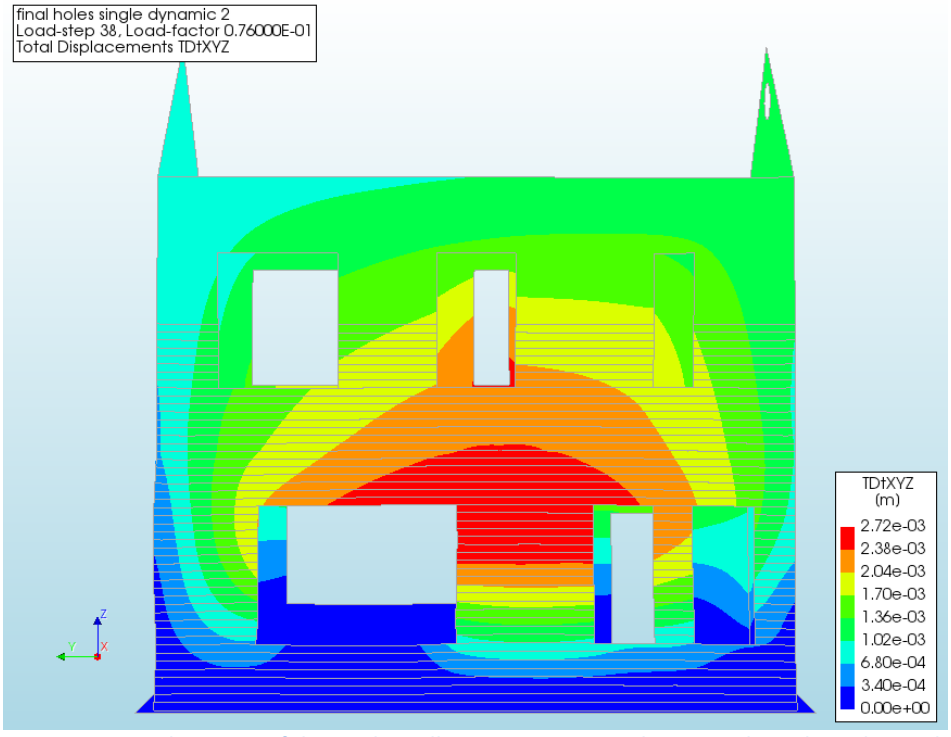


**Figure 252 - Displacement of the Single Wall Masonry House with Door and Windows due to the dynamic load at 5.56%, front view**

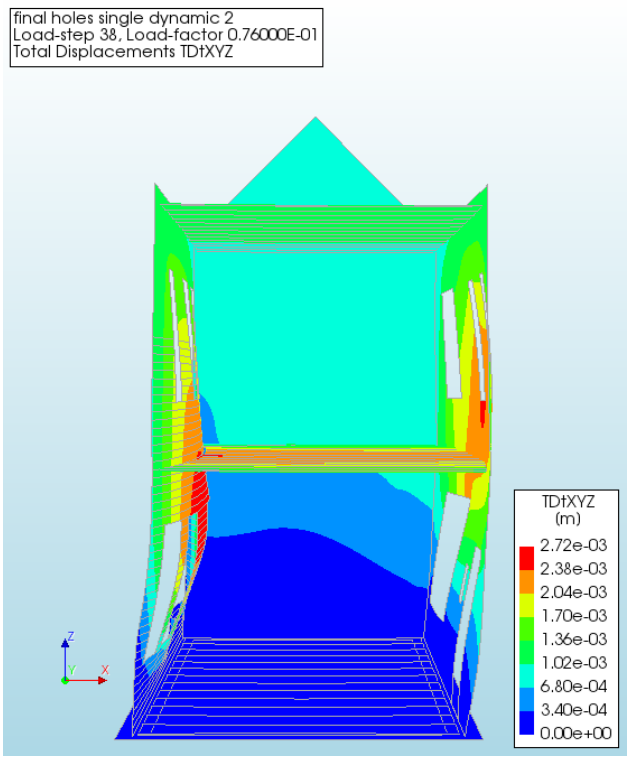


**Figure 253 - Displacement of the Single Wall Masonry House with Door and Windows due to the dynamic load at 5.56%, side view**

The crack widths in Figure 254 and Figure 255 show still relatively small cracks. Neither the bottom nor middle of the ground floor wall has yet fully cracked, whereas the top experiences no crack as of yet. The current cracking pattern is as expected, the main crack locations are in between the windows. This is similar to the cavity door and windows dynamic case but differs from the cavity door and windows static case, where the first major cracks and displacements where beneath the large window. The extra thickness of the single wall causes this section to carry the load without cracking and thus the normally expected pattern appears again.

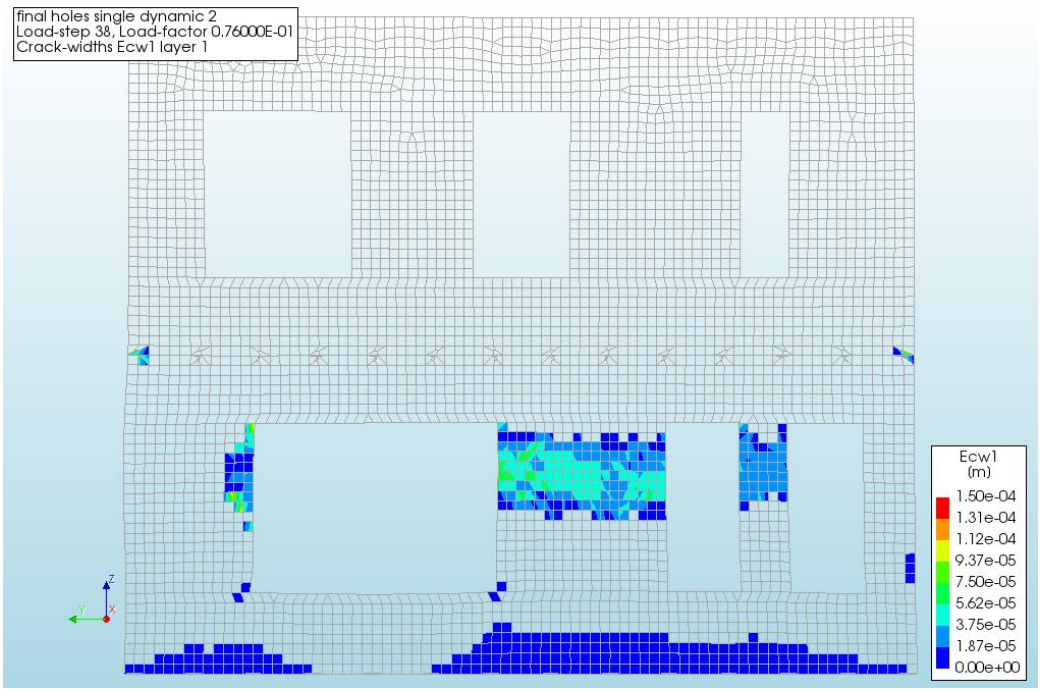


**Figure 254 - Crack widths of the Single Wall Masonry House with Door and Windows due to the dynamic load at 5.56%, front view layer 1**

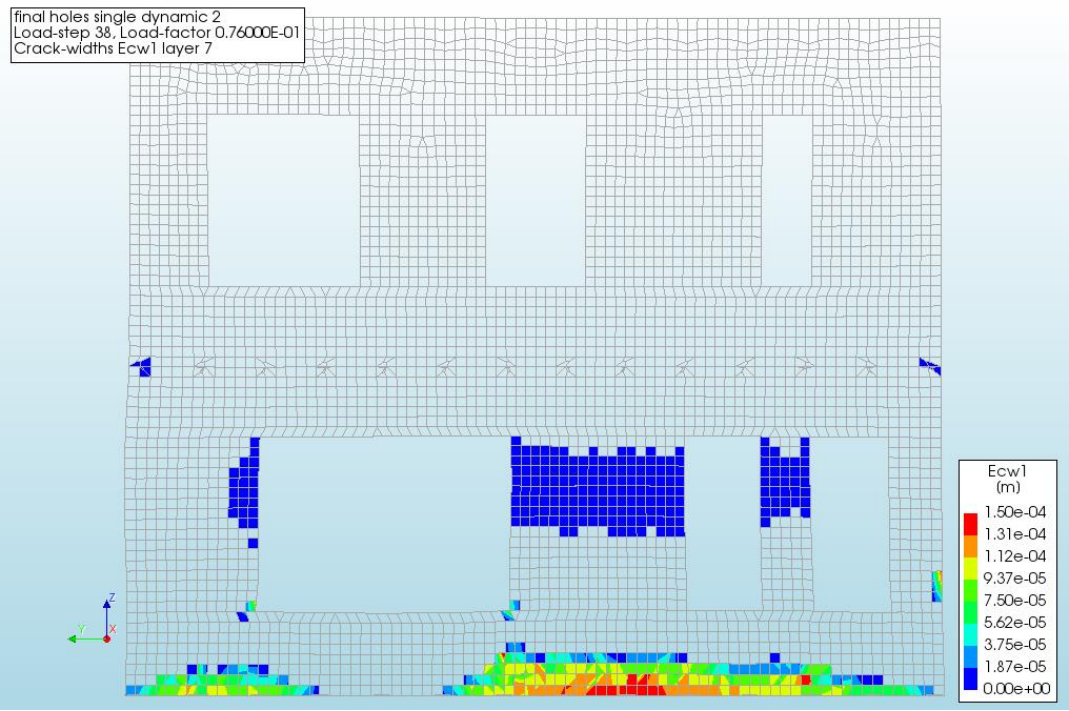


**Figure 255 - Crack widths of the Single Wall Masonry House with Door and Windows due to the dynamic load at 5.56%, front view layer 7**

## MASONRY HOUSE WITH INNER WALLS

Again, the complexity is increased, compared to the first, simple model, inner walls have been added. These should provide some out of plane support to the front walls and thus increase their resistance.

### STATIC

Being loaded with the rising water level, the first crack formed at an inundation depth of around 2.5 m. This fits with the transition from 'Converged' steps to 'Almost Converged' steps in Figure 256. The load then keeps increasing and water displacement and cracks start to occur. This starts at an inundation depth of approximately 3.85 m, which corresponds to the second 'Not Converged' step. This step has an error of 0.106, which makes it still somewhat trustworthy. This is partially confirmed by the rest of the load steps, although they are all 'Not Converged' they show a similar pattern. The failure load of this model is therefore estimated to be between an inundation depth of 4-5 m.

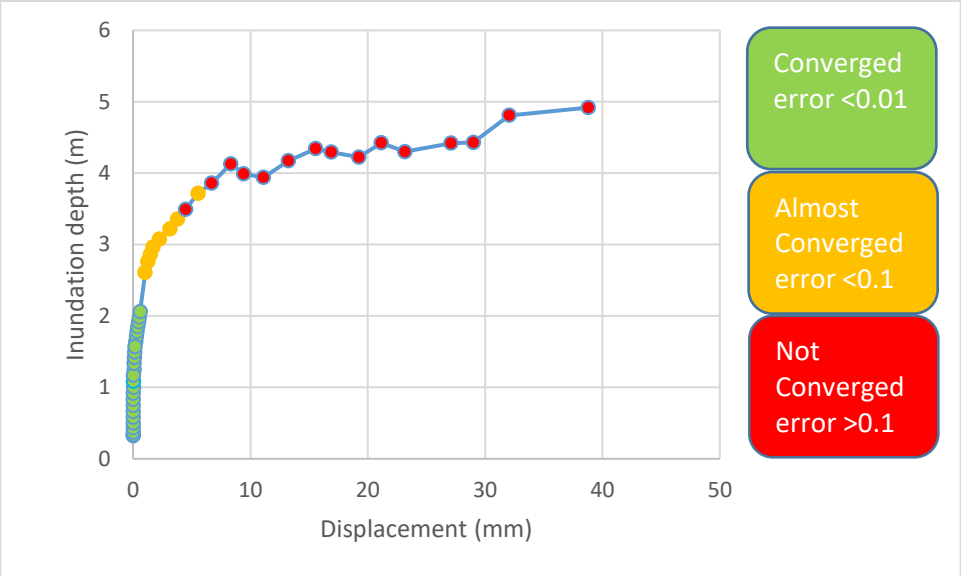


Figure 256 - Inundation depth vs Displacement of the Single Wall Masonry House with Inner Walls due to the static load

Figure 257 and Figure 258 show the displacements of the entire house. Notice the influence of the inner walls in redirecting displacements and preventing displacements. They displacement of the ground floor is caused by the inner wall at that location. This inner wall decreases the displacements of a part of the front wall, causing the inner wall itself to deform. That is a noticeable difference with the cavity inner walls static case where the inner wall seemed to divide to front wall into two distinct sections.

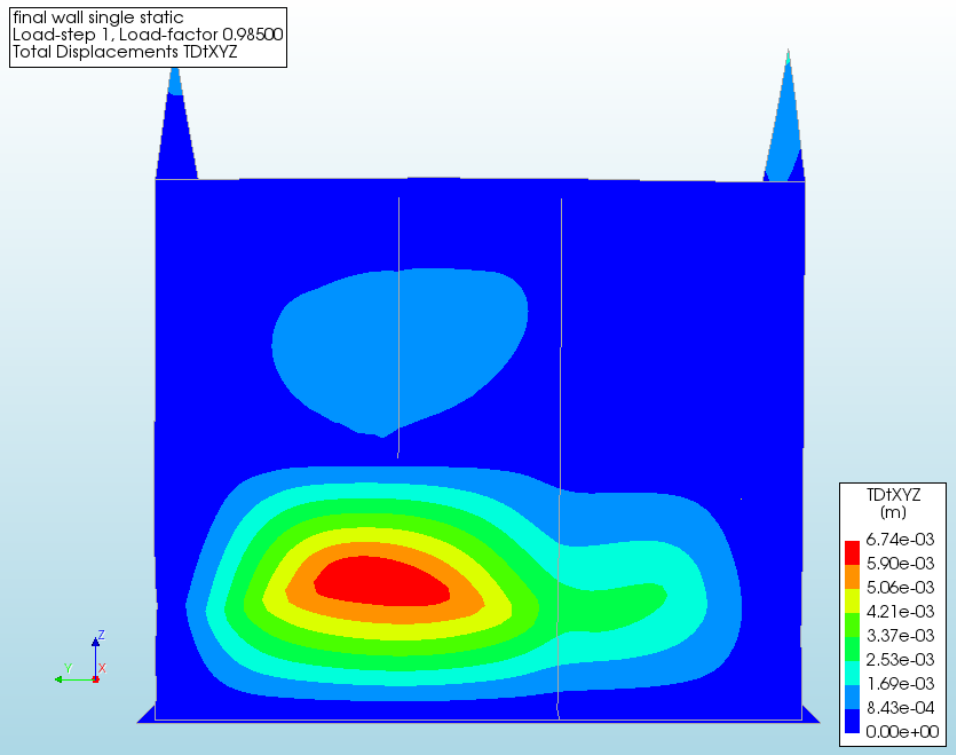


Figure 257 - Displacement of the Single Wall Masonry House with Inner Walls due to the static load, 3.85 m, front view

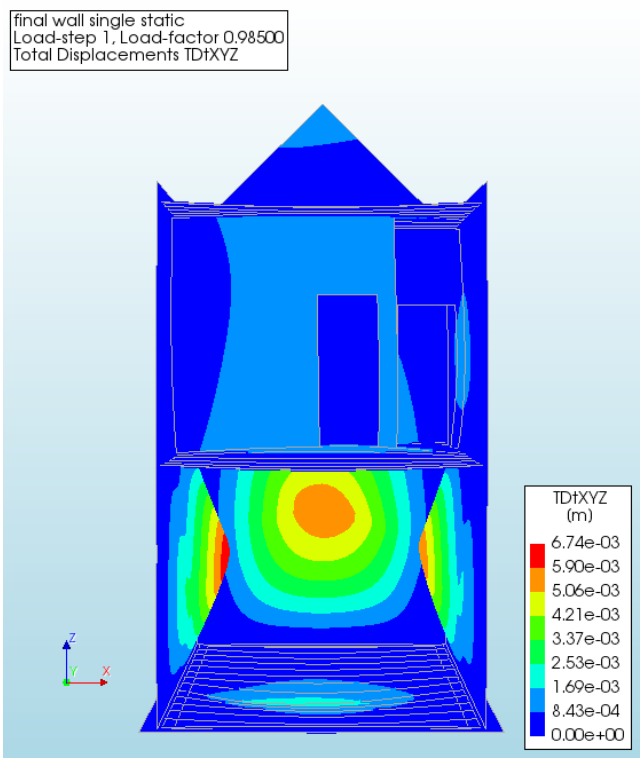


**Figure 258 - Displacement of the Single Wall Masonry House with Inner Walls due to the static load, 3.85 m, side view (without the ground floor inner wall)**

Figure 259 and Figure 260 show the crack widths and patterns. Although similar to those from the cavity inner walls static case, some differences are present. The main difference is the increased deformation of the right part of the wall also causes cracks to develop at those locations, especially at the middle of the ground floor wall. The rest of the cracks appears at the expected places, bottom, middle and top of the ground floor wall.

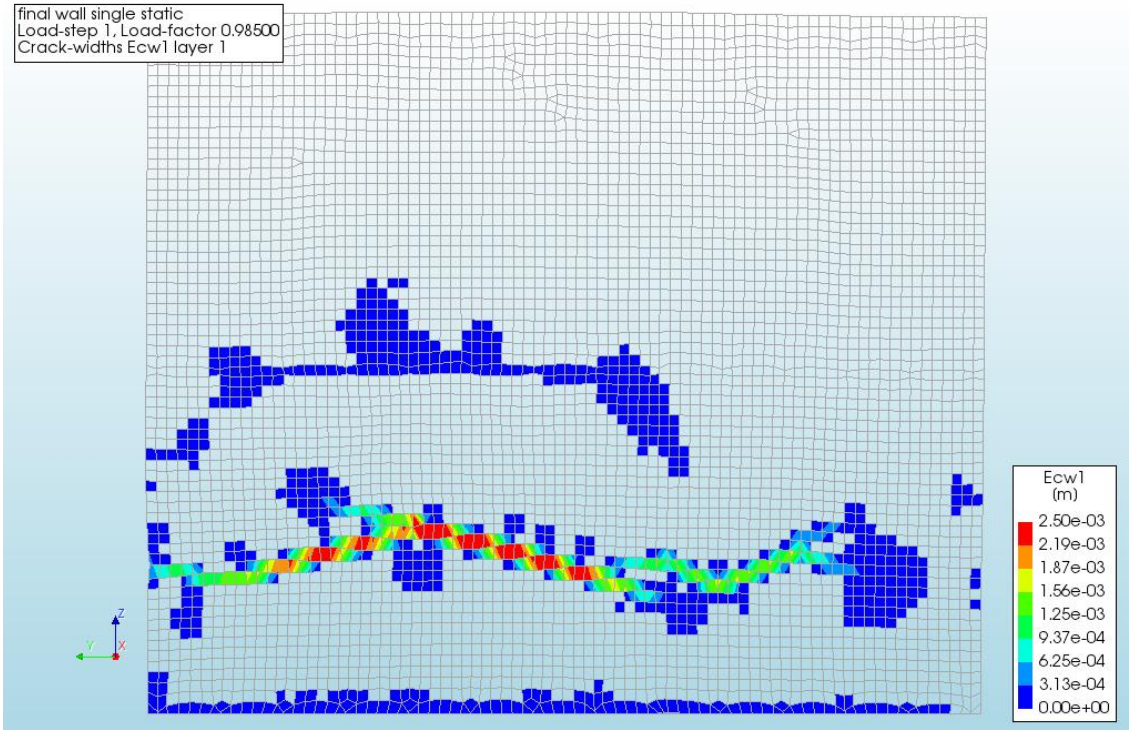


**Figure 259 - Crack widths of the Single Wall Masonry House with Inner Walls due to the static load, 3.85 m, front view layer 1**

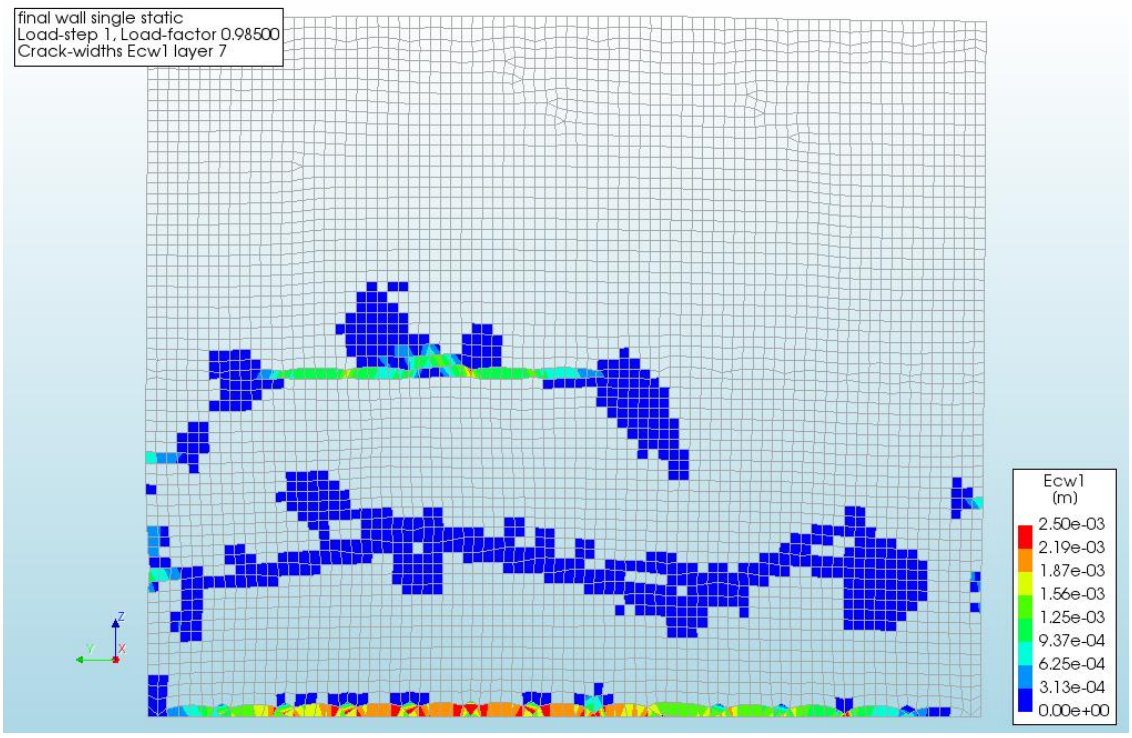


Figure 260 - Crack widths of the Single Wall Masonry House with Inner Walls due to the static load, 3.85 m, front view layer 7

### DYNAMIC

The model is loaded with an increasing amount of the dynamic load until failure. With respect to the first singe solid dynamic case, an increase in the maximum load is expected due to the presence of the inner walls. This is confirmed by Figure 261, the maximum load here is expected to be between approximately 9-11% of the total dynamic load. For the displacement and cracking patterns, the last 'Almost Converged' step is used. This step has an error of 0.035, which makes those results still fairly accurate.

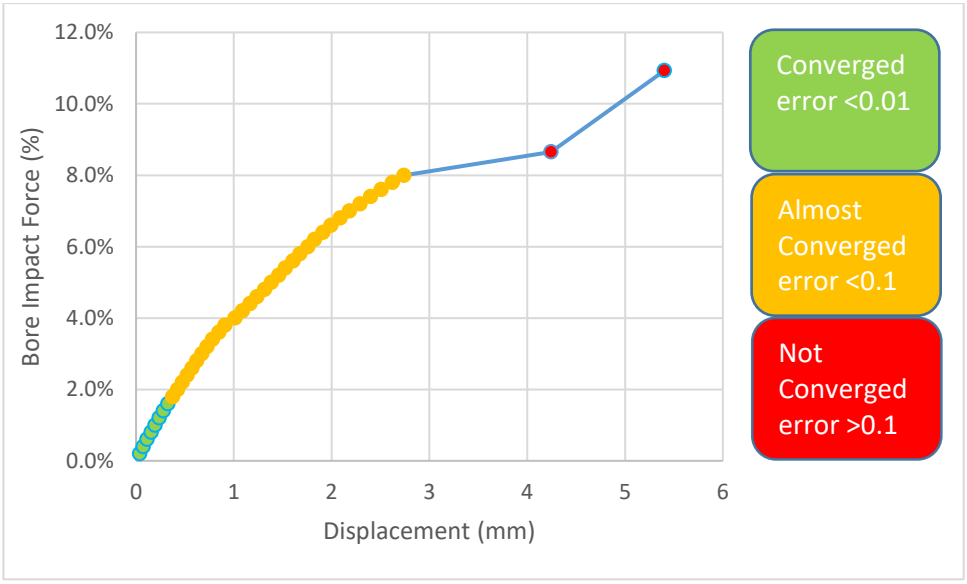


Figure 261 - Bore Impact Force vs Displacement of the Single Wall Masonry House with Inner Walls due to the dynamic load

The displacement fields are shown in Figure 262 and Figure 263. There is a resemblance between that dynamic and static displacement fields. Again, as with the static case, the inner wall decreases

the displacements at its location but not nearly as much as in the cavity inner walls dynamic case. The increased loading compared to this previous case causes the inner walls themselves to deform. In the current situation the displacement of the outer wall is not yet incredibly large, a few millimetres at the most. The inner wall follows this displacement, however, without much resistance. Relatively speaking the inner wall provides therefore much less support.

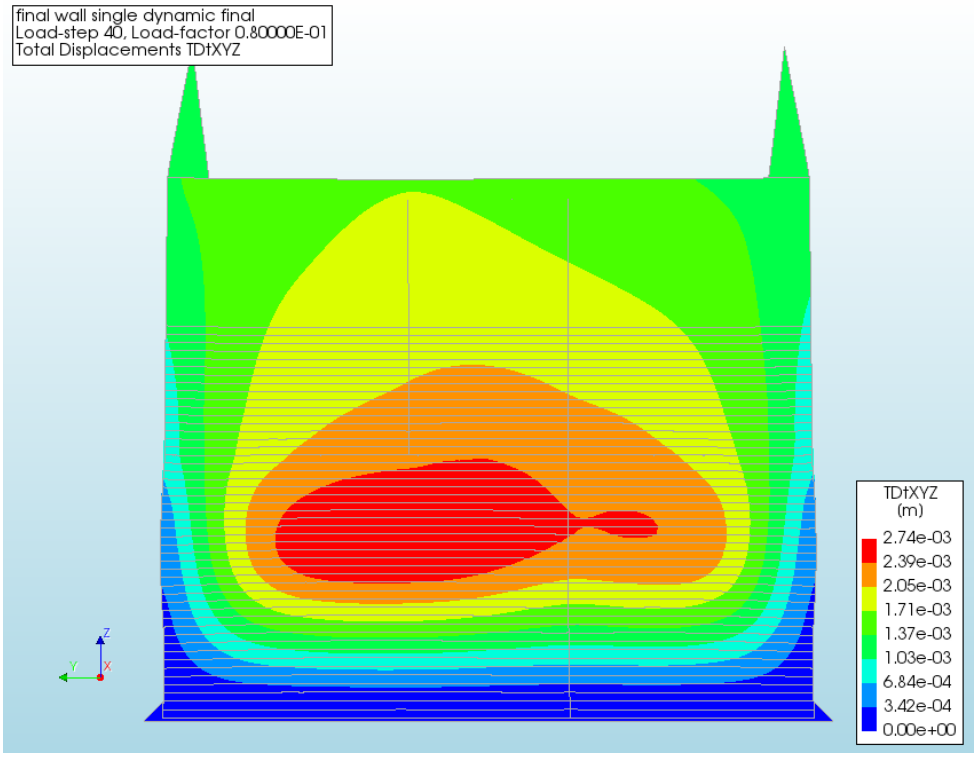


**Figure 262 - Displacement of the Single Wall Masonry House with Inner Walls due to the dynamic load, at 8.0%, front view**

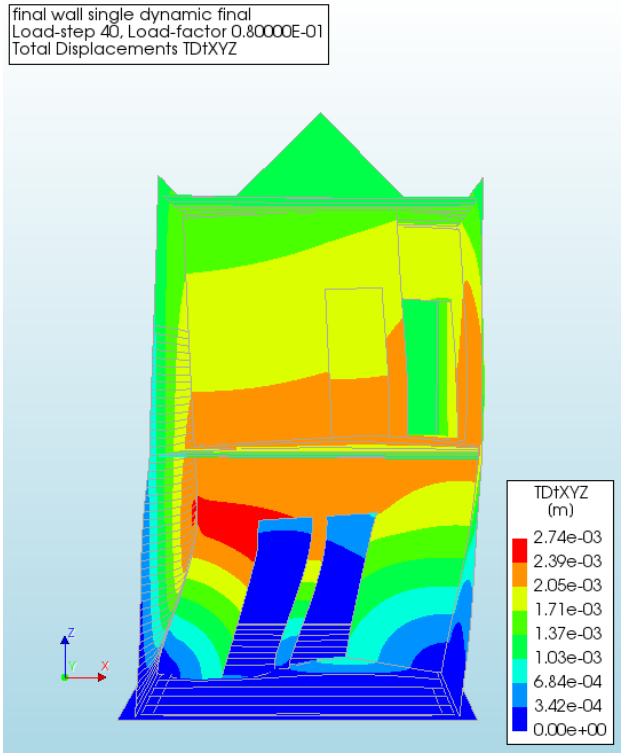


**Figure 263 - Displacement of the Single Wall Masonry House with Inner Walls due to the dynamic load, at 8.0%, side view**

The situation with the displacements is also visible for the crack widths. Instead of two distinct groups, the cracks are connected. From the size of the cracks it is clear that this is still before major cracking, shortly after this step the bottom cracks completely. This is followed by the middle of the ground floor wall and later the top of the ground floor will crack as well, as was for the cavity inner walls dynamic case and single solid inner walls static case.

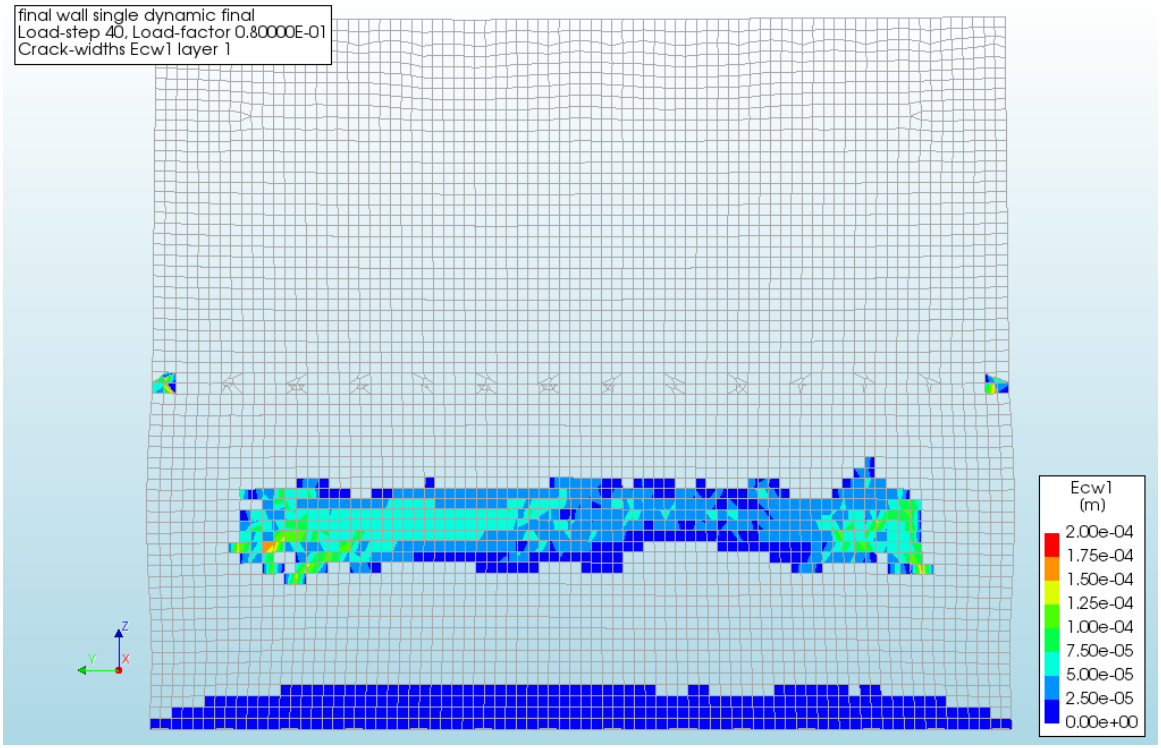


**Figure 264 - Crack widths of the Single Wall Masonry House with Inner Walls due to the dynamic load, at 8.0%, front view layer 1**

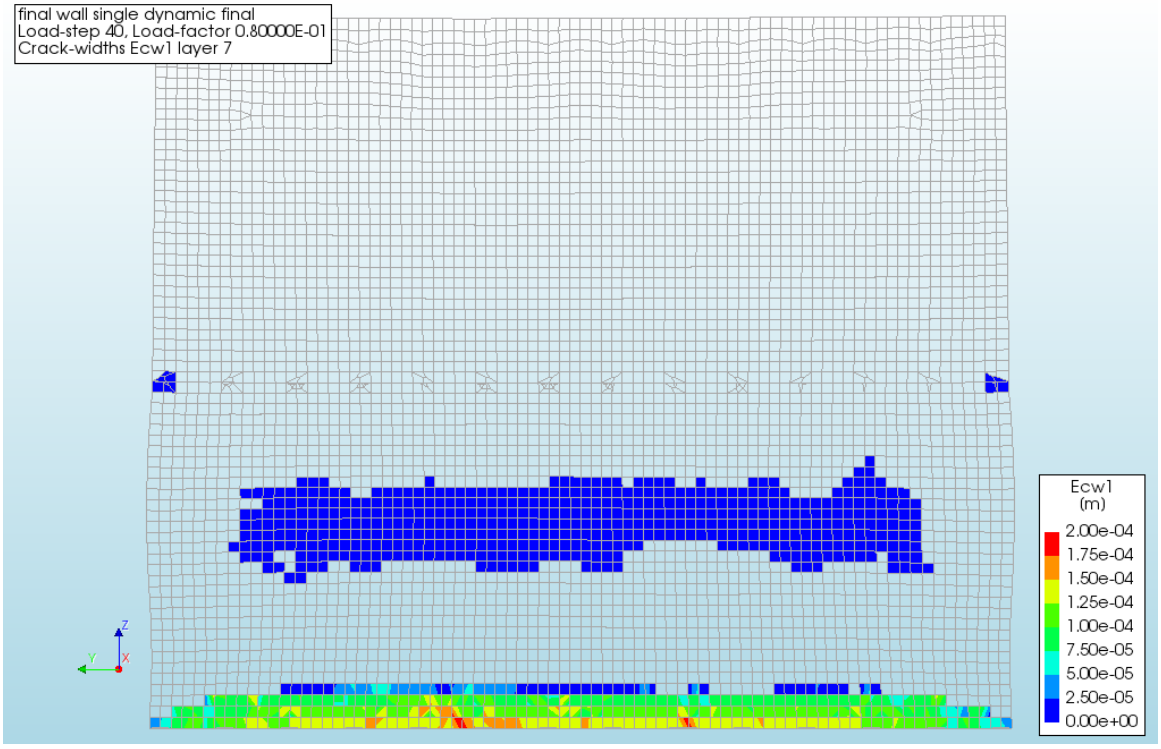


**Figure 265 - Crack widths of the Single Wall Masonry House with Inner Walls due to the dynamic load, at 8.0%, front view layer 7**

## Masonry House with Door, Windows and Inner Walls

The final model combines both the door and windows as well as the inner walls. Whether or not this will cause an increase or decrease in the resistance compared to the first dynamic cases is difficult to determine. One measure seems to increase the resistance, while the other decreases the resistance.

### Static

In contrast to the cavity door, windows and inner wall static case, now the section beneath the large window will not fail very early. However, whether or not the side wall will fail before the front wall, still needs to be checked. From Figure 266 and Figure 267 it follows that the side wall is not leading, the front wall is leading. The inundation depth causing failure therefore seems to be between 4-5 m. The front wall starts to show the typical failure behaviour at an inundation depth of approximately 4.0 m, which corresponds to the second 'Not Converged' step of Figure 266. This step is used for the displacement and cracking patterns.

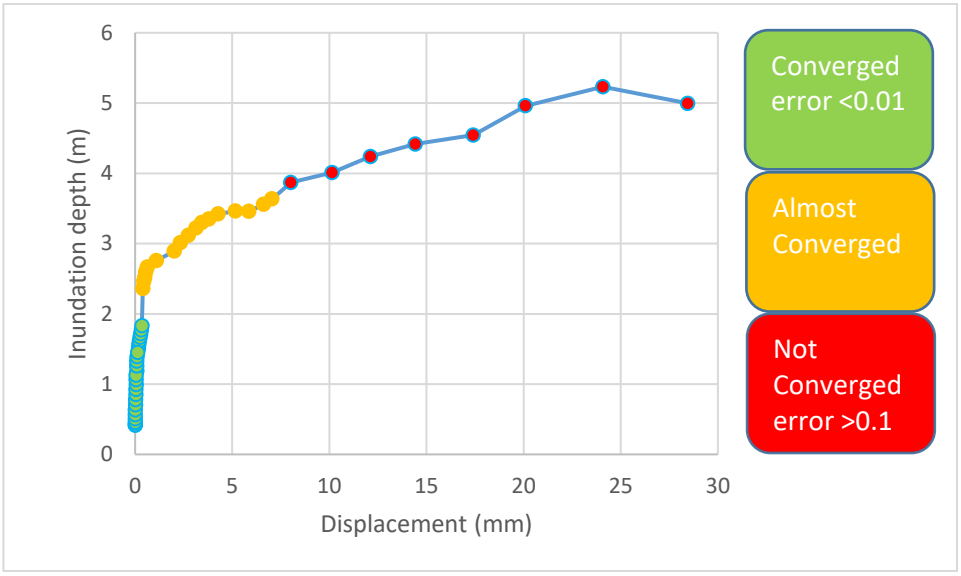


Figure 266 - Inundation depth vs Displacement of the Single Wall Masonry House with Door, Windows and Inner Walls due to the static load, front wall

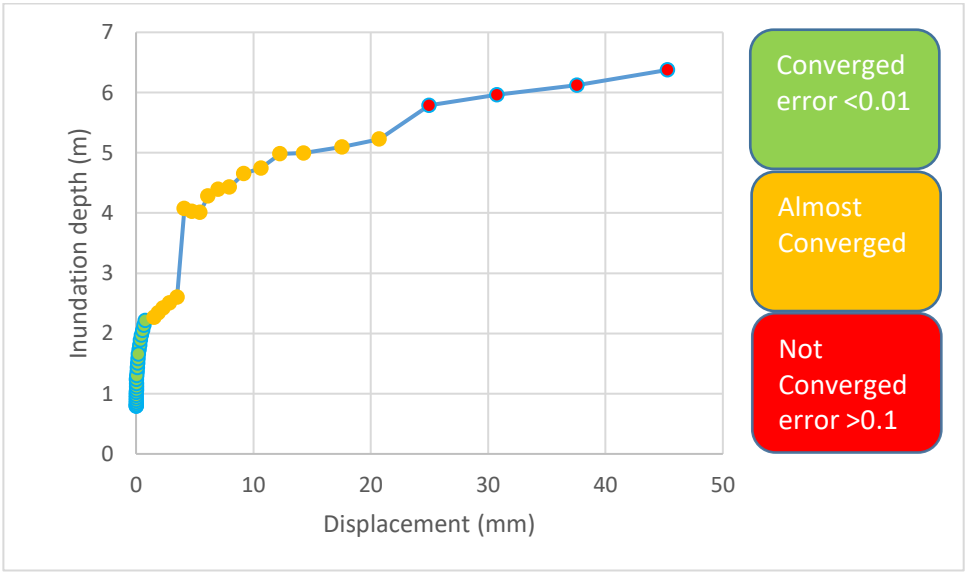


Figure 267 - Inundation depth vs Displacement of the Single Wall Masonry House with Door, Windows and Inner Walls due to the static load, side wall

Figure 268 and Figure 269 show the displacements for the house. The displacement pattern of the front wall is very similar to previous cases, see single solid inner walls cases and the single solid door, windows and inner walls static case. It seems however that the side walls deform much more. However, it actually experiences a greater load, causing the greater displacement.

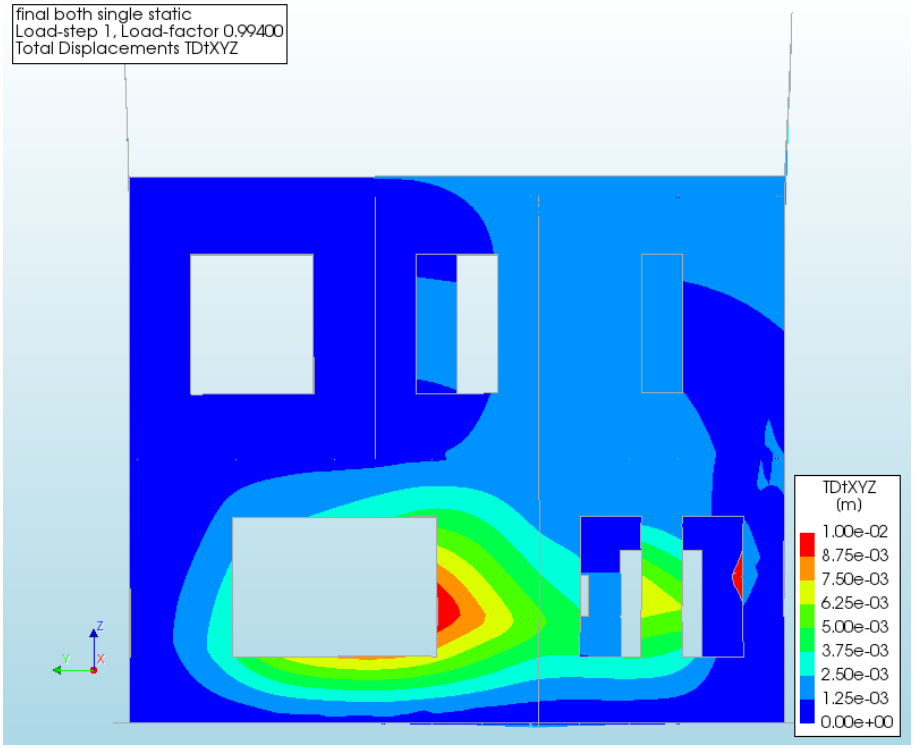


**Figure 268 - Displacement of the Single Wall Masonry House with Door, Windows and Inner Walls due to the static load, 4.0 m, front view**

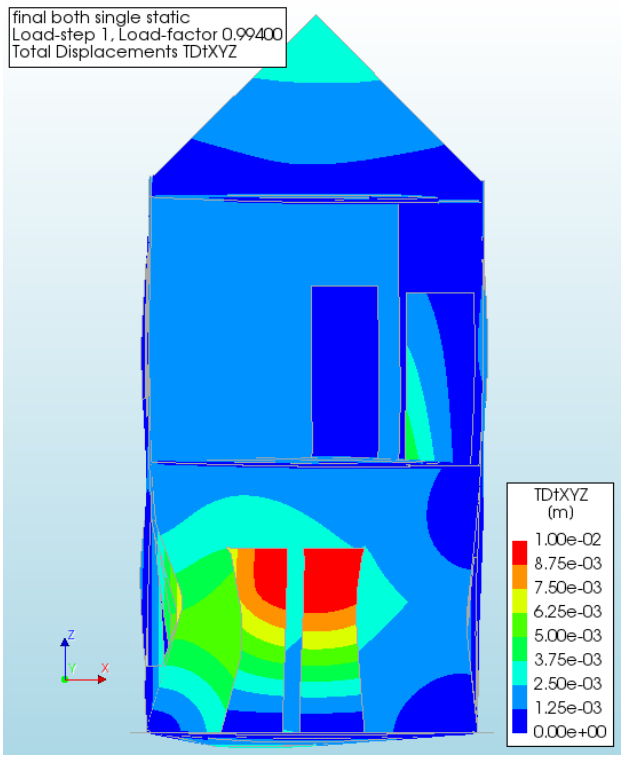


**Figure 269 - Displacement of the Single Wall Masonry House with Door, Windows and Inner Walls due to the static load, 4.0 m, side view**

As expected, there are again major crack patterns at the bottom and middle of the ground floor wall. The top of the ground floor wall has also started to crack and near the windows small crack patterns have appeared, see Figure 270 and Figure 271.

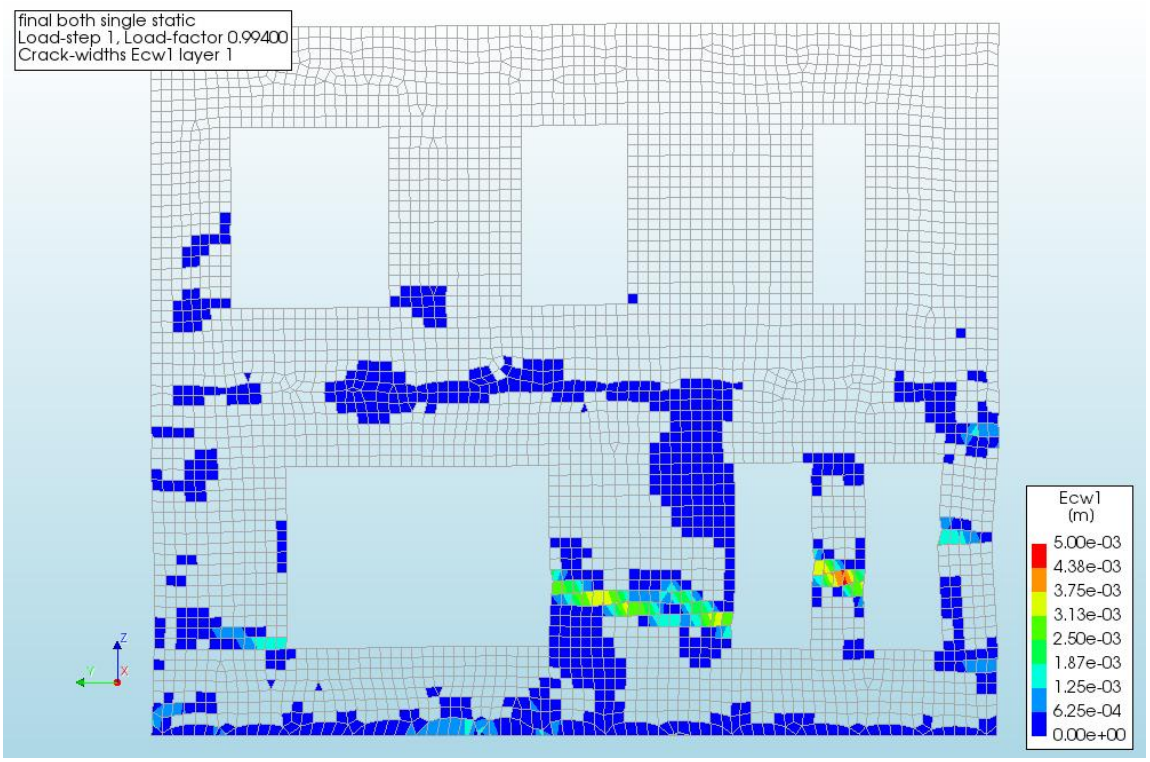


**Figure 270 - Crack widths of the Single Wall Masonry House with Door, Windows and Inner Walls due to the static load, 4.0 m, front view layer 1**

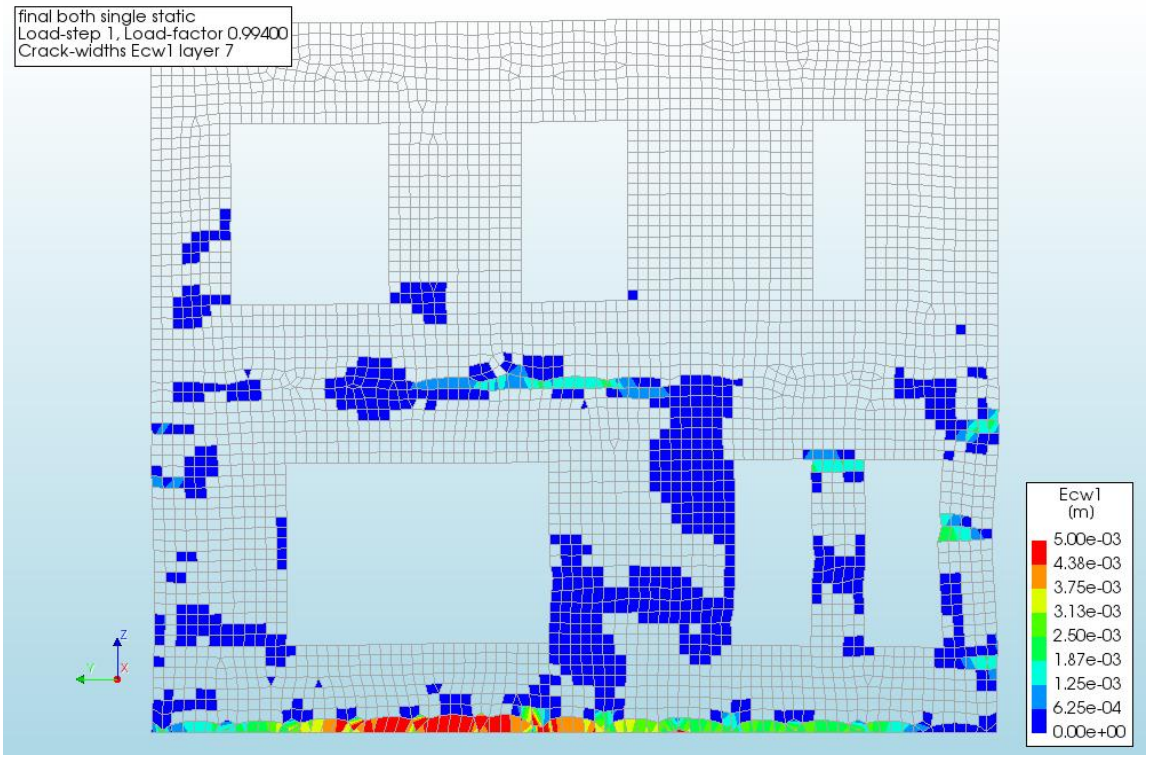


**Figure 271 - Crack widths of the Single Wall Masonry House with Door, Windows and Inner Walls due to the static load, 4.0 m, front view layer 7**

### DYNAMIC

Also, the last model is loaded with the dynamic load until failure. The cracking and displacement patterns for the last steps were all very similar. Therefore, the step with the lowest error is chosen to show these patterns. This is the last step of the 'Almost Converged' steps in Figure 272 and has an error of 0.063. This is still quite accurate, especially for determining the overall patterns. The failure load seems to be between approximately 7-10% of the total dynamic load.

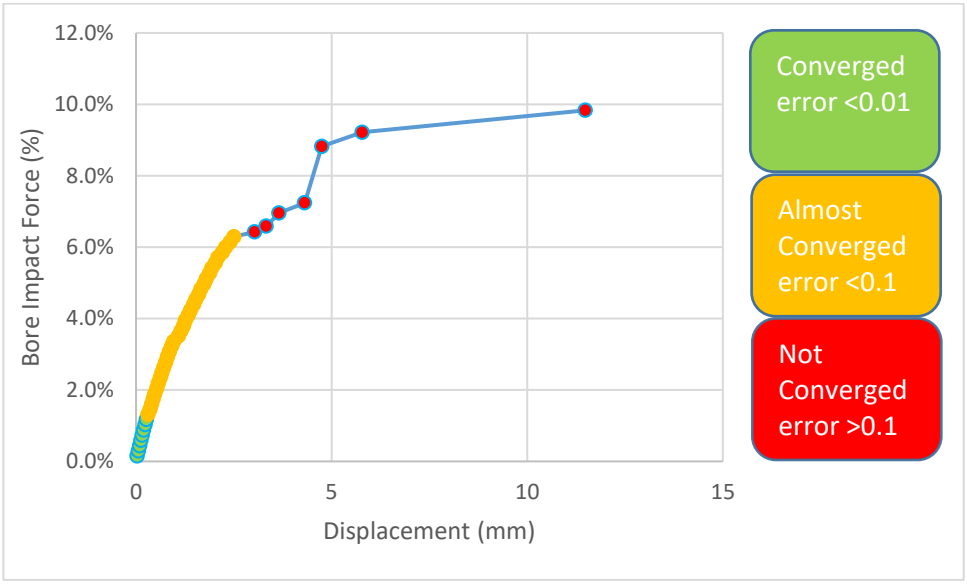


Figure 272 - Bore Impact Force vs Displacement of the Single Wall Masonry House with Door, Windows and Inner Walls due to the dynamic load

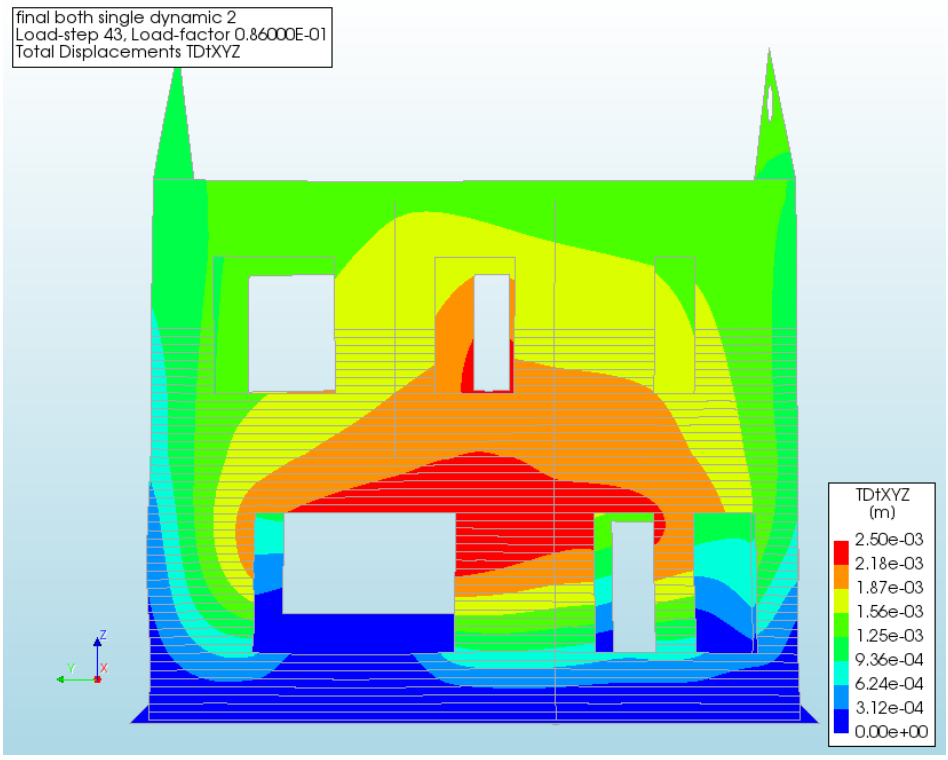


Figure 273 - Displacement of the Single Wall Masonry House with Door, Windows and Inner Walls due to the dynamic load, at 6.3%, front view

Figure 273 and Figure 274 show the displacement field of the house. The maximum displacement of the front wall will relocate towards the middle of the ground floor wall with increasing load. As is clearly visible, the inner walls seem to only have a small effect and deform already considerably. Before long, it is likely that their support will decrease even further as parts of the inner wall fail.

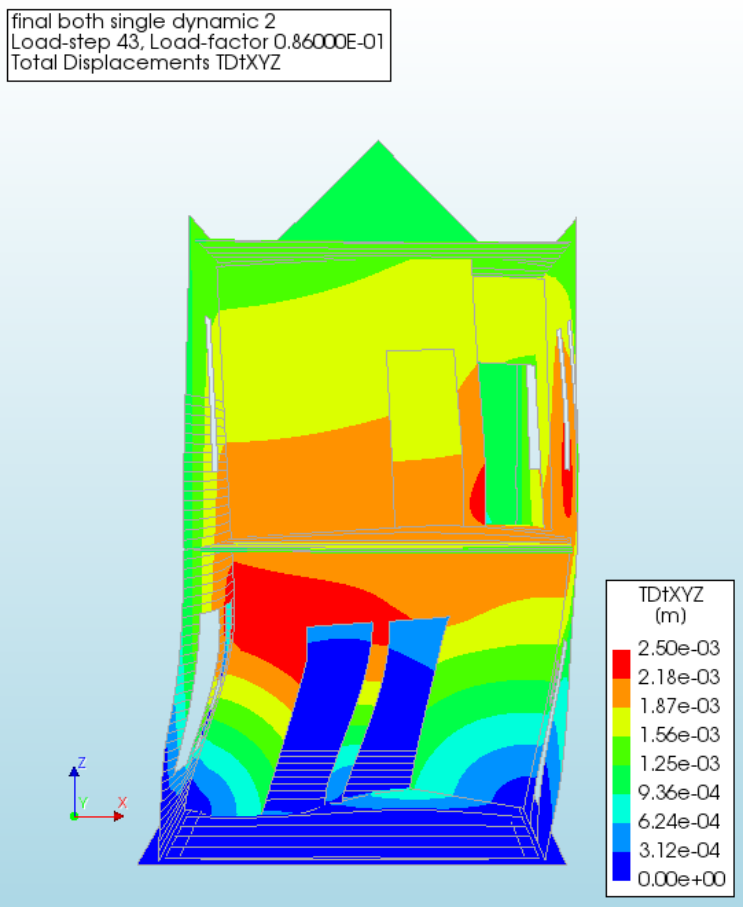


**Figure 274 - Displacement of the Single Wall Masonry House with Door, Windows and Inner Walls due to the dynamic load, at 6.3%, side view**

Figure 275 and Figure 276 show the familiar cracking patterns, largest at the bottom of the ground floor followed by the section in the middle, between the windows. The size of the cracks is still relatively small as failure has only started to occur.

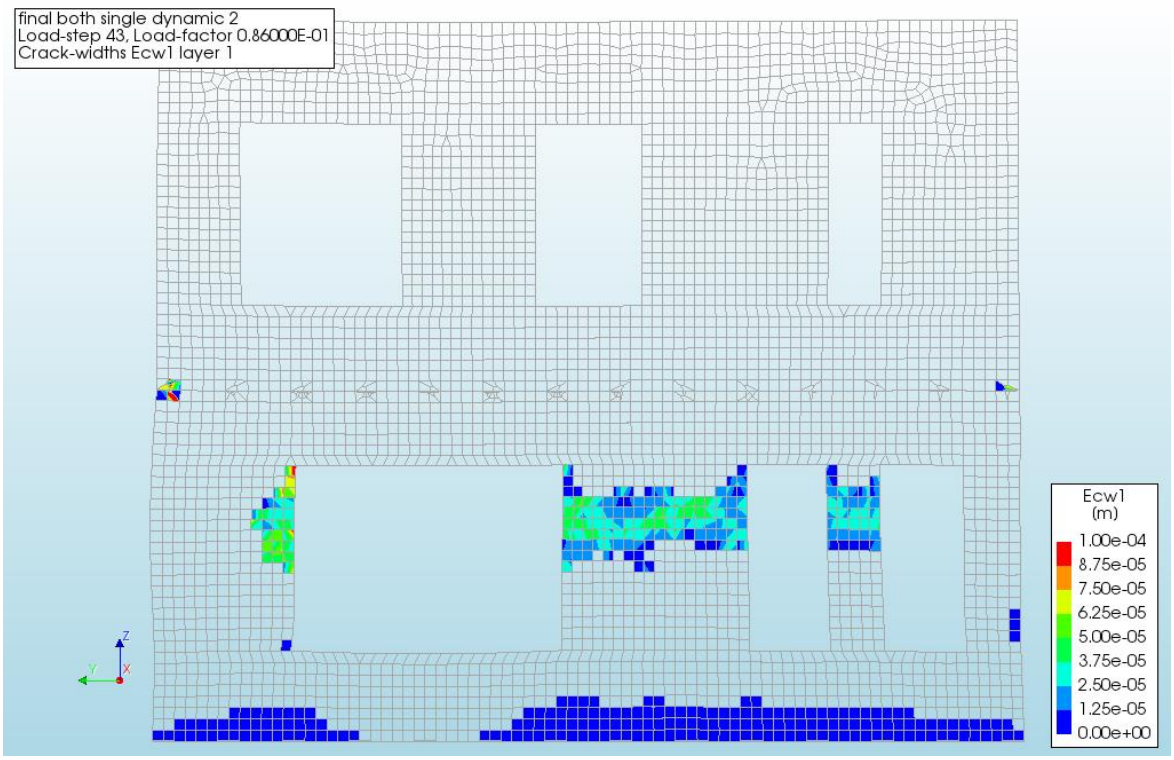


Figure 275 - Crack widths of the Single Wall Masonry House with Door, Windows and Inner Walls due to the dynamic load, at 6.3%, front view layer 1

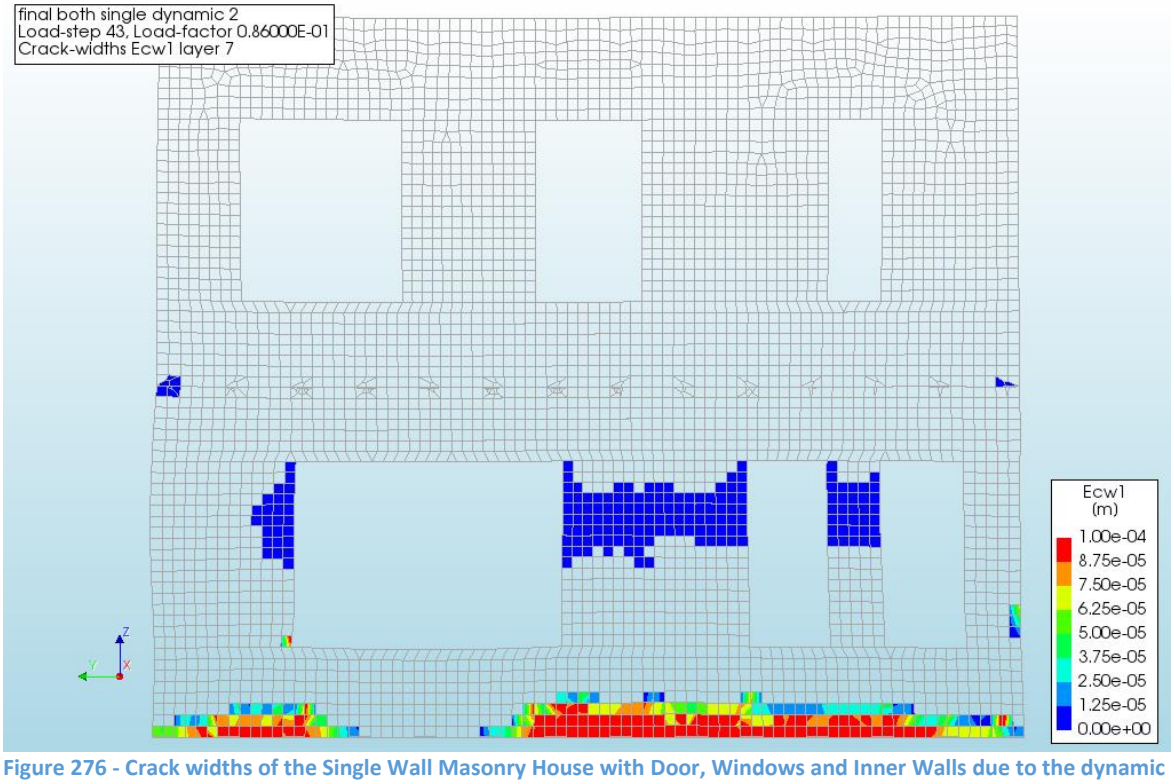


Figure 276 - Crack widths of the Single Wall Masonry House with Door, Windows and Inner Walls due to the dynamic load, at 6.3%, front view layer 7

## CONCLUSIONS

Four different cases have been investigated for the dynamic and static load. Again, each case added some complexity and realism to the original model, windows, door and inner walls. These changes also caused differences in the results.

Table 33 - Summary of the estimated failure loads of the Cavity Wall Masonry House

| | Failure load static (m) | Failure load dynamic (%) |
|---|---|---|
| **Original** | 4-5 | 5.5-6 |
| **Door and Windows** | 3.75-4.6 | 5.5-6 |
| **Inner Walls** | 4-5 | 9-11 |
| **Door, Windows and Inner Walls** | 4-5 | 7-10 |

As can be seen for the static load each extra element has little influence on the failure load. Only the door and windows show a small decrease of the failure load.

For the dynamic load this is not the case, the introduction of door and windows causes no decrease of the failure load. The inner walls do cause a significant increase of the failure load but decrease the accuracy. Combining both, an increase of the failure load compared to the original case is observed at the cost of accuracy.

The results seem somewhat contradictory. Where there is hardly any influence in the case of the static load, only a small decline for the door and windows case, there are, major differences for the dynamic load. Especially the influence of the inner walls is clearly visibly, increasing the maximum load with about 30-100%. Still, it is difficult to make any hard statements regarding these results since none of the steps near failure loads was very accurate. The results therefore have to be somewhat interpreted and estimated.

The most logical conclusion for these phenomena, again the height at which the loads act on the house. The dynamic load has its maximum at around 2.0 m. This is roughly where the inner wall of the ground floor directly connects the front and back wall, transferring part of this load to this back wall. Since the maximum of the static load is at the bottom of the wall, this transfer is much less present.

# Appendix K. Previous Load Cases

There are two distinct load cases, the hydrostatic pressure after the inundation of the flood area and the bore impact.

### STATIC

For the hydrostatic load case the models will be loaded with increasing inundation depths until, in the end, failure occurs. The hydrostatic and the bore impact pressure distributions are shown in Figure 277.

### DYNAMIC

The load for the dynamic bore impact follows from the calculations in chapter 3 and is based on a water level of 4.76 m and a velocity of 2.92 m/s. To determine the pressure due to the bore impact the maximum theoretical pressure impulse formula from 4.6.4.1 is used:

$$0.742 * \rho * h_b * u_n = 0.742 * 1000 * 4.76 * 2.92 = 10313.21 = 10.3 \left(\frac{kN}{s * m^2}\right)$$

In order to get the pressure peak, the duration of the impulse peak is required. This duration follows from Figure 35 and is approximately 0.10 sec. The pressure at the bottom is thus:

$$\frac{10313.21}{0.1} = 103132.1 = 103.1 \left(\frac{kN}{m^2}\right)$$

The pressure distributions for the bore impact over the entire wave height is then scaled using Figure 34. The hydrostatic and the bore impact pressure distributions are shown in Figure 277.

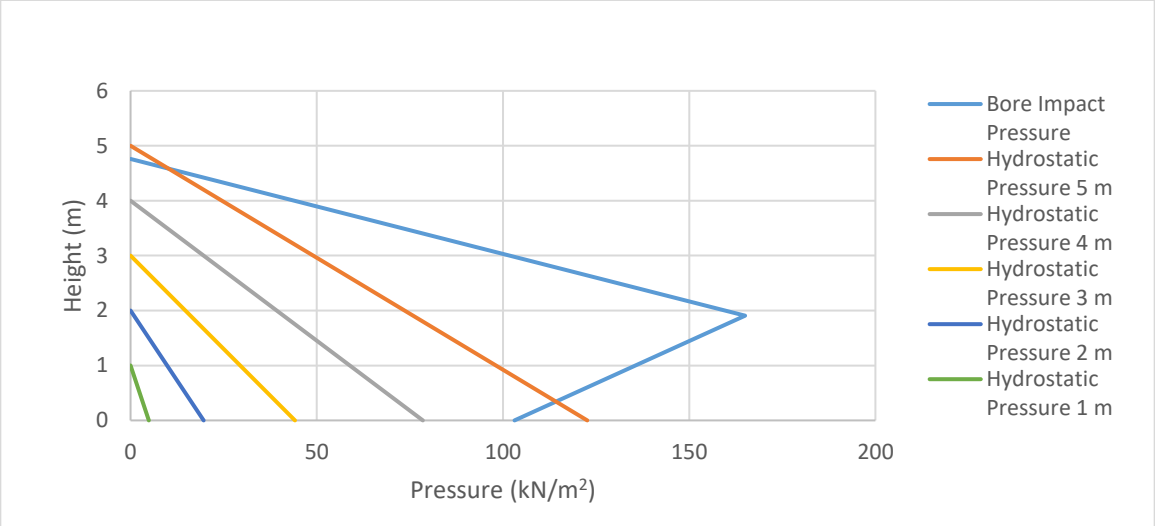


Figure 277 - Modelled Pressure Distribution Bore Impact and Hydrostatic Pressures

Figure 278 and Figure 279 show how these load case will look like in DIANA.

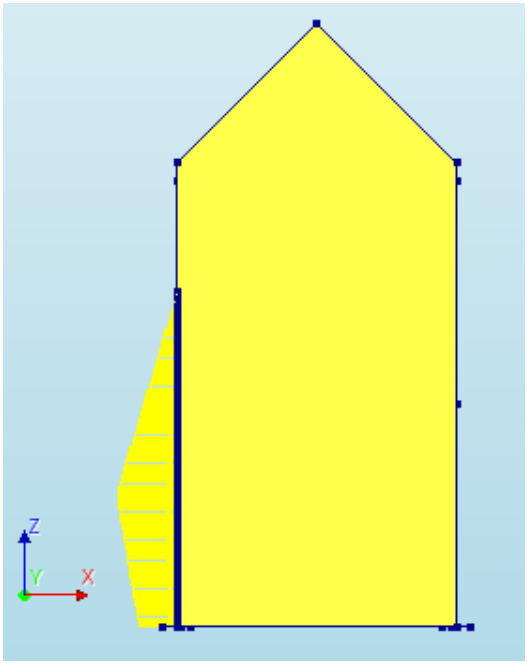


Figure 278 - Bore Impact pressure distribution in DIANA

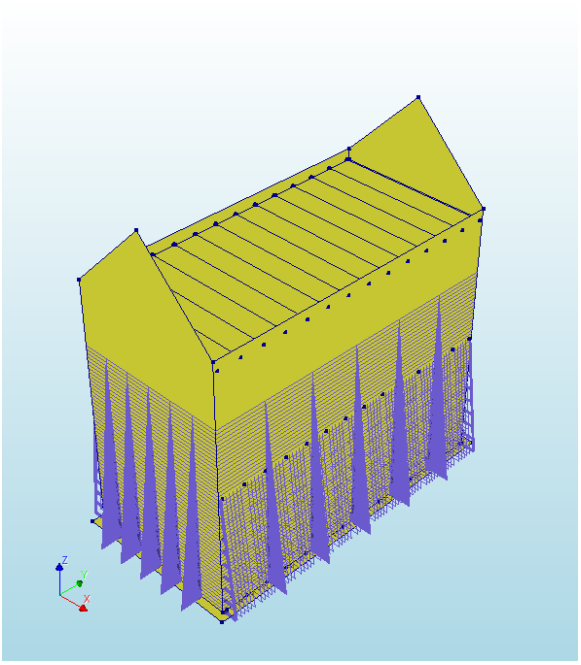

Figure 279 - Hydrostatic pressure distributions in DIANA